1991

Abrasive wear of ferrous alloys

Liqun Xu
University of Wollongong

ABRASIVE WEAR OF FERROUS ALLOYS

A thesis submitted in fulfilment of the requirements for the award of the degree of

DOCTOR OF PHILOSOPHY

from

THE UNIVERSITY OF WOLLONGONG

by

XU LIQUN B.Mech.

DEPARTMENT OF MATERIALS ENGINEERING

1991

CANDIDATE'S CERTIFICATE

This is to certify that the work presented in this thesis was carried out by the candidate in the Department of Materials Engineering, the University of Wollongong and has not been submitted to any other university or institution for a higher degree.

ACKNOWLEDGEMENTS

The research work reported in this thesis was carried out in the laboratories of the Department of Materials Engineering, at the University of Wollongong, Australia under the supervision of Associate Professor N. F. Kennon.

The author would firstly like to thank Bunge Steels Pty. Ltd., now Bisalloy Steels Pty. Ltd., and Heat Containment Industries Pty. Ltd., Unanderra, and the University of Wollongong for providing a scholarship to support this research work. The author would also like to thank the past and present chairmen of the Department, Associate Professor N. F. Kennon and Professor W. Plumbridge for the provision of laboratory facilities.

The author wishes to express her deep gratitude to Associate Professor N. F. Kennon for his kindly acceptance of her as a post-graduate student majoring in materials engineering with her background of mechanical engineering, and for his consistent support, skillful guidance and invaluable criticisms throughout her study.

The author is indebted to Associate Professor D. P. Dunne, Dr. A. Wingrove and Mr. M. Pretor for their valuable discussion and advice. The author is also indebted to Associate Professor C. D. Jiang for his continuous support and help during her study in Australia.

The author wishes to acknowledge Mr. R. Kinnell for his involvement in designing the pin-on-drum wear test machine and preparation of the original working drawings for manufacture of the machine. The author is also grateful to Mr. G. Hamilton and the entire staff of the Department of Materials Engineering for their assistance with various aspects of the programme.

The author is grateful to her dear friends, Ms X. Qian, Ms H. Wang, Ms S. Chen, Ms X. Yang, Mr. S. Huang and Professor W. Huang for their invaluable help, personal assistance and continued encouragement during her study.

Finally, the author wishes to thank her parents and brother for their continued support, understanding and encouragement during her study in Australia.

SYNOPSIS

The investigation reported in this thesis was carried out to study the abrasive wear behaviour of three groups of ferrous alloys, comprising ten carbon steels, three tool steels and four high-strength low-alloy steels, with the particular emphasis on the effect of microstructure. Wear tests were conducted using an unlubricated pin-on-drum machine, with silicon carbide, alumina and garnet abrasive papers, and a standard test condition of 20N applied load, 50mm/s sliding speed and 6m wear path.

The inter-relationships between wear resistance, microstructure, hardness and carbon content were studied using the carbon steels containing 0.10%C to 1.4%C. For constant hardness and carbon content less than 1.0%, the results showed that bainite had the highest wear resistance, followed by tempered martensite and the annealed structures. For a steel containing carbon >1.0%C, the annealed structure had wear resistance superior to the quenched and tempered structure or the spheroidized structure. Additionally, the relationship between wear resistance and hardness was linear for annealed steels, but the slope for hypoeutectoid steels was lower than for hypereutectoid steels. Further, normalizing of these steels increased both hardness and wear resistance for the eutectoid steel, but hardness only for hypoeutectoid steel.

For quenched steels, the relationship between wear resistance and hardness was rather complicated, while for tempered martensite at the same hardness level, the higher the carbon content, the higher was the wear resistance. For a particular steel, a non-linear relationship between wear resistance and hardness of tempered martensite was confirmed. This wear behaviour indicates that abrasive wear resistance is not simply related to the hardness of materials, but is determined also by the microstructural properties.

The effect of heat treatment on abrasive wear behaviour was examined using a Ni-Cr-Mo-C tool steel, with specimens being either single-quenched or double-quenched from 900°C followed by tempering at 100°C, 200°C, 300°C and 400°C. The results showed that wear resistance was optimized by double-quenching followed by 200°C tempering, for which the microstructure comprised highly dispersed fine carbides in a matrix of tempered martensite. The relationship between wear resistance and hardness was non-linear for both single- and double-quenched specimens; however, for single-quenched specimens, wear resistance increased with hardness to Hv610, then decreased with further increase of hardness. For double-quenched specimens, wear resistance increased non-linearly with hardness to Hv660, which was the highest value available in the study.

The effect of massed carbides in the microstructure on abrasive wear behaviour was measured as a function of applied load using two high-carbon high-chromium tool steels designated Chrome and XW-5. The result that Chrome was more wear resistant than XW-5 under high applied load can be attributed to the difference in the carbides in the two steels. In XW-5, only massed M_7C_3 type carbides were identified by energy dispersive spectroscopy, while in Chrome, mixed massed M_7C_3 and MC carbides were identified. Optical microscopy indicated that the carbide sizes and volume fractions were similar for both steels. It is concluded that wear resistance should be optimized for microstructures comprising mixed massed M_7C_3 and MC carbides randomly distributed in tempered martensite.

The effects of the concentrations of carbon and molybdenum on wear behaviour were studied using four high-strength low-alloy steels designated Bisalloys, which were available in the quenched condition as with martensite or bainite (high molybdenum alloy), or the quenched and tempered condition. The relationship between wear resistance and hardness after tempering a particular steel was non-linear, due to the

effect of carbides precipitated during the tempering process. Also, for the specimens at the same hardness level, bainite had higher wear resistance than tempered martensite, and for tempered martensite, the higher the carbon content, the higher was the wear resistance, consistent with results for the plain carbon steels. However, after high temperature (>300°C) tempering, tempered bainite had lower wear resistance than tempered martensite due to the large inter-carbide spacing in the bainitic structure.

A thin white surface layer was generated under the standard abrasive wear test condition on specimens with prior microstructures of bainite or low temperature tempered martensite. For plain carbon steels, the thickness of the white layer increased non-linearly with carbon content. The generation of the layer can be attributed as the prior microstructures which comprised tempered martensite or bainite containing retained austenite and fine carbides, and the severe plastic deformation which occurred during abrasion. The structure of the white layer was possibly severely deformed martensite or bainite, containing extremely fine carbides with ultra-fine-grained structures.

Microscopical studies of the worn surfaces and of wear debris indicated that microcutting was the dominant mechanism of metal removal and that microploughing, which formed grooves with prows and bulges, was a necessary precursor to microcutting, fracture and side-cut chip formation. Steels with high carbon content (annealed 1.2%C) or brittle microstructure (quenched martensite) have a great tendency for microcracking. Microploughing was significant for low carbon steels. Additionally, some secondary wear mechanisms such as adhesion and delamination, were involved in the formation of small wear debris.

It is clear that the inter-relationships between wear resistance, hardness, composition and microstructure are complex. However, it is also clear that microstructure is as

important as hardness or as composition in determining wear resistance. For a particular steel, wear resistance can be optimized by applying an appropriate heat treatment to generate the most suitable microstructure in relation to the tribological requirements of the application.

CONTENTS

Section **Page**

Section Page

Section Page

Section Page

Section Page

Section Page

Section Page

Section Page

Section Page

LIST of FIGURES

Figure op. **Page**

Figure **op. Page**

EXPRESSION OF SYMBOLS

A	specimen surface
a, a_1	constant
b, b_1	constant
α, α_1, α_2	constant
β, β_1, β_2	constant
ε, ε_o, ε_1, ε_2, ε_3	relative wear resistance
C%, C	carbon content
C_1	coefficient for wear resistance and hardness
d	diameter for pin specimen
D	diameter for drum
δ	experimental system error
Δ, ∂	error between the actual value and the measured value
σ	standard deviation for testing error
υ	coefficient variation
E	Young's modulus
f_1, f_2, f_3,	individual fraction of the components of the material
H	hardness of steels or alloys
H_a	hardness of abrasives
H_o	hardness of annealed steels
Hv	Vicker's hardness
i_1, i_2, i_3	speed ratio for gear box
K	dimensionless wear coefficient
l	length of specimens
L_D	length of the drum
L	applied Load
m	mass loss

n	number of experiment times
n_D	rotating speed of the drum
n_E	rotating speed of the electric motor
n_s	rotating speed of the guide screw
N_D	rotating number for the drum
N_s	rotating number for the guide screw
P	volume fraction of pearlite
P_r	applied pressure on the specimen
θ	semi apex angle of the abrasive cone
r	radius of the abrasive cone
S_x	distance for the specimen sliding horizontally
t	thickness of pearlitic lamellae
t_s	teeth spacing of the guide screw
V	relative sliding speed between pin specimen and drum
V_h	horizontal sliding speed of specimen
V_l	volume loss
X	wear path
x	length of the abrasive particle moved
Z_1, Z_2, Z_3, Z_4	gear teeth number
z	depth of the abrasive cone penetrated into the wearing material

Chapter 1

INTRODUCTION

Wear is encountered in many situations ranging from home to industry and is a subject of obviously practical significance. It is not surprising, therefore, to find that man has tried for many centuries to understand and control the wear process[1]. In modern times, wear has attracted investigators from numerous different scientific and technical backgrounds; however, despite this attention, the present understanding of the processes and mechanisms by which wear occurs is far from complete. The failure of mechanical components, for example, can result from excessive deformation, fracture or wear; the first two modes of failure are understood quite well and can be considered in a quantitative manner in design, whilst wear problems are usually handled in the empirical and qualitative method. Wear still remains almost impossible to forecast under any particular sliding system, because, although individual wear mechanisms are now well understood, the way in which they interact with one another depends most sensitively on the specific operating conditions[2].

In recent years, interest in the materials aspects of wear has grown dramatically as investigators have attempted to provide quantitative data relating composition, microstructure, mechanical properties and wear behaviour. However, success has been limited, and in most cases, the gap between laboratory experimental work and industrial wear is still large[3].

Wear can be defined as the progressive loss of substance from the operating surface of a counter-body occurring as a result of relative motion at the surface[4], and wear is probably the most commonly encountered industrial problem where relative movement of components is involved. Failure from wear can be gradual, rapid or even catastrophic. It may result in dimensional changes, in surface damage or under extreme cases, in fracture damage of the components necessitating eventual component replacement. Generation of hard wear debris may be more serious than the actual dimensional change of a component and may lead to acceleration of wear damage.

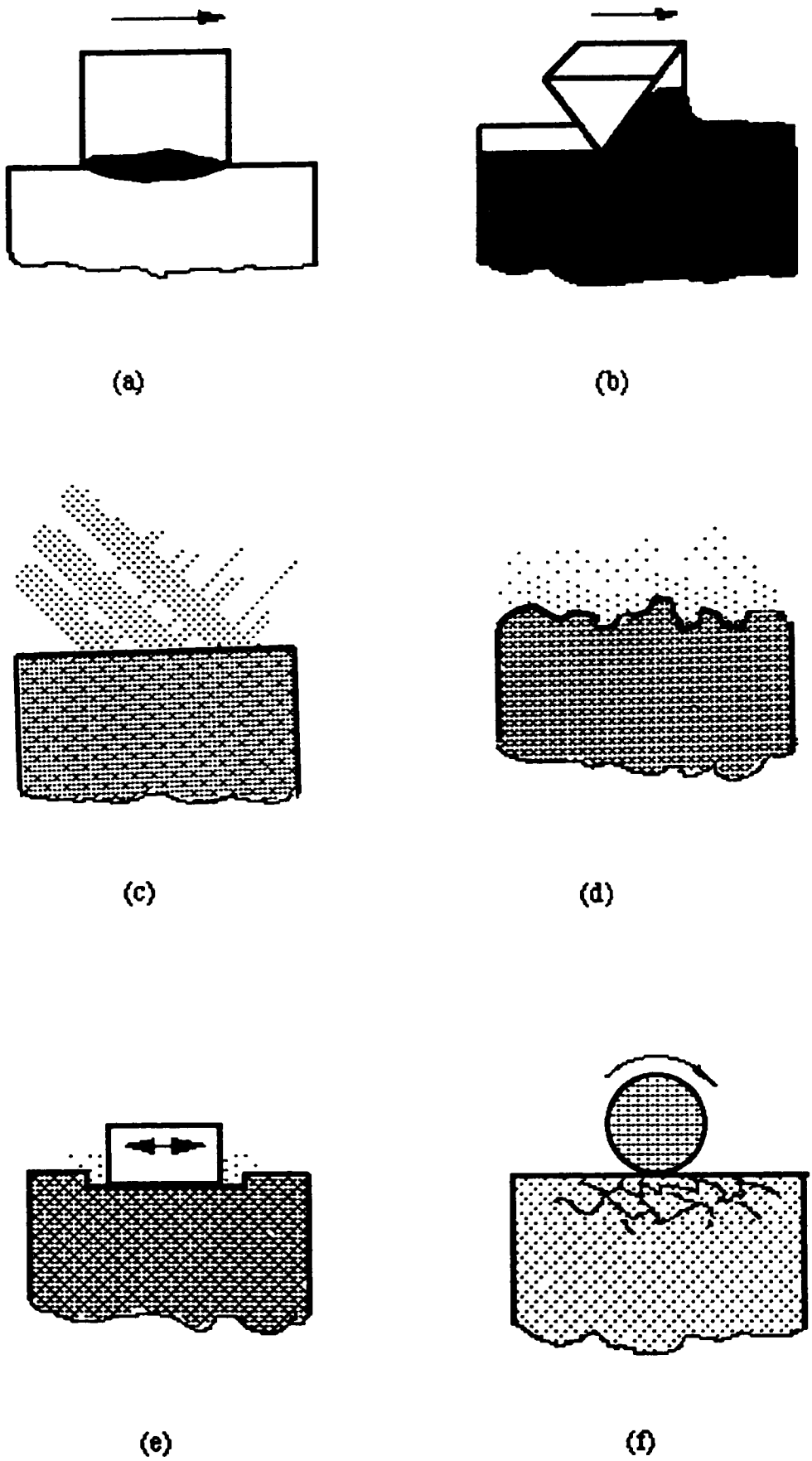

Fig.1.1 Diagrams showing wear classified by the mechanisms of debris formation: (a) adhesive wear, (b) abrasive wear, (c) erosion, (d) corrosion, (e) fretting and (f) surface fatigue.

From the beginning of the industrial revolution to industrial modernization, wear problems have imposed a significant cost to industry in material wastage, in energy wastage and in labour commitment[5]. Recently, in view of increased labour and material costs, interest in wear prevention, instead of replacement, has increased rapidly.

Wear is commonly quantified as wear rate which is defined as the quantity of material removed over unit distance or during unit time of abrasion, or wear resistance which is expressed as the reciprocal of wear rate[4]. The quantity of removed material may be measured by mass, volume or dimensional loss from a specimen. For some applications, relative wear rate is specified as the wear rate of a test specimen relative to the wear rate of some standard reference material.

According to the type of relative motion, wear processes may be classified as sliding, rolling, oscillation, impact and erosive, depending on the kinematics of the system, and may occur in the dry or the lubricated abrasion condition. The mechanism of formation of wear debris can be classified as adhesive, abrasive, erosive, corrosive, fretting and surface fatigue[6], as presented in Fig.1.1.

Adhesive wear occurs when two surfaces slide or roll relatively to each other under pressure. The traditional explanation proposed by Merchant[7] and further elaborated by Bowden and Tabor[5; 8] involves welding or adhesion of asperities followed by fracture from the joined region to remove material. More recently, Suh *et al.*[9-10] proposed an alternative mechanism based on sub-surface delamination.

Abrasive wear is material displacement caused by sliding contact with hard particles or hard protuberances[4], and is discussed in detail in Chapter 2.

Erosive wear results from the impact of particles and occurs by a combination of deformation from the normal impact of the particles and cutting action. The wear rate depends upon the attack angle between the direction of impacting particles and the wearing material, as well as the mutual materials involved.

Corrosive wear is often regarded as chemical reaction and involves the formation of new substances partially distributed on the surface of the wearing material. The new substance is often easily removed leaving the wearing surface subject to pitting corrosion.

Fretting wear occurs between two mating surfaces subjected to cyclic relative motion with small amplitude. It is usually adhesive in nature resulting from the cyclic stressing; the wear debris is very small and the surface damage is often surrounded by oxidation debris[6].

Fatigue wear occurs on metal surfaces or sub-surfaces due to repeated rolling, sliding or impacting motion at relatively low stress resulting in numerous pit-like cavities in the surface.

Industrial wear processes are often the combination of various mechanisms and approximate frequencies have been given by Eyre[11]:

Abrasive	50%	Adhesive	15%
Fretting	8%	Chemical	5%
Erosive	8%	Others	14%

This information points to the importance of abrasive wear, which is most significant over a very wide range of operating situations. In many of these cases, abrasive wear appears to be the limiting factor in the design of equipment.

The wear rate of components in a mechanical system can be related to the tribology system by which relative movement occurs, and to the materials in contact. In the case that the tribology system has been designed to satisfy specific working requirements, wear resistance can be improved significantly only by optimization of material properties. Scientists[12-13] have appealed for increasing attention to be given to the materials aspects of wear.

The present project is concerned with abrasive wear problems accounted in the applications of tool steels such as in brick-pressing and mineral processing operations, and of high-strength low-alloy steels such as in mobile crane and agriculture equipment. These working conditions are characterized by sliding abrasive wear under low sliding velocity and high work load.

The aim of the project was to study abrasive wear from the material point of view by relating wear resistance to composition, microstructure and hardness for a number of ferrous alloys. The project consists of three parts. First, the effects on wear resistance of basic abrasive wear variables such as applied load, sliding speed, work path, and material properties such as carbon content, hardness and microstructure have been investigated using ten steels containing from 0.10% to 1.4% carbon. Secondly, the effects on wear resistance of heat treatment processes such as single-quenching or double-quenching, followed by tempering were studied using a Ni-Cr-Mo-Fe-C tool steel; and the effect on wear resistance of alloying elements, especially in relation to carbide-type and distribution, was studied using two high-carbon high-chromium tool steels. Thirdly, the effects on wear resistance of the concentration of carbon and

molybdenum, and tempering temperature were investigated using four high-strength low-alloy Bisalloy steels.

Consequent upon these studies, co-relations were sought to provide a guide to optimization of wear resistance for particular steel through appropriate composition and heat treatment and to provide useful information for developing new, relevant steels with optimized wear resistance.

To limit the experimental variables to as few as possible for the abrasive wear test, two-body abrasive wear was accepted for this investigation. In Chapter 2, an introduction of abrasive wear and two-body wear testing is presented. The various factors which influence on abrasive wear will be discussed in Chapter 3, whilst a review of optimization of wear resistance from material aspects is given in Chapter 4; and an introduction of properties for relevant steels is shown in Chapter 5. Chapter 6 is concerned with the experimental work and apparatus used for this investigation; the results of which are presented and interpreted in Chapter 7. Analysis of abrasive wear damage and elucidation of the relative wear mechanisms are discussed in Chapter 8, and finally, in Chapter 9 the conclusions and recommendations based on the study are presented. The further work suggestion is presented in Chapter 10.

Chapter 2

ABRASIVE WEAR

and

WEAR TESTING

Abrasive wear occurs by penetration of hard particles or surface asperities of a material into the surface of a softer material during relative movement, and is manifest in two main ways[14].

(1) The wear counter-body contains particles of the abrasive medium (such as carbides) distributed in a softer matrix. When the matrix at the surface is removed, the particles are exposed and function as abrasive particles by simply rubbing against the surface of another counter-body.

(2) Abrasive particles, from a lubricant, contamination, or wear debris, are trapped as free abrasive particles between two sliding surfaces.

Abrasive wear can occur in a wide range of circumstances ranging from agriculture to mining and mineral processing, from refractory to textile industries and in the home. Where relative motion occurs, wear occurs. Abrasive wear is an inevitable problem for most industries, and wear resistant materials are sought for many engineering applications. However, wear resistance is not an intrinsic property of a material but depends on the tribological system and, for a specific material, is strongly dependent on the nature of the relative movement between the involved components. Therefore, it is most important for a design engineer to develop a tribology system which, under satisfactory working requirements, will minimize the wear damage.

2.1 ABRASIVE WEAR CLASSIFICATION

Abrasive wear is classified traditionally as 'two-body' or 'three-body', according to whether the functional particles are fixed within a rigid matrix or are in a loose form[13]. The situation under which only two components are involved in the interaction is known as two-body abrasion and occurs, for example, as a grinding

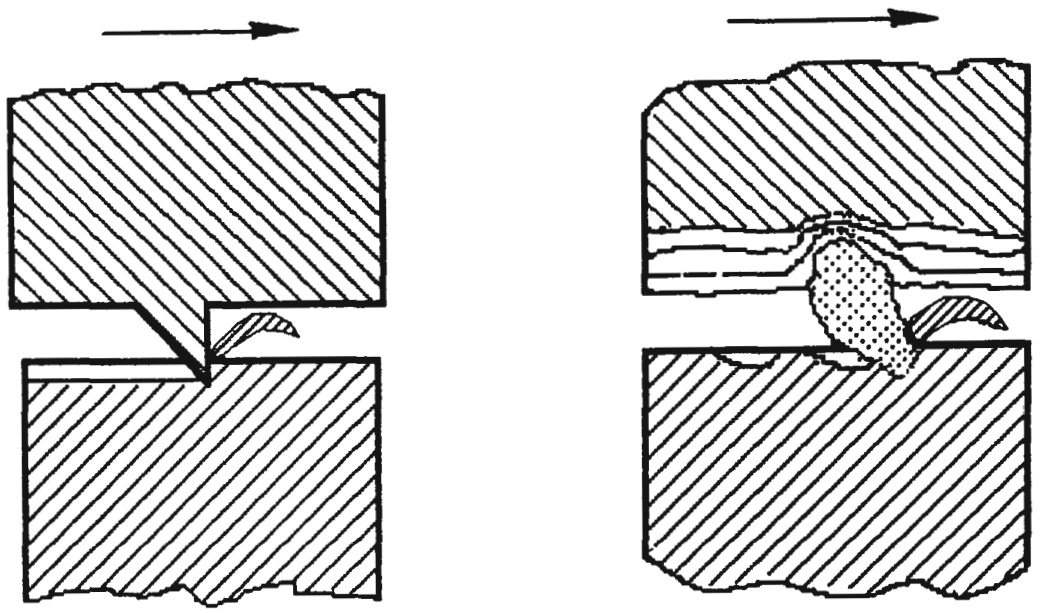

Fig.2.1 Diagrams showing the mechanism of material removal for (a) two-body abrasive wear and (b) three body-abrasive wear.

wheel removes material from a metal surface. Three-body abrasion occurs under the condition that abrasive particles are trapped between two solid sliding surfaces such as in mining drilling or in bearings. The mode of material removal for both two-body and three-body abrasive wear are shown diagramatically in Fig.2.1.

The widely used classification system for abrasion proposed by Avery[15-16] categorized abrasive wear as gouging, high stress and low stress depending on the stress levels applied on the system.

(1) Gouging abrasion may result from impact and may occur during abrasion with abrasive papers or a grinding wheel. Large particles of debris are removed from the wear surface under very high stress and consequently, the particles may be heated to quite high temperature and may appear as sparks in dim-light. Impact load, fracture, metal flow and work hardening are factors associated with this type of wear.

(2) Under high stress abrasion, the abrasive particles are often broken by contact stresses, and generally, progressive fragmentation occurs when the contact stress exceeds the crushing strength. The high stress causes plastic flow and then detachment of ductile constituents or fracture of hard constituents.

(3) Low stress scratching abrasion occurs when the imposed stress does not exceed the fracture strength of the abrasive particle, as in the work condition on a conveyor in mineral processing plants. Under low stress abrasion, some plastic deformation is associated with the wear process, but very little work hardening occurs and the wear rate is quite low.

2.2 ABRASIVE WEAR and TESTING

2.2.1 Abrasive Wear

In practice, abrasive wear occurs mostly by three-body abrasion, while two-body abrasion is encountered primarily in material removal operations such as filing, turning, milling, shaping, drilling and grinding. Despite the importance of three-body abrasion, the majority of abrasive wear studies deal with the two-body problem, possibly because the variables in two-body abrasive wear are comparatively easy to control so that simple test procedures can be used. Additionally, a theoretical model for the wear mechanism can be deduced because the material removal process is relatively clearly defined.

The differences among different types of laboratory abrasive wear tests, or between laboratory wear test results and practical wear situations, are serious questions. It was reported[17] that wear rates measured for the same material by three different types of wear test can differ by a ratio factor as high as 12. Also, there seems to be no consistent relationship between wear resistance and hardness or microstructural properties of materials. It is important, therefore, to standardize laboratory wear testing to correlate the tests with field conditions. This requirement may impose new approaches on wear testing but eventually should result in fewer, rather than more, types of wear test. It is optimistic to suggest that one or two basic abrasive wear tests could replace most, or even all of the present abrasive wear tests. However, at the present time, the suggestion is unrealistic and abrasive wear tests remain numerous and complex.

2.2.2 Abrasive Wear Testing

Abrasive wear testing is still in the stimulation stage. The major point for wear testing is that a methodology should be established for approaching the practical wear

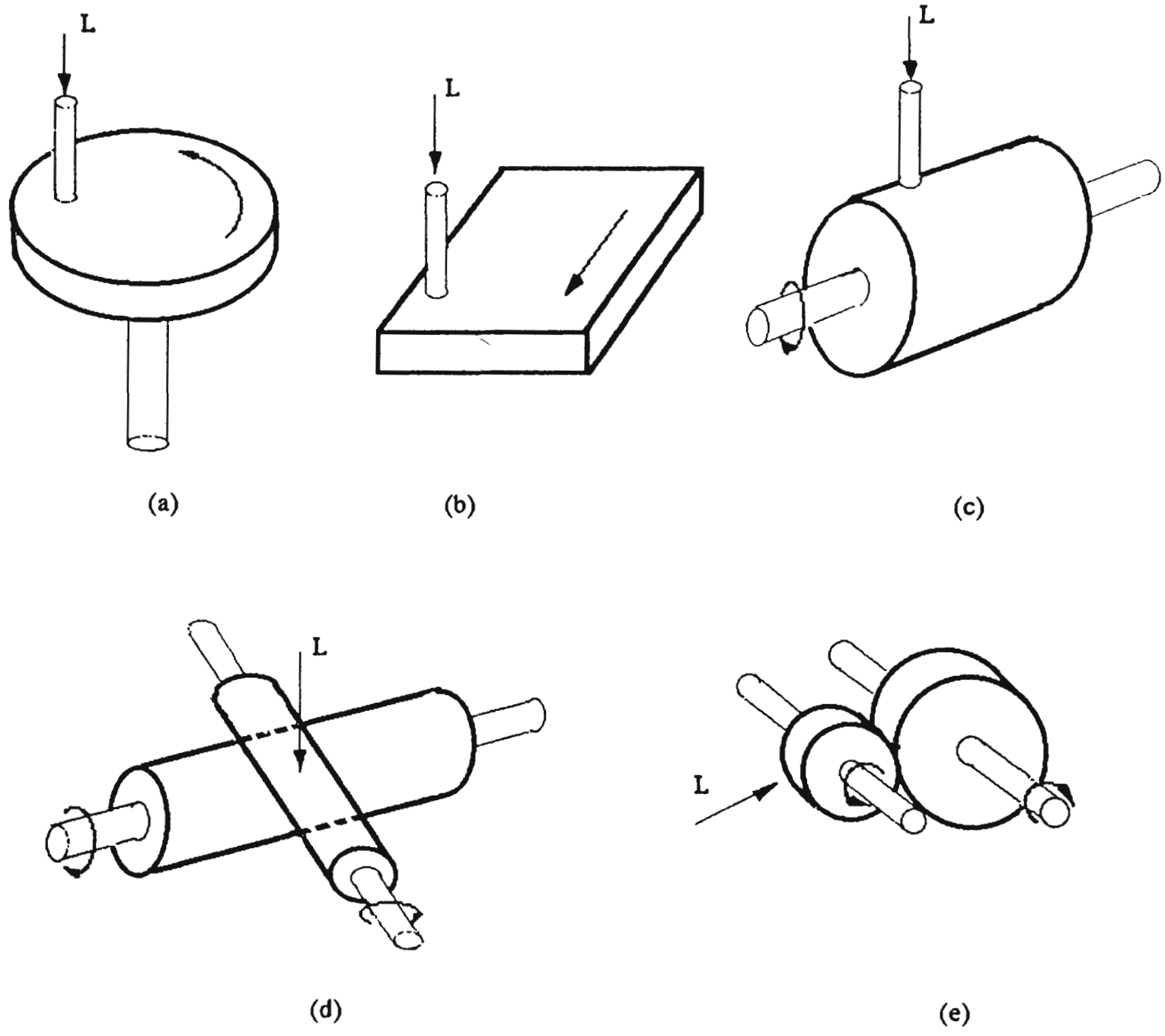

Fig.2.2 Diagrams showing basic wear models applied for wear test devices: (a) pin- on-disk, (b) pin-on-plate, (c) pin-on-drum, (d) cylinder-on-cylinder and (e) ring-on-ring.

problems. Massieon[18] suggested that the test apparatus can be simple, but test results should be interpretable from the laboratory test to the practical application. The choice of abrasives should be based on real work conditions and a reference material may be necessary.

2.2.2.1 Two-Body Abrasive Wear Testing

Two-body abrasive wear can occur by mechanisms such as cutting, ploughing and cracking to cause removal of solid material from the sliding surface and the basic mechanism of abrasive wear has been the subject of many investigations[19-21]. Khruschov and Babichev[22] identified two processes that occur when abrasive particles contact with a wearing surface.

(1) Plastically impressed grooves, which do not involve material removal, are formed.

(2) Metal particles in the form of wear debris or microchips, are separated from the wearing surface.

During the wear test, these two processes often occur simultaneously, due to numerous abrasive particles which take part in wear action at the same time.

The popularly used configurations of two-body abrasive wear testers can be classified as pin-on-disk, pin-on-plate, pin-on-drum, cylinder-on-cylinder and ring-on-ring, as shown diagrammatically in Fig.2.2.

In the **pin-on-disk** configuration, a loaded pin (often the specimen) is pressed onto a rotating disk, usually sliding along a spiral locus, which results in inconstant relative speed between pin and disk. The most widely used pin-on-disk apparatus was

designed by Khruschov Babichev[22] and later modified by the British National Engineering Laboratory[23].

In the **pin-on-plate** apparatus, a loaded pin, either turning or not and often the specimen, is impressed upon a sliding plate. The relative speed is constant for each stroke but discontinuous over the whole wear path. A typical pin-on-plate machine was developed in the Climax Laboratory[24] in America.

In the **pin-on-drum** apparatus, a loaded pin (the specimen) is pressed on a rotating drum at a constant relative speed generating a helical track on the abrasive medium attached to the drum. Wear debris can be collected easily in a tray located underneath the rotating drum. The pin-on-drum machine was developed by Mutton and Watson[25].

In a **cylinder-on-cylinder** apparatus, the geometry of the contact conditions is similar to the geometry of contacting balls, but more scope is available for variation of the ratio of rolling to sliding as each cylinder can be driven independently. In variations of this type, one cylinder can be reciprocated in various directions and the relative movement of the crossed cylinders enables the load to be confined to a small area of contact. An applied model was developed by Kasak and Neumeyer[26].

A **Ring-on-ring** device was introduced by Merritt[27] in 1935 for simulating gear contact conditions and makes possible variations of contact conditions with respect to both speed and load.

2.2.2.2 Three-body Abrasive Wear Testing

According to the surface characteristics involved, three-body abrasive wear can be classified as 'closed' and 'open'[14]. Closed three-body abrasive wear occurs when

loose abrasive particles are trapped between two sliding or rolling surfaces which are close to each other. A such kind of typical testing machine was designed by Toporov[28] and developed by Rabinowicz *et al.*[29]. Open three-body abrasive wear occurs when the two wearing surfaces are far apart or only one surface is involved in the wear process such as the condition of mineral conveyor. This kind of test machine was developed by Misra[30].

There are more variables involved in three-body abrasive wear testing than in two-body testing. A most important variable is the flow rate of the abrasive particles which is quite difficult to maintain constant. Another factor which needs to be considered in three-body abrasive wear testers is the friction force generated between the abrasive particles and the abrasive-carriage tube which influences the effective load. Therefore, the calibration of the three-body abrasive wear testers is quite complex.

Chapter 3

TWO-BODY ABRASIVE WEAR

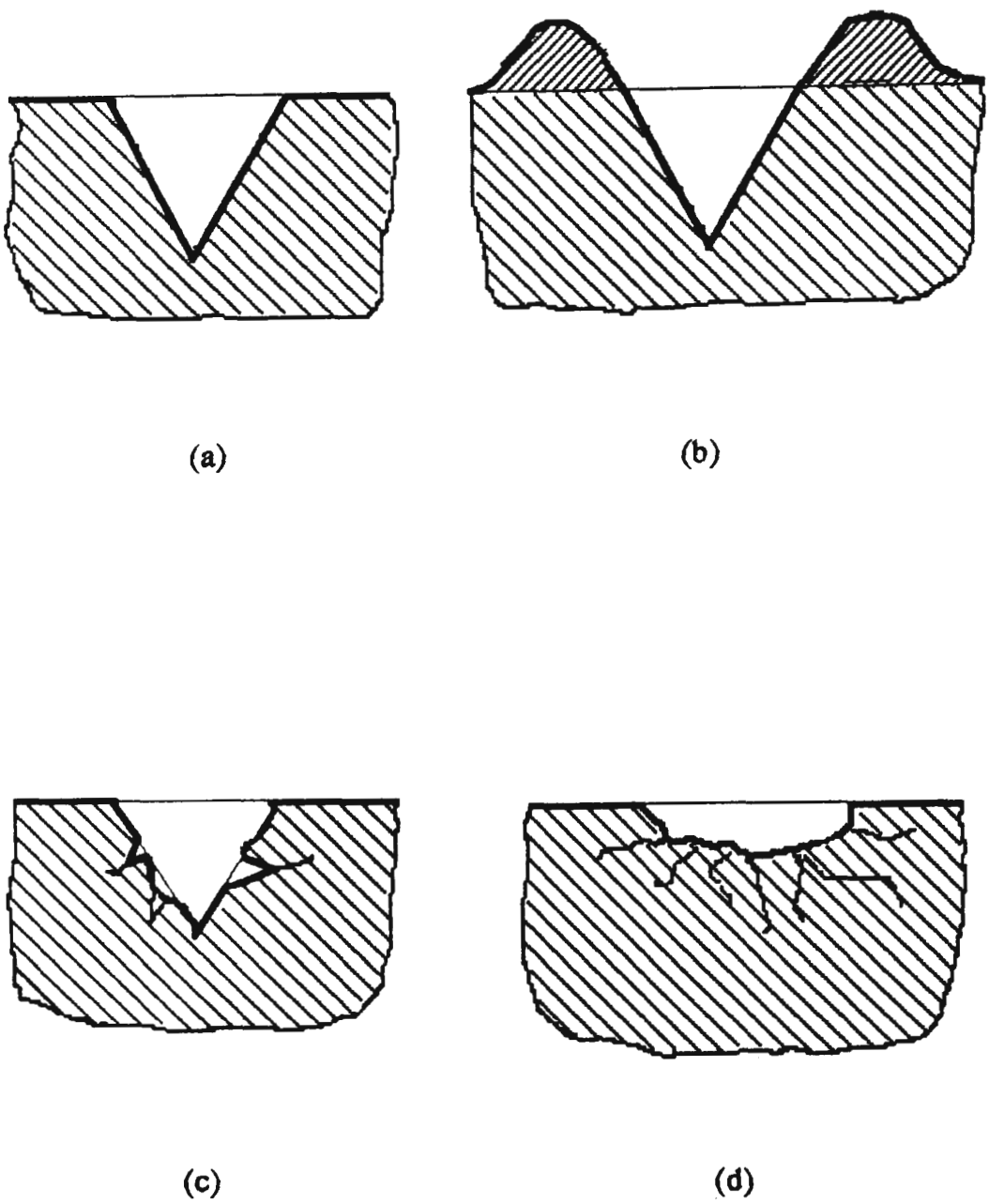

Fig.3.2 Diagrams showing the mechanisms of material removal: (a) microcutting, (b) microploughing, (c) microcracking and (d) microfatigue.

Figure 3.1 **Diagram showing the important factors for two-body abrasive wear; modified from Zum-Gahr[13]**

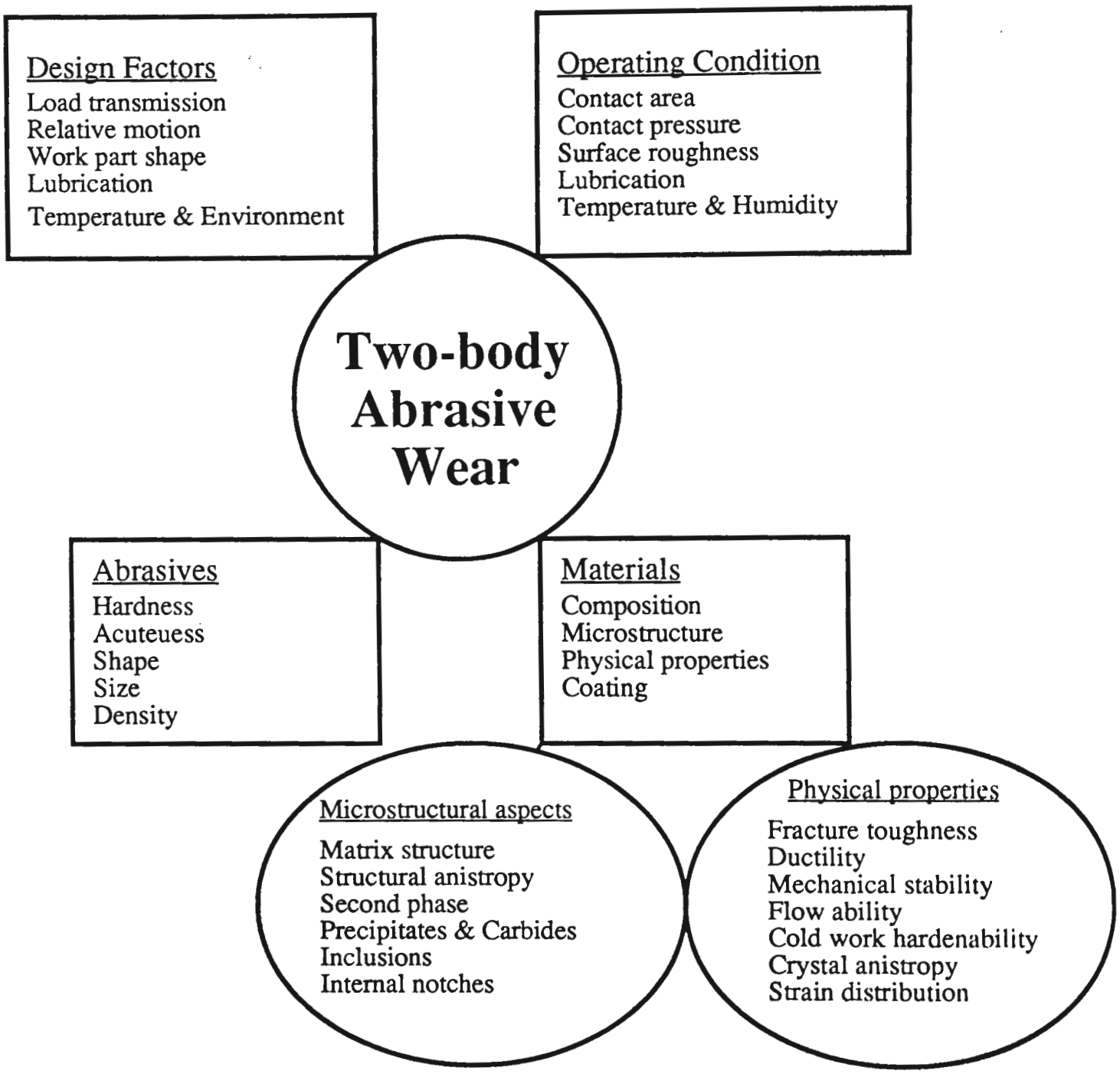

Two-body abrasive wear can be defined as wear due to penetration of hard particles or surface asperities of a harder counter-body into the softer surface in sliding contact[13], as shown in Fig.1.1(b). Material is removed by cutting action or fracture cracking which arises when one of the rubbing surfaces is rough and functions as a rasp. Figure 3.1 shows important factors which influence the two-body abrasive wear[13] and, in which the influence of hardness, alloy composition and microstructural parameters are central to this thesis.

3.1 MECHANISMS OF TWO-BODY ABRASIVE WEAR

In the practical wear environment it is quite common to encounter very complex processes in which several types of wear occur simultaneously and for which, each wear process may involve a number of wear mechanisms. Both the wear rate and the mechanism of material removal are affected considerably by the applied load, the abrasive particle geometry and the wearing material properties. In most practical situations, material is removed by the mechanisms of microcutting, microploughing, microcracking and microfatigue shown in Fig.3.2.

3.1.1 Microcutting

The mechanism of microcutting in metal removal is very similar to the mechanical machining. A ribbon-like chip, with serrations on one side and a smooth surface on the other, is the typical and common product of the cutting action. Investigators[31-32] considered individual abrasive particles as machining tools with randomly distributed rake angle and cutting edge.

During the abrasion process, ribbon-like chips can be identified for microcutting that occurs when the value of 'attacking angle'† is equal to or larger than a 'critical

† the angle measured between the wearing surface and rake face which is the surface of the effective cutting abrasive containing the cutting edge[31].

attacking angle[††] [32] which is determined primarily by the coefficient of friction between the contacting surfaces[33]. Additionally, Hokkirigawa and Kato[34] proposed that the critical value of attacking angle decreased with the increase in hardness.

There is controversy about the proportion of contacting abrasive particles that produce chips. Mulhearn and Samuels[35] concluded that only about 10% of the particles in unused abrasive paper have favourable attacking angle and act as cutting points, whilst Larsen-Badse[36] estimated later that approximately 50% of the particles in abrasive paper contacted with the specimen surface and remove material from the specimen.

3.1.2 Microploughing

Microploughing is characterized by abrasive particles plastically deforming the wear material to form bulges at the groove edges and an end prow[37]. There is no direct material removal involved, but material in a bulge or prow may be removed by shearing by following abrasive particles either by microcutting or by microcracking.

Pure microploughing occurs, theoretically, when the attacking angle of the abrasive particles (under abrasion condition) is less than the critical value. As the critical attacking angle cannot be actually determined, pure microploughing can be observed only under experimental condition which are specially designed for the purpose. Practically, there is no sharp transition from microcutting to microploughing[37], however, microploughing may often accompany cutting action or be a precursor for microcracking[38].

3.1.3 Microcracking

Generally, microcracking is likely to occur during high stress abrasive wear, and is strongly influenced by material properties, such as fracture toughness and hard phase

---

[††] the value of attacking angle that the abrasive start cutting chip.

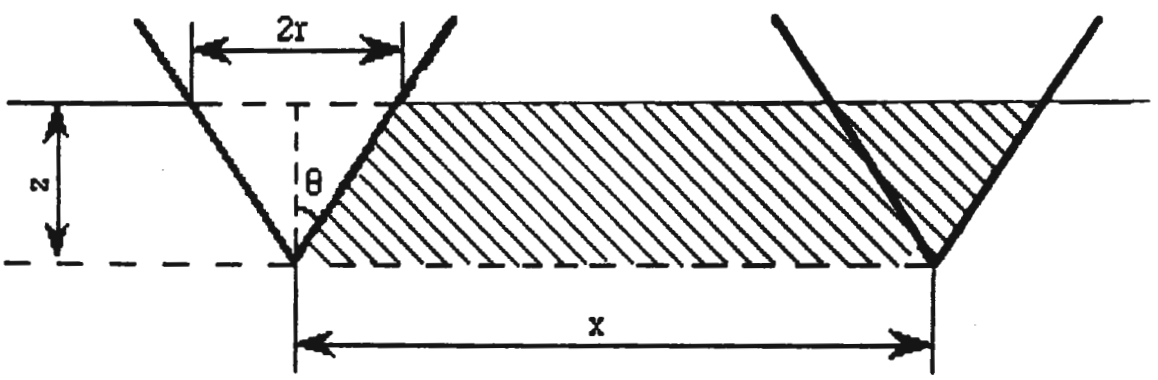

Figure 3.3 Model of abrasive wear due to Rabinowicz[42].

distribution. The more brittle materials, such as steels with martensitic structure, undergo frequent microcracking[13]. Additionally, microcracking often occurs at the interface with a hard phase, such as allotriomorphs of cementite at grain boundaries in hypereutectoid steels[39] or some alloyed carbides[13]. Therefore, the probability for formation of wear debris due to microcracking depends on the applied contact pressure, the hardness and the microstructural properties of the wearing material.

3.1.4 Microfatigue

During abrasive wear, no material is removed by the mechanism of pure microploughing as described in §3.1.2. However, deformed material at the bulges of a groove and the ploughed prows at the end of a groove will be fatigued if it is strained repeatedly by successive abrasive particles. Microfatigue occurs by material detachment from the wearing surface when the fatigue limit is exceeded, even though the applied stress may be low. Heilmann and Ridney[40] showed evidence for fatigue during sliding wear and suggested that fatigue of material can generate wear debris.

Commonly, mcrofatigue occurs in very ductile material under low stress abrasion, where microploughing is the predominant wear mechanism and little microcracking can occur.

3.2 THEORETICAL EXPRESSIONS FOR TWO-BODY ABRASIVE WEAR

A quantitative expression for mechanical wear under pure cutting conditions was proposed by Archard[41] and developed by Rabinowicz[42]. This model was considerably oversimplified as the abrasive particle was assumed to be conical as shown in Fig.3.3, and suggested that the abrasive cone penetrates the soft surface to a depth z, dependent upon hardness H which was considered to be a function of the applied load L per unit indented area, i.e.[43]:

$$H = \frac{L}{\pi r^2}$$

From Fig.3.3, it is observed that the volume V_l of the soft material removed during a horizontal sweep of the cone is a prism with base area z*x and length x. Thus

$$V_l = r \cdot x \cdot z \qquad \text{or}$$

$$V_l = r^2 \cdot x \cdot \cot\theta$$

$$V_l = \frac{L \times \cot\theta}{\pi H} \qquad (3\text{-}1)$$

where θ is the semi apex angle of the cone. If a constant K is inserted as $\frac{\cot\theta}{\pi}$ in equation (3-1)[41], it becomes:

$$V_l = \frac{K L x}{H} \qquad (3\text{-}2)$$

where V_l = volume removed

L = applied load

H = hardness of the wear material

K = dimensionless wear coefficient, $K = \frac{\cot\theta}{\pi}$

x = work distance

Equation (3-2) expresses some of the basic observations on wear, although other work[35] showed it to be a severe oversimplification. Experimental evidence obtained under specific conditions, however, verified[42] that the volume of material removal in abrasive wear was, in fact, directly proportional to the load and to the work distance and inversely proportional to the hardness of the softer material.

More detailed equations were proposed by Khruschov and Babichev[19; 44-45]. For pure metals and annealed steels , they proposed that:

$$\varepsilon = C \cdot H \qquad (3\text{-}3)$$

where ε is wear resistance and C is a coefficient of proportionality.

For heat-treated steels:

$$\varepsilon = \varepsilon_o + C_1(H-H_o) \qquad (3\text{-}4)$$

where ε_o and H_o are wear resistance and hardness for annealed steels and C_1 is a coefficient of proportionality for the steel tested.

For the structurally inhomogeneous material, a linearly additive relationship was proposed:

$$\varepsilon = f_1\varepsilon_1 + f_2\varepsilon_2 + f_3\varepsilon_3 \cdots\cdots\cdots, \qquad (3\text{–}5)$$

where f_1, f_2, f_3 are respectively the individual fractions of the components of the material; thus $f_1+f_2+f_3+\cdots=1$ and correspondingly, ε_1, ε_2, ε_3, respectively, are values of the wear resistance.

Spurr and Newcomb[46] proposed that volume loss should be related to the elastic modulus of the wearing material, rather than the hardness, as follows:

$$V_l = \frac{K L x}{E} \qquad (3\text{-}6)$$

where E is Young's modulus.

More recently, Zum-Gahr[47-48] and Larsen-Basse[49] correlated wear resistance semi-empirically with fracture toughness; the relationship was rather complicated due to inclusion of effects such as size and shape of the abrasive particles, microstructural features and fracture toughness.

3.3 EFFECT OF OPERATIONAL VARIABLES

For the two-body abrasive wear test, the operational variables commonly refer to the applied load, speed, wear path, specimen size and abrasive paper.

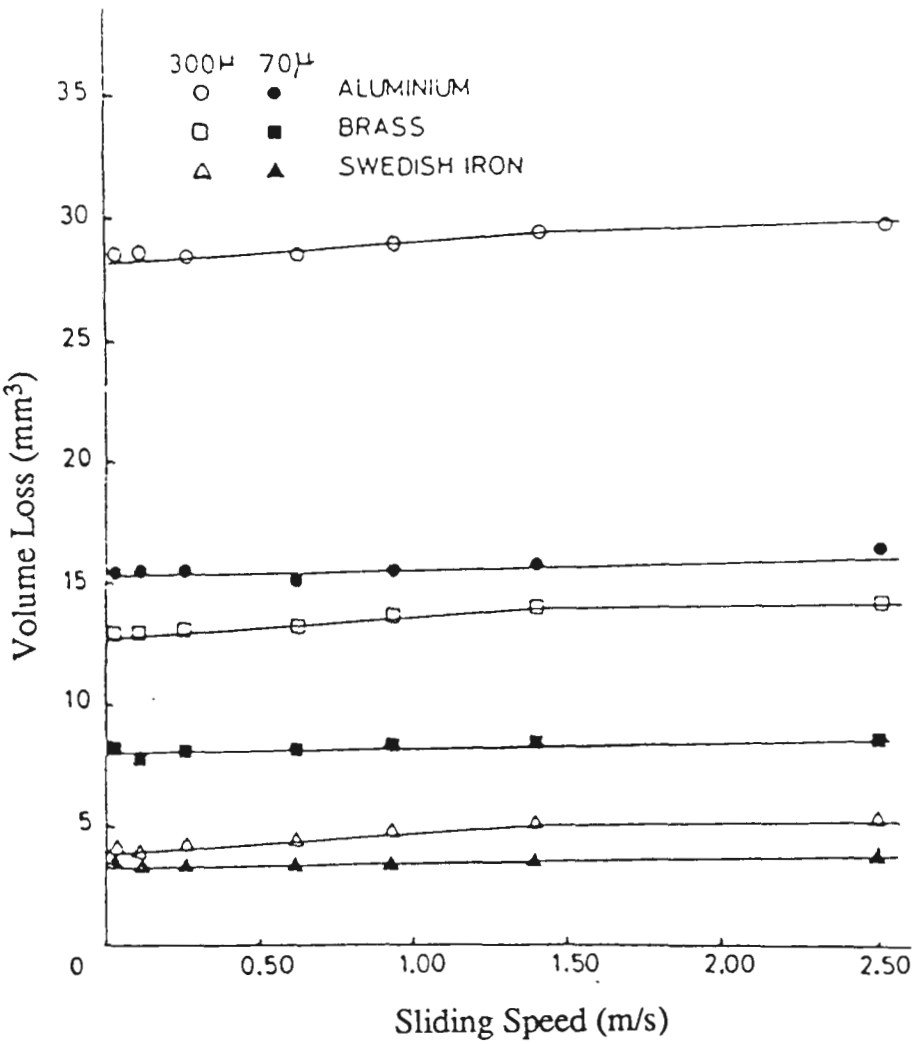

(a)

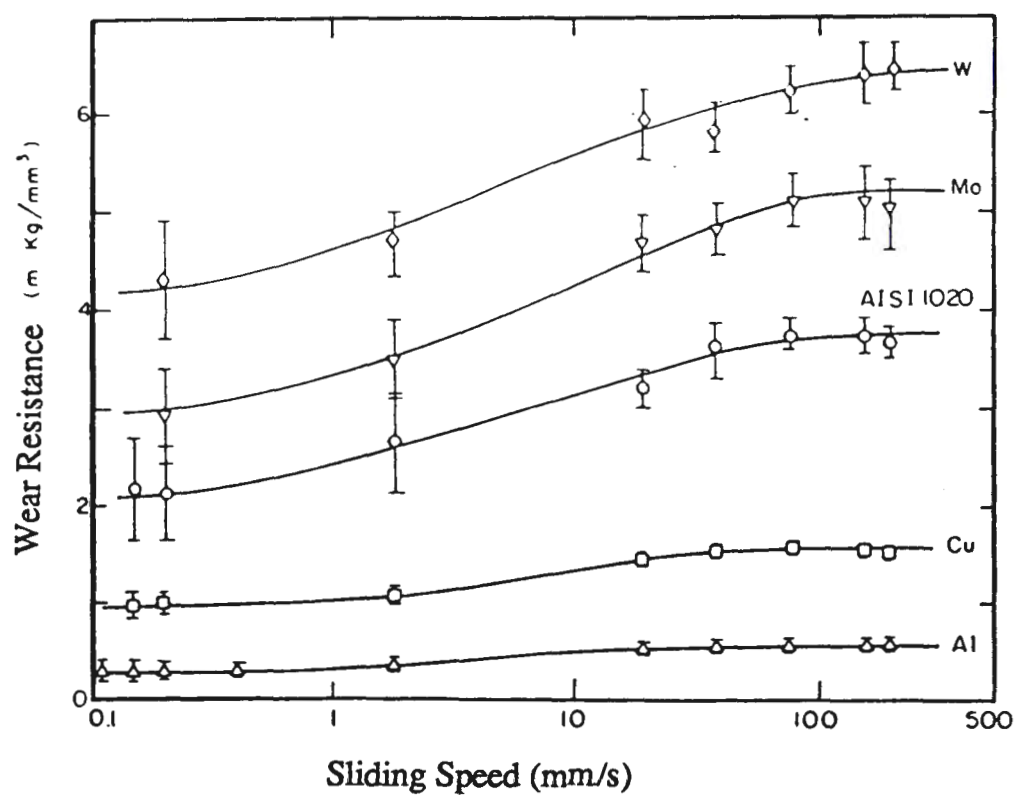

(b)

Fig.3.6 Diagram showing sliding speed as a function on (a) wear rate (measured as volume loss)[52] and (b) wear resistance[50].

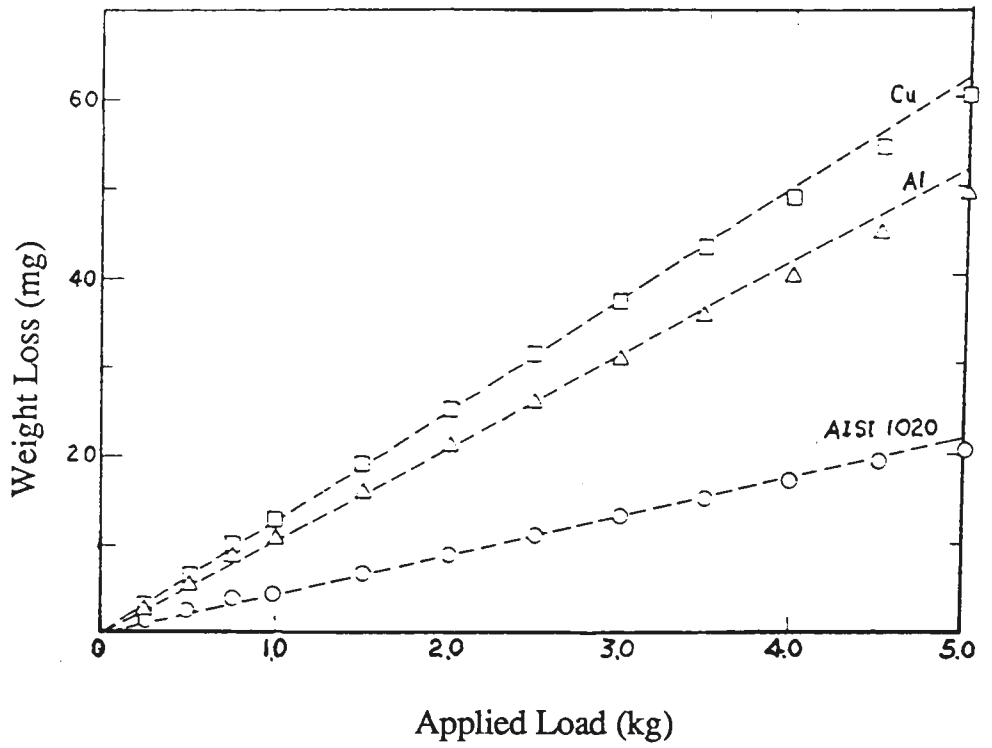

Fig.3.4 Diagram showing the relationship between wear rate (measured as weight loss) and applied load[50].

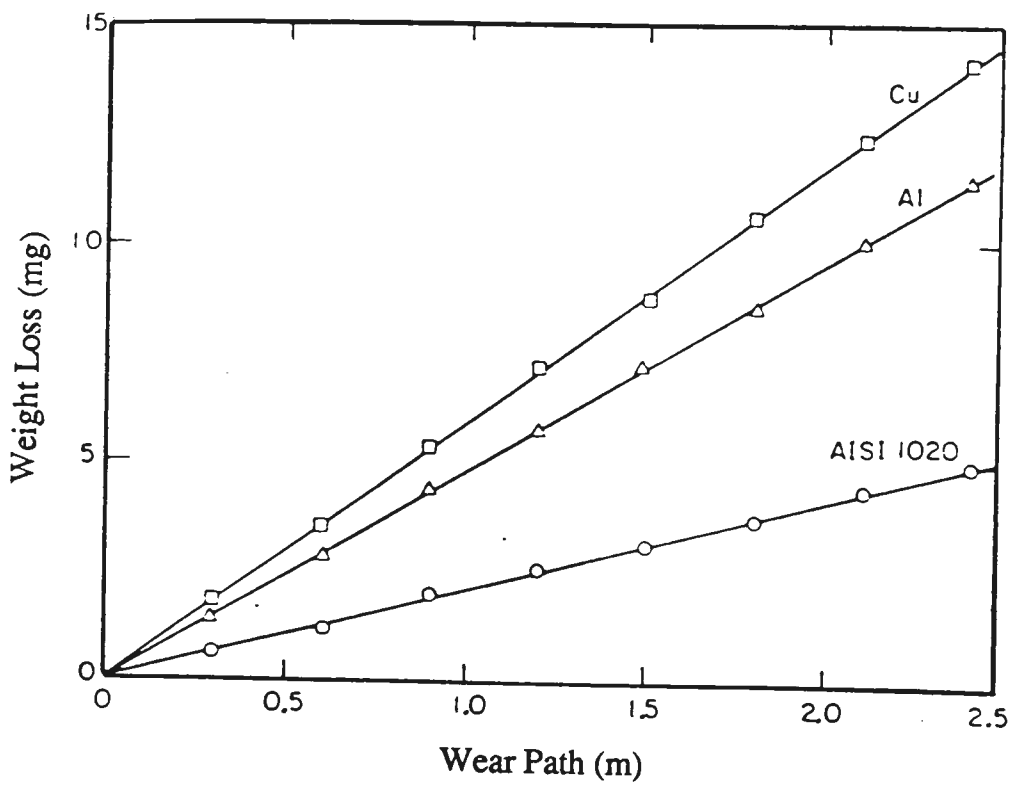

Fig.3.5 Diagram showing the relationship between wear rate (measured as weight loss) and wear path[50].

3.3.1 Applied Load

Some investigations[19; 50] showed that wear rate was directly proportional to the normal load, Fig.3.4. However, Larsen-Badse[51] found the relationship to be not strictly linear, but influenced by the size of abrasive particles and specimen diameter, while Nathan and Jones[52] concluded that the deviation from linearity was greater for the smaller size of abrasive particles. Richardson[23] stated that although volume loss increased linearly with load, the wear rate per unit load decreased with increase of the applied load. Further, Wang and Li[53] found that wear rate was also proportional to the applied load for amorphous alloys. Larsen-Badse[36] attributed the increase of wear rate with applied load to an increase in both the number of groove formations and the average groove width which would increase with the applied load up to a certain value.

Additionally, Rabinowicz *et al.*[29] suggested that mass loss was also linearly related to applied load under three-body testing conditions, for which Aronov *et al.*[54] proposed that the coefficient of friction was independent of the applied load in the steady state friction range.

3.3.2 Wear Path

Wear path is normally measured in time units for metal to metal two-body wear testing; and in length units for the test using abrasive paper. Nathan and Jones[52] reported a linear relationship between wear rate and length of wear path for abrasion with hard abrasives, as shown in Fig.3.5. This relationship was later confirmed by Misra and Finnie[50] and Smith[55].

3.3.3 Sliding Speed

Khruschov and Babichev[22] and Nathan and Jones[52] established that, at low sliding speed, wear rate increased slightly with the speed, while in the high speed range, wear rate was almost independent of speed (Fig.3.6(a)). Nathan and Jones suggested that

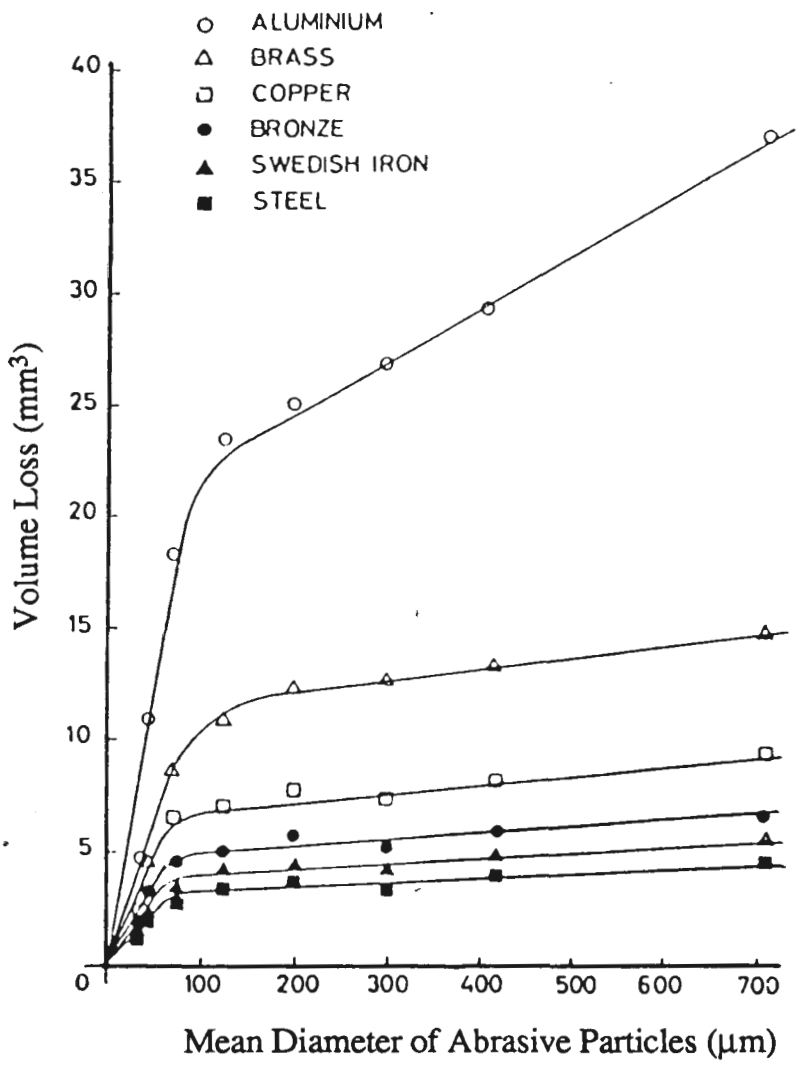

Fig.3.7 Diagram showing wear rate (measured as volume loss) related to grit size of abrasive[52].

frictional heating may account for the increase in rate. More recently, Misra and Finnie[50] found that wear resistance for the range of materials increased with sliding speed up to 65 mm/s, then was less dependent upon the speed when further increased (Fig.3.6(b)), and attributed the behaviour to effects of strain rate and flow stress. Additionally, Wang and Li[53] found that wear rate of amorphous alloys increased with sliding speed.

3.3.4 Specimen Size

In abrasive wear testing, it is practical to choose the specimen size in such a way that deterioration of abrasive particles contacting the specimen is minimal. It is important to use specimens with sufficiently small cross-sections that the metal removed by an abrasive particle will not fill the interstices between abrasive particles, which reduces the effectiveness of abrasion. Wear rate per unit area of specimen was reported[56] to increase with the decrease in the length of the specimen in the sliding direction. Further, Larsen-Badse[51] suggested that wear rate was, for practical purposes, linearly related to the specimen surface area when the size of abrasive particles was above some 'critical value'.

3.3.5 Abrasive Paper

From the material removal point of view, the size, shape, hardness and density of the abrasive particles have considerable influence on wear resistance.

3.3.5.1 Abrasive Size

Nathan and Jones[52] proposed that wear rate increased rapidly with increase in the size of abrasive particles to a critical size and then increased slowly and linearly with further increase in the size of abrasive particles, Fig.3.7. Clearly, for hard materials such as steel, the wear rate is nearly constant for abrasive particles larger than the critical size.

On the other hand, Richardson[57] showed that, under the abrasion of relatively soft particles, wear rate did not continually increase with the increase in size of the particles but reached a maximum at a critical size, then decreased with further increase in size.

Under three -body abrasive wear testing, Rabinowicz *et al.*[29] reported that wear rate was nearly independent of the size of abrasive particles.

There have been many explanations proposed to account for the influence of the size of abrasive particles on wear rate. Of these, the explanation of 'pick-up' which refers to adhesive of abrasive particles on the specimen surface appears to be most widely accepted. Avient *et al.*[56; 58] suggested that the amount of pick-up of abrasive particles on the specimen increased rapidly as the size of the particles decreased, thus the smaller abrasive particles resulted in a low wear rate as they embedded in the wearing surface. Johnson[59] used an electron microprobe to analyse pick-up of silicon carbide particles during abrasion of annealed aluminium, and found that the amount of pick-up increased with increase in length of abrasion track, with the increase in applied pressure and with decrease in size of abrasive particles.

3.3.5.2 Abrasive Shape

The shape of the abrasive particles determines cutting efficiency during abrasion as it determines the 'attacking angle', which influences the percentage of abrasive particles taking part in the cutting action.

Patterson and Mulhearn[60] found that, during abrasion, angular particles caused more volume loss than round particles by producing more chips. Moore and Swanson[61] compared relative wear resistance under two-body and three-body testing conditions, and found significant differences in wear resistance for angular abrasive particles and only minor differences for rounded particles.

3.3.5.3 Abrasive Hardness

Wear rate increases with the hardness of abrasive particles up to a critical value, then remains approximately constant, from which Khruschov[62] concluded that wear rate depended on the relative hardness of the abrasive particles and the metal. However, Khruschov[63] also concluded that wear rate did not depend upon the relative hardness for the condition that the abrasive was considerably harder than the abraded metal. For the condition that the hardness of the abrasive was less than the hardness of the abraded metal, the wear rate decreased rapidly with increase in the hardness difference. For the condition that hardness of the abrasive and the abraded metal are about the same, the wear rate depended on the difference in hardness in a rather complex way. Later, Rabinowicz[64] confirmed that the relationship between wear resistance and hardness was strongly influenced by the relative hardness of wearing material and the abrasive particles.

Blank and Luchsinger[65] found that wear rate also depended on the relative hardness between the abrasive and carbides, such as M_7C_3, in steel. Further, Gundlach and Parks[66] concluded that hardness of the abrasive particles had a greater influence on wear resistance for austenitic and martensitic white irons than for steels. When the abrasive particles were as hard as, or harder than the massed carbides present in the microstructure, the wear resistance for cast austenitic irons was greater than for martensitic irons. When the abrasive was softer than the carbides, the martensitic irons had greater wear resistance.

3.3.5.4 Abrasive Density

Misra[14] found that wear rates obtained with different batches of abrasive paper differed significantly and attributed this difference to density variation of abrasive particles on the paper. Generally, the higher the density of abrasive particles, the

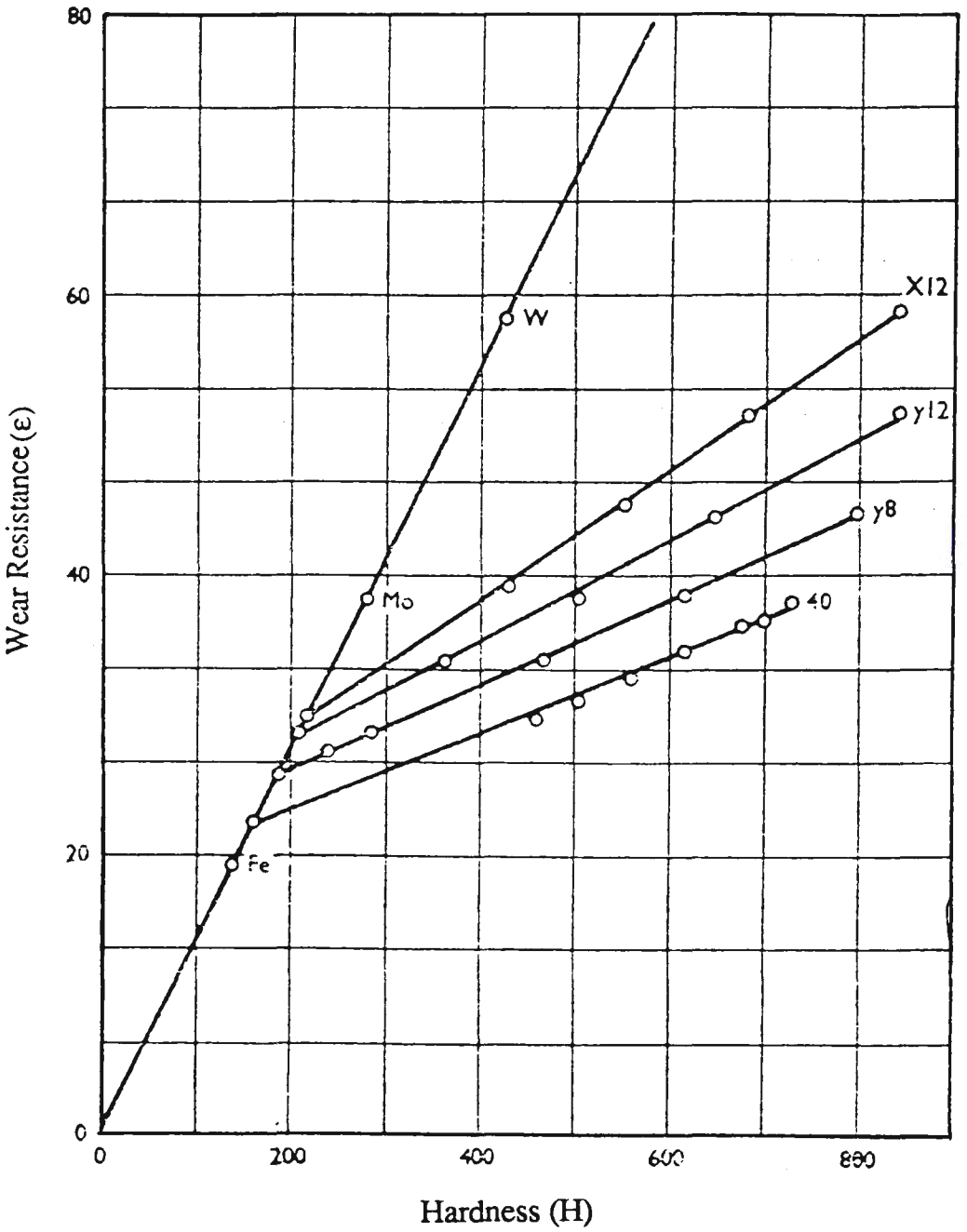

Fig.3.8 Diagram showing relationship between relative wear resistance and hardness for pure metals and heat treated steels[44].

greater the number of abrasive particles that contact the wearing surface, and hence the higher the wear rate.

3.4 EFFECT OF MECHANICAL PROPERTIES

It has been traditionally understood that for a particular tribology system, wear rate was related to mechanical properties such as hardness or fracture toughness. Although microstructural effect on wear resistance has attracted recent interest, mechanical properties remain important factors in abrasive wear and wear testing.

3.4.1 Hardness

Of all properties, hardness is the most important factor in wear; and there is a large amount of literature dealing with the influence of hardness on wear resistance. Hardness effects can be divided into bulk hardness, surface hardness and microhardness.

3.4.1.1 Bulk Hardness

For the effect of bulk hardness on wear rate (or resistance), Archard[41] proposed a linear relationship between wear rate and hardness (equation 3-2), and which was later confirmed[42]. Khruschov and Babichev[67] concluded empirically (Fig.3.8) that for pure metals and annealed steels, wear resistance are linearly related to hardness and the relationship extrapolates through the origin (equation 3-3), providing a further confirmation of Archard's equation. Additionally, wear resistance did not change with hardness increase resulted from mechanically work-hardening[68]. For heat treated steels with different levels of hardness, the relationship was linear but not extrapolate through the origin (equation 3-4). Finally, wear resistance of structurally heterogeneous metallic materials was much lower than that of pure metals at the same hardness level.

Later work[23; 37] confirmed the linear relationship between wear resistance and hardness for annealed pure metals. More recently, however, Tylczak[69] has argued that a linear relationship could exist only within the same type of structures, such as body-centred cubic or face-centred cubic.

For tempered martensitic steels with different hardness levels, Murray *et al.*[37] proposed an S-shaped relationship between wear resistance and hardness.

Further, Hokkirigawa and Li[70] proposed that wear mechanism is related to hardness of material, for which the degree of cutting mode (the ratio of wear volume to apparent groove volume) increased with increasing hardness.

3.4.1.2 Surface Hardness

Surface hardness which is measured at the worn surface, provides more information about the abrasive wear process and effects of such factors as flow stress and surface hardenability[71]. Richardson[72] concluded that wear resistance was in fact best estimated empirically from the hardness at the worn surface and was proportional to the maximal surface hardness. Further, Alison and Wilman[73] studied the abrasion work hardening behaviour of hexagonal and cubic metals, and found that wear resistance and surface hardness were linearly related, but that the work hardening for hexagonal metals for cubic metals were different.

Larsen-Badse[74] concluded that the hardness value of a heavily cold-worked, abraded surface was best related with wear resistance. Additionally, if the work hardening exponent for the bulk-hardness indentation is the same for the chip removal, the wear resistance should be a direct function of bulk hardness.

3.4.1.3 Microhardness

The effect of microhardness on wear resistance will be reviewed in §3.5 as a microstructural effect.

3.4.2 Toughness and Ductility

Toughness is the parameter indicating the ability of a metallic material to withstand high unit stress together with unit strain without complete fracture[75], whilst fracture toughness is the parameter which influences the critical applied pressure, above which fracture and mass removal (spalling) of material occurs[76]. Ball and Böhm[77] concluded that toughness was as important as hardness in determining wear resistance under severe abrasion conditions.

Ductility is the parameter which, for metallic materials, indicates the ability to sustain large permanent deformation by tension[75]. Garrison *et al.*[78-79] found that ductility significantly influenced wear resistance; and pointed out that the product of wear rate and bulk hardness decreased with increasing ductility.

3.4.3 Plastic Flow and Fracture Properties

Plastic flow is often observed as deformation on the worn surface and is often measured as stress or strain on the area at which plastic flow occurs. Fracture becomes an important influence on wear rate when the plastic flow reaches a critical value.

Glaeser[80] found that severe deformation occurred during wear processes. Kramer and Balasubramanian[81] reported that a work-hardened layer formed on the plastically deformed surface of specimens was as thick as 50-60μ which was measured by the stress required for the formation of slip bands, in aluminium monocrystals, polycrystalline 2012-T6 aluminium and iron-3%Si.

Hornbogen[82] related wear rate to applied strain, the relationship follows Archard's law under the condition that the applied strain was less than the critical strain of the material. However, when the applied strain exceeded the critical value, the probability of microcracks increased and consequently wear rate increased.

Moore and King[83] indicated that both plastic deformation and fracture generated mass loss for brittle materials during abrasive wear. Plastic deformation was favoured when the applied load was low and the ratio of fracture toughness to hardness for the material was high; otherwise, fracture was favoured. The higher the fracture toughness for the material, the deeper the critical indentation for an abrasive particle that penetrates into the wearing materials, and the fewer is the microcracks that occur during wear processes; thus wear rate decreased with the increase in fracture toughness under the condition that the fracture mechanism was dominant.

More recently, Zum-Gahr[84] developed a theoretical model and stated that the wear process changed from microploughing-microcutting to predominantly microcutting-microcracking when the applied load exceeded a critical value. In this case, increasing fracture toughness of a wear material increases the ploughing tendency and enhances wear resistance. Additionally, Zum-Gahr[85] found that the critical value of surface hardness was confined by the fracture of the material.

3.4.4 Elastic Modulus and Elastic Limit

Spurr and Newcomb[46] reported that the amount of metal removal depended upon the elastic recovery of the surface, and wear rate was inversely proportional to the modulus of elasticity, E. Later, Khruschov[62] correlated wear resistance of metallic materials to the modulus, and indicated that this expression was only true for pure metals and annealed steels. Further, Khruschov and Babichev[86] concluded that wear

resistance was obviously not a single-valued function of either the modulus, or the hardness.

Larsen-Badse[74] demonstrated that wear resistance of quenched and tempered steels could be expressed by hardness with a constant exponent which derived from the stress-strain relation of the material, whilst Bhansali and Silence[87] concluded that hardness increased linearly with the elastic modulus for pure metals, for homogeneous alloys strengthened by solid solution hardening and for the steel strengthened by precipitation hardening, but the increasing rates were different.

Rosenfield[88] found that wear rate increased with increase in applied load and decrease in local strain at the near-surface of the specimen. Further, Moore *et al.* [89] stated that the strain level near the worn surface was extremely high compared with the strain under conventional deformation processes, and the strain that occurred during abrasion was proportional to the size of the abrasive particles and to the square root of the applied load.

3.5 EFFECT OF MICROSTRUCTURES

Wear resistance was proposed to be influenced not only by hardness and composition of the steels, but also by microstructures[90] which have a considerable influence on the mechanical properties of a material and therefore, must also influence abrasive resistance[91].

Microstructural factors comprise mainly the matrix structures, dispersed phases, grain size and structural defects. As mechanical properties strongly relate to microstructures, optimization of wear resistance by microstructure control is becoming practical in prolonging the work-life for some equipment and so reducing the cost of productivity.

The review of microstructural effects on abrasive wear in this Chapter mainly concerns ferrous alloys.

3.5.1 Matrix Structures

For steels, Serpik and Kantor[92] indicated that wear resistance increased progressively as the microstructure changed from spheroidite to pearlite, and martensite to bainite at equal hardness. This conclusion was confirmed later by Moore[93], and Zum-Gahr[90] attributed the higher wear resistance of bainite to the large amount of retained austenite in the bainitic structure. More recently, Kwok and Thomas[94] found that highly dislocated lath martensite together with retained austenite appears to be preferable for which has higher wear resistance than either bainitic-martensitic or ferritic-pearlitic microstructures. The wear rate was minimized by a combination of austenite and martensite in which the martensite had high hardness[95].

Zum-Gahr and Doane[96] studied the influence of matrix structures on wear rate in high chromium-molybdenum white cast iron and concluded that the highest wear rate occurred for predominantly austenitic structures which had partially transformed to ferrite and carbide aggregates. Further, Zum-Gahr[97] concluded that a structure having a predominantly austenitic matrix had a lower wear rate than did a martensitic matrix under abrasion with silicon carbide, which is harder than the massed carbides in irons, and that wear rate was influenced by both the composition and the matrix structure.

3.5.2 Dispersed Phases

Second phase particles dispersed in a matrix are very important in improving properties such as machinability and hardness that increase wear resistance. Second phases include precipitates such as carbides or in addition, soft microstructural constituents such as retained austenite or ferrite.

3.5.2.1 Precipitates

Zum-Gahr[98] investigated an Fe-Ni-Al alloy and showed that the wear rate could be reduced by as much as 25% by changing the microstructure from a solid solution to a solid solution containing precipitated particles and dislocations. Further, Zum-Gahr[76] indicated that precipitation of inter-metallic compounds includes soft (coherent) and hard (non-coherent) particles and the highest wear resistance was obtained for microstructures with fine dispersed semi-coherent particles.

3.5.2.2 Carbides

Carbides are the most important second phase in the microstructures of wear resistant materials being much harder than metallic compounds, for instance, carbides of type M_3C are at least three to four times as hard as the compound Fe_3Al[90]. The influence of carbides on wear resistance depends on the hardness relative to the matrix. Carbides in a soft matrix increase wear resistance while carbides in a hard matrix provide internal notches and wear resistance suffers[75]. The finely dispersed carbides in steel increase abrasion resistance, according to a Hall-Petch relationship as abrasion resistance is inversely proportional to the square root of cementite particle spacing[74; 99-100]. More detail of the effect of carbides on wear resistance will be reviewed in Chapter 5.

3.5.2.3 Soft Phases

Generally, the soft phases in ferrous alloys are ferrite and austenite. Moore[93] and Larsen-Badse[100] proposed that for ferritic-pearlitic steels, wear resistance and bulk hardness decreased linearly with an increase in the volume fraction of ferrite. For ferritic-cementitic or spheroidized steels, wear resistance increased with increasing carbide size and decreasing mean free path. Additionally, Zum-Gahr[101] concluded that for particular volume fraction of ferrite in ferritic-pearlitic and ferritic-martensitic

steels, wear resistance increased with increasing hardness of pearlite or martensite, respectively.

Retained austenite in a martensitic microstructure can transform to martensite to some extent by stress from abrasion work-hardening[102]. A transformable amount of retained austenite was favourable in enhancing wear resistance for tool steels and white cast irons, whilst an excessive amount of retained austenite resulted in a reduced wear resistance. Su *et al.*[103] studied a high-carbon high-chromium blade steel and found that a decrease in the amount of retained austenite was beneficial to the wear resistance.

3.5.3 Grain Size

Generally, reducing the microstructural grain size leads to improvement of mechanical properties such as yield stress, ductility and hardness, which in turn, increases wear resistance[90]. Feng[104] studied the effect of grain size on wear using pure copper specimens with the grain size in the range from 0.10 to 15 mm and found that wear rate decreased gradually with decreasing grain size. A rapid decrease of wear rate occurred at the grain size of 0.2mm which is approximately the size of the large wear debris. Yamamoto *et al.*[105] concluded that the relationship between wear resistance and grain size was significantly affected by environmental factors.

3.5.4 Inclusions

Inclusions such as manganese sulphide, oxides, silicates and aluminates on the surface of specimens reduce wear resistance. Tumuluru[106] observed that a decrease in the number of sulphide inclusions significantly decreased wear rates for steel, while modification of inclusion morphology by addition of calcium and aluminium contributed to poor wear resistance.

3.5.5 Internal Notches

Internal notches embrace such features as microcracks, pores, inclusions and lamellar or spheroidal graphite. Internal notches in materials produce high internal stress resulting in an increased possibility of crack propagation and consequential increase in wear rate. Leach and Borland[107] reported that an increase in the number of graphite flakes in cast iron either by reducing the flake size or by increasing the carbon content resulted in a significant increase in wear rate.

3.5.6 Anisotrophy

Structural anisotrophy can occur as a result of unidirectional solidification, deformation, or precipitation of a second phase in a stress field. Mechanical properties are related strongly to crystalline anisotrophy; thus wear rate is also influenced by structural anisotrophy. A study of abrasive wear of pearlitic steels[108] showed that the direction of lamellae in the pearlitic colonies near abraded grooves was parallel to the abrading direction. Zum-Gahr[90] concluded that whenever a microstructure consists of two phases with different hardness and shape, the volume fraction of the second phases such as carbide, was insufficient to assessment for the wear resistance as the anisotrophy of second phases was also a relevant factor.

Finally, Herold-Schmidt and Hinsberger[109] reported that wear resistance for materials with an anisotropic microstructure was much better than for materials with an isotropic microstructure. In addition, the high wear resistance was obtained with the long axis of martensite oriented perpendicularly to the sliding direction.

3.6 EFFECT OF OTHER FACTORS

Other factors commonly encountered in two-body abrasive wear are frictional heating and humidity, neither of which is controllable.

3.6.1 Frictional Heating

Frictional heating has little influence on wear resistance during low speed abrasion[23; 62]. At high speed, however, Nathan and Jones[52] and Kwok and Thomas[110] attributed an increase in wear rate with increasing speed to frictional heating. Moore[111] concluded that no satisfactory explanation could be deduced from the measurement of frictional heat using a thermo-couple. The temperature rise was thought to modify the physical, chemical and mechanical properties on the contact surface of specimens, even though the overall effect of frictional heat on the abrasion process was insignificant.

3.6.2 Humidity

High humidity was reported[20] to increase the wear rate by about 15% because water vapour, which is similar to other lubricants, increased the effectiveness of the abrasion. In laboratory wear tests, the effect of moisture on wear rate is usually small[19]. Larsen-Badse and Sokoloki[112] concluded that the effect of humidity depended strongly on experimental conditions, particularly on the abrasion length for individual abrasive particles. At higher humidity levels, the influence on wear rate for softer materials was greater than for harder materials.

Chapter 4

OPTIMIZATION of WEAR RESISTANT MATERIALS

Wear resistant materials comprise four main groups[13; 113]: metallic alloys, ceramics, composites and polymers. Metallic alloys are the most widely used materials for equipment components subjected to wear and these tool steels and white cast irons appear as special groups because of their high wear resistance and special properties. However, some metallic alloys, especially those containing chromium, tungsten, vanadium and molybdenum etc., are progressively being substituted by ceramics or composites due to the cost. Ceramics have considerable hardness and high wear resistance, and are particularly beneficial for equipment working under the condition that chemical contamination is involved. The main disadvantage of ceramics is brittleness at ambient temperature, so that current development is concerned mainly with ceramic coating on a metallic substrate. Composites comprise phases of at least two different groups of materials, and bonding stress is the important factor for wear resistance. Polymers appear as new group in wear resistant materials, and wear properties are less well established than for metallic alloys or ceramics.

This Chapter solely concerns ferrous alloys as the main group of iron-based alloys in metallic alloys, for which, the optimization of wear resistance is generally obtained by appropriate heat treatment or composition control, or both.

4.1 EFFECT OF COMPOSITION

Composition of ferrous alloys refers mainly to concentration of carbon and alloying elements which are most important factors in determining mechanical properties and microstructural parameters such as matrix structure and the type, and volume fraction and distribution of carbides.

4.1.1 Carbon Content

Carbon ranks as the most important element in influencing microstructure, hardness and thus wear resistance. During heat treatment of ferrous alloys, carbon is largely responsible for improving hardness by reaction with alloying elements and in providing a minor contribution to hardenability by shifting the T-T-T curve to the right[114].

White and Honeycombe[115] found that reduction of the carbon content in high-purity Fe-Mn-C alloys led to the formation of more α- or ε-martensite and thus decreased wear resistance, because α-martensite (lath martensite) is less wear resistant than β-martensite (plate martensite) at the same hardness level[116]. Further, Kehoe and Kelly[117] proposed that the initial dislocation density in martensite increased linearly with carbon content and the strength of martensite depended on the square root of the carbon content.

Watson *et al.*[118] suggested that variations in the carbon content, resulting in varying volume fractions of eutectic carbide in white cast iron, altered wear resistance. Hogmark and Vingsbo[119] concluded that the wear rate of alloyed carbon steels was mainly influenced by material parameters such as heat treatment, carbon content and carbide distribution.

The effect of carbon content on wear resistance for carbon steels is reviewed in §5.1.

4.1.2 Carbide Forming Elements

Carbide forming elements in ferrous alloys refer generally to those which actively react with carbon to form carbides, and include titanium, tungsten, vanadium, chromium and molybdenum. Doane[24] suggested that various combinations of alloying elements

in ferrous alloys can provide the appropriate microstructure for a particular application through the appropriate heat treatment, and also that the morphology and hardness of carbides could be altered by appropriate control of alloying elements. Sidorin and Dolgova[120] studied the effect of vanadium content on wear resistance of a tool steel, and concluded that wear resistance increased as the vanadium content increased from 0 to 2%, then decreased as the content exceeded 2% due to formation of VC which reduced the carbon and alloying elements in solution in the martensitic matrix.

4.1.3 Alloying Elements in Matrix

The effect of alloying elements on hardness of a martensitic matrix in tempered steels, very much depends on the tempering temperature. Grange *et al.*[121] quantitatively studied the effects of manganese, nickel, chromium, molybdenum, and vanadium in 0.2% carbon steel, and found that for untempered martensite, none of the alloying elements increased hardness, but they all retarded softening at tempering temperatures above 200°C. The increased hardness of tempered steels, due to alloying elements, depended greatly on the tempering temperature and the kind and the amount of alloying elements. Only nickel had essentially the same effect at all tempering temperature above 200°C. Manganese had a great effect over the tempering temperature range of 430°C to 650°C. For strong carbide forming elements, the highest hardness occurred at the tempering temperature of 430°C for chromium, 540°C or 590°C for molybdenum, and 650°C for vanadium, and vanadium was the most potent alloying element at tempering temperatures above 320°C.

Minemura *et al.*[122] found that ferrite forming alloying elements were beneficial to wear resistance in metastable austenitic alloys in the Fe-Cr-C, Fe-Mo-C and Fe-W-C systems, because those elements contributed high hardness and strength as well as good ductility. Also, Berns and Fischer[123] found that wear rate decreased with

increasing hardness of matrix microstructures from stable austenite to martensite and unstable retained austenite, which was obtained by changing the amounts of alloying elements in the matrix.

4.1.4 Alloying Elements in Carbides

Berns and Fischer[123] proposed that alloying elements such as vanadium, tungsten and titanium in Hadfield's steels and tool steels, and in iron-based hardfacing alloys led to the precipitation of massed MC carbides, while molybdenum and chromium led to formation of massed M_2B and $M_{23}B_6$ borides as well as M_7C_3 carbides. The formation of carbides proved to be beneficial to wear resistance; however, wear rate was reduced more by the formation of MC- than by M_7C_3-carbides in ferrous alloys.

4.2 HEAT TREATMENT

Heat treatment is an important means for developing required mechanical, physical and microstructural properties of steels, and therefore is an important method for optimizing the wear resistance for particular steels. Commonly, heat treatment methods include annealing, spheroidizing, normalizing, isothermal transformation, quenching and tempering.

4.2.1 Annealing, Normalizing and Spheroidizing

Annealing treatment is carried out by full austenitization followed by slow cooling to obtain the equilibrium structures. It is generally applied to soften a product.

Normalizing is the process of austenitization and then cooling in air. The structures after normalizing are usually finer than after annealing because of the higher cooling

rate and consequently, normalized structures offer higher hardness compared with coarse annealed structures[125].

Spheroidizing is a heat treatment applied commonly to hypereutectoid steels to avoid the formation of net-work cementite[126]. The spheroidal carbides form directly from austenite at nuclei which are remnants of prior carbides, during cycles of heating and cooling around the austenitizing temperature. The hardness of spheroidized products and of annealed products are similar.

4.2.2 Isothermal Transformation

Products of isothermal transformation are generally upper or lower bainite. Only lower bainite is suitable for industrial applications because of moderate mechanical properties, such as toughness and hardness which is slightly lower than martensite, while upper bainite is far too brittle for practical applications. Further review of bainitic structure is given in the §5.1.

4.2.3 Quenching

Quenching treatment involves cooling from an austenitizing temperature at a rate which is sufficiently high to avoid the formation of diffusional products. Quenched structures, which include martensite, retained austenite and undissolved carbides, are metastable, hard and brittle so that quenching is often followed by a tempering treatment to improve properties.

4.2.4 Tempering

Tempering is normally applied after quenching to stabilize the microstructure, to obtain dimensional stability and to diminish internal stress generated by quenching. Temperature and duration time at the tempering temperature are important factors in

determining the microstructures and the mechanical properties of the heat treated product.

4.2.4.1 Precipitation of Carbide

For carbon steels tempered in the temperature range from 20°C to 150°C, the supersaturation of carbon atoms in the martensitic tetragonality provides driving force for carbide formation and in this stage, transition carbide starts to form. This transition carbide was identified as having a hexagonal structure and designated ε-carbide[146]. For tempering at temperatures up to 250°C, the ε-carbides are metastable and coherent with the martensitic matrix, while above 250°C, the ε-carbides are replaced by cementite which then coalesces to large particles. Above 500°C all traces of the martensite disappeared[127].

4.2.4.2 Transformation of Retained Austenite

Retained austenite transforms to carbides and ferrite with corresponding increase in hardness during tempering at temperatures between 200°C to 300°C. Alloying elements such as chromium, manganese and silicon, have a strong effect on the temperature and the rate of transformation; while nickel, copper, molybdenum, tungsten and vanadium have little effect; and cobalt has no effect[127].

4.3 WHITE LAYER

'White layer' is a term used to refer to those surface layers which appear featureless and white under optical microscopical observation after normal etching procedures[128]. The characteristics of white layers are commonly recognized as resistance to etching by conventional agents, high hardness and increased wear resistance[128-134]. However, white layers have been found to vary in structure,

thickness and properties with respect to the original structure of the steel and the conditions under which they were generated. Hence the characteristics of the white layer are still a subject of considerable controversy.

4.3.1 Hardness

Eyre and Baxter[130] reported that the hardness of the white layer could be between Hv700 and Hv1200 for the steels and cast irons, while for a 0.24%C carbon steel, the hardness value was measured as Hv1100. Babei *et al.*[131] found the microhardness of the white layer to be considerably greater than the hardness of the original structure.

Additionally, Tomlinson *et al.*[132] and Glenn and Leslie[135] found that the hardness at and near the surface changed through a transition zone to the bulk material. Furze and Griffiths[136] confirmed the presence of a transition zone and pointed out that the hardness of white layer could be 3.3 times as that of the transition zone. Furthermore, Bailey *et al.*[137] studied the surface integrity in machining with a variety of cutting speeds and found that the microhardness at the surface, where a white layer had formed, was extremely high, but decreased very rapidly beneath the surface in the transition zone, then increased to the original hardness for the bulk material.

4.3.2 Advantages for Wear Resistance

Tomlinson *et al.*[132] proposed that the white layers provided a wear resistant surface and that the extent of increased wear resistance depended on the thickness of the layer. Later, Griffiths and Furze[129] confirmed that surface modification at the white layer had some tribological advantages, while more recently, Jost and Schmidt[138] concluded that, for metastable Fe-Mn-C austenite, the white layer can provide a very effective microstructural mechanism for increased wear resistance.

Babei *et al.*[131] developed the white layer for the specimens, which were refined and quenched and low temperature tempered, of a steel designated 50Kh, and found that the wear rate decreased by 4.5 and 1.5 times, respectively, compared with corresponding polished specimens. They attributed the decrease in wear rate to the structure of white layer which comprised the increased concentrations of carbon and alloying elements, the amount of finely dispersed carbides and the increased density of defects in the crystalline lattice.

4.3.3 Structures

The structure of white layers is still a subject of investigation. Grozin and Iankevich[134] classified white layers into seven groups with the respect to the original microstructures, which were: (1) martensitic, (2) austenitic-martensitic, saturated with nitrogen and carbon, (3) ferritic-martensitic, (4) austenitic-martensitic, tempered martensite, (5) ferritic-cementitic, (6) carbidic (chromium carbides) and (7) precipitated structures. However, the white layer was reported to be generated with the involvement of phase transformation[128; 139], and the microstructure of the white layer related not only to the original structures, but also the conditions under which the white layer was generated.

Kuznetsov *et al.*[133] reported that the white layer was some type of aggregate containing a large number of fine carbides. Later, Babei *et al.*[131] proposed that the white layer consisted of fine lath martensite with finely dispersed carbides and some retained austenite; and, Wingrove[140] found that the white layer consisted of shear bands in an abnormal martensitic structure with a high density of dislocations. More recently, Jost and Schmidt[138] observed that, in metastable Fe-Mn-C austenite, a white layer was formed by friction-induced martensitic transformation.

Turley *et al.*[128; 141] and Glenn and Leslie[135] argued that there was little evidence for carbides in electron micrographs from white layers; within the layer, there was very fine body-centred-cubic subgrain structure with a general loss of carbides. They explained that some of the carbides had been literally annihilated by the dispersion of carbon to dislocations, vacancies and, more particularly, subgrain boundaries. Also, Eyre and Baxter[130] attributed the high hardness of white layers to a fine dispersion of an extremely small crystalline structure, and proposed that such a structure was produced by a combination of surface temperature flashes and extensive cyclic deformation. Additionally, Blunt *et al.*[139] pointed out that the white layer was possibly produced by deformation combined with quenching after the rapid temperature flash.

4.3.4 Mechanisms of White Layer Formation

Furze and Griffiths[136] classified the occurrence of white layers into three main types:

(i) formed by machining or deformation;
(ii) found at the surface of engineering components; and
(iii) resulting from laboratory experiments.

All white layers have two common features: a high hardness by comparison with the bulk hardness and an apparently featureless structure when observed with low power microscopy[142].

Traditionally, it was proposed by Griffiths[142-143] that there were three main mechanisms for generating a white layer:

(i) rapid heating and quenching which results in transformation structures;

(ii) surface reaction with the environment; and

(iii) plastic flow which produces a homogeneous structure or a very fine grained structure.

Turley[128] confirmed that structures in the white layer produced by intense plastic deformation, consisted of fine subgrains, as the temperature rises caused by the abrasion operation were too small to be taken into account. Additionally, Wilson[144] attributed white layer generation to the precipitation of ε-carbide during tempering in the range of 100°C to 200°C and could be suppressed by previous plastic deformation.

However, the study of the mechanism of white layer formation is far from complete, as the structure of the white layer is still controversial and the process of white layer generation is complex.

Chapter 5

INTRODUCTION

to

the PROPERTIES of

RELEVANT STEELS

The steels investigated for this project comprised ten carbon steels, three tool steels and four Bisalloys which are a type of high-strength low-alloy steel, with varieties of microstructures obtained by appropriate heat treatments.

5.1 CARBON STEELS

Carbon steels are the most common steels used in industry because of their wide range of properties and comparatively low cost. The properties of carbon steels are determined by carbon content and by microstructure, which is generated by appropriate heat treatment.

5.1.1 Equilibrium Structures

Under equilibrium conditions, carbon steels are austenitic at high temperature and, at room temperature, comprise ferrite, ferrite and pearlite (hypoeutectoid structures), pearlite (eutectoid structure) and pearlite and cementite (hypereutectoid structures), depending on the carbon content[145].

Austenite is face-centred-cubic and stable only at high temperature for plain carbon steels. Generally, austenite has high ductility and toughness, and low hardness.

The eutectoid transformation in steels produces a unique microstructure termed "pearlite", which consists of lamellae of ferrite and cementite with carbon content is of 0.77%[146]. The thickness of the lamellae is determined mainly by the cooling rate during transformation and the amounts of cementite and ferrite can be calculated using the lever rule. The combined mechanical characteristics such as hardness, toughness and ductility, of pearlitic structures are moderate.

Ferrite is body-centred-cubic at room temperature and when present with pearlite, forms the so-called hypoeutectoid structure. Ferrite (<0.002%C[126]) forms below the A3 temperature in carbon steels that contain less than 0.77%C[126]; and for hypoeutectoid steels, the amount of ferrite decreases with increase in carbon content to zero at 0.77%C.

When the carbon content is more than 0.77%, the structure comprises pearlite and cementite, the so-called hypereutectoid structure, and the amount of cementite increases with increase in carbon content to the limit at 2.06%C[126]. The mechanical properties of both hypoeutectoid and hypereutectoid structures depend on the relative amount and identity of proeutectoid constituent. Generally, the larger the amount of ferrite in hypoeutectoid steels, the higher the toughness and the lower is the hardness. The larger the amount of cementite in hypereutectoid steels, the higher is the hardness and the more brittle is the steel.

5.1.2 Heat Treatments and Microstructures

Commonly applied heat treatments for carbon steels are annealing, normalizing, spheroidizing, quenching, tempering and austempering. Details of these heat treatment procedures have been described in §4.2.

Annealing produces structures containing ferrite and cementite with relatively low hardness and high ductility.

Normalized structures are very similar to annealed structures for the hypoeutectoid and eutectoid products, but the size of the ferritic colonies (hypoeutectoid) and the thickness of the pearlitic lamellae in normalized structures are smaller or less than those in annealed structures. For hypereutectoid structures, proeutectoid carbides form as partially spheroidized agglomerates[146] or as allotriomorphs on prior austenitic grain

boundaries, and fracture toughness is improved compared with fully annealed structures containing net-work cementite[147].

Spheroidized structures are characterized by spheroids of carbide in a ferritic matrix for steels with all carbon contents. Toughness and ductility are improved, compared with annealed structures, however, hardness is almost unchanged.

Martensite is formed during cooling at a rate higher than the 'critical rate' and is the typical structure for quenched products. Normally, two major morphologies of martensite, lath and plate, develop in heat treatable carbon steels, depending mainly on carbon content. The lath designation is used to describe the units of martensite that form in low- and medium-carbon steels, while the plate designation accurately describes the shape of the martensite units that form in high-carbon steels[146].

Lath martensite is characterized by the tendency of many laths to align parallel to one another in large volume of the parent austenitic grain. Dislocations are the major structural heterogeneity in lath martensite; although fine transformation twins are also found to some extent[146].

Plate martensite is recognized by many different orientations of the plates due to twenty-four variants of the irrational habit planes[146]. However, microcracks often develop in the plates, particularly, in the large martensite plates[148], as a result of impingement of plates with other habit plate variants[149]. Therefore, high carbon plate martensite is quite brittle and sensitive to microcracking. Microcracks in martensite can be reduced by decreasing the grain size of austenite which leads to the formation of small plates[146], or by lowering the carbon content which changes the morphology to lath martensite[150].

Bainite is a mixture of ferrite and cementite, and is formed under continuous cooling or isothermal transformation conditions. There are two major morphologies or forms of bainite[127]: upper bainite that forms in the temperature range below that for pearlite formation, and lower bainite which forms at temperatures closer to Ms. Upper bainite has a feathery appearance, with carbides located between ferritic laths. Consequently, microcracks occur frequently along these carbides, resulting in brittleness and low toughness[127]; therefore, upper bainite is generally not applicable in industry. Lower bainite has an appearance which is very similar to plate martensite under optical microscopy; however, the carbides in lower bainite are finely dispersed in a plate-shaped ferritic matrix, are responsible for the dark etching response, and are resolved only under transmission electron microscopy[146]. Lower bainite has moderately good toughness, ductility and hardness, which varies slightly with carbon content. Additionally, isothermally formed lower bainite may contain as much as 20% residual austenite, which is three to four times as much as in martensitic structures[76].

5.1.3 Hardness

The hardness of carbon steels varies with microstructures and carbon content. For the same kind of the microstructure, the higher the carbon content, the harder is the steel[39]. For the same steel, however, the hardness decreases from quenched martensite, to bainite, to normalized structures and finally to annealed structures and spheroidite[126]. For tempered martensite, hardness is determined by the tempering temperature and carbon content.

5.1.4 Toughness

Toughness is an important property for higher carbon steels, which are selected primarily for applications necessitating high hardness and wear resistance.

Krause[151] indicated that the fracture behaviour of hardened high carbon steel is very much dependent on the austenitizing treatment applied prior to quenching and tempering. Steels austenitized at temperatures below A_{cm} retain a dispersion of carbide particles that induce trans-granular fracture, whilst austenitizing above A_{cm} dissolves all carbide particles but may cause phosphorus segregation to austenitic grain boundaries. The best fracture toughness is obtained for the structure that austenite associated with a minimum of micron-sized retained carbide particles.

5.1.5 Wear Properties

Khruschov and Babichev[44-45; 62] proposed a linear relationship between wear resistance and hardness, which was later confirmed[23; 100], and an additive rule of wear resistance for inhomogeneous structures. Further, Serpik and Kantor[92] found that, for annealed structures, wear resistance increased with hardness for hypoeutectoid steels, but decreased with hardness for hypereutectoid steels due to the formation of cementite allotriomorphs along prior austenite grain boundaries; for spheroidized structures, however, wear resistance increased with carbon content even beyond 0.80%. Additionally, they reported that, at the same hardness, wear resistance increased in the structural sequence from spheroidite to pearlite and from tempered martensite to bainite. More recently, Wayne *et al.*[152] confirmed that pearlitic structures in AISI 1045 steel offer much higher wear resistance than the spheroidized structures.

The volume fraction of pearlite is evidently important in controlling the wear rate of annealed carbon steels, and it has been agreed[92-93] that wear resistance is, in fact, proportional to this volume fraction in hypoeutectoid steels. Furthermore, the original orientation of the colony and the mean inter-lamellar spacing influence wear resistance[108; 153]. Wear of hypereutectoid steels is controversial[67; 92] as the effect

of networks of cementite is not clear and most of the correlations have been proposed without adequate exploration of the mechanisms by which wear occurs.

For tempered structures, Larsen-Badse[74; 100] suggested that wear resistance should be a linear function of the logarithm of the tempering temperature above 250°C and of the square root of the mean free distance between the dispersed carbides. Mutton and Watson[25] concluded that the relationship between wear resistance and hardness for particular tempered steels was non-linear.

5.2 TOOL STEELS

Alloy tool steels represent a small, but extremely important fraction of total steel production, since they are essential to the processing of all other steels and engineering materials[114]. Tool steels are used to make tools for cutting, forming or shaping material into a part or component of equipment adapted to a definite application[154]. Also, tool materials need to have unique characteristics to be particularly suitable for many structural applications[155]. For the purpose of cutting and structural application, tool steels should be hard, tough and wear resistant, although the relative importance of these properties varies from application to application.

5.2.1 Composition

The composition of tool steels varies with the application purpose, but the main groups include[114]: cold-work steels, hot-work steel and high-speed steels, as shown in Table 5.1.

Table 5.1 Main Groups of Tool Steels[114]

Designation	Type
	Cold-work steels
W2-W7	Water-hardening tool steel
O1-O7	Oil-hardening tool steel
A2-A7	Air-hardening tool steel
S1-S5	Shock-resistant tool steel
D1-D7	High-carbon high-chromium tool steel
F1-F3	Carbon-tungsten tool steel
L1-L7	Low-alloy, special-purpose tool steel
P1-P20, PPT	Low-carbon mold steels
	Hot-work tool steels
H11-H43	Hot-work tool steels
	High-speed steels
T1-T15	Tungsten high-speed tool steels
M1-M36	Molybdenum high-steed tool steels

In **cold-work steels**, generally, the water-, oil- and air-hardening steels (W, O, A groups) have carbon content in the range of 0.60 to 2.25% and the hardenability is controlled by the amount and variety of alloying elements. The shock-resisting tool steels (S group) have a lower carbon content (0.50%) to improve toughness. The high-carbon high-chromium tool steels (D group) have large amounts of chromium (12%) and other carbide formers to produce an air-hardening composition with excellent wear resistance, which is very useful for thread-rolling dies or brick molds. The wear resistance of carbon-tungsten tool steels (F group) is improved by the presence of tungsten carbides, and for low-alloy and special purpose tool steels (L group) is improved by large amounts of strong carbide formers. The low-carbon mold steels (P group) have the lowest carbon content among all the tool steels and the wear resistance is improved by machine or press hardening.

The **hot-work steels** contain large amounts of the strong carbide formers, such as chromium, tungsten, molybdenum and vanadium, and resist softening at operating

temperatures. The carbon contents are normally below 0.65% to provide moderately good toughness at high strength levels.

The **high-speed steels** contain high levels of carbon with tungsten, molybdenum, chromium and vanadium, which react with carbon during heat treatment to form variety of carbides that provide high wear resistance during high speed cutting.

5.2.2 Heat Treatments

Heat treatment of tool steels is dependent upon the composition and the application, but is considerably complicated as the individual tool steels vary from plain carbon grades to the complex high-speed steels[156]. Ghomashchi and Sellars[157] proposed that, for an M2 grade high-speed tool steel, matrix structure, and carbide size and distribution changed with time at the austenitizing temperature.

5.2.3 Microstructures

Microstructures of tool steels vary with the composition and application; however, the basic microstructure is very similar, comprising tempered martensite and dispersion of carbides.

The matrix of tempered martensite is obtained by water-, or oil-, or air-quenching followed by tempering at a particular temperature for an appropriate time which is determined by the toughness requirement of the application.

Carbides are either primary, which are undissolved during austenitizing, or secondary which are precipitated during tempering. The popular carbides used in tool steels are the types of: Cr_7C, Cr_3C_2, $Cr_{23}C_6$, VC / V_4C_3, W_2C / WC, Mo_2C, TiC, etc. depending upon the carbide formers in the steels and heat treatment method applied.

5.2.4 Hardness

The hardness of tool steels varies with the matrix structure and the amount and the type of carbides. The hardness values common carbides and other relevant materials are given in Table 5.2[145; 158].

Table 5.2 Hardness Value for Common Carbides and Relevant Minerals[145; 158]

Carbide	Hardness Hv	Knoop HK
Cr_7C_3	2100	
$Cr_{23}C_6$	1650	
Cr_3C_2	2700	
VC / V_4C_3	2800	
W_2C	3000	
WC	2400	
TiC	2800	
Fe_3C	1300	
Mo_2C	1570	
Al_2O_3	2100	
SiC	3200	
Quartz	1000	
Glass		500-600
Zircon		1340
Diamond		8000
Garnet		1360

5.2.5 Wear Properties

Wear resistance of tool steels depends strongly on the amount, the size and the distribution of massed carbides. For most cases, wear resistance increases with increase in the amount or the size of carbides at the wearing surface. The toughness and the bonding stress between the carbides and the matrix are also important factors for wear resistance, but their functions depend very much on the wear condition.

5.2.5.1 Effect of Matrix

Normally, for a particular microstructure, wear resistance increases with increase in hardness, and for the same hardness, high carbon martensite has higher wear resistance than other structures when the tempering temperature is below 230°C[159]. Additionally, martensite tempered to below HRC50 has similar wear resistance to a bainitic structure and, under severe impact conditions, the wear resistance of both tempered martensite and bainite is inferior to that of a pearlitic structure[159].

For tool steels with non-martensitic matrices, Rigney[159] pointed out that austenite provides better wear resistance than ferrite at a comparable carbide content. Further, the softer the matrix, the lower will be the wear resistance and the greater the tendency for carbides to be extracted.

5.2.5.2 Effect of Carbide Types

Berns *et al.*[123; 160] developed a group of new improved abrasion resistant alloys having a microstructure of carbides embedded in a strong matrix. The precipitation of massed MC-carbides proved to be more beneficial than massed M_7C_3-carbides to wear resistance of these steels. Further, Berns and Trojahn[161] reported that the MC carbides associated with net-work M_7C_3 eutectic carbides improved wear resistance, and MC carbides significantly increased wear resistance under abrasion of hard media such as corundum. Ghomashchi[162] identified the MC carbides in high-speed steels as a vanadium-rich carbide or a tungsten-rich carbide. Additionally, Kasak and Neumeyer[26] concluded that the wear behaviour of high hardness steels depended greatly on the identity and the size of carbides, with the amount of MC-type carbides being the prevalent factor for high-speed steels.

5.2.5.3 Effect of Carbide Volume Fraction

Massed carbides are the important constituents in tool steels. Carbide volume fraction is a relatively useful parameter in hypoeutectic alloys, and for most cases, wear resistance increases with an increase of carbide volume fraction[13]. Also, the mean free path between the massed carbides is an important parameter in describing wear resistance; for the same carbide size, the higher the volume fraction, the smaller will be the inter-carbide spacing. Silence[163] concluded that wear resistance increased directly with volume of the hard constituent (such as carbide), particularly with massed carbides. Additionally, Shchulepnikova[164] concluded, for three-body abrasion, that wear resistance of steel depended primarily on the amount of the massed carbides. The additive rule advanced by Khruschov and Babychev[45] was confirmed to be applicable to the results from this three-body wear test.

5.2.5.4 Effect of Carbide Size and Distribution

Bhansali and Silence[87] and Desai *et al.*[165] stated that wear resistance increased monotonically with increase in carbide size and observed that many of the smaller carbides were often found to be wholly contained within micro-machined chips, indicating that small carbides contributed little to wear resistance. More recently, Berns and Fischer[123] confirmed by study of new tool steels that an increase in carbide size and a decrease in inter-carbide spacing resulted in reduced wear rate. Additionally, Silence[163] confirmed with three-body abrasive wear testing, that wear resistance was promoted by maximizing of the size of the carbide particles.

In hypereutectic alloys wear is strongly influenced by the morphology of massed carbides[65] because abrasive particles, with size larger than the free distance between massed carbides, cannot penetrate substantially into the matrix[13]. Su *et al.*[103] found that unidirectional carbide arrangement perpendicular to the wearing surface, improves wear resistance of blade steels. More recently, Junyi and Yuding[166] indicated that

materials with carbide fibres perpendicular to the wearing surface showed higher wear resistance than for other orientations.

5.2.5.5 Effect of Hardness

To ascertain the effect of bulk hardness on wear resistance of tool steels, Venne[167] reviewed certain ranges of relevant steels and concluded that, for mining applications, good materials for gouging abrasion resistance had a hardness of about HB600.

Clearly, the hardness of massed carbides is a decisive factor for wear resistance. Blank and Luchsinger[65] proposed that wear mechanisms depended on the alloy composition and structure, the relative hardness of abrasive particles and carbides, the size of abrasive particles and the applied load. In relation to the dependence of wear resistance on the hardness of abrasive particles and massed carbides, Fang *et al.*[168] proposed that the wear resistance increased with increasing hardness ratio of the massed carbides to the abrasive (Hv/Ha) when the ratio exceeded 0.8. Further, Berns and Fischer[123] proposed that MC-carbides in tool steels provided better wear resistance than M_7C_3-carbide and, Xu and Kennon[38] confirmed that the hard VC contributed to a higher wear resistance than Cr_7C_3 in high-carbon high-chromium steels under higher stress abrasion.

5.2.5.6 Effect of Toughness

Toughness is an important factor in determining the wear resistance of tool steels, particularly, under the condition that fracture is the dominant mechanism for metal removal. In this case wear resistance increases dramatically with increase of fracture toughness.

Diesburg and Borik[169] indicated that the best toughness, associated with best abrasion resistance, was achieved in cast irons without pearlite in the matrix;

additionally, the coalescence of massed carbides in high-chromium steels by heat treatment increased the fracture toughness.

5.3 HIGH-STENGTH LOW-ALLOY STEELS

High-strength low-alloy (HSLA) steels is a comparatively new family of steels becoming identifiable only in 1958 but having rapidly developed into industrial applications in the 1960's[170]. High-strength low-alloy steels comprise a specific group of steels with composition specially developed to provide improved values of mechanical properties and greater resistance to atmospheric corrosion than plain carbon steels[171]. High-strength low-alloy steels are generally developed with emphasis on mechanical property requirements rather than on composition limits, and therefore, they are defined in terms of high yield strength[172], with a wide range of compositions and microstructures under various heat treatment conditions[173].

High-strength low-alloy steels were developed primarily to obtain improved strength-to-weight ratio by an increase in nominal unit stress. The main applications of high-strength low-alloy steels are to replace carbon steels to save weight and enhance strength[174-177] for structural applications, or for some special applications such as vessels which require high resistance to sea-water corrosion[178], or oil pipes for petroleum industry where stress corrosion and crack resistance are important[179].

High-strength low-alloy steels include four main categories[174]:

(a) as-rolled pearlitic structural steels with yield strengths of 275 to 345 MPa;
(b) microalloyed steels, with moderately good properties resulting from a combination of alloying additions and controlled hot rolling;

(c) carbon steel grades, either normalized or quenched and tempered, having good yield strengths and, if specified, good toughness or impact strength; and

(d) quenched and tempered steel grades having good yield strength to meet requirements of steels with grade ASTM A514.

5.3.1 Chemical Elements

Commonly used alloying elements in high-strength low-alloy steels include manganese, silicon, copper, chromium. nickel, molybdenum, niobium, aluminium, vanadium, titanium and zirconium[174], besides elements of carbon, boron and nitrogen. The amount and variety of elements used in the steel are determined by the application.

Additionally, Meyer *et al.*[180] studied effects of microalloying elements in high-strength low-alloy steels and concluded that it was possible to improve substantially the mechanical properties of the steel by microalloying with niobium, vanadium, titanium, zirconium and boron, which have strong effects on such structural parameters as grain size, transformation structure, dislocation density, precipitates, and texture. In normalized steels, grain refinement can be obtained by precipitates of coarse NbC, dispersive fine VC and fine but stable TiN.

5.3.2 Heat Treatments and Microstructures

Appropriate heat treatments and consequential microstructures of high-strength low-alloy steels vary with application and composition, and the mechanical properties relate largely to microstructure, grain size and presence of precipitates[181]. Generally, heat treatment methods applied to high-strength low-alloy steels are the normalizing, and quenching and tempering, and the corresponding microstructures are pearlite or pearlite and ferrite, and tempered martensite or bainite. Alternatively, the alloys are used in the rolled condition.

Because of the sensitivity of recrystallization and nucleation phenomena to fine-scale variations in composition and processing, there are significant differences in high-strength low-alloy steels produced in different plants, merely due to subtle differences in steel-making and rolling practice[172]. Therefore, the optimization of a high-strength low-alloy steel developed by one particular plant may not hold adequately for other plants.

5.3.3 Wear Properties

Wear properties of high-strength low-alloy steels depend mainly on the amount and the variety of elements in the steel as well as the applied heat treatment. Commonly, wear properties are similar to those of carbon steels because the industrial applications for the two kinds of steels are very similar, and the amount of the alloying elements added in high-strength low-alloy steel is comparatively low, therefore, the abrasion wear resistance increases with hardness[182].

Bhat *et al.*[183] proposed that under high stress two body abrasive wear, using hard abrasives, microstructural constituents such as fine secondary alloy carbides, coarse undissolved massed carbides and retained austenite improved abrasive wear resistance. In low alloy steels, the highest wear resistance was obtained with a microstructure consisting of martensite, lower bainite and retained austenite.

Chapter 6

EXPERIMENTAL MATERIALS and METHODS

Experimental work carried out for this project comprised abrasive wear tests and metallographic studies.

To study metallurgical aspects of the mechanism of abrasive wear, a tribological system was set up to simulate practical work conditions of high stress and low sliding speed, with minimum variables that could be controlled easily to the same conditions for all wear tests. A two-body abrasive wear testing model was, therefore, relevant to this investigation, as it incorporates few variables and is appropriate to the main purpose of the project. Generally, a wear testing machine designed for laboratory use must duplicate actual wear conditions as closely as possible, provide for reasonably short testing duration, and require simple geometry for the specimen.

6.1 WEAR TESTING APPARATUS

For this study, a pin-on-drum configuration was selected as the two-body abrasive wear testing machine for the following reasons.

(1) The configuration can be smaller in size than a pin-on-disc tester that provides the same wear path.

(2) The relative speed is constant over the entire wear path, and the wear debris can be easily collected in a tray underneath the rotating drum.

(3) The worn surface of the pin specimen is slightly concave resulting from the contact with the cylindrical surface of the drum and although more difficult to metallographically examine directly than the flat surface produced by other

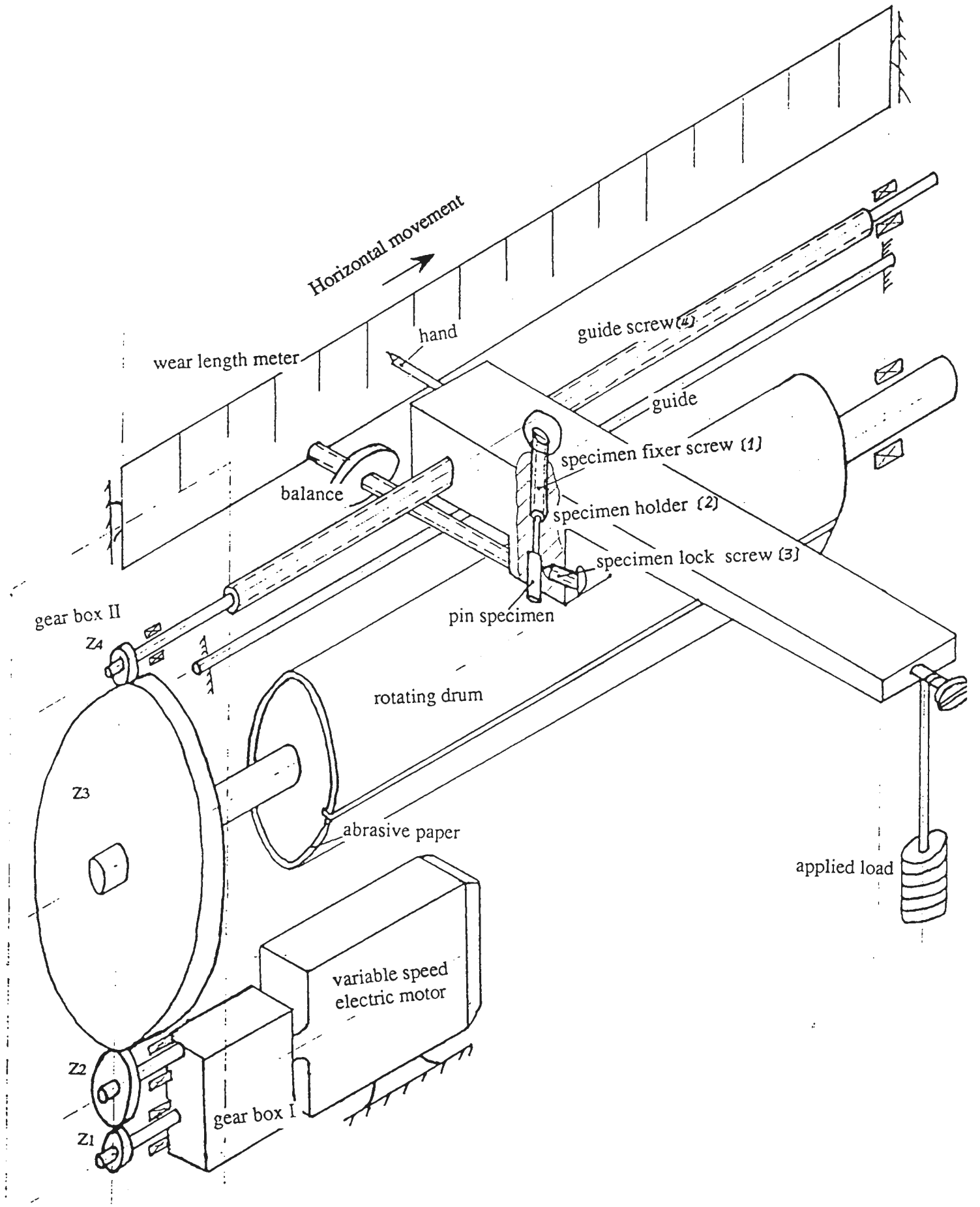

Figure 6.2 **Diagram of the pin-on-drum wear testing machine**

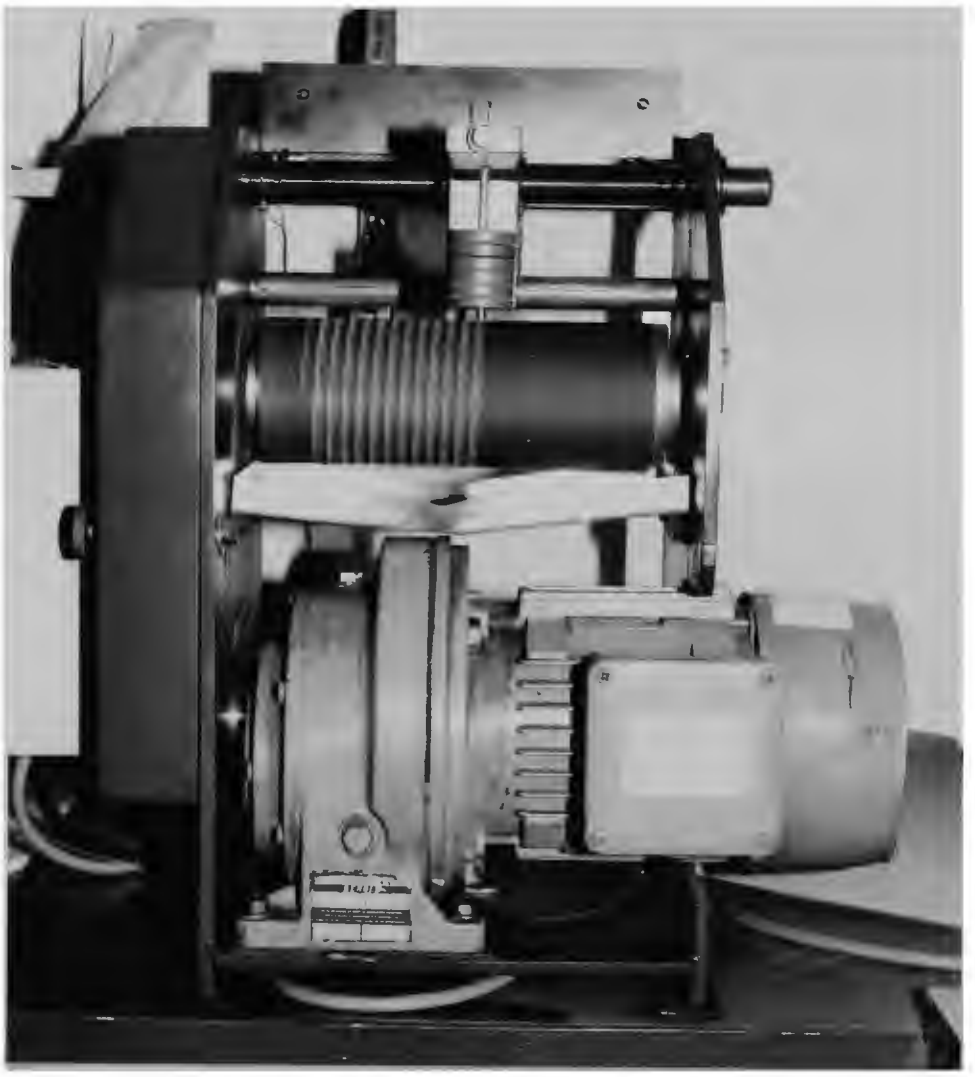

Fig.6.1 Photograph of the pin-on-drum machine used for this study.

configurations, it enables a very effective taper section to be prepared by light polishing of the concave surface as described in §6.6.2.2.

6.1.1 Pin-on-drum Machine

The pin-on-drum wear testing machine was constituted as shown in the photograph in Fig.6.1 and the diagram in Fig.6.2; the main design data are given in Table 6.1. The pin specimen was 6 mm in diameter with allowable length of 20mm to 35mm, and could be adjusted by the screw (1), on the top of the specimen holder (2), to fully contact the drum. Screw (3) could be used to lock the specimen in position. The rotating drum was 86mm in diameter with length of 300mm and driven by a variable speed electrical motor through the gear boxes I and II. Simultaneously, the electric motor drove the guide screw (4) thereby driving the arm of the specimen holder to move the specimen horizontally in relation to the rotating drum. The details of the structural design is given in Appendix 2.

Table 6.1 Designing Data for Pin-on-Drum Machine

Machine parts	Data
Motor	Variable speed 60 -- 1200 rpm
Gear box I -- Motor	Speed reduction ratio: $i_1 = 1:10$
Gear Box II -- Gear --Speed reduction ratio	$Z_1 = 20$, $Z_2 = 40$, $Z_3 = 180$, $Z_4 = 22$ $i_2 = Z_1/Z_3 = 1:9$, $i_3 = Z_3/Z_4 = 90:11$
Guide screw	$t_S = 1$ mm
Drum	D = 86 mm, L_D = 300 mm
Pin	d = 6 mm, l = 20 -- 35 mm

The relationship between the sliding speed of the specimen holder arm and the rotating speed of the drum was as follows:

$$V_h = n_s \cdot t_s = i_3 \cdot t_s \cdot n_D = 8.2\, n_D \qquad (6.1)$$

where V_h is the horizontal sliding speed of the specimen, n_s and t_s, respectively, are the rotating speed and teeth spacing of the guide screw (4) and n_D is the rotating speed of the drum. Using equation (6.1), the relationship between the sliding distance of the specimen in a horizontal direction and the number of rotations of the drum can be derived as:

$$S_X = N_s \cdot t_s = i_3 \cdot t_s \cdot N_D = 8.2\, N_D \qquad (6.2)$$

where S_X is the horizontal distance of sliding, N_s and N_D, respectively, are the numbers of rotation for the guide screw and for the drum. When the drum rotates through 1 turn (N_D=1), the specimen slides 8.2 mm (S_{X1} = 8.2mm is larger than the specimen diameter, 6mm), ensuring that all of the surface of the specimen continuously contacts virgin abrasive paper along a helical locus.

The wear path (X) is the length of the helical locus on the cylindrical drum; therefore, the wear path from each rotation of the drum can be calculated from a triangular function as the circumferential length of the drum (πD) and horizontally sliding distance of specimen for each rotation of the drum (S_{X1}):

$$X_1^2 = (\pi D)^2 + (S_{X1})^2 \qquad (6.3)$$

The total wear path, X, however, is the product of the wear path from each drum turn and the total number of drum rotations, N_D; i.e.:

$$X = N_D \sqrt{(\pi D)^2 + (S_{X1})^2} = \frac{\sqrt{(\pi D)^2 + (S_{X1})^2}}{i_3 t_s} S_X = \frac{270.3}{8.2} S_X \qquad (6.4)$$

where N_D was replaced by the equation (6.2). The horizontal distance of the specimen movement and corresponding wear path are given in Table 6.2, for which the

maximum wear path was designed as 7 meter to utilize the 300mm available length of the drum and the test wear path was selected to be 6m.

Table 6.2 Wear Path and Horizontal Distance of Specimen Movement

Wear Path X (m)	Horizontal Distance Sx (mm)
0.5	15.1
1.0	30.3
1.5	45.5
2.0	60.6
2.5	75.7
3.0	90.9
3.5	106.1
4.0	121.2
4.5	135.4
5.0	151.5
5.5	166.7
6.0	181.8
6.5	197.0
7.0	212.1

The relative sliding speed between the specimen and the drum is the wear path per unit time, which can be derived from the equation (6.4) as:

$$V = n_D\sqrt{(\pi D)^2 + (S_{X1})^2} = i_1 i_2 n_E\sqrt{(\pi D)^2 + (S_{X1})^2} = 3.0\, n_E \qquad (6.5)$$

where n_E is the rotating speed of the electric motor. The relationship between the relative sliding speed of the specimen and the rotating speed of motor is given in Table 6.3.

Table 6.3 Sliding Speed of Specimen Related to Rotating Speed of Motor

Motor Speed (rpm)	60	200	500	800	1000	1200
Sliding Speed (mm/s)	3	10	25	40	50	60

Load was applied to the specimen by adding weight at the end of the arm connected with the specimen holder; the actual load was determined using a spring balance to weigh at the screw (1) during wear testing. The relationship between added weight and applied load at a sliding speed of 50 mm/s is shown in Table 6.4. For results to be comparable, it was important that the guide screw was kept clean to ensure that friction between the guide and the arm was minimal.

Table 6.4 Applied Load Related to the Added Weight (V=50mm/s)

Added weight (g)	125	250	400	550	700
Applied load (N)	10	20	30	40	50

6.1.2 Operational Variables

The wear tests were carried out to simulate working condition under high stress and low sliding speed. It was essential to have available appropriate variables such as applied load, sliding speed and wear path, and therefore the pin-on-drum machine was constructed and operated with the following three features.

1) The sliding speed range of 3 to 60 mm/s was obtainable by varying the rotating speed of the electric motor.

2) The range of applied loads was 10 to 50 N by changing the weight at the end of the specimen holder arm.

3) The maximum wear path was 6m which could be controlled manually with the accuracy of ±10mm.

All the wear tests were conducted under normal laboratory conditions and at ambient temperature.

6.1.3 Estimation of System Error

Wear rate is expressed as the volume loss which was measured as mass loss from the specimen. The testing system error, δ, is considered to comprise errors resulting from mass weighing, and uncertainty in wear path, specimen size and working pressure, and can be estimated as follows.

$$\delta = \frac{\Delta V_l}{V_l} = \frac{\partial m}{m} + \frac{\partial X}{X} + \frac{\partial A}{A} + \frac{\partial P_r}{P_r} \qquad (6.6)$$

where V_l, m, X, A and P_r, respectively, are the actual values of volume loss, mass loss, wear path, specimen surface area and applied pressure; and

ΔV_l is the volume loss difference between the actual value and the measured value,

∂m is the weighing difference between the actual value and the measured value due to inaccuracy in the electronic balance; for the electronic balance used in this wear testing, $\partial m \leq \pm 0.05$mg,

∂X is the wear path deviation from the prescribed length of the path; for an experienced operator, $\partial x \leq \pm 10$mm,

∂A is the deviation for the prescribed specimen surface area due to machining inaccuracy, i.e. the machining size and allowance for this specimen is $6^{\pm 0.05}$mm, then $\partial A/A \leq \pm 1.7\%$, and

∂P_r is the working pressure deviation caused by the specimen surface area inaccuracy, thus $\partial P_r/P_r \leq \mp 1.6\%$, where $\partial A/A$ and $\partial P_r/P_r$ diminish each other, and therefore $(\partial A/A + \partial P_r/P_r)$ was estimated to be less than 0.2%.

Under normal test conditions, mass loss should be more than 5mg for a testing wear path of 6m. Therefore, the maximum system error for the designed pin-on-drum tribology system can be estimated using equation 6-6:

$$\delta = \frac{\Delta V_1}{V_1} = \frac{\partial m}{m} + \frac{\partial X}{X} + \frac{\partial A}{A} + \frac{\partial P_r}{P_r} \leq \frac{0.05}{5} + \frac{0.01}{6} + (0.2\%) < 1.5\%$$

where ∂m_{max} is 0.05mg, m_{min} is 5mg, ∂X_{max} is 0.01m, X is 6m, $(\frac{\partial A}{A} + \frac{\partial P_r}{P_r})_{max}$ is 0.2%. The result that $\delta < 1.5\%$ shows that the abrasive wear testing conducted on this machine is reliable.

6.2 WEAR TESTING

Wear testing was carried out using the pin-on-drum machine, shown in Figs.6.1 and 6.2, with a pin specimen 6mm in diameter and about 30mm in length. The specimen was run-in very well before actual wear testing was performed, and the operational variables selected for the wear testing of each specimen are shown in Appendix 1. Wear rate was measured by determining the mass loss using an electronic balance which could be read to an accuracy of 0.0001g, after the specimen had been cleaned ultra-sonically with acetone and dried with hot air. The mass loss of a particular wear test was the difference of the weight between before and after wear test.

A reference material, annealed 0.10%C steel, was selected for all tests so that relative wear rate could be expressed as the mass loss of the test specimen in relation to the

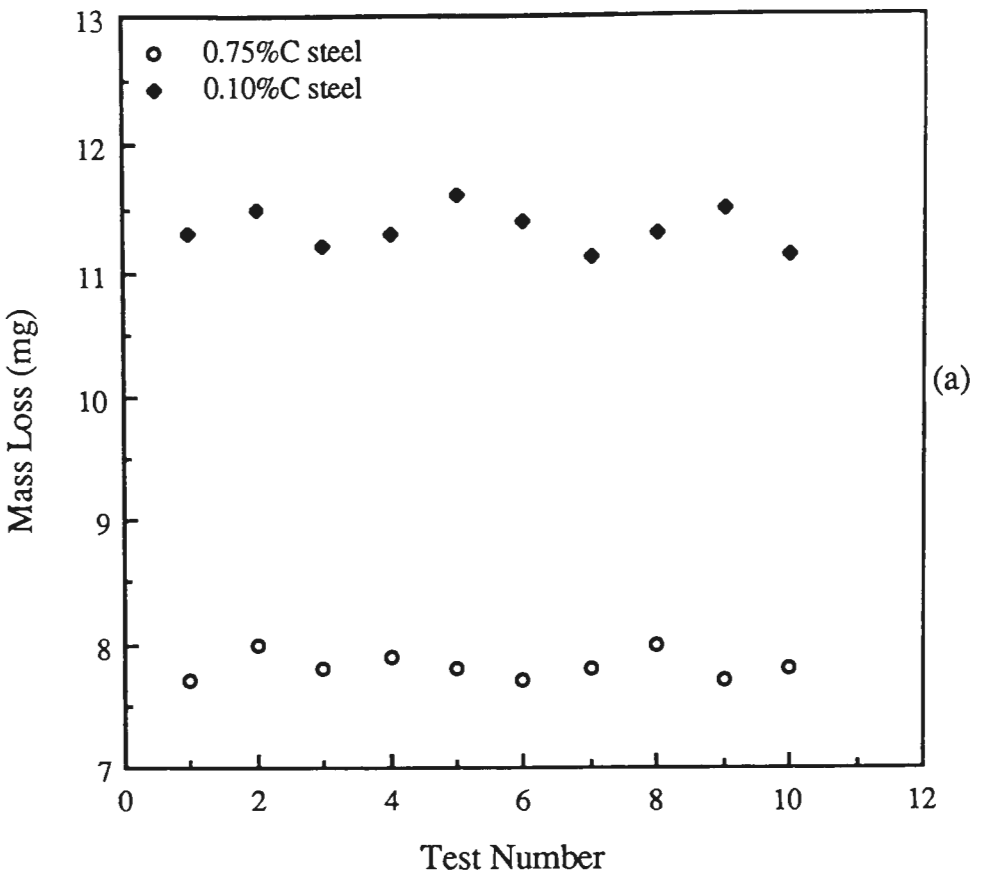

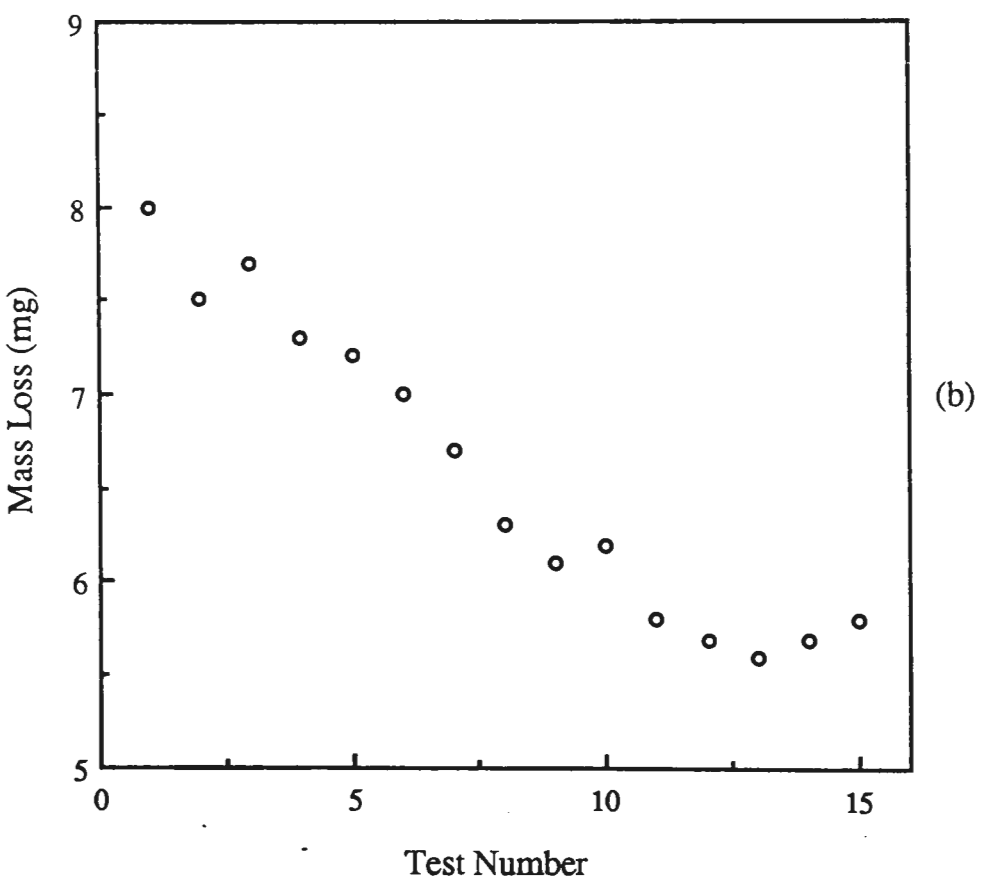

Fig.6.3 Mass loss from repeated tests for annealed steels: (a) 0.10%C and 0.75%C using fresh abrasive paper for each test and (b) 0.75%C using repeatedly the same abrasive paper.

mass loss under individual condition for the reference material. Relative wear resistance is expressed as the reciprocal of relative wear rate.

6.2.1 Reproducibility

Testing error was estimated according to the statistical formulae proposed by Pollard[184]:

$$\sigma = \sqrt{\frac{1}{n-1}\sum_{n=1}^{n}(m_i - \overline{m})^2} \tag{6.7}$$

where σ is the standard deviation from the arithmetic mean, $\overline{m}$; and

$$\overline{m} = \frac{1}{n}\sum_{n=1}^{n} m_i \tag{6.8}$$

Therefore, the coefficient variation is given by:

$$\upsilon = \frac{\sigma}{\overline{m}} \tag{6.9}$$

The reproducibility of the mass loss was examined using annealed 0.10%C and 0.75%C steels on the same day by the same operator under the same operating conditions of an applied load of 20N, a speed of 50mm/s and wear path of 6m, with unused 180# grit silicon carbide abrasive paper for each test. The mass loss for ten successive tests for each material is shown in Fig.6.3(a). The standard deviation for the ten determinations was 0.17 for the 0.10%C steel and 0.11 for the 0.75%C steel, and the coefficient of variation was 1.5% for the 0.10%C steel and 1.4% for the 0.75%C steel, which being less than 5%, indicates that the results are reliable.

Mass loss measured for the annealed 0.75%C steel under the operating conditions of an applied load of 20N, a speed of 50 mm/s and wear path of 6m repeatedly using the same 180# grit silicon carbide abrasive paper, Fig.6.3(b), shows that mass loss

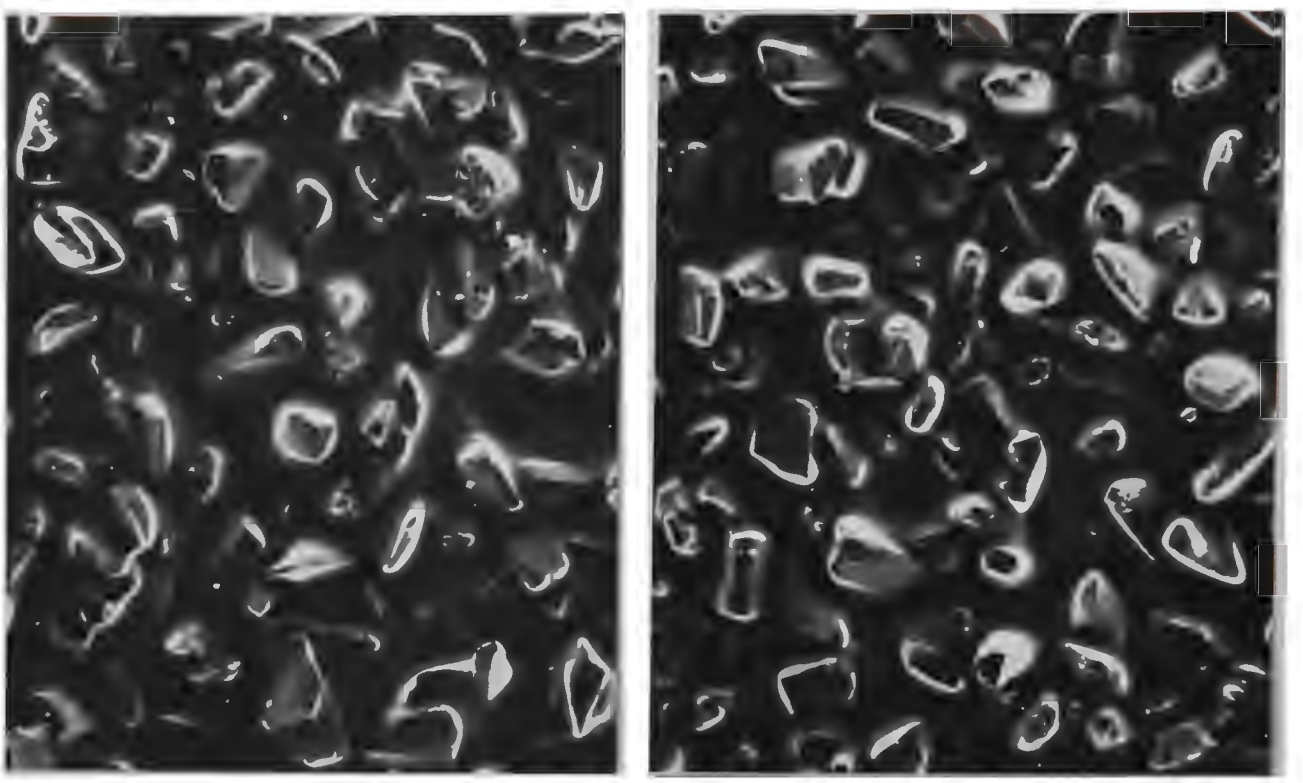

(a) (b)

Fig.6.4 Scanning electron micrographs showing abrasive papers from: (a) batch I and (b) batch II. X70.

decreased significantly with the repeated testing, and possibly became constant after about 10 repetitions. This result emphasized the importance to the reliability and the reproducibility of test data in using fresh abrasive paper for each test.

It is important to choose an acceptable reliability criterion to obtain meaningful results from any test. The criterion chosen for this project was 95% reliability, requiring that every result be determined as the average of four meaningful repetitions, for which the coefficient variation should be less than 5%. Consequently, any test result was considered to be unreliable if the resultant coefficient deviation exceeded 5%, and was discarded.

6.2.2 Abrasive Papers

Dry abrasive paper of size 230 x 280 mm^2 was used to cover the drum with one end located in a slot of the drum and the other end affixed to the drum with double-sided adhesive. Commercial silicon carbide, alumina and garnet abrasive papers were selected for the wear testing, and the hardness values of the abrasive materials are shown in Table 5.2. Abrasive papers from only one manufacturer, Carborundum Abrasives Pty. Ltd., Australia, were used in the tests, and a grit size 180#, for which the mean diameter of abrasive particles is approximately 80μ[20], was selected considering that:

(1) the mass loss during one wear path should be significant;

(2) the results should not be affected significantly by grit size variation, for as Nathan and Jones[52] showed for steel specimens, wear rate increased with the abrasive particle size to about 70μ, then became almost constant with increasing the size of abrasive, and

(3) the wear surface can be observed clearly using optical and scanning electron microscopy.

The mass loss measured from the same specimen abraded using two different batches of the silicon carbide abrasive paper was significantly different, even though the two batches of paper carried the same specification, and were manufactured by the same company. The losses were 11.3mg for batch I and 8.7mg for batch II under the testing condition of an applied load of 20N, a sliding speed of 50 mm/s and a wear path of 6m.

Scanning electron microscopical examination showed that the density of abrasive particles in the batch I paper was lower than in the batch II paper (Fig.6.4), and it is likely that this variation accounted for the difference in mass loss. To avoid such error in experimentation, all groups of wear tests included the standard reference specimen so that experimental results could be normalized and were reported as relative wear rate or relative wear resistance. It is expected that this procedure minimized error resulting from variation in the abrasive papers.

6.3 SPECIMEN MATERIALS

Specimen materials used for this project comprised three groups:

(a) carbon steels and single phase metals,
(b) tool steels comprising a Ni-Cr-Mo-C steel and two high-carbon high-chromium steels, and
(c) four Bisalloys together with an Hadfield's Manganese Steel (H.M.S) for comparison purposes.

For high-carbon high-chromium steels, Chrom is a commercial steel Chromewear 300 of Harbison-Walker Refractories, Division of Dresser Industries Inc. America, and XW-5 is the commercial steel ASSAB XW-5 of AUS STD D3A(D6A) Australia. Bisalloy is high-strength low-alloy steels which is heat treated by quenching and tempering, and produced by Bisalloy Steels Pty. Ltd., Unanderra, NSW, Australia.

Details of composition of the materials are shown in Table 6.5.

Table 6.5 (a) Composition of Carbon Steels (%)

Material	C	P	Mn	Si	S	Ni	Cr
0.10%C	.10	.012	.40	.015	.015	.032	.026
0.38%C	.38	.019	.64	.14	.015	.011	.004
0.45%C	.45						
0.58%C	.58	.021	.39	.074	.041	.13	.03
0.75%C	.75	.017	.84	.25	.016	.021	.021
0.80%C	.80						
0.85%C	.85						
1.0%C	1.0						
1.2%C	1.2						
1.4%C	1.4						

Table 6.5 (b) Composition of Tool Steels (%)

Material	C	Si	Mn	Cr	V	Mo	W	Ni
XW-5	2.05	.30	.80	12.5	--	--	1.30	--
Chrome	2.70	.40	.70	8.25	4.5	1.12	--	--
Ni-Cr-Mo	.38	.99	.88	1.03	--	.50	--	2.68

Table 6.5 (c) Composition of Bisalloys (%)

Material	C	P	Mn	Si	S	Ni	Cr	Mo	Cu	Al	Sn	Ti
BIS A	.085	.014	1.32	.19	.005	.019	.61	.003	.012	.025		.023
BIS B	.18	.020	1.12	.38	.003	.025	.84	.003	.024	.030	.003	.018
BIS C	.18	.017	1.08	.38	.002	.026	.84	.190	.015	.036	.002	.024
BIS D	.27	.018	1.32	.21	.003	.023	.022	.003	.025	.025	.002	.023
H.M.S	1.0		12									

6.3.1 Carbon Steels and Pure Metals

Ten steels with carbon content from 0.10% to 1.4% were studied to determine the influence of the basic operational variables on wear resistance and inter-relationships between hardness, carbon content and microstructure. The steels were heat treated to annealed, quenched and tempered, and bainitic structures, as shown in Table 6.6, and together with a 1.2%C specimen in the original spheroidized condition. Steels were heat treated by first austenitizing at a temperature about 50°C above A_1 (<0.77%C steels) or A_{cm} (>0.77%C steels) for half an hour in an argon filled furnace, then cooling appropriately. The inter-lamellar spacing of pearlite in the annealed structures was controlled to be between 0.3 and 0.7μm so that the pearlitic constituent of the microstructure could be considered to have similar wear characteristics in all steels.

Four hardness groups, Hv140, Hv220, Hv260, Hv500, were identified either with the same microstructure for different steels, or different microstructures for the same steel, to study inter-relationships between hardness, carbon content and microstructure.

The specimen designation comprised two numerals followed by one or two letters, and additional numerals for tempered martensitic specimens. The first group of numeral indicates the carbon content of the specimen, i.e. 38 means 0.38%C. The letter, N refers to a normalizing treatment, the other letters identify constituents of the

microstructure: F indicates ferrite, P for pearlite, C for cementite, S for spheroidized structure, B for bainite and M for martensite. In tempered martensite, the M is followed by numerals indicating the tempering temperature.

A group of annealed pure metals comprising aluminium, copper, nickel and chromium was also studied for comparison of the hardness effect on wear resistance.

Table 6.6 Heat Treatment, Hardness, Microstructure for Carbon Steels

Material	Heat treatment	Hardness Hv	Microstructure .	Specimen
0.10%C	Annealed	80	Ferrite & Pearlite	10F
0.10%C	Quenched	250	Lath Martensite	10M
0.38%C	Annealed	140	Ferrite & Pearlite	38FP
0.38%C	Normalized	180	Ferrite & Pearlite	38NFP
0.38%C	Q & T	140	Tempered Martensite	38M650
0.38%C	Q & T	220	Tempered Martensite	38M600
0.38%C	Q & T	300	Tempered Martensite	38M450
0.38%C	Q & T	400	Tempered Martensite	38M300
0.38%C	Q & T	500	Tempered Martensite	38M200
0.38%C	Q & T	470	Tempered Martensite	38M250
0.38%C	Quenched	650	Martensite	38M
0.45%C	Annealed	160	Ferrite & Pearlite	45FP
0.58%C	Annealed	190	Ferrite & Pearlite	58FP
0.58%C	Q & T	190	Tempered Martensite	58M650
0.58%C	Q & T	500	Tempered Martensite	58M250
0.58%C	Quenched	700	Martensite	58M
0.75%C	Annealed	220	Pearlite	75P
0.75%C	Normalized	300	Pearlite	75NP
0.75%C	Q & T	220	Tempered Martensite	75M650
0.75%C	Q & T	300	Tempered Martensite	75M500
0.75%C	Q & T	400	Tempered Martensite	75M350

Cont. Table 6.6 Heat Treatment, Hardness, Microstructure for Carbon Steels

Material	Heat treatment	Hardness Hv	Microstructure	Specimen
0.75%C	Q & T	500	Tempered Martensite	75M250
0.75%C	Q & T	650	Tempered Martensite	75M150
0.75%C	Quenched	780	Martensite	75M
0.75%C	Austempered	500	Bainite	75B
0.80%C	Annealed	230	Pearlite	80P
0.85%C	Annealed	240	Pearlite	85P
1.0%C	Annealed	250	Pearlite & Cementite	100PC
1.0%C	Q & T	250	Tempered Martensite	100M650
1.0%C	Quenched	780	Martensite	100M
1.2%C	Annealed	260	Pearlite & Cementite	120PC
1.2%C	Received	260	Spheroidized Cementite	120S
1.2%C	Q & T	260	Tempered Martensite	120M650
1.2%C	Q & T	500	Tempered Martensite	120M250
1.2%C	Quenched	750	Martensite	120M
1.4%C	Annealed	270	Pearlite & Cementite	140PC

6.3.2 Tool Steels

6.3.2.1 Ni-Cr-Mo-C Tool Steel

An air-hardening Ni-Cr-Mo-C tool steel was used to obtain information about optimization of wear resistance though appropriate heat treatment procedures. The steel was austenitized at 900°C for 30 minutes, then either single-quenched by air-cooling, or double-quenched, by air-cooling and then re-heating to 900°C and air-cooling again. Both kinds of quenched specimens were tempered at 100°C, 200°C, 300°C and 400°C to produce tempered martensitic structures with various hardnesses as shown in Table 6.7. In the specimen designation, TS refers to tool steel and the first numeral indicates

single-quenching [1], or double-quenching [2], and the second numeral indicates tempering temperature, 1 designating 100°C, 2 designating 200°C and so on.

Table 6.7 Heat Treatment and Hardness of the Ni-Cr-Mo-C Tool Steel

Specimen	Austenitizing Temperature	SQ	DQ	Tempering Temperature	Hardness (Hv)
TS 10	900°C	X	--	--	610
TS 20	900°C	--	X	--	590
TS 11	900°C	X	--	100°C	605
TS 21	900°C	--	X	100°C	590
TS 12	900°C	X	--	200°C	615
TS 22	900°C	--	X	200°C	660
TS 13	900°C	X	--	300°C	595
TS 23	900°C	--	X	300°C	570
TS 14	900°C	X	--	400°C	565
TS 24	900°C	--	X	400°C	470

6.3.2.2 High-Carbon High-Chromium Steels

Two high-carbon high-chromium steels were used to study the effect of composition on microstructure, especially on carbide-type, and the influence on wear resistance; the compositions are given in Table 6.5(b). The heat treatments of the two alloys, as given in Table 6.8, followed the suppliers recommendations of quenching, then double tempering to produce a microstructure of massed carbides in a matrix of tempered martensite.

Table 6.8 Heat Treatments and Hardness for High-Chromium High-Carbon Steels

Material	Quenching	Tempering (1h)	Hardness
XW-5	960°C 1/2h, oil-cooled	150°C twice	HRC65
Chrome	960°C 1/2h, air-cooled	200°C twice	HRC66

6.3.3 Bisalloys

Bisalloys are a kind of high-strength low-alloy steels and comprised four alloys with different compositions which, as shown in Table 6.5(c), differ mainly in the levels of carbon and molybdenum. Details of heat treatment with hardness values are given in Table 6.9. In the specimen designation, the capitalized letter after BIS indicates the specimen alloy, relating to composition, i.e. A means the specimen was alloy A. The numeral after the letter indicates the tempering temperature: 0 for untempered, 1 for 100°C, 2 for 200°C, and so on.

Typical characteristics of composition and heat treatment for each alloy are as follows:

Alloy A is low carbon (0.085%), low molybdenum (0.003%), which was quenched or quenched and tempered to provide two specimens.

Alloy B is normal carbon (0.18%), low molybdenum (0.003%), which was quenched or quenched and tempered to provide six specimens with different hardness levels.

Alloy C is similar to alloy B, but with 0.19% molybdenum, and was quenched or quenched and tempered to provide four specimens for study of the effect of molybdenum concentration.

Alloy D has a higher carbon of 2.7% and was quenched and 200°C tempered to be used for comparison with relevant specimens of BIS B alloy.

Table 6.9 Heat Treatment and Hardness for Bisalloys

Alloy	Quenching	Tempering T (°C)	Hardness (Hv)	Specimen
BIS A	900°C (1/2h) WQ	--	350	BIS A0 *
BIS A	900°C (1/2h) WQ	600°C	230	BIS A6 *
BIS B	900°C (1/2h) WQ	--	460	BIS B0
BIS B	900°C (1/2h) WQ	200°C	450	BIS B2
BIS B	900°C (1/2h) WQ	300°C	440	BIS B3 *
BIS B	900°C (1/2h) WQ	400°C	385	BIS B4 *
BIS B	900°C (1/2h) WQ	500°C	350	BIS B5
BIS B	900°C (1/2h) WQ	600°C	255	BIS B6 *
BIS C	900°C (1/2h) WQ	--	430	BIS C0
BIS C	900°C (1/2h) WQ	200°C	430	BIS C2
BIS C	900°C (1/2h) WQ	400°C	405	BIS C4 *
BIS C	900°C (1/2h) WQ	600°C	300	BIS C6 *
BIS D	900°C (1/2h) WQ	200°C	465	BIS D2 *
Hadfield	900°C (1/2h) WQ	--	250	H.M.S

* referred to in Figure 7.44

6.4 MICROSCOPY

Optical microscopy, scanning electron microscopy and transmission electron microscopy were used to examine the microstructures, the size and distributions of carbides, the white layer on abraded surface, retained austenite in martensitic steels, the wear topography and the abrasion grooves and plastic deformation under the worn surface.

6.4.1 Optical Microscopy

Optical microscopical observations were conducted by a Leitz MM6 metallograph to examine:

(a) the pre-test microstructures of specimens,

(b) the worn subsurface on slight taper sections and transverse sections of the abraded grooves for pearlitic specimens which shows plastic deformation zone, and the white layer on a 5° taper section,

(c) the distribution of the massed carbides in high-carbon high-chromium tool steels and

(d) distinguish between Cr_7C_3 and VC carbides, after special-purpose etching.

Additionally, the retained austenite in martensitic specimens was measured using a Nickon UFX-II optical microscope equipped with a computer-aided image analyzer and the results were confirmed using the linear intersect method from optical microscopical observation using an oil-immersion lens.

6.4.2 Scanning Electron Microscopy

Scanning electron microscopy was used to observe:

(a) wear topography,

(b) wear debris,

(c) plastic deformation of the worn subsurface on pearlitic specimens, which showed the grooving mechanisms clearly in the slight-taper section (obtained by light polishing of the concave specimen surface).

All observations were conducted using a Hitachi S450 Scanning Electron Microscope with Tracor Northern 2000 Energy Dispersive X-Ray Analysis System equipped with the computer programs for semi-quantitative analyses.

Wear debris was distinguished from abrasive particles by back scattered imaging using a Robinson detector and confirmed with an energy dispersive X-ray capability map. Additionally, the compositions of massed carbides in high chromium-carbon steels were determined by energy dispersive X-ray capability for semi-quantitative analysis.

6.4.3 Transmission Electron Microscopy

Transmission electron microscopical observations were carried out on JEOL 2000FX Stem Transmission Electron Microscope to study:

(a) the size and distributions of precipitated carbides in martensitic and bainitic specimens and
(b) the structures of martensite and bainite in some quenched specimens.

6.5 HARDNESS MEASUREMENT

Hardness of metallographic specimens was measured using a Vicker's hardness testing machine with a load of 10kg. Hardness values were determined from the average of 10 measurements.

6.6 SPECIMEN PREPARATION

The specimens consisted of those used for the wear testing and microscopy. Also, 5° taper sections through worn surfaces were specially prepared for observing the 'white layer' generated during abrasion of some specimens. Wear debris was collected and analysed by scanning electron microscopy to assist in elucidating to wear mechanisms.

6.6.1 Wear Test Specimens

The wear test specimens were mechanically machined into cylinders with diameter of $6^{\pm 0.05}$ mm and length of about 30mm; the allowable length for the specimen was 20 to 35mm. The specimen was run-in under test conditions until the wearing surface matched the contour of the outer surface of the drum before the actual testing on fresh abrasive paper was conducted.

6.6.2 Optical Microscopical Specimens

Optical microscopical observation was carried out for routine examination of the microstructure of the specimen materials and, after wear testing, for observation of the presence of the 'white layer' and the subsurface structure in taper sections, transverse sections and longitudinal sections.

6.6.2.1 Metallographic Specimens

Metallographic specimens were prepared by mounting a small piece of the specimen material in bakelite, then hand grinding using 180, 240, 320, 400, 600 and 1200 grit abrasive papers followed by polishing to a specular finish using 6μm and 2μm diamond. Microstructures were observed using Leitz MM6 optical microscope after appropriate etching (§6.6.2.4).

6.6.2.2 Taper Sections

For observing the worn subsurface, two kinds of taper section were used to study the worn subsurfaces and to observe the 'white layer', a taper section was obtained by slightly polishing the concave worn surface resulting from the pin-on-drum configuration.

A standard 5° taper section was prepared for observing the white layer. The details of the 5° taper section technique can be described as follows. The worn surface was coated first with copper and then nickel immediately after wear testing for protection. Copper was vacuum-coated to a thickness of a few tens of micrometers using a Dynavac mini-coater, specifically to distinguish the white layer from the heavy nickel coating. Nickel was electro-plated to a thickness of about 1mm to protect the worn surface during making of the 5° taper by the standard method. A small slot, cut in the specimen with a diamond saw after wear testing identified the abrasion direction and was used as a guide for grinding the 5° taper. This procedure ensured that the thickness of the white layer could be measured accurately.

Details of nickel electro-plating device designed for this work are given in Appendix 3.

6.6.2.3 Transverse and Longitudinal Sections

Longitudinal sections of the abrasion groove were obtained by cutting a Cu-Ni coated pin specimen along the direction of the abrasion groove, then mounting in bakelite. These specimens were used for examining the plastic deformation zone under the abrasion groove in annealed materials. Transverse sections of the abrasion groove were obtained, in the same way, by cutting the Cu-Ni coated specimen in the direction normal to the abrasion groove, and were used for observing plastic deformation under the grooves and for confirming the thickness of the white layer in tempered martensitic and bainitic specimens.

6.6.2.4 Etchants

The etchants used in this investigation are shown in Table 6.10. Nital was used for the specimens of carbon steels, Ni-Cr-Mo-C tool steel and Bisalloys. NaOH-$KMnO_4$[145] was used for the high-carbon high-chromium steels so that chromium carbides could

be distinguished from vanadium carbides by optical microscopical observation. The two high chromium-carbon steels were etched in Picric-HCl-Ethanol[185].

Table 6.10 Etchants for the Metallographic Observation

Material	Etchants	Purpose
Carbon Steels	2.5% Nital Picric(100ml)-HCl(10drops)	Microstructure, White layer Retained austenite
Ni-Cr-Mo-C tool steel	5% Nital	Microstructure, White layer
Bisalloys	5% Nital	Microstructure, White layer
High Cr-C steels	HCl(5%)+Picric(3g)+Ethanol NaOH(4g)-KMnO4(10g)-H2O	Microstructure, White layer Distinguish Cr_7C_3 and VC

6.6.3 Scanning Electron Microscopy Specimens

Most of the worn specimens, the taper section specimens and metallographic specimens were suitable for scanning electron microscopical observation. Only the wear debris samples required special preparation which comprised two steps. First, wear debris together with detached abrasive particles were glued, using varnish, to a stage which was a specimen holder specially made for scanning electron microscopy. The sample was then coated with carbon, using a Dynavac high vacuum coating system to render it conductive; the carbon did not affect the intensity of energy dispersive map. The metallic wear debris was distinguished from worn-off abrasive particles by the back scattered image which showed metallic material to be bright. This distinction was confirmed by energy dispersive analysis and X-ray capability mapping.

6.6.4 Transmission Electron Microscopy Specimens

Transmission electron microscopy specimens were prepared mainly as thin foils, using the standard method described by Modin[186]. The 3mm diameter foil was hand

ground to a thickness of 100 to 150 μm, then further thinned by electro-polishing on a Struers Tenupol-2 with solution of 5% Perchloric acid, with operating conditions as shown in Table 6.11.

Table 6.11 Electro-Thinning Conditions for Martensitic Specimens

Specimen material	Voltage	Flow rate	Temperature
Carbon steel	60 V	1.5	Ambient
Ni-Cr-Mo-C tool steel	40--60 V	1.5	Ambient
BIS B3 &C3	100 V	1.5	Ambient
BIS B4 & C4	100 V	2.5	Ambient
BIS B0 & B2, C0 &C2	90 V	1.5	Ambient
BIS B5 &C5, C4 &C5	70 V	1.5	Ambient
BIS A	80 V	1.5	Ambient

Chapter 7

EXPERIMENTAL RESULTS

Experimental results for this study comprises results of the abrasive wear tests and associated microstructural observations. Abrasive wear tests were carried out on the pin-on-drum machine, described in §6.1.1, to measure the wear properties which are expressed as wear rate or relative wear resistance, for the steels that were investigated. Wear rate was measured as mass loss by weighing the specimen before and after wear testing using an electronic balance with the accuracy of 0.0001g; and relative wear rate was expressed as the ratio of the mass loss from the test specimen to that of the reference material.

Microstructural study of the specimen materials, the worn surface, the subsurface and the wear debris, was used to elucidate the prevailing wear mechanisms and to relate wear resistance to the microstructural properties and hardness. This study was carried out using optical microscopy, scanning electron microscopy and transmission electron microscopy.

The experimental results include the survey of operational variables that were important for establishing a standard for the wear testing, and the examination of wear and microstructural properties for ten carbon steels, three tool steels and four Bisalloys.

7.1 OPERATIONAL VARIABLES

The effects on wear rate of the operational variables of sliding speed, applied load and wear path were measured by mass loss from specimens of several carbon steels. Wear tests were carried out for one variable by maintaining the other two constant, for instance, if the applied load was the variable for one group of tests, the sliding speed and wear path were kept constant, as shown in Appendix 1. The standard testing condition was 20N applied load, 50mm/s sliding speed and 6m wear path.

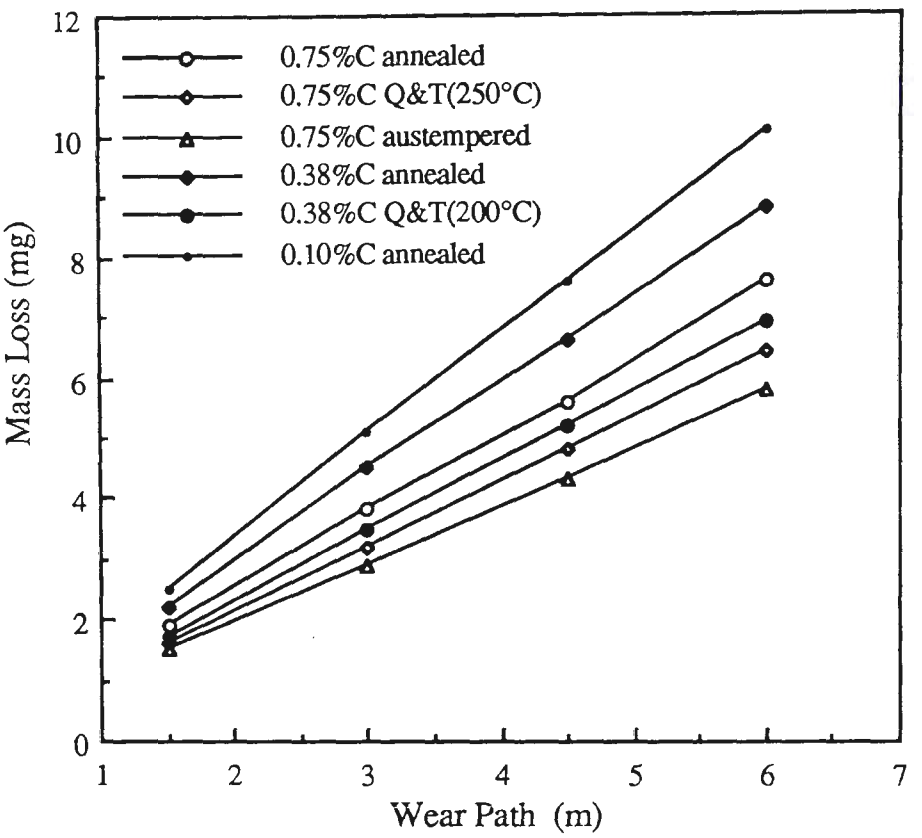

Fig.7.4 Diagram showing relationship between mass loss and wear path for carbon steels. Wear test condition: L=20N and V=50mm/s, 180# silicon carbide paper.

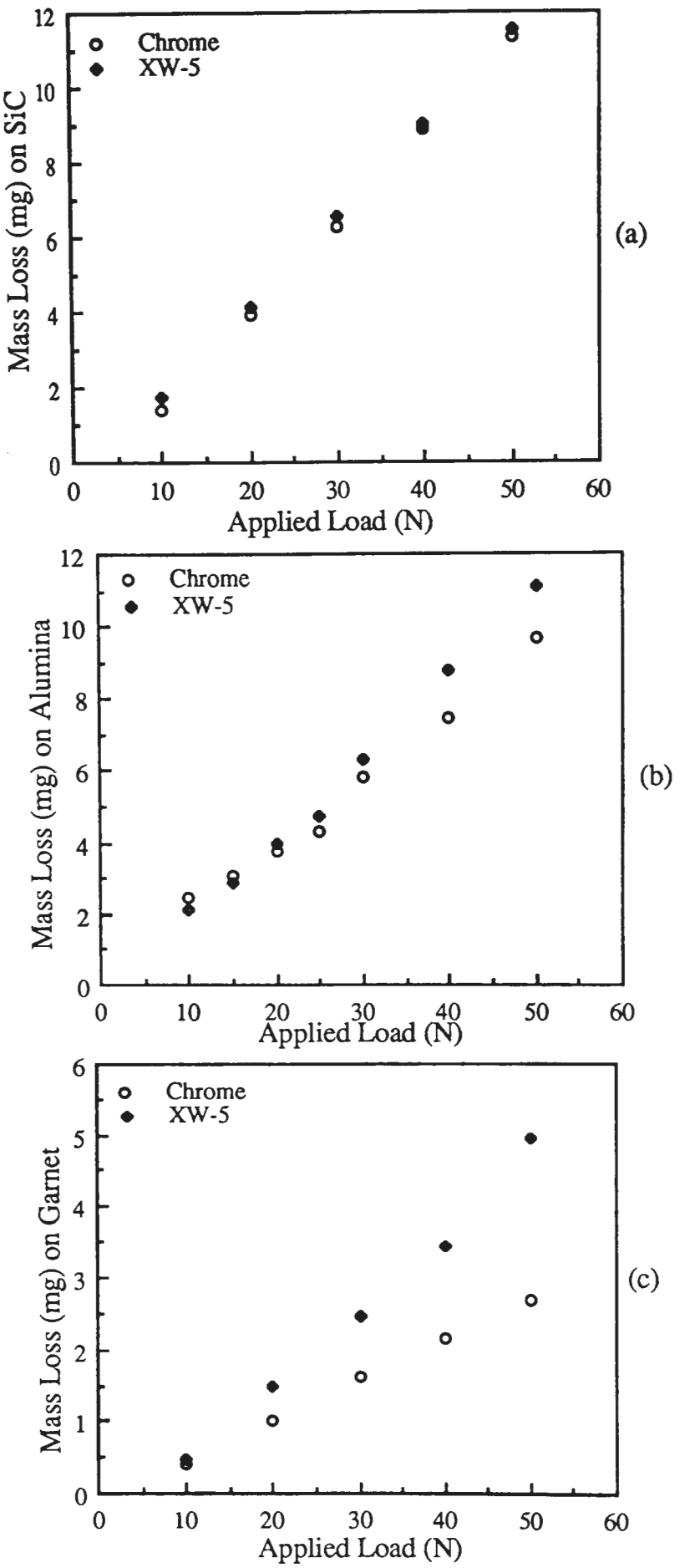

Fig.7.3 Diagram showing relationships between mass loss and applied load for high-carbon high-chromium specimens, Chrome and XW-5, abraded with abrasive papers: (a) 180# silicon carbide, (b) 120# alumina and (c) 180# garnet. Wear test condition: V=50mm/s, X=6m.

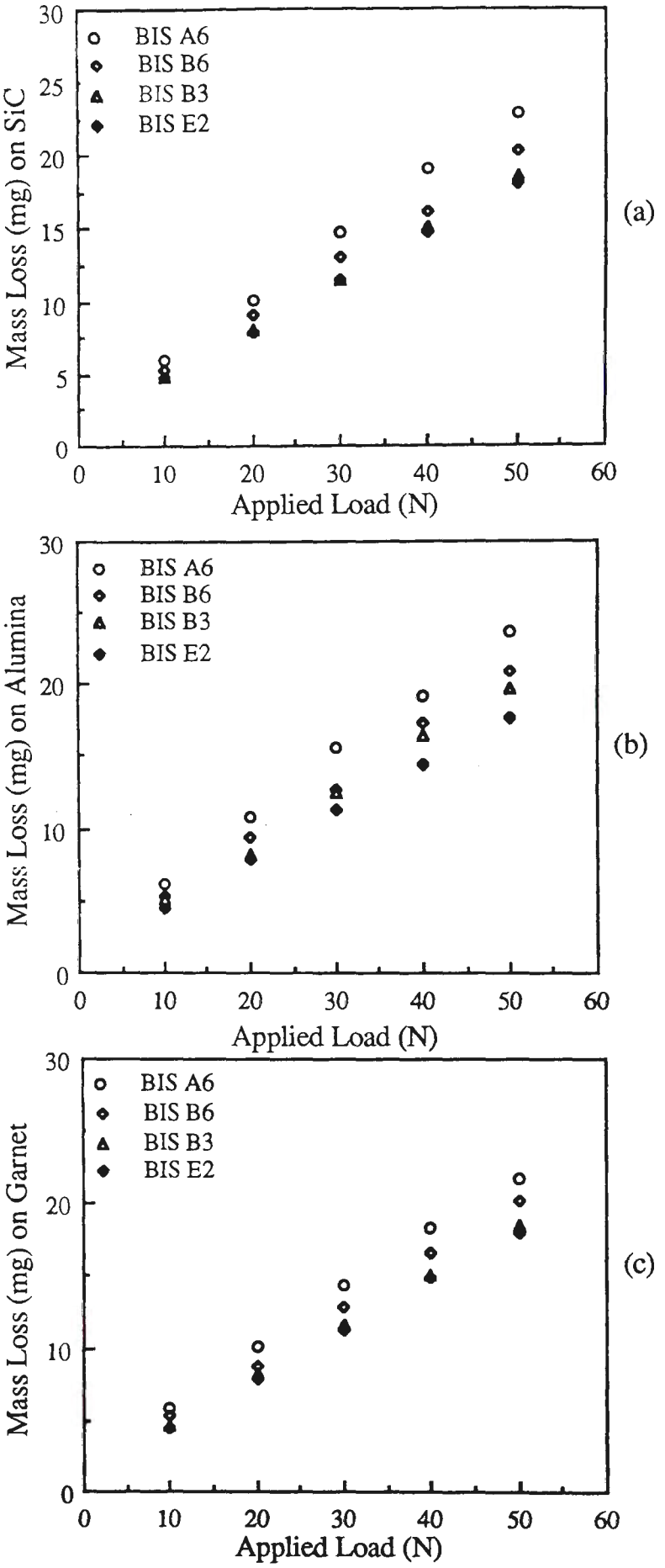

Fig.7.2 Diagrams showing relationships between mass loss and applied load for Bisalloy specimens abraded with 180# abrasive papers of: (a) silicon carbide, (b) alumina and (c) garnet. Wear test condition: V=50mm/s and X=6m.

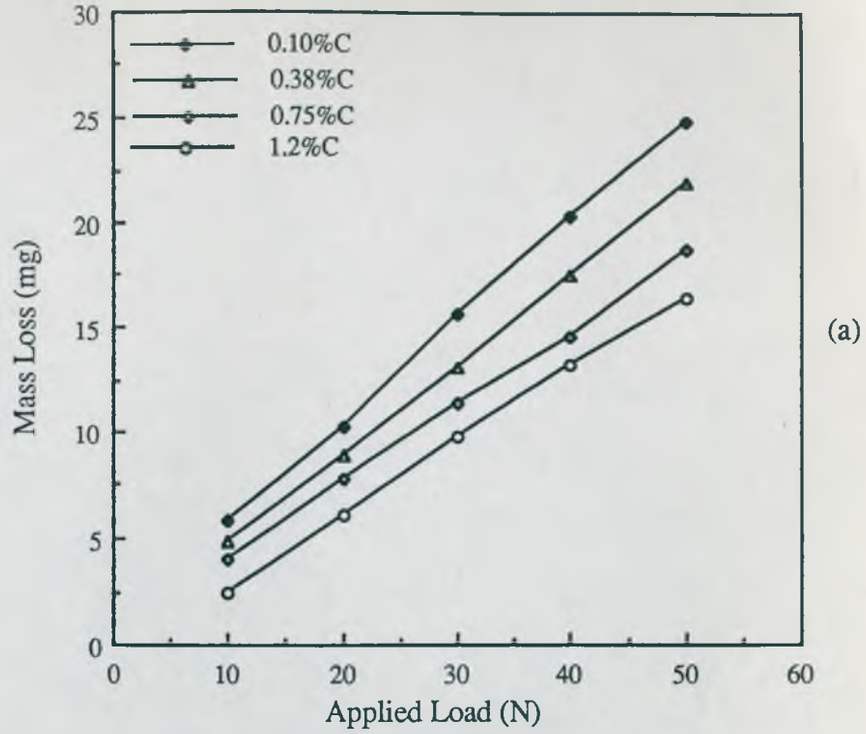

(a)

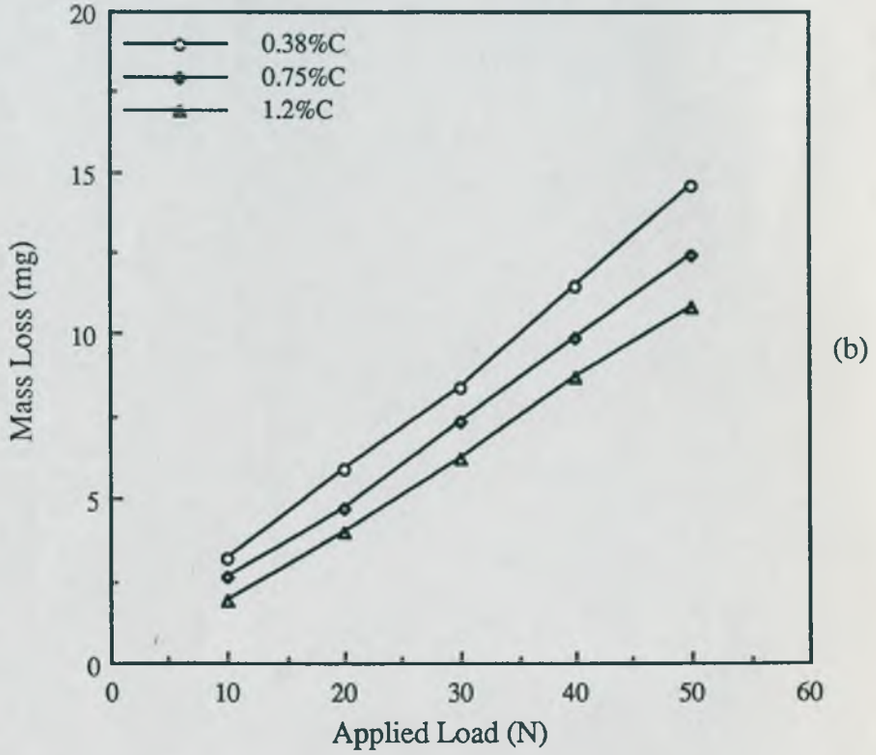

(b)

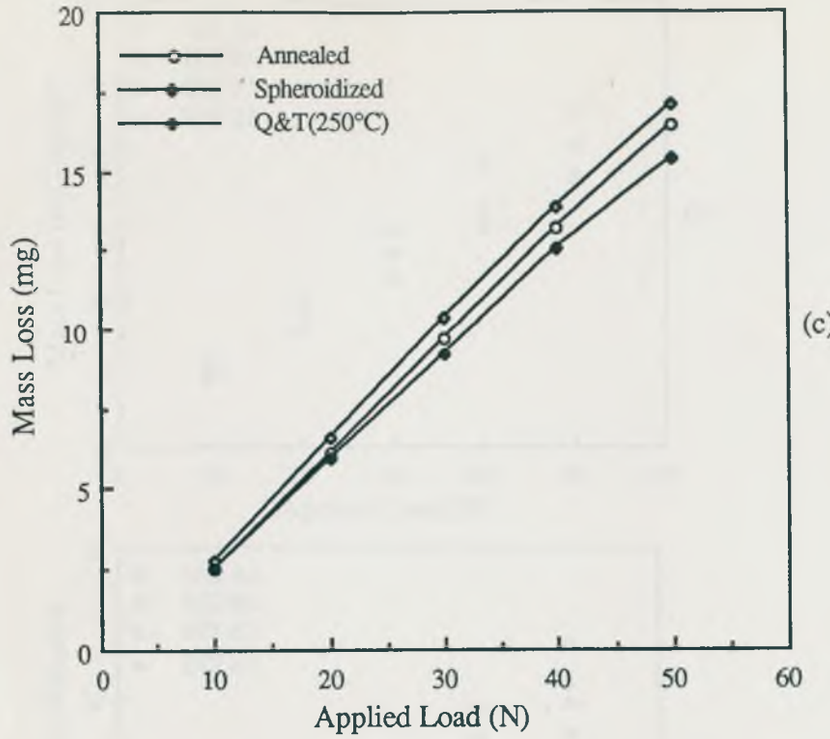

(c)

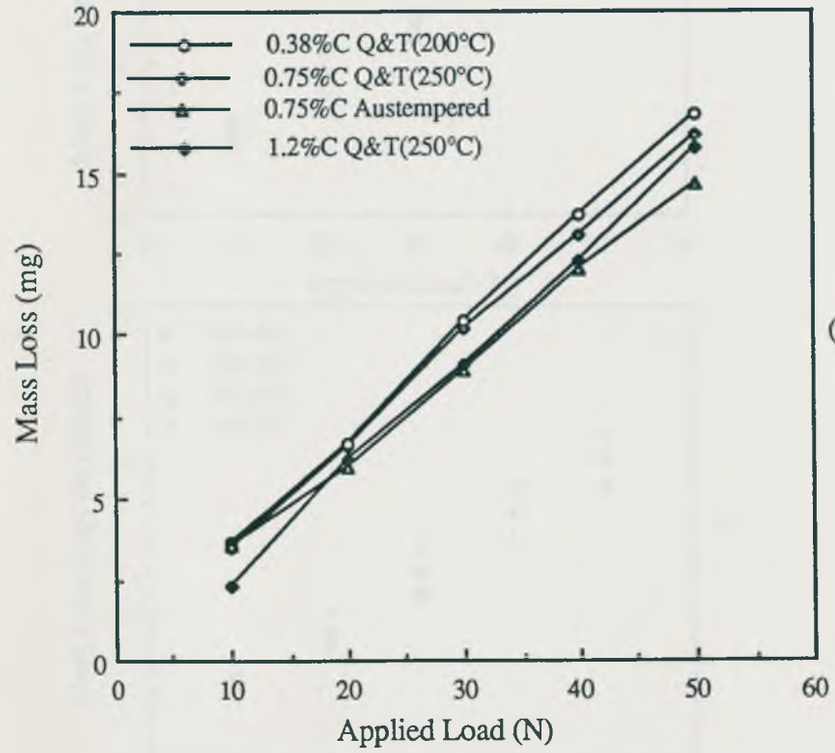

(d)

Fig.7.1 Diagrams showing relationships between mass loss and applied load for carbon steels: (a) annealed structures, (b) quenched martensitic structures, (c) 1.2%C steel in the annealed, the spheroidized and the quenched and 650°C tempered conditions and (d) Hv500 specimens with tempered martensitic and bainitic structures. Wear test condition: V=50mm/s and X=6m, 180# silicon carbide paper.

7.1.1 Applied Load

Figure 7.1 shows mass loss as a function of applied load for specimens of several carbon steels. Clearly, for all steels and structures examined, mass loss probably increased linearly with load over the 10N to 50N range under conditions of 50mm/s sliding speed and 6m wear path, using 180# silicon carbide abrasive paper.

For Bisalloy specimens, mass loss was proportional to the applied load over the 10N to 50N range, as shown in Fig.7.2, for test conditions of 50mm/s sliding speed, 6m wear path, 180# silicon carbide, alumina and garnet abrasive papers. It appears from these diagrams that the relationships between mass loss and applied load were independent of the hardness of the abrasive. Further details of the results of mass loss related to applied load are given in §7.4.3.

Figure 7.3 presents the relationships between mass loss and applied load for specimens of high-carbon high-chromium steels, Chrome and XW-5, abraded with 180# silicon carbide, 120# alumina and 180# garnet abrasive papers. For both silicon carbide and garnet papers, the relationships were linear, however, the slope of the linearity for silicon carbide paper was much higher than for garnet paper (Figs.7.3(a) and (c)). Further, for alumina paper, the relationships appeared to be non-linear. For an applied load less than 15N, mass loss of Chrome was higher than XW-5, whilst for an applied load was more than 25N, mass loss of Chrome was lower than XW-5 as shown in Fig.7.3(b), with a minor discontinuity in the relationships at about 25N.

7.1.2 Wear Path

Figure 7.4 shows that mass loss was linearly dependent upon wear path for carbon steels under the test condition of 20N applied load and 50mm/s sliding speed, 180# silicon carbide abrasive paper. Clearly, wear rate expressed as mass loss per unit wear path is independent of the length of wear path.

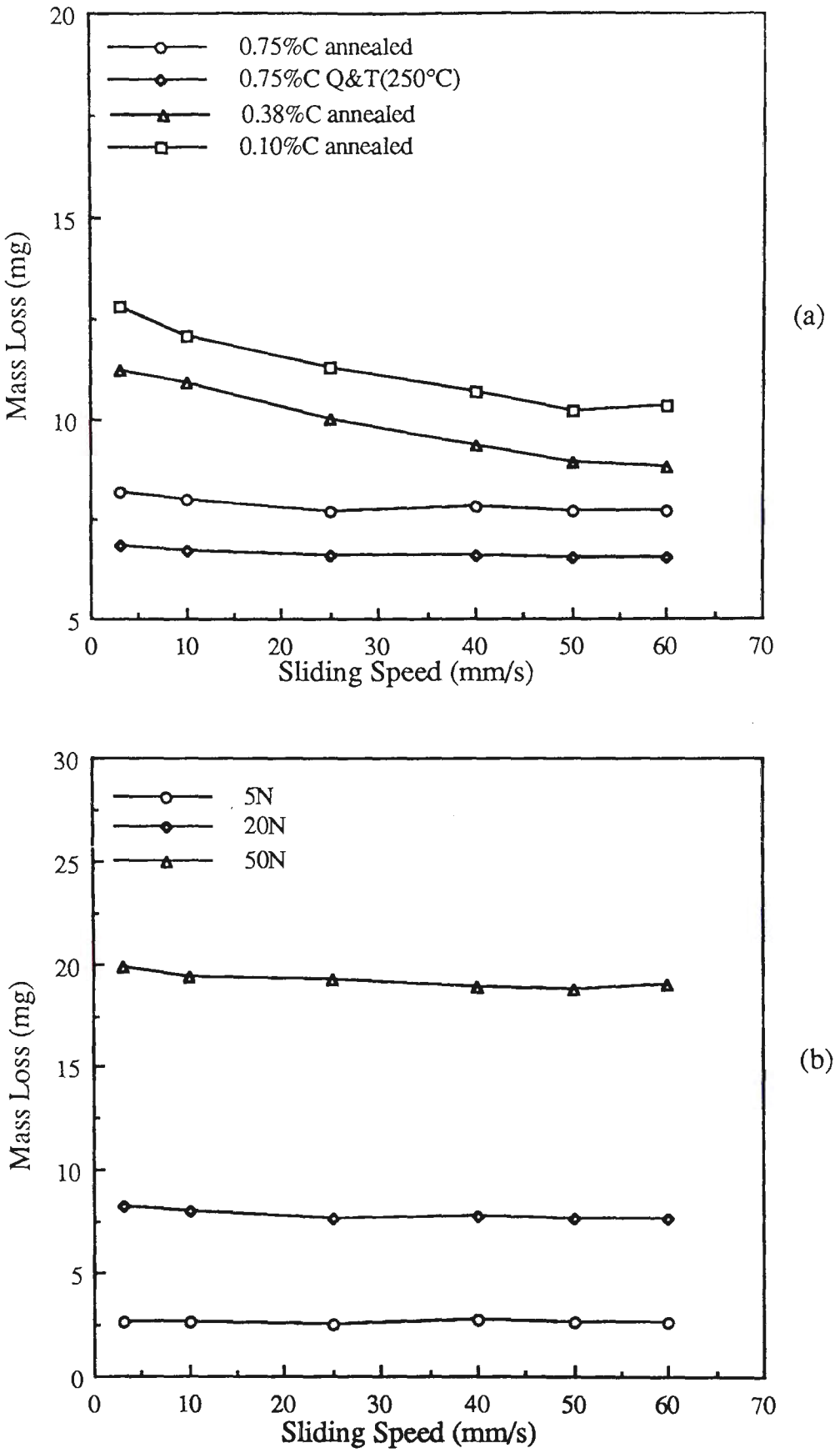

Fig.7.5 Diagrams showing relationships between mass loss and sliding speed for: (a) carbon steels under an applied load of 20N and (b) annealed 0.75%C steel under applied loads of 5N, 20N and 50N. Wear test condition: X=6m, 180# silicon carbide paper.

7.1.3 Sliding Speed

Figure 7.5 shows mass loss as a function of sliding speed from 3mm/s to 60mm/s. It is evident from Fig.7.5(a) that for the harder specimens (annealed, and quenched and 250°C tempered 0.75%C steel), mass loss was almost constant over the sliding speed range examined at 20N applied load and 6m wear path. For the softer specimens (annealed 0.10%C and 0.38%C steels), mass loss decreased with sliding speed from 3mm/s to 50mm/s, then became a approximate constant with a further increase in the speed. However, under the applied load of 50N, mass loss from the annealed 0.75%C steel decreased slightly with increase in sliding speed from 3mm/s to 25mm/s, then became almost constant, as shown in Fig.7.5(b). Clearly, the decreasing rate for the 0.10%C steel is much higher than for the 0.75%C steel. Further, mass loss was almost independent of sliding speed for annealed 0.75%C steel under the applied load of 5N and 20N.

7.1.4 Effect of Abrasive

Figure 7.3 indicates that mass loss from specimens of high-carbon high-chromium steels was influenced significantly by the hardness of the abrasive, and it is evident that the harder the abrasive, the higher was the mass loss. Relationships between the mass loss and the applied load were probably linear for the condition that the abrasive particles were much harder (silicon carbide), or softer (garnet) than the massed carbides in the specimen steels, but were non-linearly complicated for the case that the abrasive particles (alumina) were about as hard as the massed carbides (Cr_7C_3). For specimens of carbon steels and Bisalloys, the hardness of the abrasive particles affected the value of mass loss only, with no significant effect on the relationship between mass loss and applied load.

The density of abrasive particles in the silicon carbide abrasive paper clearly influenced mass loss which, as described in §6.2.2, showed that the higher density of abrasive particles, the lower was the mass loss.

7.2 CARBON STEELS and PURE METALS

Ten steels containing from 0.10% to 1.4%C were used to study relationships between wear resistance, hardness and microstructures, with the main focus on annealed structures, using 180# silicon carbide abrasive paper.

Four pure metals with hardness ranging from Hv60 to Hv170 are used for comparison purpose.

7.2.1 Effect of Carbon Content

7.2.1.1 Microstructure

Under normal conditions as mentioned in §6.3.1, hypoeutectoid structures occur in steels containing less than 0.75%C, pearlitic structures occur in steels containing about 0.80%C and hypereutectoid structures occur for carbon concentrations larger than 0.85%C[124]; see Table 6.5(a) and Table 6.6.

The volume fraction of pearlite increases linearly with carbon content for hypoeutectoid structures, and decreases linearly for the hypereutectoid structures. The relationship between the volume fraction of pearlite, P, and the carbon content, C, (%), can be expressed for hypoeutectoid steels as:

$$P = a\,C \tag{7.1}$$

and for hypereutectoid steels as:

$$P = a_1\,C + b_1 \tag{7.2}$$

where a, a1 and b1 are constants that can be calculated by a least square analysis of experimental data, Table 7.1.

Table 7.1 The Least Square Mathematical Relationships and Constants for Annealed Structures

Structure	Variables	Relationship	Figure
Hypoeutectoid	P, C	P = 1.26 C	
Hypereutectoid	P, C	P = -0.17 C + 1.136	
Hypoeutectoid	Hv, C	Hv = 214 C + 60	7.6(a)
Hypereutectoid	Hv, C	Hv = 54 C + 195	7.6(a)
Hypoeutectoid	ε, C	ε = 0.503 C + 0.951	7.7
Hypereutectoid	ε, C	ε = 0.209 C + 1.19	7.7
Hypoeutectoid	ε, Hv	ε = 0.0023Hv + 0.81	7.8(a)
Hypereutectoid	ε, Hv	ε = 0.0039Hv + 0.44	7.8(a)

For the quenched specimens, optical microscopical observations indicated clearly that carbon content affected both the size of the martensitic plates and the amount of retained austenite. The 1.2%C steel contained about five times the amount of retained austenite present in the 0.75%C steel, and additionally, there were microcracks in the martensitic structure.

For the quenched and 250°C tempered specimens with hardness level of Hv500, no significant differences in the microstructural appearance were evident either for steels with different carbon content or for the same steel with martensitic and bainitic structures. Similarly, for 650°C tempered martensitic structures, no differences in appearance of steels with different carbon contents could be detected. Transmission electron microscopical study of the Hv500 specimens indicates that the higher the carbon content, the higher was the density of precipitated carbides, and the smaller was the mean spacing between the similarly sized carbides, as shown in Table 7.2.

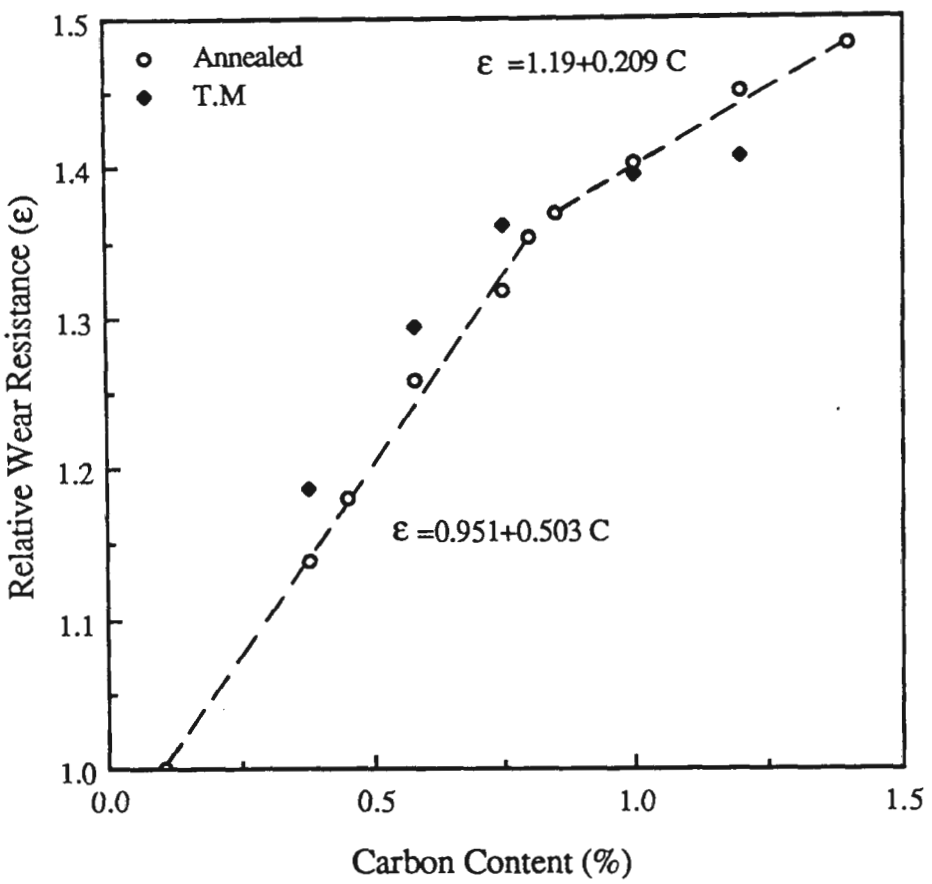

Fig.7.7 Diagram showing relationship between relative wear resistance and carbon content for carbon steels in the annealed and the quenched and 650°C tempered conditions. Wear test condition: V=50mm/s, L=20N and X=6m, 180# silicon carbide paper.

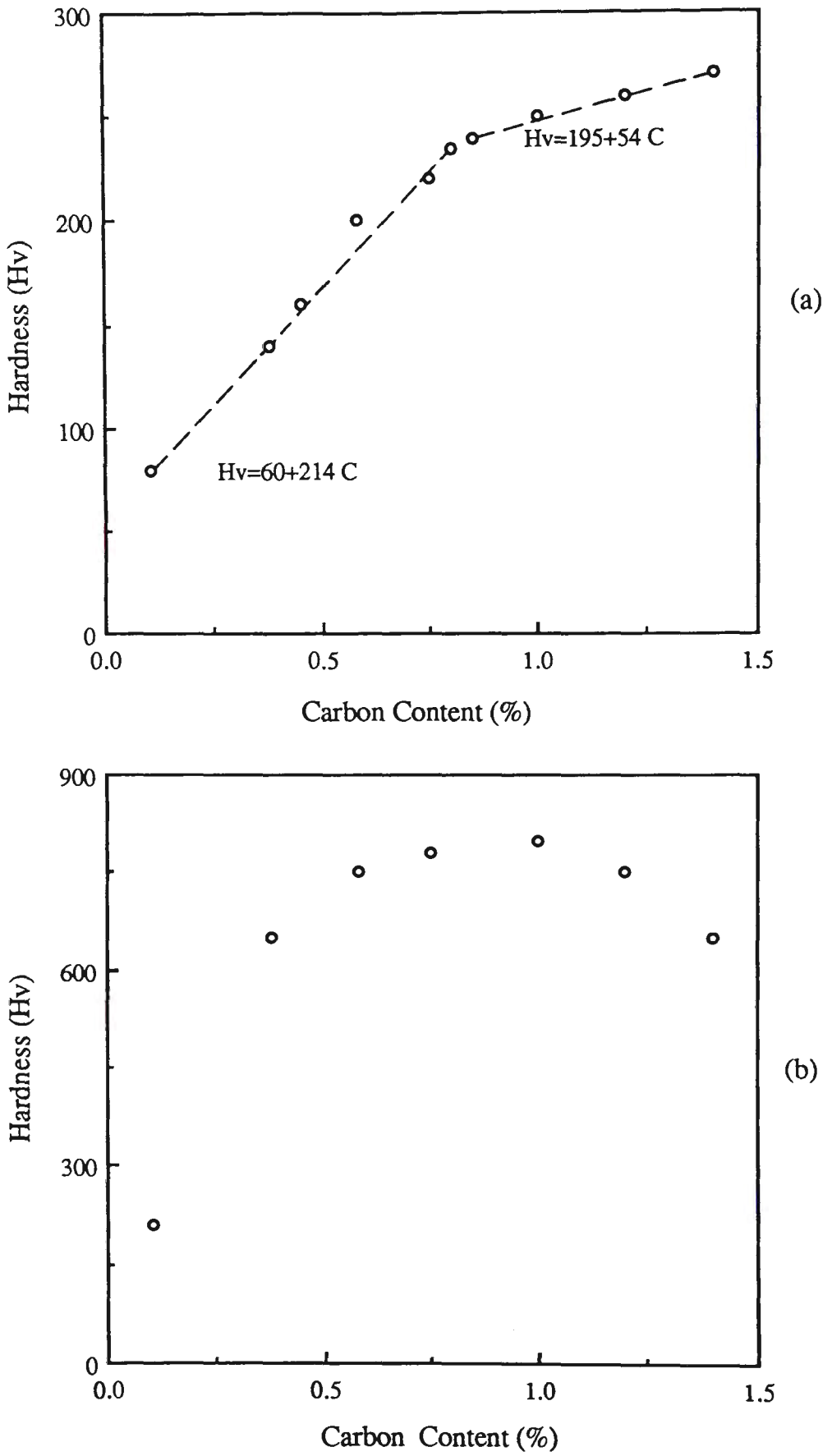

Fig.7.6 Diagrams showing hardness as a function of carbon content for carbon steels in: (a) annealed and (b) quenched conditions.

Table 7.2 Mean Inter-carbide Spacing (λ) and Retained Austenite (A) for Martensitic Specimens

	0.38%C	0.58%C	0.75%C	1.2%C
A (%)	--	--	3	15
λ (nm)	75	60	50	30

7.2.1.2 Hardness

The relationship between hardness and carbon content for annealed and for quenched steels with carbon content in the range 0.10 to 1.4% is well established, as shown in Fig.7.6. For the annealed steels, the relationship was linear within each of the hypoeutectoid or the hypereutectoid ranges, and can be expressed as:

$$Hv = \alpha_1 C + \beta_1 \qquad (7.3)$$

where Hv is hardness, C is the carbon content (%) and α_1 and β_1 are constants determined by the least square analysis of the experimental data, as given in Table 7.1. It is clear from Fig.7.6(a) that value of α_1 for hypoeutectoid steels was higher than for hypereutectoid steels.

For the quenched condition, hardness increased with carbon content to a maximum value at about 1.0%C, then decreased with further increase of carbon content; the relationship was approximately parabolic, Fig.7.6(b).

7.2.1.3 Wear Resistance

Figure 7.7 shows relative wear resistance as a function of carbon content for steels containing 0.10 to 1.4%C, which were austenitized at about 50°C above A_1 (hypoeutectoid steels) or A_{cm} (hypereutectoid steels), then slowly cooled (annealed), or quenched and 650°C tempered (TM). Clearly, for annealed specimens, the relative wear resistance (ε) was linearly related to carbon content C (%), according to the relationship:

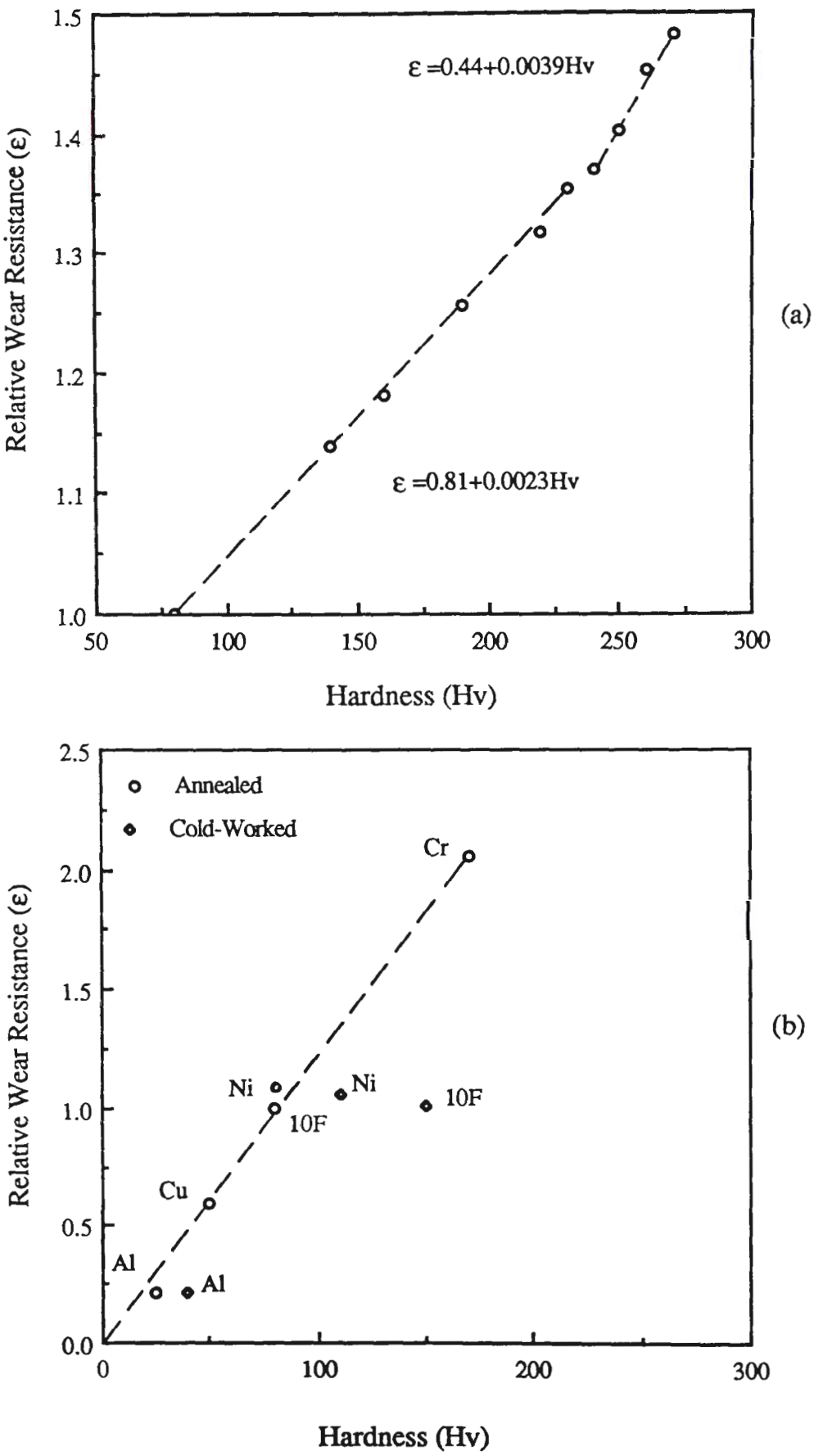

Fig.7.8 Diagrams showing relationships between relative wear resistance and hardness for: (a) annealed carbon steels and (b) single phase metals in annealed and cold worked conditions. Wear test condition: V=50mm/s, L=20N and X=6m, 180# silicon carbide paper.

$$\varepsilon = \alpha_2 C + \beta_2 \qquad (7.4)$$

where α_2 and β_2 are the constants determined by the least square analysis of the experimental data, as given in Table 7.1. It is clear from Fig.7.7 and Table 7.1 that α_2 for hypoeutectoid steels was higher than for hypereutectoid steels.

As shown in Fig.7.7, for specimens containing less than 1.0%C, the relative wear resistance of 650°C tempered specimens was higher than that of annealed specimens, while for specimens containing 1.2% carbon, tempered specimens were less wear resistant than annealed specimens, even though the hardness was at the same level of Hv260.

Relative wear resistance was linearly related to hardness for annealed specimens with the same structure, Fig.7.8(a). The linear relationship can be expressed as:

$$\varepsilon = \alpha Hv + \beta \qquad (7.5)$$

where α and β are constants determined by the least square analysis of the experimental data, as given in Table 7.1. It is clear from these data that:

(i) the value of α for hypoeutectoid steels is less than that of hypereutectoid steels;
(ii) the linear extrapolations of the relationship between wear resistance (ε) and hardness (Hv) do not pass through the origin.

By comparison, the relative wear resistance for single phase metals was linearly related to hardness, Fig.7.8(b), and the linear extrapolation appears to pass through the origin. Further, hardness increase resulting from cold work does not seem to affect relative wear resistance.

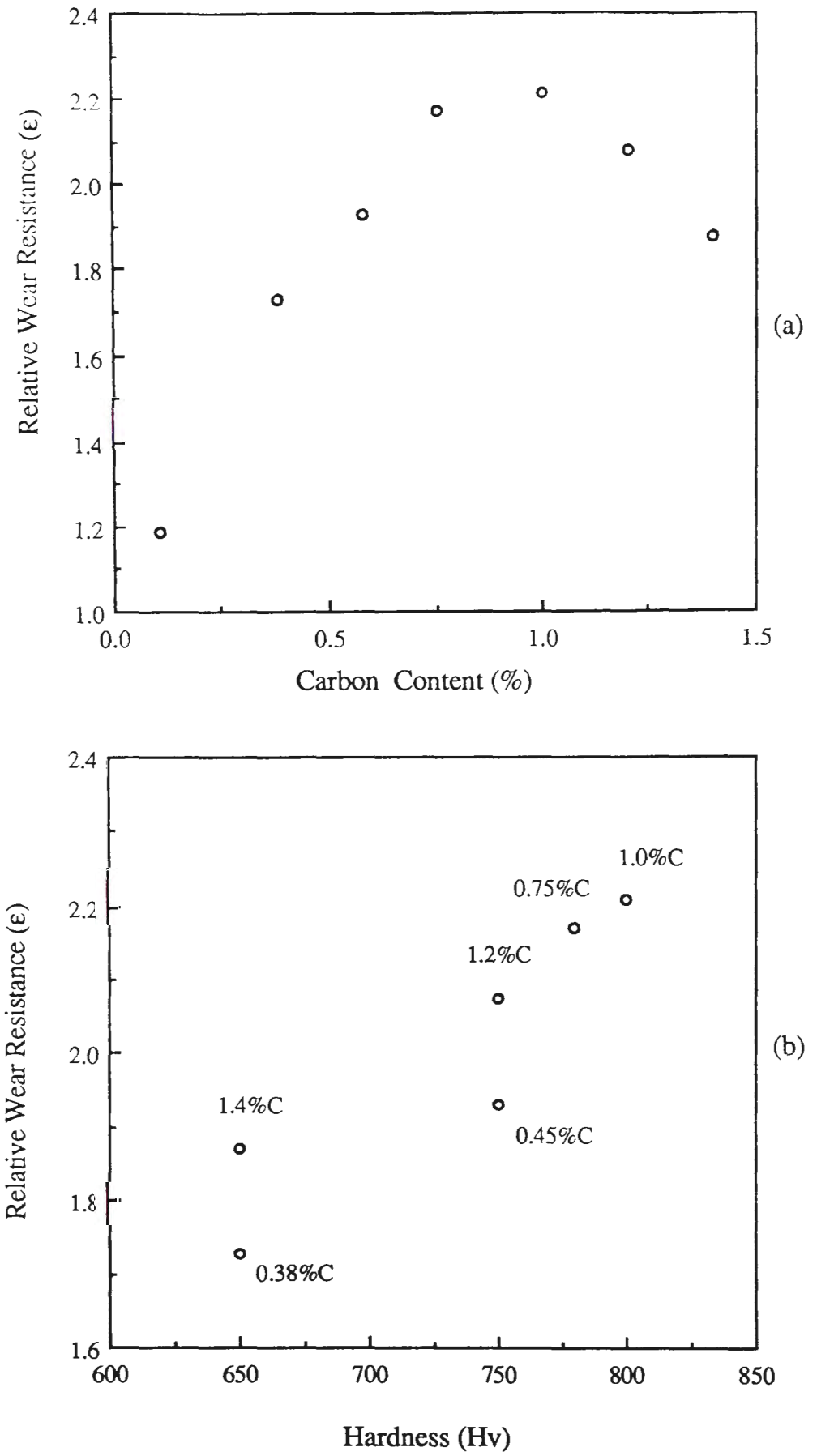

Fig.7.9 Diagrams showing relative wear resistance influenced by: (a) carbon content and (b) hardness for carbon steels in the quenched condition. Wear test condition: V=50mm/s, L=20N and X=6m, 180# silicon carbide paper.

For quenched specimens, relative wear resistance increased non-linearly with carbon content to about 1.0%C, then decreased with a further increase in carbon content, as shown in Fig.7.9.

7.2.2 Effect of Heat Treatment

7.2.2.1 Annealing, Normalizing and Spheroidizing

For the purposes of comparison, annealing and normalizing treatments were applied to the 0.38%C and 0.75%C steels, and annealed and spheroidized specimens were were prepared from the 1.2%C steel. Details of the structure, hardness and relative wear resistance (ε) for these steels are given in Table 7.3.

Table 7.3 Structural Characteristics and Hardness Values for Annealed, Normalized and Spheroidized Steels

Annealed	Normalized	Spheroidized
0.38%C Steel		
Hypoeutectoid	Hypoeutectoid	
Normal pearlitic lamellae	Thinner pearlitic lamellae	
Normal pearlitic colonies	Smaller pearlitic colonies	
Hv140	Hv180	
$\varepsilon = 1.13$	$\varepsilon = 1.15$	
0.75%C Steel		
Pearlite	Pearlite	
Normal lamellae (thickness t)	Thinner lamellae (thickness 1/6 t)	
Hv220	Hv300	
$\varepsilon = 1.31$	$\varepsilon = 1.45$	
1.2%C Steel		
Hypereutectoid		Spheroidized structure
Lamellar carbides		Spheroidal carbides
Hv260		Hv260
$\varepsilon = 1.45$		$\varepsilon = 1.26$

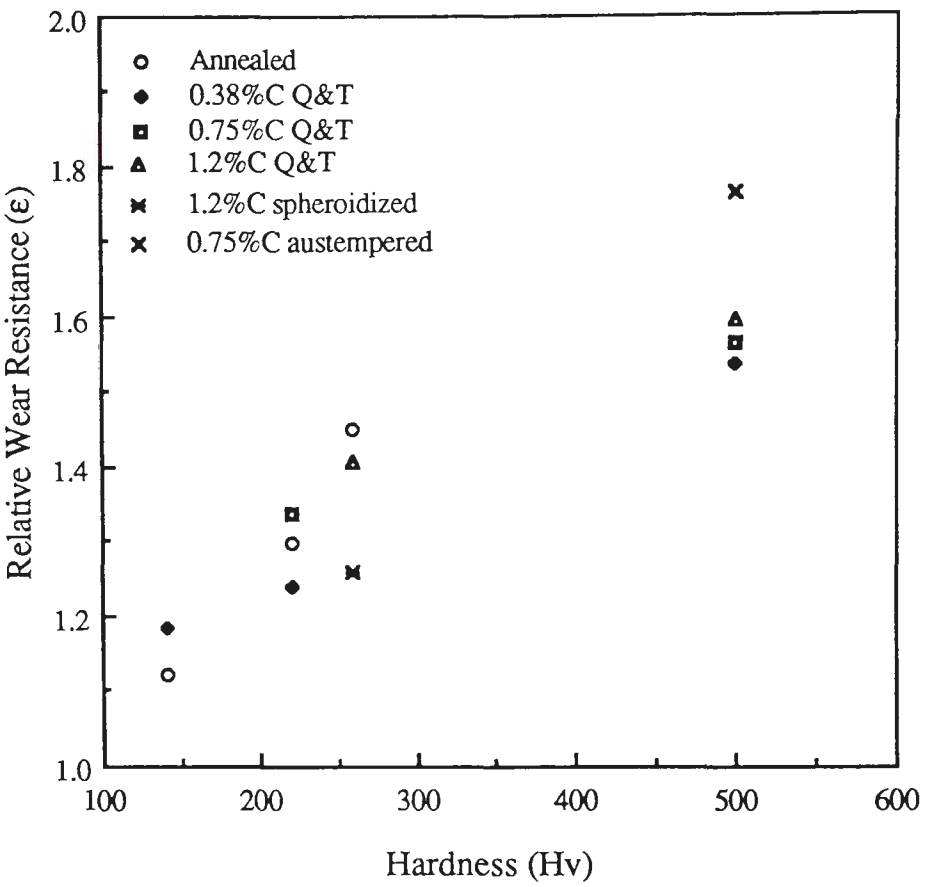

Fig.7.11 Relative wear resistance for hardness groups Hv140, Hv220, Hv260 and Hv500. Wear test condition: V=50mm/s, L=20N and X=6m, 180# silicon carbide paper.

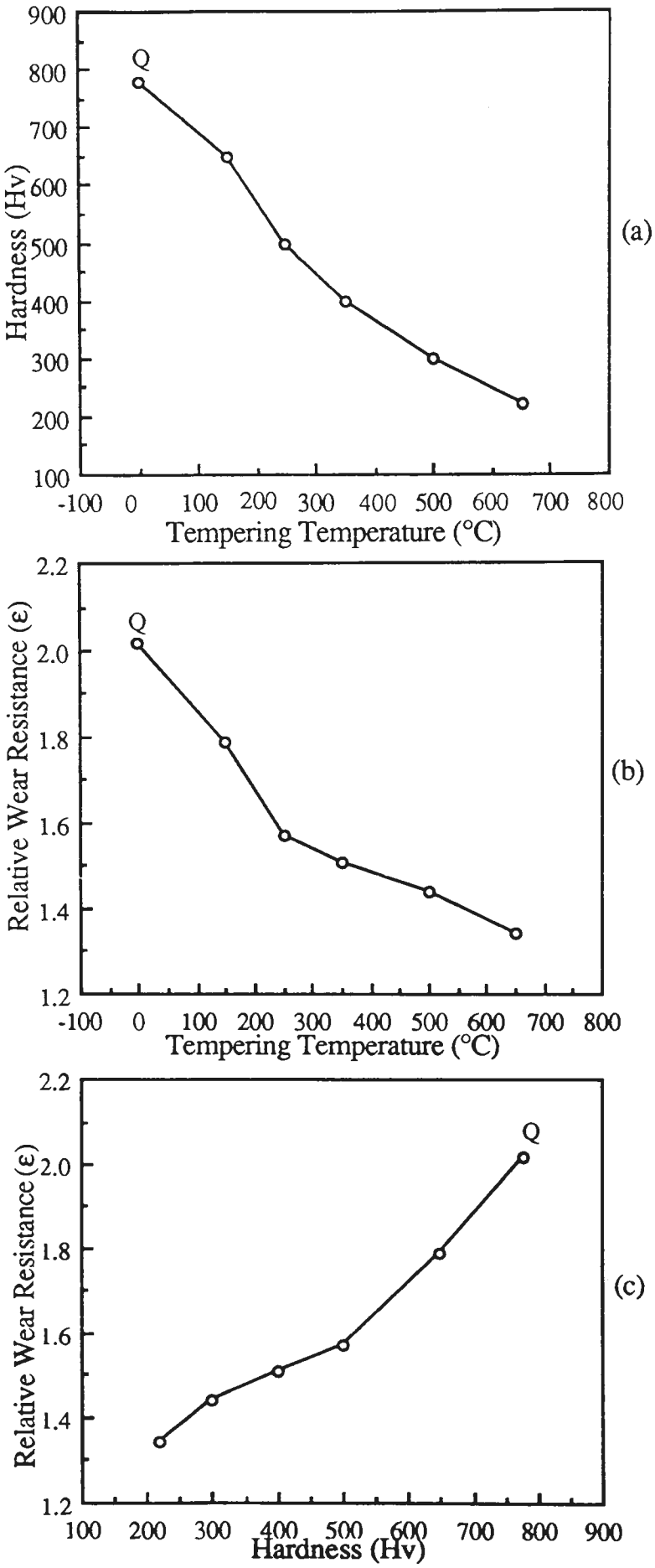

Fig.7.10 Diagrams showing relationships between: (a) hardness and tempering temperatures, (b) relative wear resistance and tempering temperature and (c) relative wear resistance and hardness for 0.75%C steel in the quenched (Q) and quenched and tempered conditions. Wear test condition: V=50mm/s, L=20N and X=6m, 180# silicon carbide paper.

7.2.2.2 Quenching, Tempering and Austempering

The relative wear resistance as functions of carbon content and of hardness for quenched structures is shown in Fig.7.9, and the amount of retained austenite related to the carbon content measured by computer-aided image analysis and by liner intercept analysis is shown in Table 7.2.

For the 0.75%C steel in the quenched and in the quenched and tempered conditions, hardness decreased non-linearly with tempering temperature, as shown in Figs.7.10(a) and (b). Consequently, relative wear resistance increased non-linearly with hardness in three stages for which the increasing rate was highest for stage III (>Hv500) and least for for stage II (from Hv300 to Hv500), as shown in Fig.7.10(c).

An austempered bainitic structure in the 0.75%C steel had a higher relative wear resistance than the quenched and tempered martensitic structure at the same hardness level; see Fig.7.11.

7.2.2.3 Wear Resistance, Hardness and Microstructure

Figure 7.11 shows the inter-relationships between wear resistance, hardness and microstructure. It is clear that, for the same hardness and carbon content less than 1.0%, bainite had the highest wear resistance followed by the quenched and tempered structures and then the annealed structures; additionally, for tempered martensite, the higher the carbon content, the higher was the relative wear resistance.

For specimens of the 1.2%C steel with the same hardness level, the annealed structure had the highest relative wear resistance, followed by tempered martensite and the spheroidized structure.

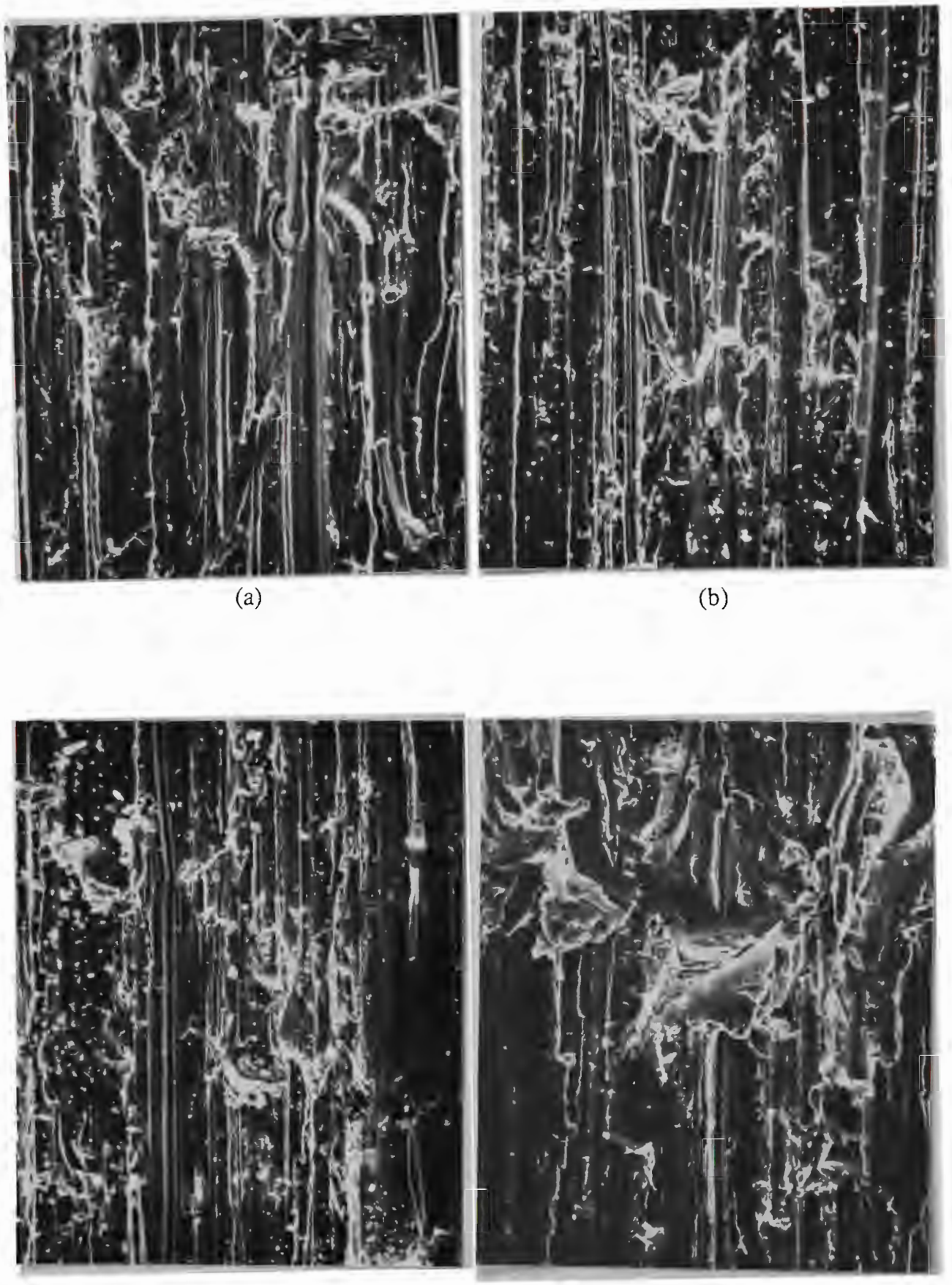

Fig.7.12 Scanning electron micrographs showing topography of wear surface for 0.75%C steel in: (a) annealed, (b) quenched, (c) quenched and 250°C tempered and (d) quenched and 650°C tempered conditions. X500. Wear test condition: V=50mm/s, L=20N and X=6m, 180# silicon carbide paper.

7.2.3 Wear Debris

7.2.3.1 Topography of Wear Surface

Wear topography of annealed steels shows that the lower the carbon content, the larger the amount of material that flowed plastically; while the higher the carbon content, the more fracture cracking that was observed. No significant differences in wear topography were observed between the steels 0.38%C and 0.45%C, the steels 0.58%C and 0.75%C, or the steels 1.2%C and 1.4%C, indicating that the transition from the plastic flow to the fracture cracking was gradual. The wear topography of annealed 0.75%C steel is shown in Fig.7.12(a).

For the quenched and 650°C tempered 0.75%C steel specimens, of which Fig.7.12(d) shows that cut chips were formed on the abraded surface, the topography was similar to that for the corresponding annealed specimens, but with more fracture debris on the worn surface of the specimen of the 1.2%C steel, and more plastic flow on the specimen of the 0.38%C steel.

For the quenched and tempered specimens at the hardness level of Hv500, fewer cut chips, with the smaller size, were produced during the abrasion process, compared with those on the 650°C tempered specimens. Figure 7.12(c) shows wear topography of the 250°C tempered specimen of 0.75%C steel, which was very similar to the topography of the specimens of the 200°C tempered 0.38%C steel, 250°C tempered 1.2%C steel, and the 250°C austempered 0.75%C steel.

For quenched specimens, the large number of fragments of debris on the worn surface (Fig.7.12(b)) indicated that fracture cracking occurred during the wear process. The occurrence of fracture in specimens of the 0.38%C steel and the 1.2%C steel was similar to the occurrence in the 0.75%C steel.

(a) (b)

Fig.7.16 Scanning electron micrographs showing wear chips from annealed carbon steels: (a) machined chip with serrations at one surface, annealed 0.38%C, and (b) cut chip with ploughed prow head, bainitic 0.75%C. X500. Wear test condition: V=50mm/s, L=20N and X=6m, 180# silicon carbide paper.

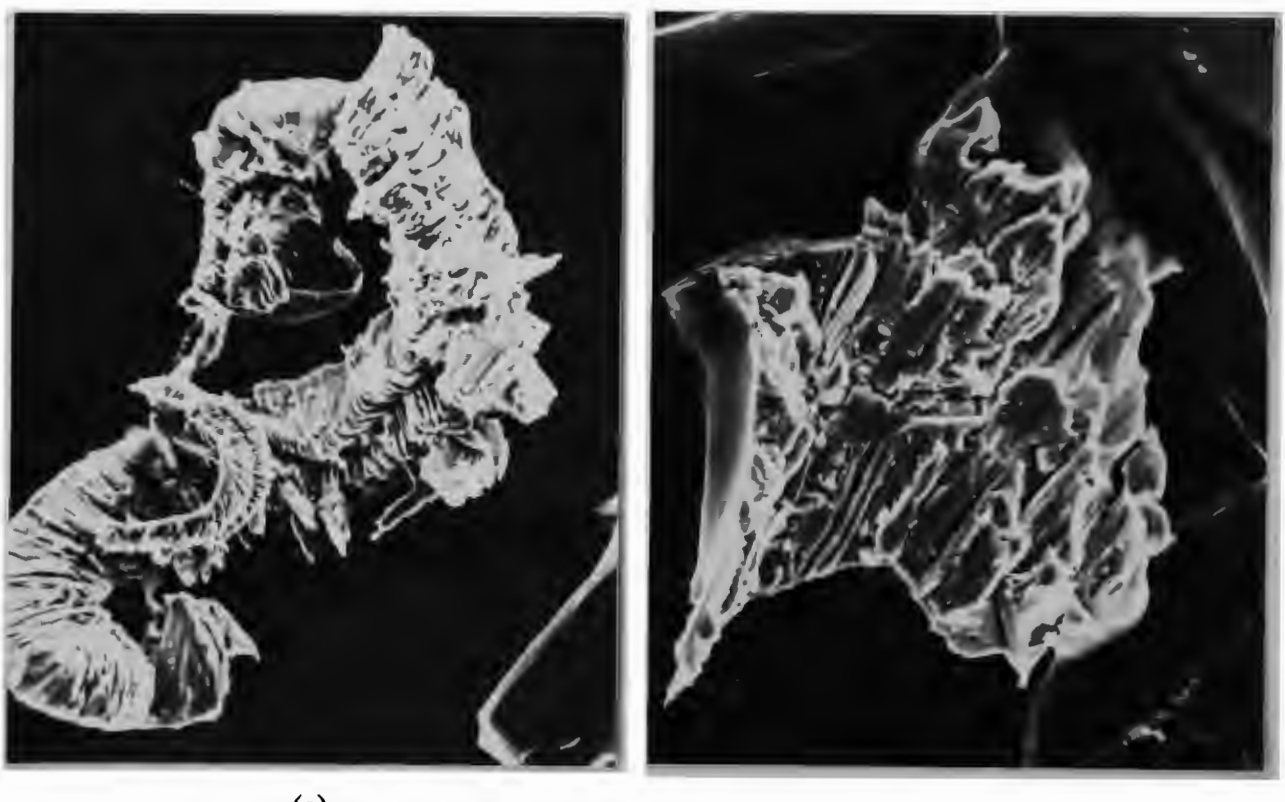

(a) (b)

Fig.7.17 Scanning electron micrographs showing: (a) cut and side-formed cut chips for 0.75%C tempered martensitic specimen and (b) fracture debris for annealed 1.2%C. X700. Wear test condition: V=50mm/s, L=20N and X=6m, 180# silicon carbide paper.

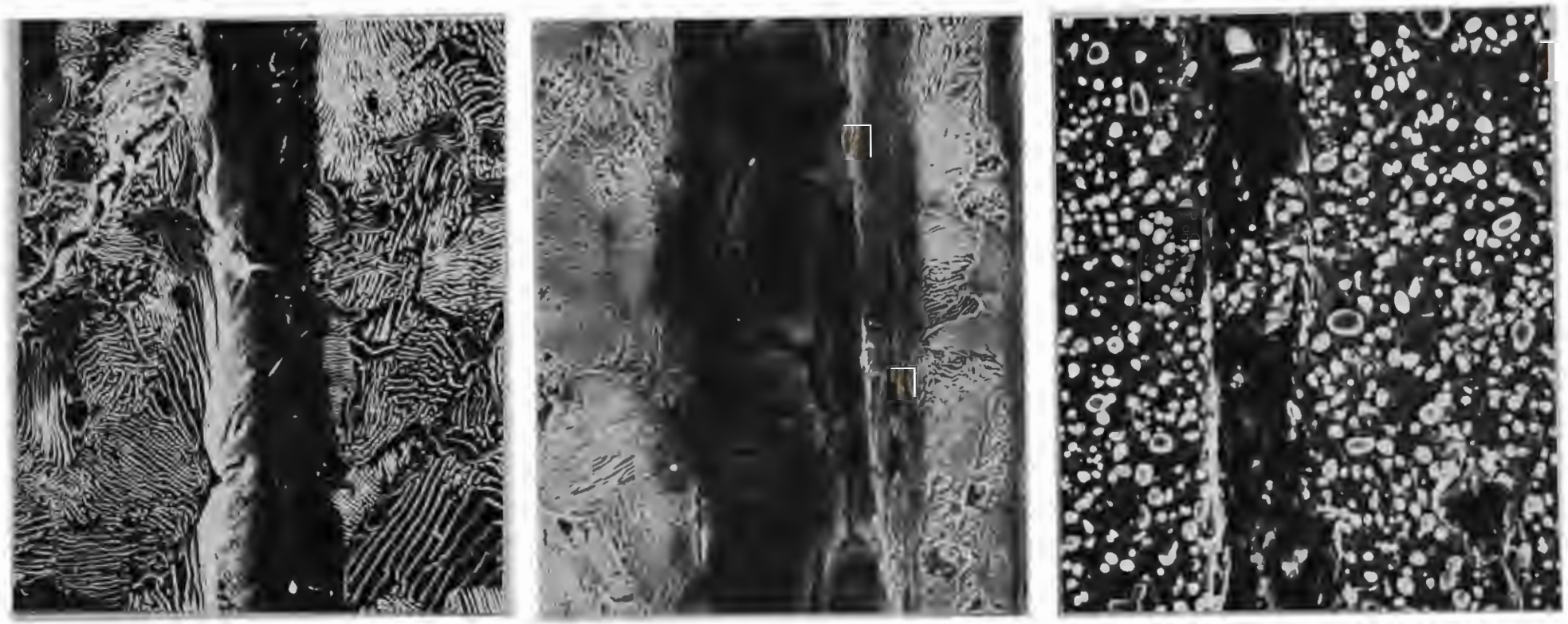

(a) (b) (c)

Fig.7.15 Scanning electron micrographs showing abrasion grooves for carbon steels: (a) cracking along cementite network in annealed 1.2%C steel, (b) cracking along cementite network at the bottom of a groove in annealed 1.4%C steel and (c) small particles of cementite in spheroidized 1.2%C steel. X1.5K. Wear test condition: V=50mm/s, L=20N and X=6m, 180# silicon carbide paper.

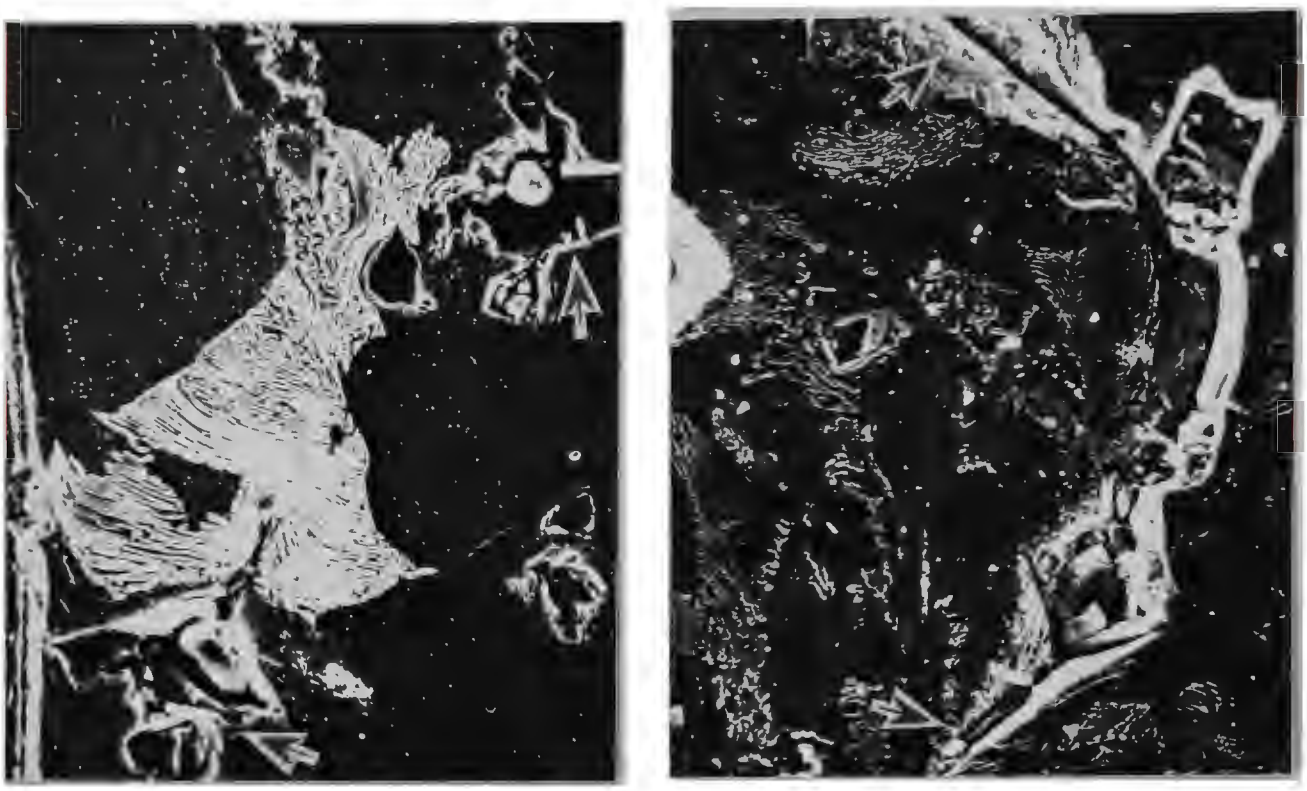

(a) (b)

Fig.7.14 Scanning electron micrographs showing microcracking at the bottom of abrasion grooves for annealed steels containing: (a) 0.10%C and (b) 0.38%C; arrows indicate microcracking loci. X1.2K. Wear test condition: V=50mm/s, L=20N and X=6m, 180# silicon carbide paper.

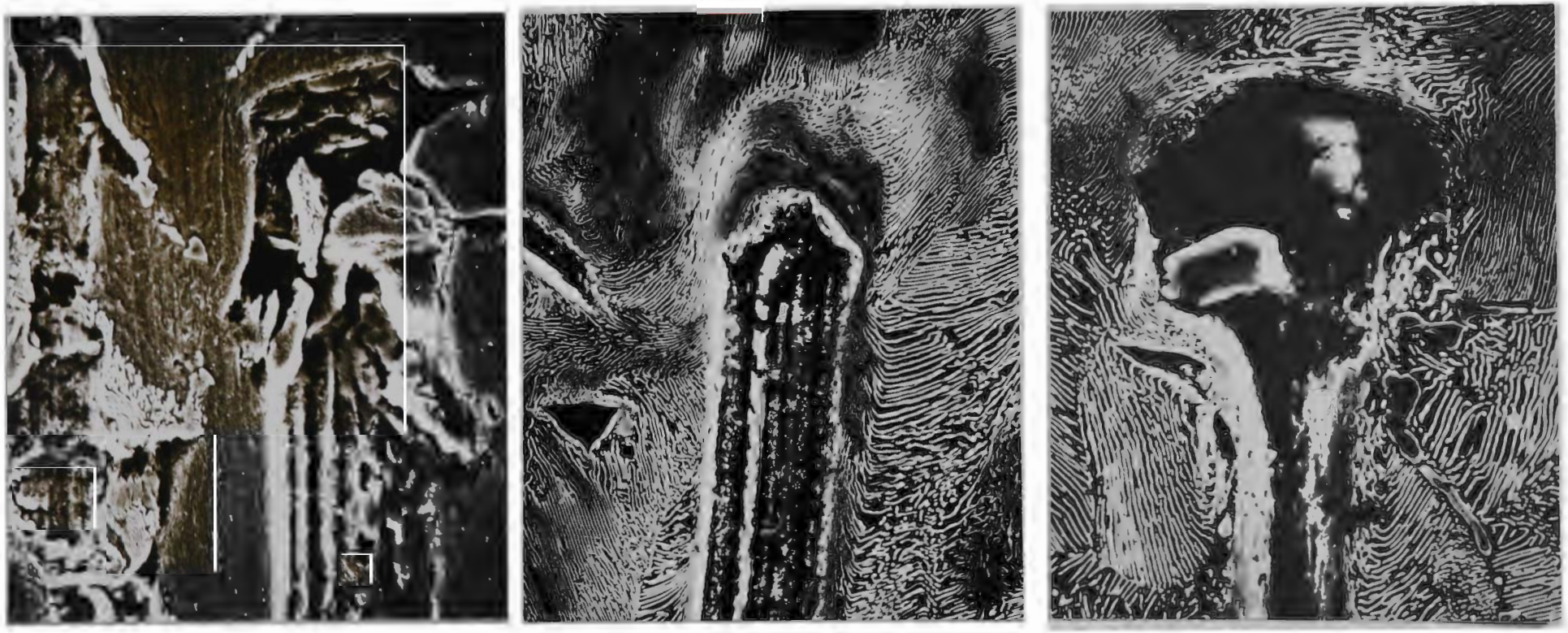

(a) (b) (c)

Fig.7.13 Scanning electron micrographs of worn subsurfaces of annealed steels showing abrasion groove ends for (a) 0.10%C, (b) 0.75%C and (c) 1.2%C. X1.0K. Wear test condition: V=50mm/s, L=20N and X=6m, 180# silicon carbide paper.

7.2.3.2 Microploughing, Microcutting and Microcracking

Scanning electron microscopical observations of the subsurface, which is the surface-layer just under the wear surface, was observed on the taper section for annealed specimens and indicates that the abrasion grooving mechanism varied with carbon content (Fig.7.13). It is evident that for a specimen with very low carbon level (0.10%C steel), the main wear mechanism was microcutting, but significant microploughing was involved in producing the large abrasion groove, as shown in Fig.7.13(a). Additionally, microcracking occurred at the bottom of the groove, and microcracking loci were halted at, or avoided, the pearlitic colonies, as shown in Fig.7.14.

For the pearlitic specimen of 0.75%C steel, material was mainly removed by microcutting characterized by a sharp ended groove, Fig.7.13(b), together with some microploughing. It appears that in the thin plastic deformation zone, the ferritic lamellae were deformed more severely than the cementite lamellae. For hypereutectoid steels, the abrasion groove was shallow and the deformed zone was very thin; occasionally, microcracking occurred along the grain boundary allotriomorphs of cementite (Fig.7.15(a)), and spalling could be observed at the groove end, Fig.7.13(c). Further, the higher the carbon content, the severer the microcracking that occurred, as shown in Fig.7.15(b)).

Analyses of wear debris for the annealed specimens were consistent with the study of the wear surface topography and the subsurface, as shown in Fig.7.16. The most common debris was ribbon-shaped wear chips with a ploughed prow head, a smooth surface on the tool (abrasive particle) side and serrations on the other surface. Also, cut chips together with side-formed cut chips, Fig.7.17(a), and flattened fracture debris (Fig.7.17(b)) were observed. Additionally, microcracking along grain boundary

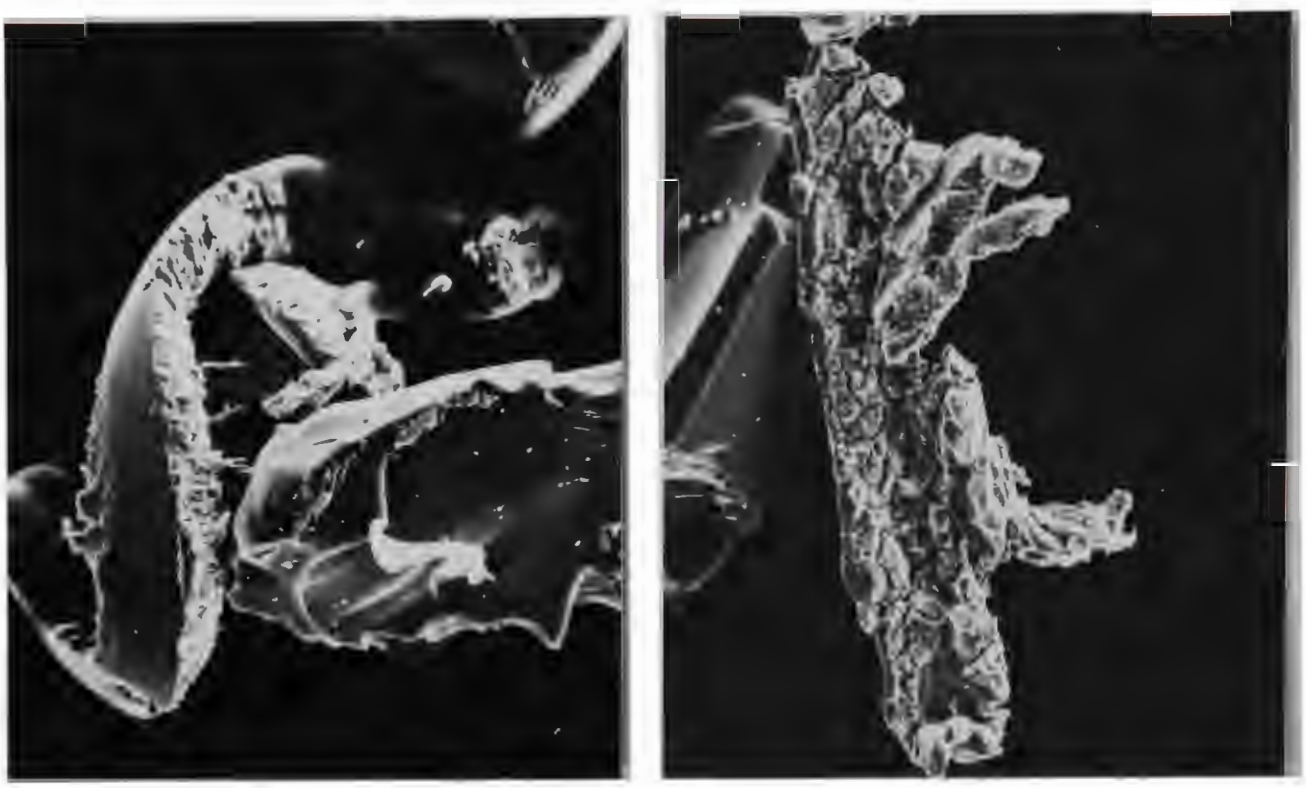

(a) (b)

Fig.7.18 Scanning electron micrographs showing: (a) cut chip and (b) fracture debris for the spheroidized 1.2%C steel. X400. Wear test condition: V=50mm/s, L=20N and X=6m, 180# silicon carbide paper.

cementite was also detected at the fracture debris from the annealed specimen of 1.2%C steel, as shown in Fig.7.17(b).

For the spheroidized structure, cutting grooves were clearly observed at the subsurface of the taper section specimen; and spheroidal carbides were often removed during the first wear pass as the spheroidal carbides were much smaller than the groove width, as shown in Fig.7.15(c). Additionally, scanning electron microscopical study of wear chips for the spheroidized structure (Fig.7.18) showed that both cut and fracture debris was larger than for the annealed structure (Figs.7.16 and 7.17).

Wear topography observations and wear debris analyses for the 0.75%C steel in the quenched, the quenched and low temperature tempered and the austempered conditions, indicated that microcutting was the predominant mechanism for metal removal in all cases. For the quenched and the quenched and low temperature tempered specimens of 0.38%C and 1.2%C steels, both wear topography and debris showed no significant differences compared with the 0.75%C steel and the predominant mechanism was therefore microcutting.

Further, it appears that, for most cases, microcracking made only a the minor contribution to metal removal, as the fracture debris, such as shown in Fig.7.17(b), was observed to be a small fraction of the total wear debris.

7.2.3.3 Plastic Deformation

For the annealed structures, scanning electron microscopical observation of the worn subsurface indicated that the amount of plastically deformed material decreased with increase in carbon content, as shown in Fig.7.13.

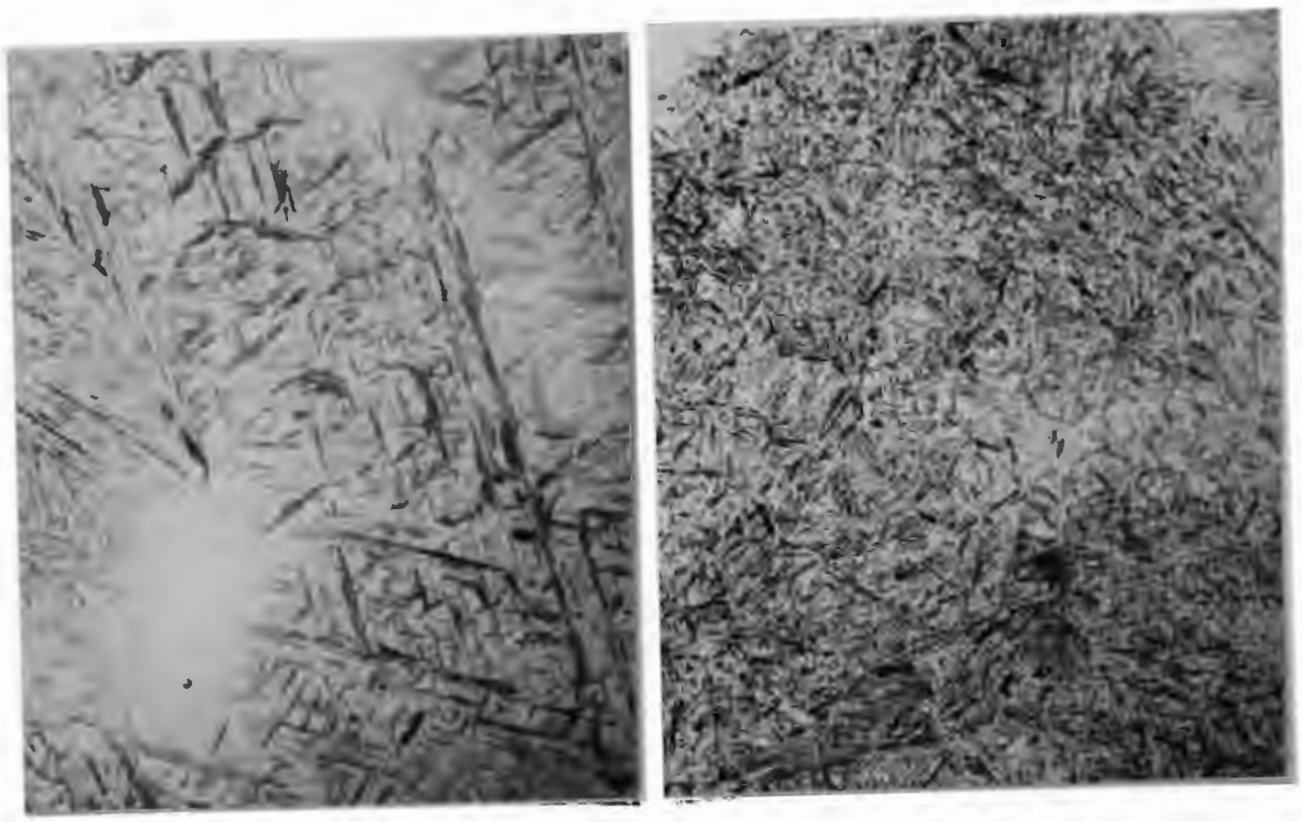

(a) (b)

Fig.7.20 Optical photomicrographs showing microstructures for specimens of Ni-Cr-Mo-C steel after: (a) single-quenching, specimen 10; and (b) double-quenching, specimen 20. X250. Etchant: 5% nital.

(a) (b)

Fig.7.21 Transmission electron micrographs showing microstructures of Ni-Cr-Mo-C steel: (a) martensite and bainite in single-quenched specimen and (b) martensite and spheroidal carbides in double-quenched specimen. X30K.

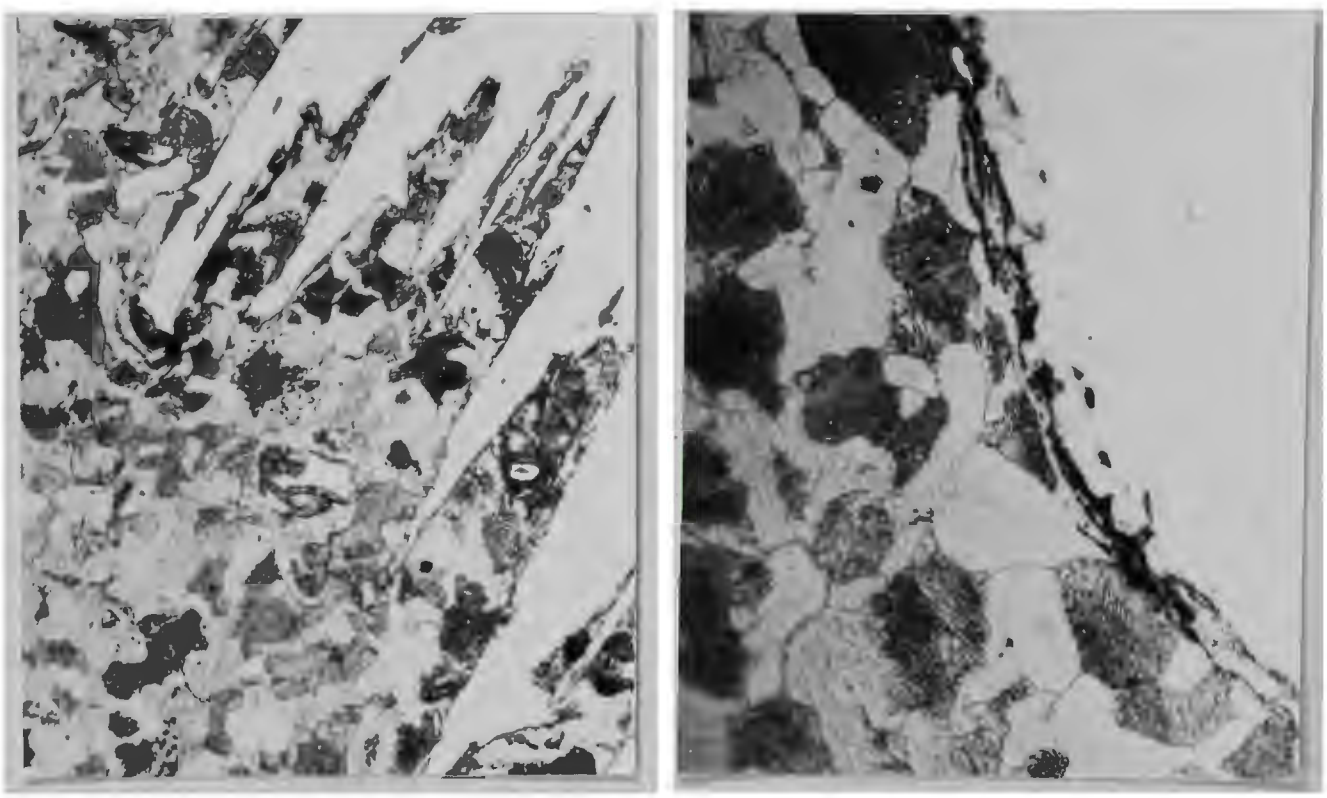

(a) (b)

Fig.7.19 Optical photomicrographs of wear subsurface showing plastic deformation for the annealed 0.38%C steel: (a) 5° taper section and (b) longitudinal section at the bottom of the abrasion groove. X600. Etchant: nital. Wear test condition: V=50mm/s, L=20N and X=6m, 180# silicon carbide paper.

Optical microscopical observation of the 5° taper surface showed the plastic deformation took place during abrasion process (Fig.7.19(a)), which was consistent with scanning electron microscopy of the worn subsurface. Also, optical microscopical observation of a longitudinal section of the abrasion grooves showed the true thickness of the deformation zone and confirmed the presence of a plastic zone under the groove, as shown in Fig.7.19(b). The dark layer on the surface is the copper coating which, together with nickel coating, protects the worn surface; the banded pearlitic lamellae shows that plastic deformation occurred during abrasion.

7.3 TOOL STEELS

7.3.1 Ni-Cr-Mo-C Tool Steel

An air-hardening Ni-Cr-Mo-C tool steel was used to study the effects of heat treatment on wear resistance. The specimens were either single-quenched or double-quenched from 900°C followed by tempering at 100°C, 200°C, 300°C and 400°C, as described in §6.3.2 and shown in Table 6.7. The heat treatment associated with best wear resistance for this steel can be deduced from wear tests carried out on these specimens. Abrasive papers used for wear testing of this steel were 180# silicon carbide and garnet.

7.3.1.1 Microstructure and Carbide Characteristics

Photomicrographs of single-quenched and double-quenched specimens are shown in Fig.7.20. It is clear that the martensitic plates in the single-quenched specimen, 10, were much larger than those in the double-quenched specimen, 20. Transmission electron microscopical examination showed that the single-quenched specimen contained bainite in addition to the martensite, Fig.7.21(a), while the double-quenched specimen, 20, contained martensite together with spheroidal carbides up to 60nm in diameter (Fig.7.21(b)); no bainite could be detected in the structure.

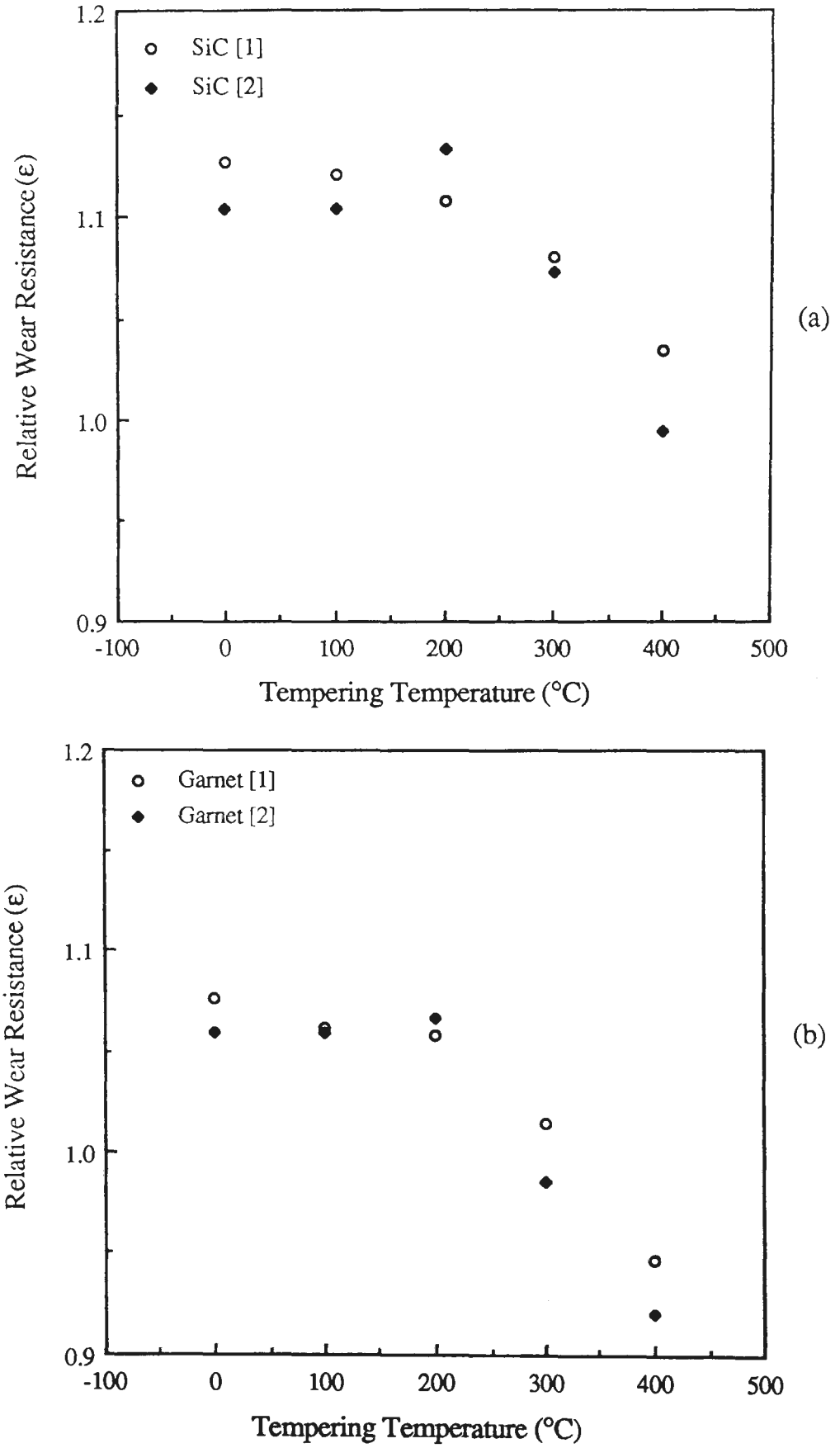

Fig.7.23 Diagram showing relative wear resistance as a function of tempering temperature for single-quenched [1] and double-quenched [2] specimens of Ni-Cr-Mo-C steel, 180# abrasive paper of: (a) silicon carbide and (b) garnet. Wear test condition: V=50mm/s, L=20N and X=6m.

(a) (b)

Fig.7.22 Transmission electron micrographs showing carbide morphologies for 200°C tempered specimens of Ni-Cr-Mo-C steel: (a) single-quenched specimen 12 and (b) double-quenched specimen 22. X80K.

Transmission electron microscopical study of the 100°C tempered specimens, 11 and 21, showed the microstructure to be martensite together with bainite in the single-quenched specimen, 11, and martensite together with carbides in the double-quenched specimen, 21. Both structures were similar to the quenched structures, 10 and 20, as described above.

The 200°C tempered specimens, 12 and 22, comprised tempered martensite or tempered bainite (which were not distinguishable) together with carbides. In specimen 12, the carbides were predominantly lath shaped, 5 to 10 nm in thickness, as shown in Fig.7.22(a), and in specimen 22, were predominantly spheroids, 5 to 10 nm in diameter, Fig.7.22(b).

The microstructures of the 300°C tempered specimens, 13 and 23, were also tempered martensite, or bainite, with carbides which were similar in the shape to those present in the 200°C tempered specimens, being predominant lath-shaped in the single-quenching specimen, 13, and predominantly spheroidal in the double-quenched specimen, 23. However, the carbides in the 300°C tempered specimens had grown or coalesced to an average characteristic dimension of about 50nm.

Transmission electron microscopy of the 400°C tempered specimens, 14 and 24, indicated that the carbides in the single-quenched specimen, 14, were much smaller than those in the double-quenched specimen, 24.

7.3.1.2 Heat Treatment

Figure 7.23 shows the relative wear resistance as a function of tempering temperature for abrasion on silicon carbide and garnet papers. It is clear for both abrasives that, for the single-quenched specimens, relative wear resistance decreased non-linearly with

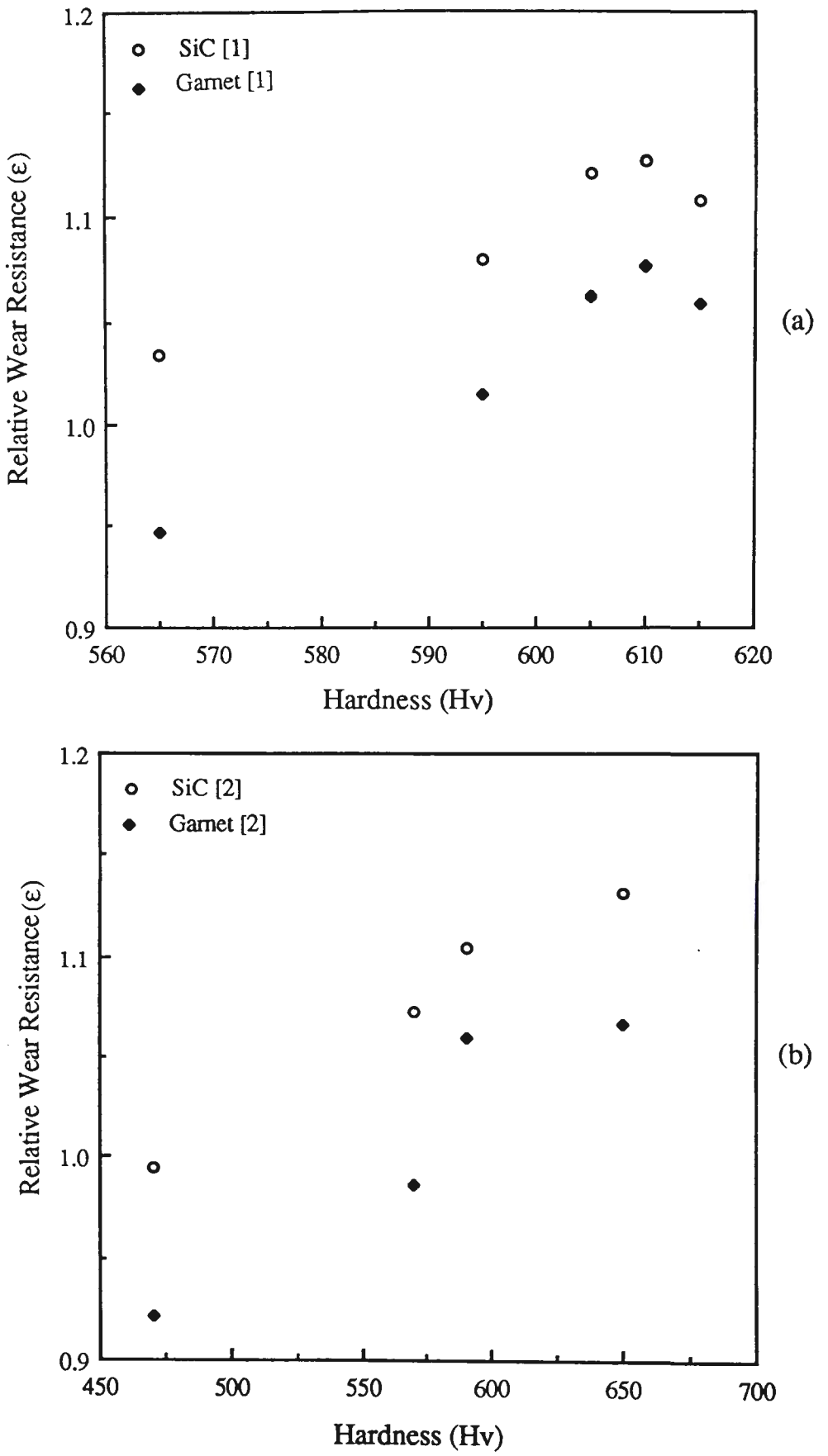

Fig.7.25 Diagrams showing relative wear resistance as a function of hardness for the specimens of Ni-Cr-Mo-C steel after: (a) single-quenching [1] and (b) double-quenching [2]. Wear test condition: V=50mm/s, L=20N and X=6m, 180# silicon carbide and garnet.

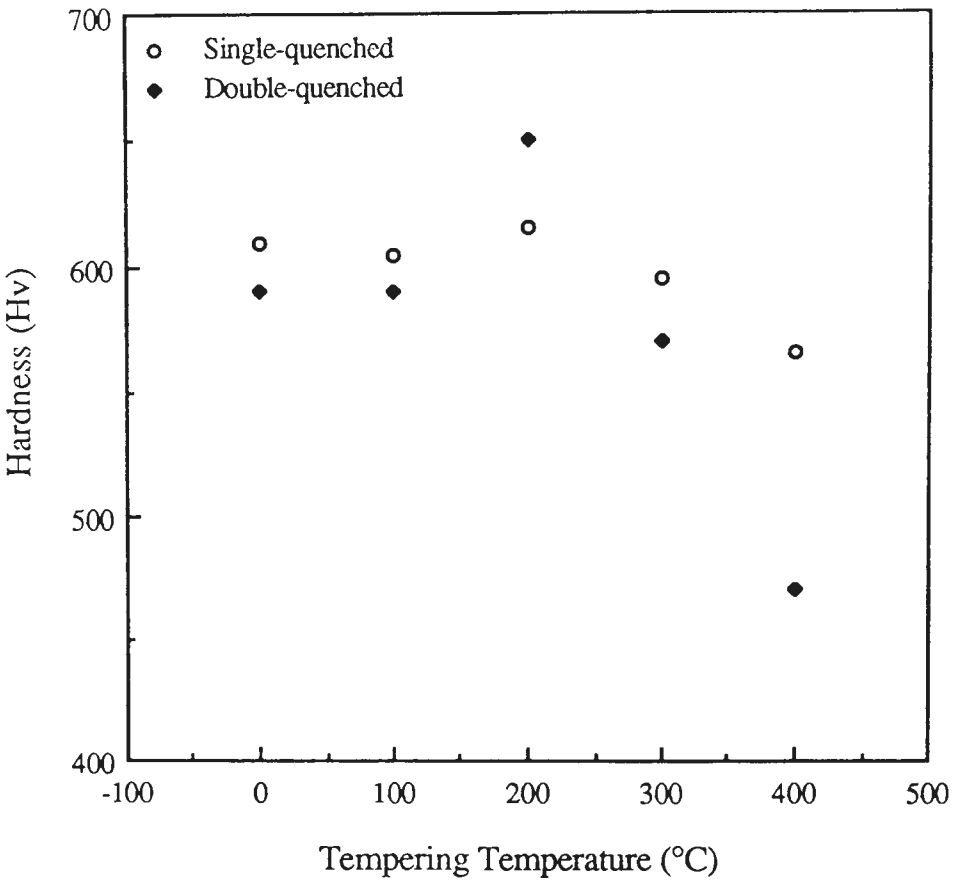

Fig.7.24 Diagram showing the relationship between hardness and tempering temperature for single- and double-quenched specimens of Ni-Cr-Mo-C steel.

tempering temperature, while for double-quenched specimens, relative wear resistance increased with tempering temperature to a maximum value at about 200°C, then decreased with further increase in tempering temperature. The maximum value of ε for the double-quenched specimen was higher than for the single-quenched specimen. Further, the results shown in Fig.7.23 indicated that relative wear resistance was also dependent upon the abrasive medium, being higher for silicon carbide (Hv3200[144]) than for garnet (Hv1360[144]).

7.3.1.3 Hardness

Figure 7.24 shows the relationship between hardness and tempering temperature. Clearly, the maximum hardness occurred at about 200°C for both single-quenched and double-quenched specimens, and the maximum value for the double-quenched specimen, 22, was higher than for the single-quenched specimen, 12. Additionally, the decreasing rate of hardness with increase in tempering temperature was higher for double-quenched specimens than for single-quenched specimens in the temperature range of 200°C to 400°C.

Figure 7.25(a) shows that relative wear resistance had a maximum value at a hardness of about Hv610 for single-quenched specimens. For double-quenched specimens (Fig.7.25(b)), relative wear resistance increased non-linearly with hardness at least to Hv660, the highest value available in the study. Additionally, the form of relationship curves between relative wear resistance and hardness for both single-quenched and double-quenched specimens was not influenced significantly by the abrasives, although there were difference in actual values of ε.

7.3.1.4 Wear Debris

Scanning electron microscopical study of the worn surface topography for the specimens of the Ni-Cr-Mo-C steel showed that the higher the temperature, the more

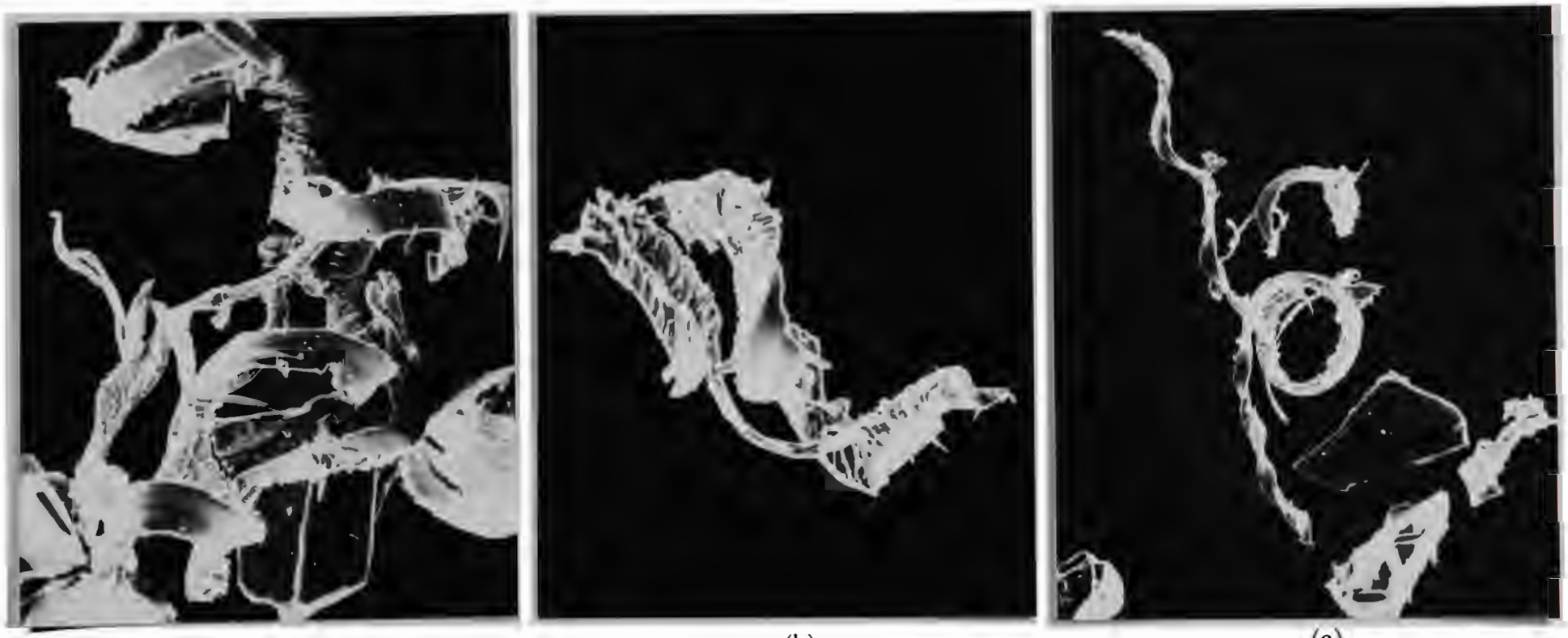

Fig.7.27 Scanning electron micrographs showing wear debris from specimen 12 of Ni-Cr-Mo-C steel: (a) ribbon-like microcut chip, (b) side-formed cut chips as precursors for large cut chips and (c) side-formed cut chips attached at sides of large cut chips. X350. Wear test condition: V=50mm/s, L=20N and X=6m, 180# silicon carbide paper.

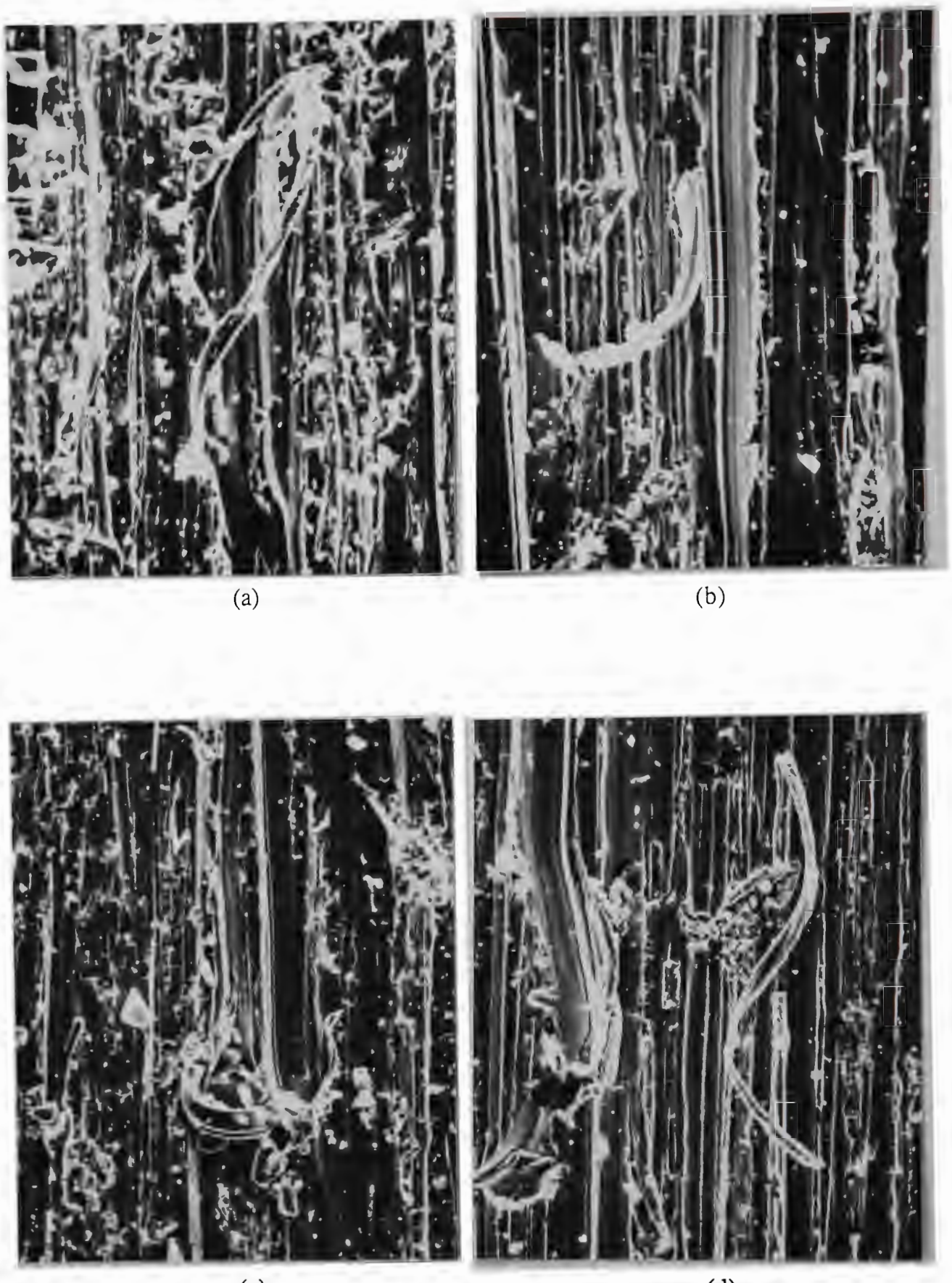

Fig.7.26 Scanning electron micrographs showing topography of wear surface for the specimens of Ni-Cr-Mo-C steel: (a) fracture debris and large cut chips in specimen 14, (b) side-formed cut chips in specimen 21, (c) cut chip in specimen 24, and (d) cut chip formed on built-up bulge in specimen 13. X500. Wear test condition: V=50mm/s, L=20N and X=6m, 180# silicon carbide paper.

fracture debris and large cut chips that were formed, Fig.7.26(a), while, the lower the temperature, the more side-formed cut chips that were formed, Fig.7.26(b). Microcutting was apparently the predominant mechanism for metal removal under conditions where the abrasive particle acted as a machining tool in cutting a large chip, and formed built-up bulges at the two edges of the groove and a prow at the end of the groove, Fig.7.26(c). The bulges were often cut by a following abrasive particle, as shown in Fig.7.26(d). Occasionally, a cutting abrasive particle fractured at the end of the groove to leave an embedded fragment (Fig.7.26(c)). Finally, there was no apparent difference in the wear behaviour which could be suggested by the worn surface topography for single-quenched and double-quenched specimens.

The abrasion groove formed by harder silicon carbide abrasive was slightly different from that formed by softer garnet abrasive under the same test conditions. In the case of garnet particles, there seemed to be no 'sharp' cutting action and fracture often occurred during the abrasion process. Additionally, less fracture debris was observed on the wear surface topography.

Scanning electron microscopical study of the wear debris from silicon carbide paper, confirmed that the dominant mechanism for metal removal was microcutting characterized by long ribbon shaped chips as shown Fig.7.27(a). The side-formed cut chips attached at the end of the large cut chips, (Fig.7.27(b)), or at sides of the large cut chips (Fig.7.27(c)), indicate that side-formed cut chips were either precursors or by-products for the main cutting action. Wear debris from abrasion by garnet paper were larger in size and less curled compared with the debris from silicon carbide abrasive paper. Significantly, cutting was the dominant mechanism for chip formation, where the chip was smooth at the face towards the machining tool (abrasive particle) with clear serrations at the other surface. Occasionally, a ploughed prow was apparent at the head of the cut chip.

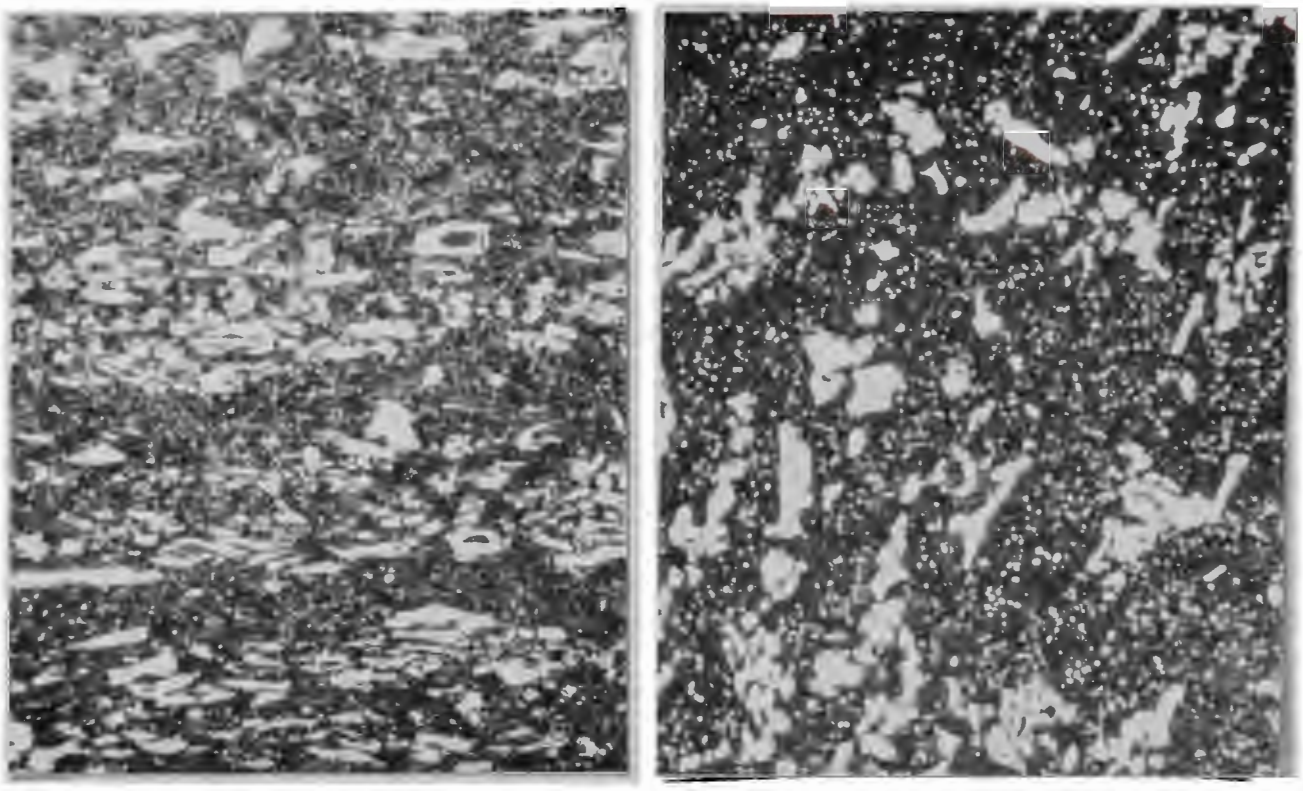

(a) (b)

Fig.7.30 Optical photomicrographs showing microstructures of high-carbon high-chromium steels: (a) Chrome and (b) XW-5. X250. Etchant: Picric-HCl-Ethanol.

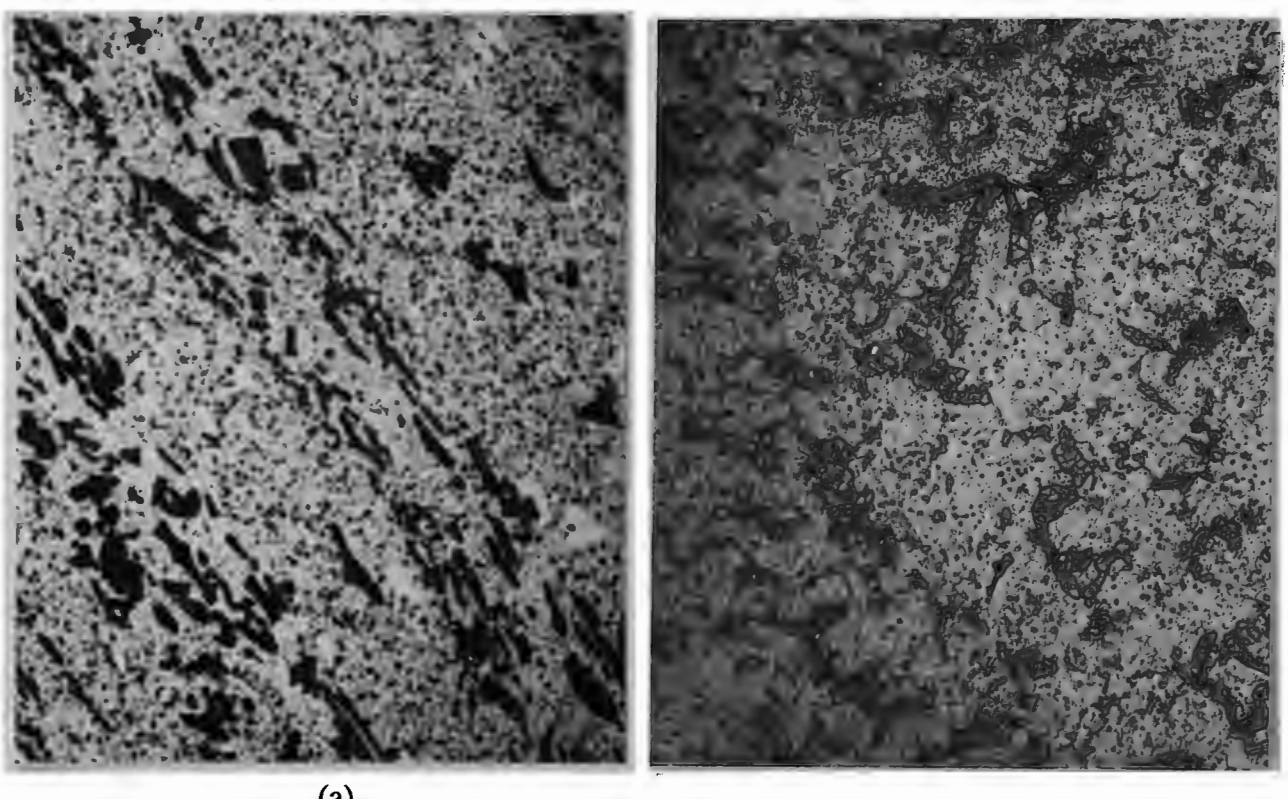

(a) (b)

Fig.7.31 Optical photomicrographs showing massed carbides in high-carbon high-chromium steels: (a) directional M_7C_3 (dark) and VC (white) carbides in Chrome and (b) random M_7C_3 carbides in XW-5. X250. Etchant: NaOH-$KMnO_4$.

(a) (b) (c)

Fig.7.29 Scanning electron micrographs of worn abrasive papers showing wear debris: (a) in a crater in a silicon carbide particle; X850, (b) on the surface of a garnet particle; X400, and (c) in the gap between garnet particles; X700. Wear test condition: V=50mm/s, L=20N and X=6m, specimen 13 of Ni-Cr-Mo-C steel.

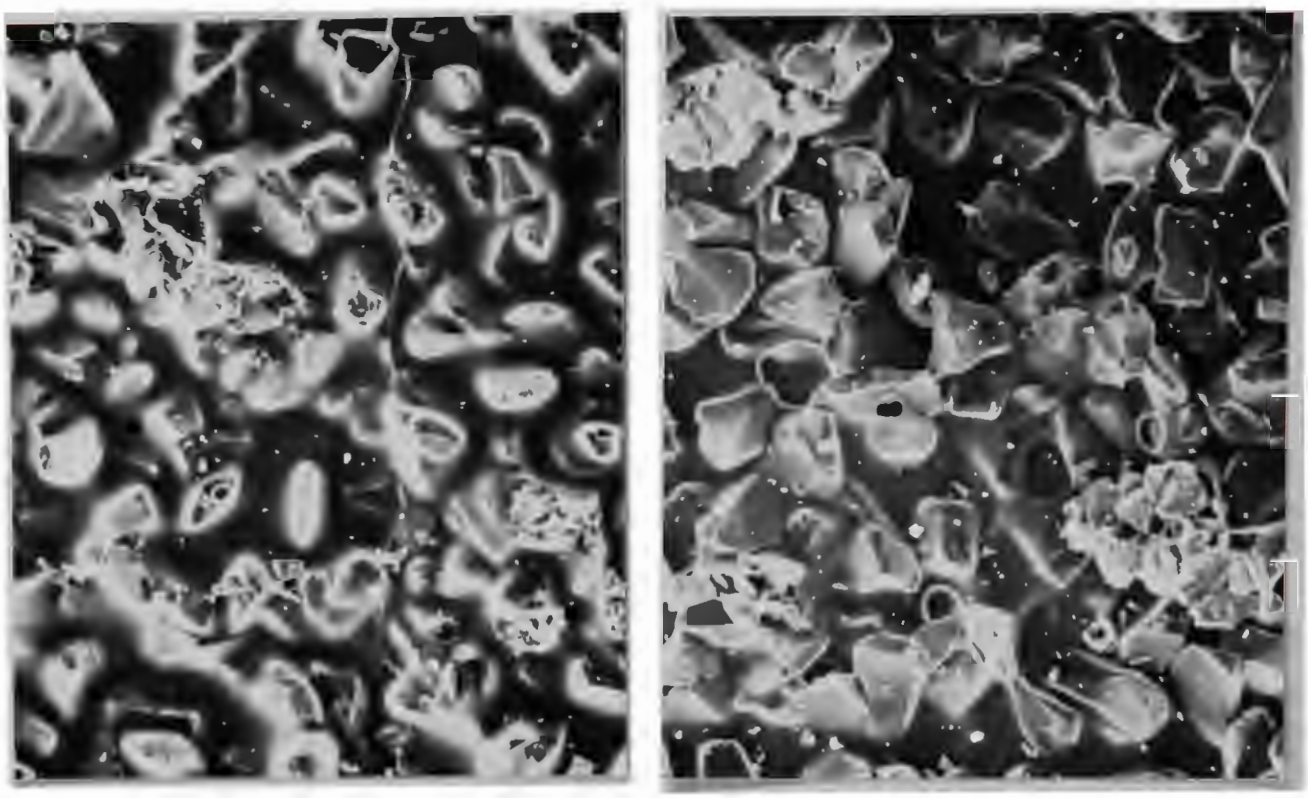

(a) (b)

Fig.7.28 Scanning electron micrographs of worn 180# abrasive papers: (a) silicon carbide and (b) garnet. X70. Wear test condition: V=50mm/s, L=20N and X=6m, specimen 13 of Ni-Cr-Mo-C steel.

Scanning electron microscopical study of worn silicon carbide and garnet abrasive papers showed presence of fracture debris, Fig.7.28. More fragments were present on the silicon carbide paper than on the garnet paper, and some wear debris was located in craters in the abrasive particles (Fig.7.29(a)), on the surface of abrasive particles (Fig.7.29(b), and in the spaces between abrasive particles (Fig.7.29(c)).

7.3.2 High-Carbon High-Chromium Steels

Two high-carbon high-chromium steels termed Chrome and XW-5, about which details are given in §6.3.2, were used to study the effect of composition on massed carbide type, and the consequential influence on wear resistance. Abrasive wear tests were carried out using 120# alumina that is the most close to the practical work condition, 180# silicon carbide and 180# garnet papers.

7.3.2.1 Microstructures

Optical microscopical examination of specimens of Chrome and XW-5 showed that microstructures of both steels were massed carbides associated with fine carbides in a matrix of tempered martensite, Fig.7.30.

7.3.2.2 Carbides

The massed carbides were distributed unidirectionally in Chrome and randomly in XW-5, as shown in Fig.7.30. The major dimension of the carbides was 3 to 10μm, while the secondary small carbides were less than 1μm in diameter, and the total volume fraction of carbides was estimated to be 30-40% for both alloys. Clearly, the massed carbides in Chrome had a more regular morphology than those in XW-5.

The photomicrographs shown in Fig.7.31 were obtained after etching with a special purpose reagent[144], and indicate that the massed carbides in Chrome were mixed

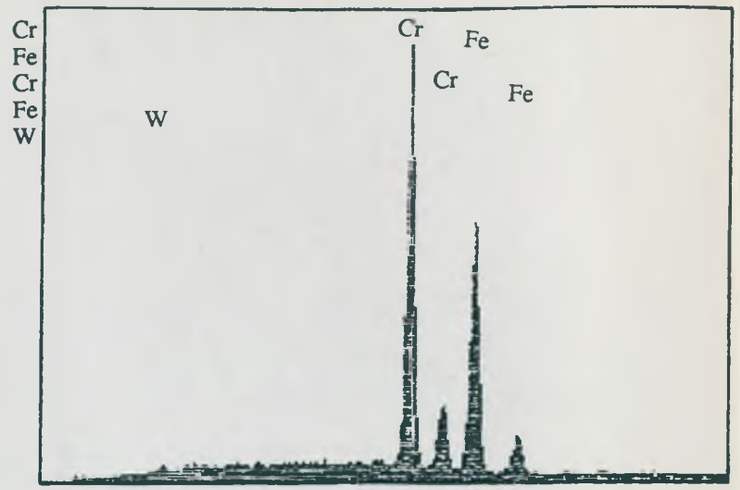

(a)

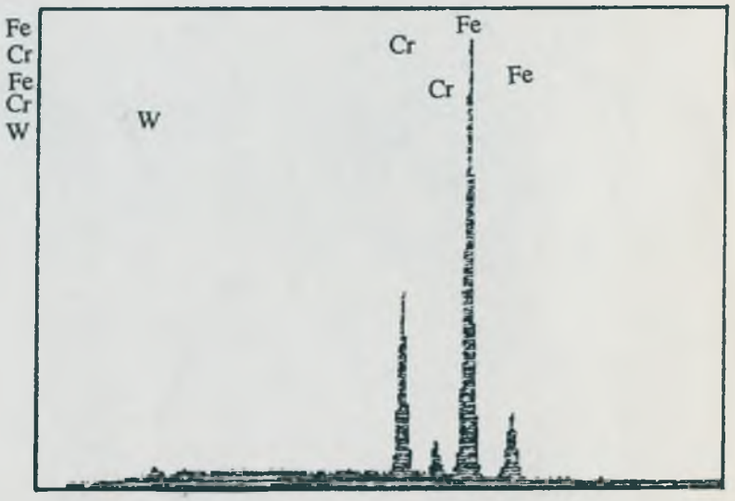

(b)

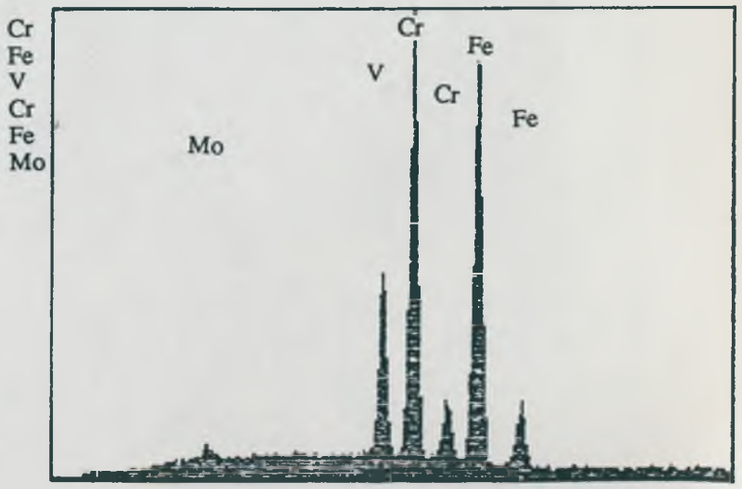

(c)

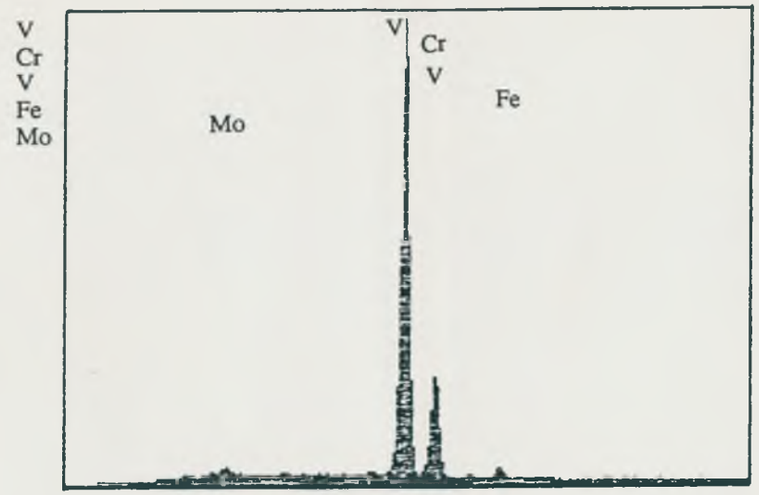

(d)

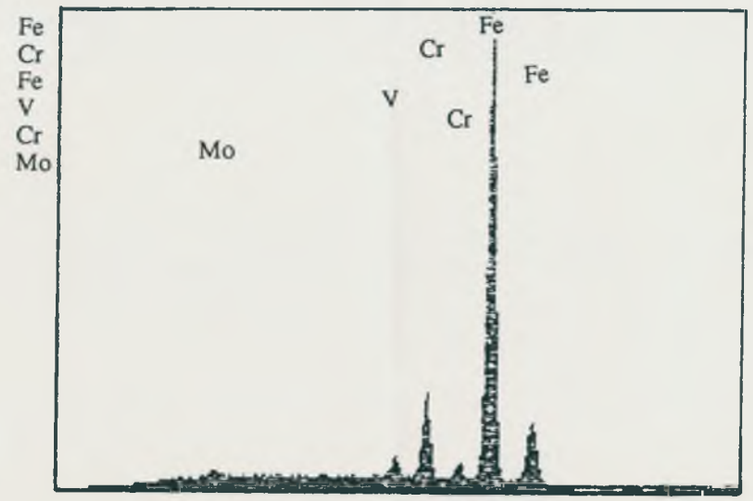

(e)

Fig.7.32 Energy dispersive X-ray capability maps showing typical carbides for high-carbon high-chromium steels: (a) massed carbides in specimen XW-5 and (b) small carbides in specimen XW-5, (c) massed carbides with high chromium in specimen Chrome, (d) massed carbides with high vanadium for specimen Chrome, (e) small carbides for specimen Chrome.

M_7C_3 (coloured purple under optical microscopy) and VC (unaffected), while those in XW-5 were unique M_7C_3 type.

Energy dispersive X-ray capability maps of typical carbides for both Chrome and XW-5 are shown in Fig.7.32 and the elements present and concentration determined by a computer aided semi-quantitative method are given in Table 7.4. It is clear from Fig.7.32 and Table 7.4 that, according to typical compositions of specific carbides[144], the massed carbides in XW-5 were Cr_7C_3 (containing up to 50%Fe), and those in Chrome were mixed Cr_7C_3 type and VC (containing more than 80%V). The small carbides (less than 1μm in diameter) were Fe_3C for both alloys.

Table 7.4 Chemical Composition of Carbides for Chrome and XW-5 (wt%)

Carbide	Cr	V	W	Mo	Fe	Carbide-type[144]
Massed (XW-5)	50.15	--	2.55	--	46.90	Cr_7C_3
Secondary (XW-5)	10.84	--	5.86	--	83.05	Fe_3C
Massed (Chrome)	31.94	13.36	--	4.19	49.96	Cr_7C_3
Massed (Chrome)	7.51	84.14	--	5.19	3.16	VC
Secondary (Chrome)	8.80	2.41	--	3.64	83.85	Fe_3C

The hardness of VC is higher than Cr_7C_3; Fe_3C has the lowest hardness, as shown in Table 5.2.

7.3.2.3 Wear Rate

Wear rates measured by mass loss for specimens of both alloys is presented in §7.1.1 in Fig.7.3.

7.3.2.4 Wear Debris

Scanning electron microscopical study of the wear topography indicated that microcutting was the major mechanism for abrasion groove formation; occasionally,

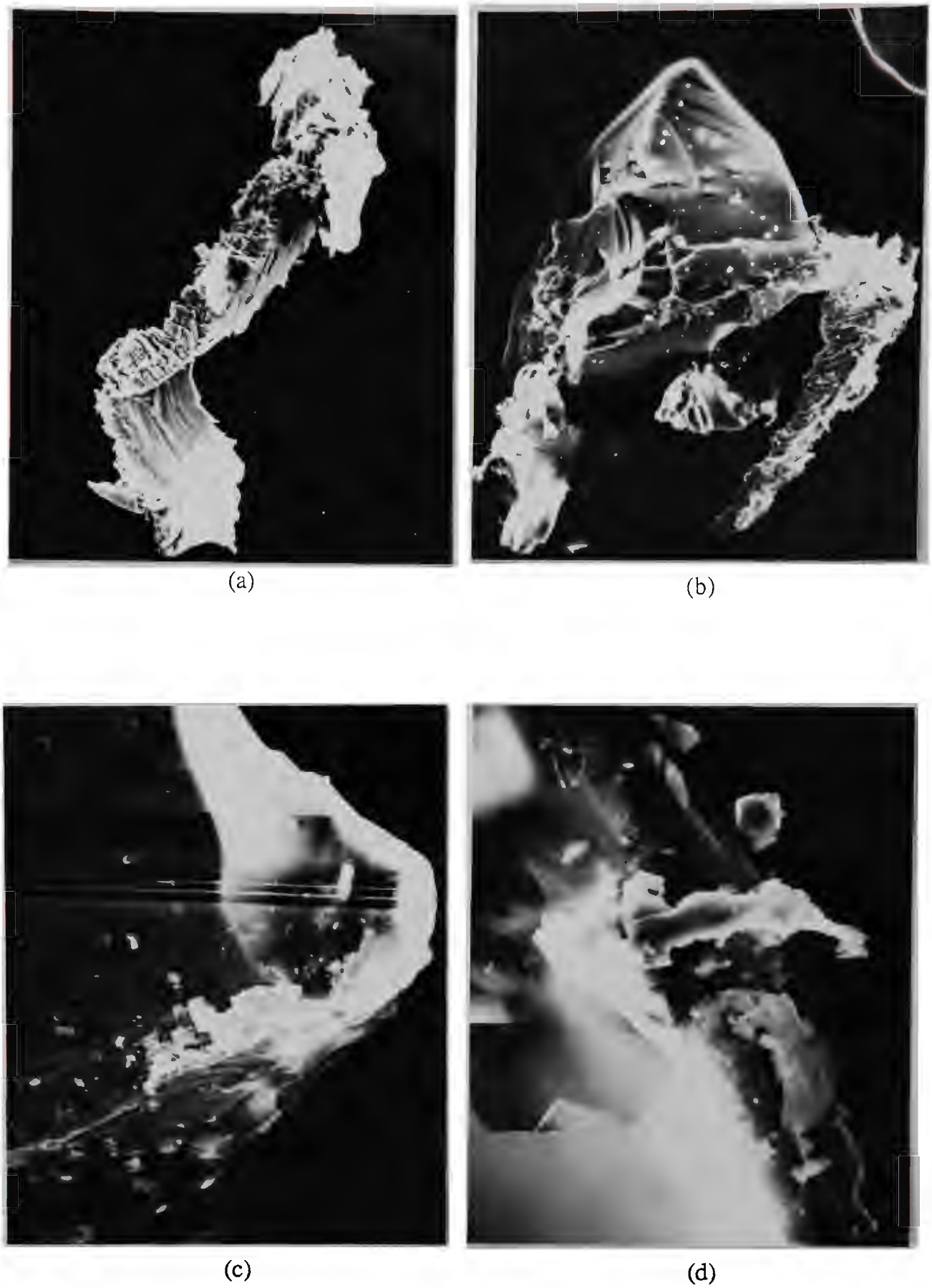

Fig.7.35 Scanning electron micrographs of wear debris for high-carbon high-chromium steels: (a) cut chip with prow ahead and serrations at one surface, XW-5; X450, (b) cut chip adhering to an abrasive particle, XW-5; X550, (c) built-up-edge formed on cutting area of the abrasive particle, Chrome; X1.5K, and (d) detached carbide, XW-5; X3.0K. Wear test condition: V=50mm/s, L=20N and X=6m, 120# grit alumina paper.

(a) (b)

Fig.7.33 Scanning electron micrographs of wear topography for high-carbon high-chromium steels showing abrasion grooves formed mainly by microcutting associated with microcracking for: (a) Chrome and (b) XW-5. X500. Wear test condition: V=50mm/s, L=20N and X=6m, 120# grit alumina paper.

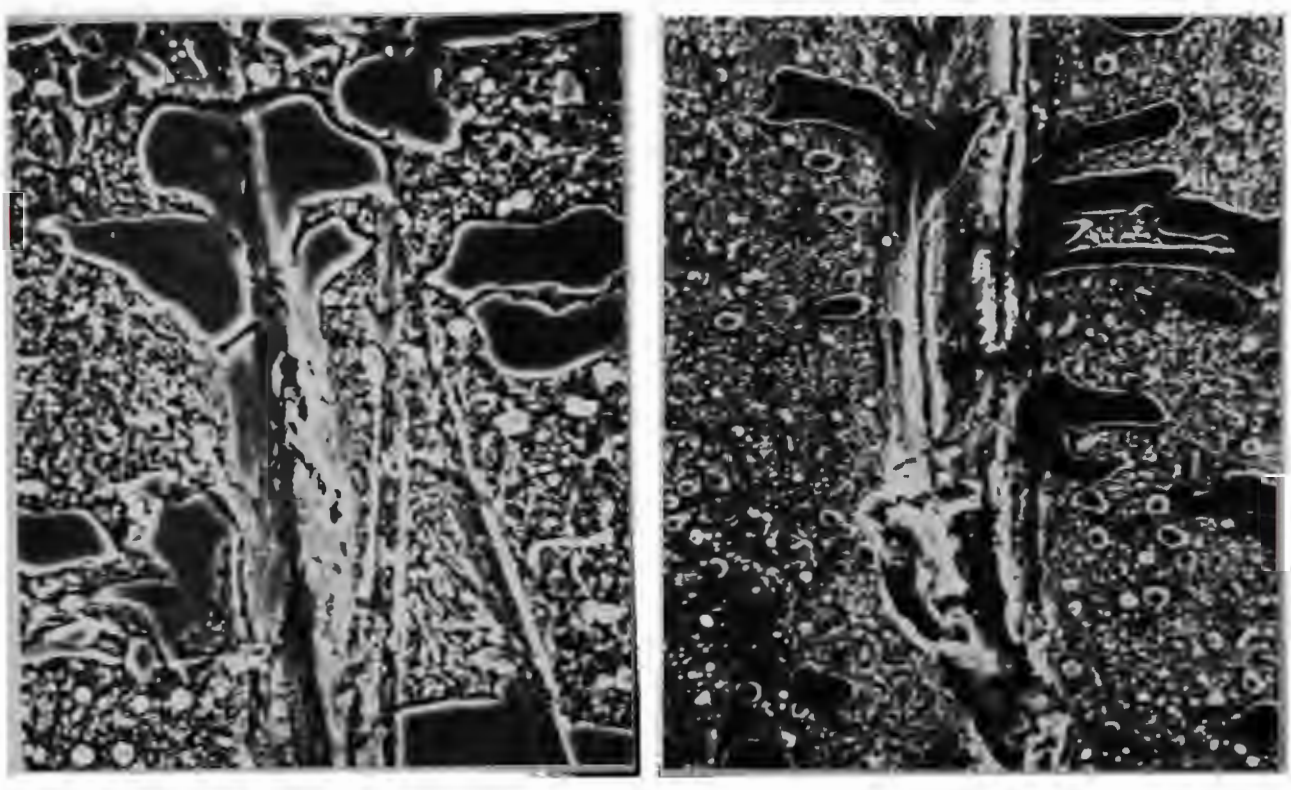

(a) (b)

Fig.7.34 Scanning electron micrographs of worn subsurface for high-carbon high-chromium steels showing massed carbides: (a) fractured and (b) extracted. X1.5K. Wear test condition: V=50mm/s, L=20N and X=6m, 120# grit alumina paper.

fracture was also observed on the worn surface of both specimens (Fig.7.33), which could be a secondary mechanism for metal removal.

Scanning electron microscopical observation of the subsurface exposed on taper section specimens showed that, during the wear process, massed carbides acted as an obstacle to grooving, but then fractured (Fig.7.34(a)), or became extracted (Fig.7.34(b)) by further abrasion.

Study of the wear debris confirmed that microcutting was the dominant mechanism for metal removal, as the cut chip was characterized by a ploughed prow head and serrations on one surface, as shown in Fig.7.35(a). Additionally, an adhesive mechanism was involved in the cutting action, marked by a cut chip adhering to the cutting area of an abrasive particle (Fig.7.35(b)) or built-up-edge formed at the cutting edge of the abrasive particle (Fig.7.35(c)). Additionally, carbides became detached from the matrix, (see Fig.7.34(b)), to form wear debris (Fig.7.35(d)).

7.4 BISALLOYS

Bisalloys, which are the kind of high-strength low-alloy steel heat treated by of quenching or quenching and tempering, were used to study the effects of the concentrations of carbon and molybdenum, and heat treatment, on wear resistance. The compositions of the four alloys used in this study are given in Table 6.5(c) and the designation of heat treatment for the specimens are shown in Table 6.9 and described in §6.3.3. Abrasives used for the testing were 180# silicon carbide, alumina and garnet papers.

Hadfield's Manganese Steel (H.M.S) was also examined for comparison purposes.

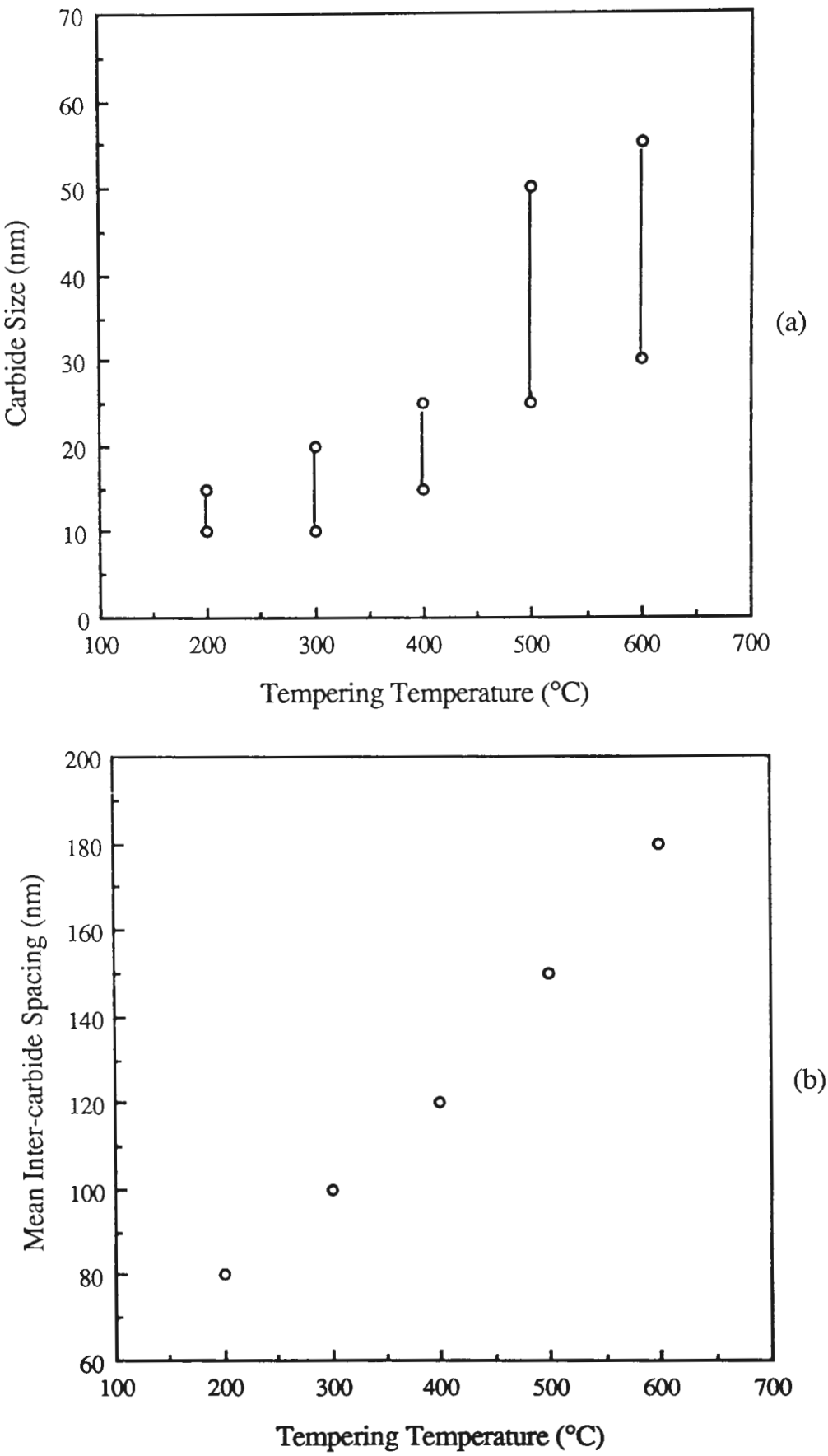

Fig.7.39 Diagrams showing the effect of tempering temperature on: (a) carbide size and (b) mean inter-carbide spacing for specimens of BIS B alloy.

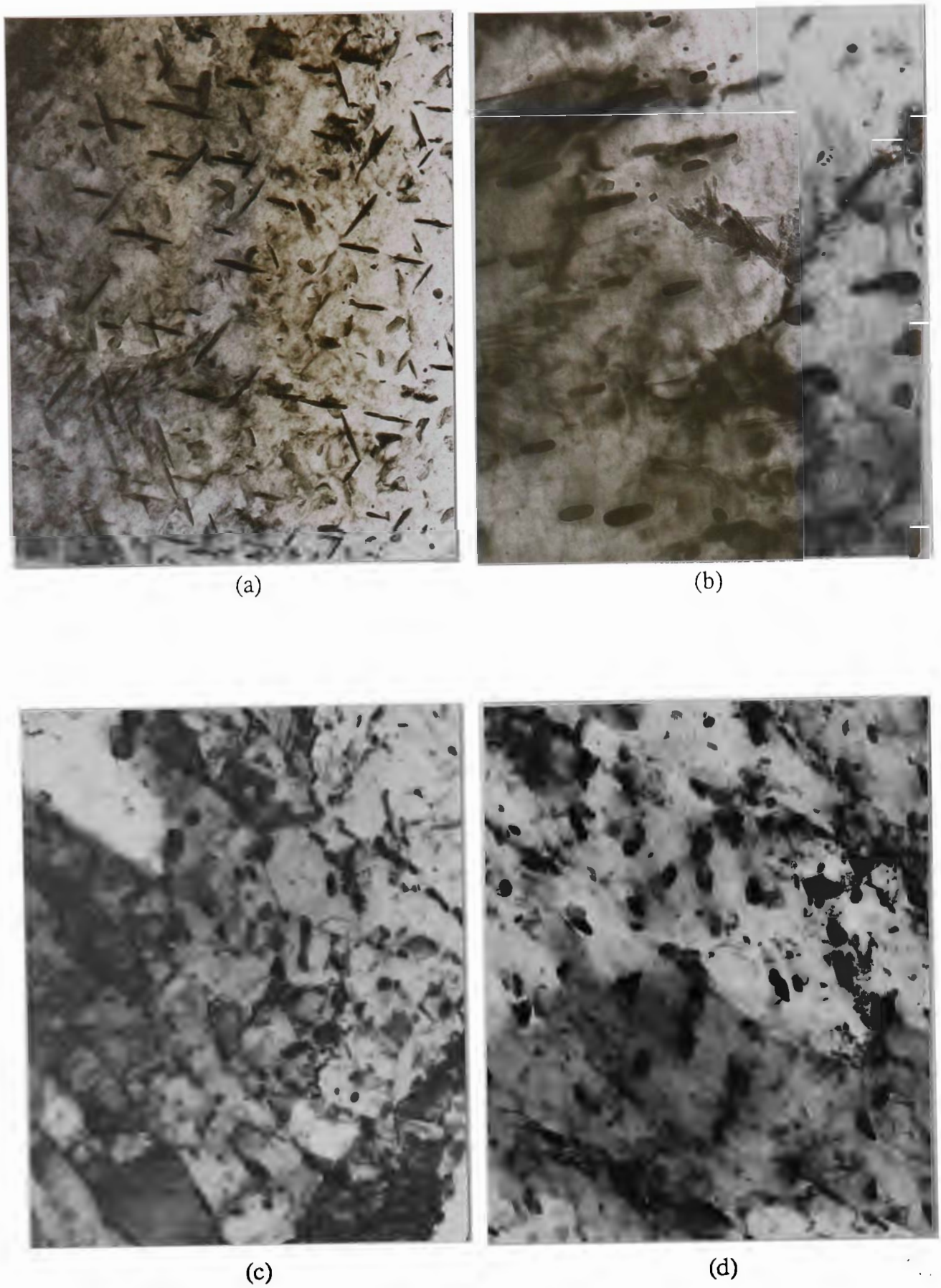

Fig.7.38 Transmission electron micrographs showing precipitated carbides for Bisalloy specimens: (a) BIS B4, (b) BIS A6, (c) BIS B6 and (d) BIS C6. X40K.

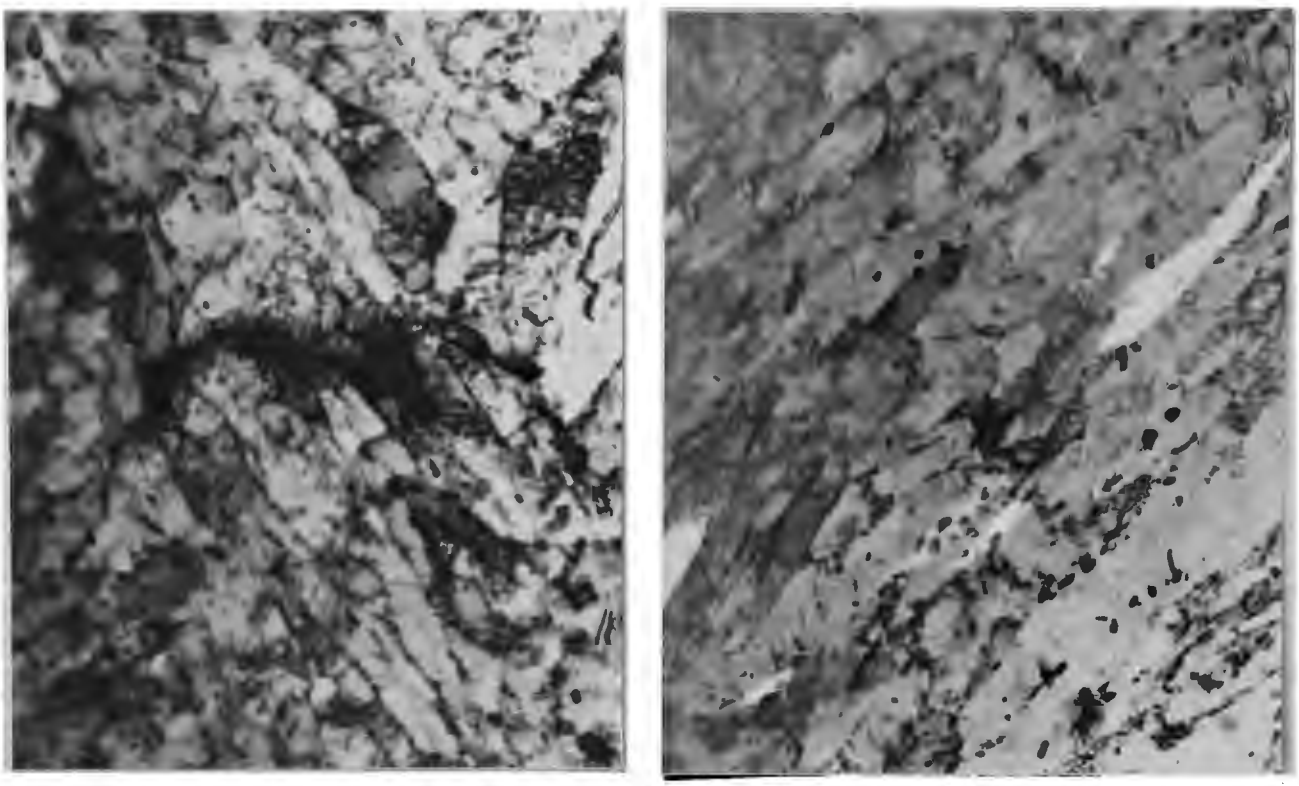

(a) (b)

Fig.7.37 Transmission electron micrographs showing the structures for 600°C tempered specimens: (a) BIS B6 and (b) BIS C6. X 20K.

Fig.7.36 Transmission electron micrographs showing the bainitic structure of quenched BIS C alloy. X20K.

7.4.1 Microstructure

Microstructures of the four Bisalloys were studied by both optical and transmission electron microscopy. Optical microscopical observations showed martensitic or bainitic structures, which were indistinguishable, for Bisalloys, and austenite for Hadfield's Manganese Steel.

Transmission electron microscopy showed the quenched BIS C alloy (0.18%C and 0.19%Mo), BIS C0, to be bainitic structure, Fig.7.36, while quenched BIS A alloy (0.85%C), BIS A0, and quenched BIS B alloy (0.18%C), BIS B0, were lath martensite. However, after tempering both BIS B alloy (0.18%C and 0.003%Mo) and BIS C alloy (0.18%C and 0.19%Mo) at 400°C and 600°C, there were no significant differences between the tempered martensite in specimens BIS B4 and BIS B6 and tempered bainite in specimens BIS C4 and BIS C6, respectively, as shown in Fig.7.37.

7.4.2 Carbides

The precipitated carbides in tempered Bisalloy specimens were mostly lath-like with a few spheroids in lower temperature tempered specimens, such as shown in Fig.7.38(a), whilst for 600°C tempered specimens, the carbides were mostly spheroidal, as shown in Figs.7.38(b), (c) and (d). For a particular alloy, such as BIS B (0.18%C), both the carbide size and the mean inter-carbide spacing increased with tempering temperature, as shown in Fig.7.39.

After similar tempering treatments, both the carbide size and the inter-carbide spacing in specimens of BIS C alloy, which contained 0.19%Mo, were slightly larger than those in BIS B alloy, which contained 0.003%Mo, as shown in Table 7.5 and Figs.7.38(c) and (d).

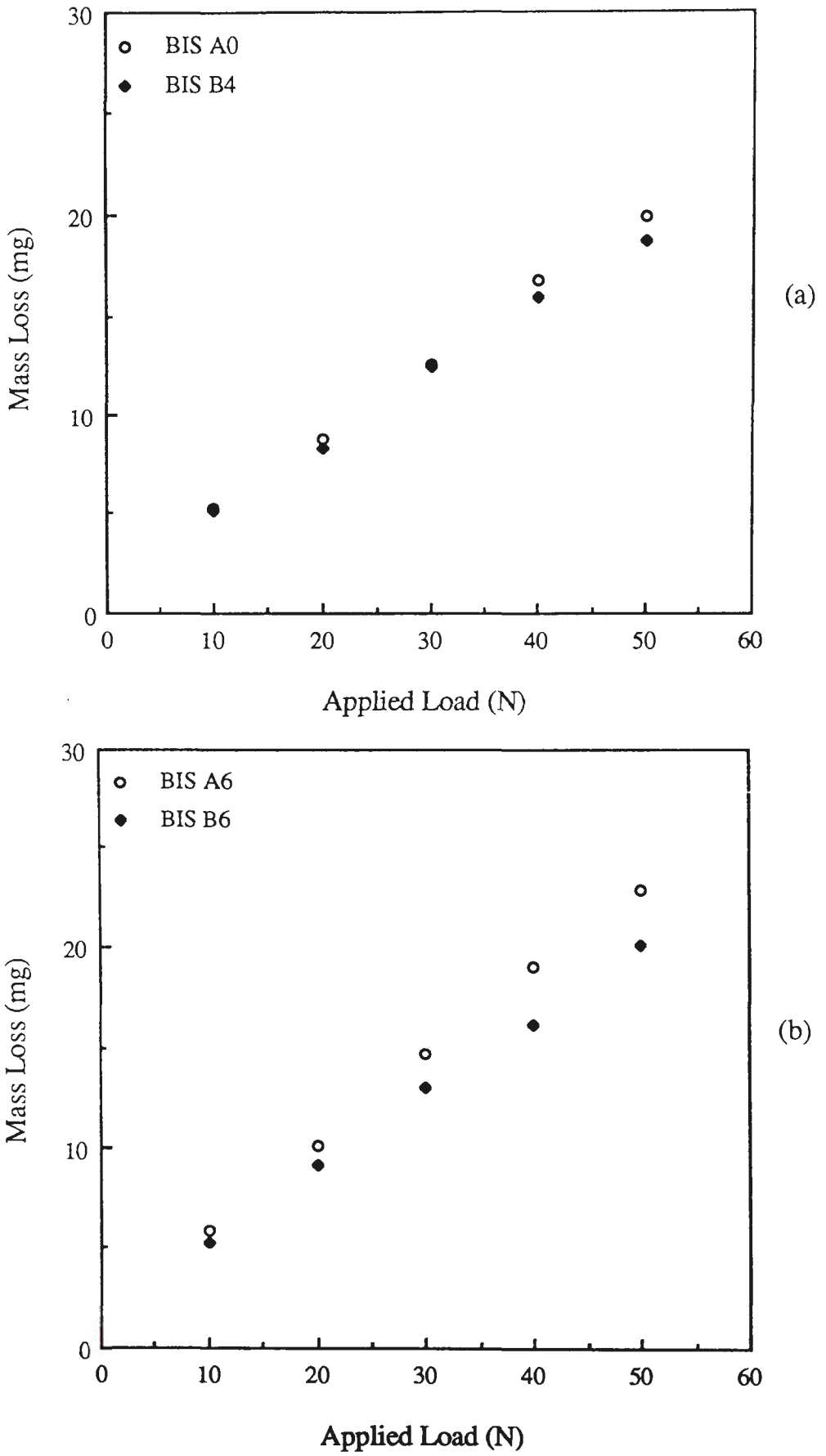

Fig.7.40 Diagrams showing the relationships between mass loss and applied load for the specimens: (a) BIS A0 and BIS B4 with the same hardness level and (b) 600°C tempered BIS A6 and BIS B6. Wear test condition: V=50mm/s, L=20N and X=6m, 180# silicon carbide paper.

Table 7.5 Carbide Size and Mean Inter-carbide Spacing for Bisalloy Specimens

Specimen	Carbide Size d (nm)	Mean Inter-carbide Spacing λ (nm)
BIS A5	20-30	250
BIS A6	35-45	300
BIS B2	10-15	80
BIS B3	10-20	100
BIS B4	15-25	120
BIS B5	25-30	150
BIS B6	30-55	180
BIS C2	10-20	80
BIS C4	25-50	150
BIS C6	40-60	180
BIS D2	20-30	100

For the specimens tempered at 600°C with different carbon content, such as BIS A6 (0.085%C) and BIS B6 (0.18%C), the size of the carbides was very similar; however, the lower carbon alloy (BIS A6) had a larger mean inter-carbide spacing than the higher carbon alloy (BIS B6), as shown in Table 7.5 and Figs.7.38(b) and (c).

7.4.3 Wear Resistance

7.4.3.1 Carbon Content

For specimens at the same hardness level under abrasion with silicon carbide paper, mass loss from quenched BIS A alloy (0.085%C), BIS A0, was higher than that from 400°C tempered BIS B alloy (0.18%C), BIS B4, and the difference between the mass loss was more significant at higher applied loads as shown in Fig.7.40(a). Similar wear behaviour was also observed under the abrasion with softer garnet paper.

For the 600°C tempered specimens, BIS A6 and BIS B6, mass loss from BIS A6 was significantly higher than from BIS B6, Fig.7.40(b).

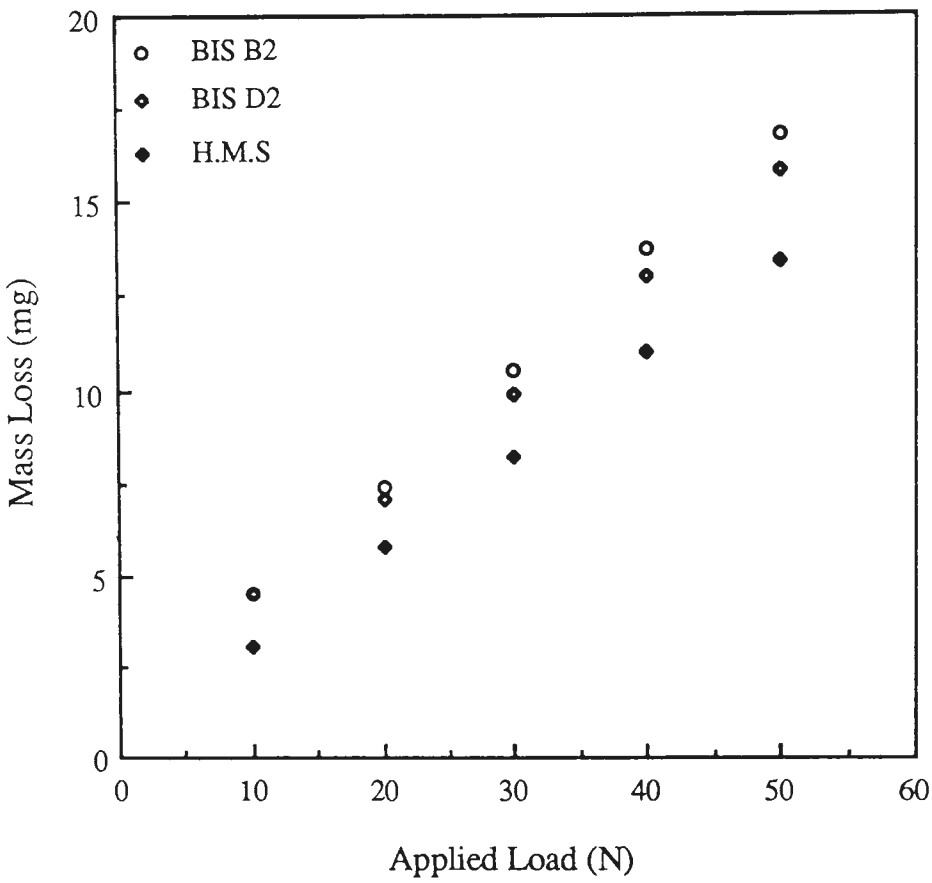

Fig.7.43 Diagrams showing relationship between mass loss and applied load for specimens BIS B2, BIS D2 and H.M.S.. Wear test condition: V=50mm/s, L=20N and X=6m, 180# silicon carbide paper.

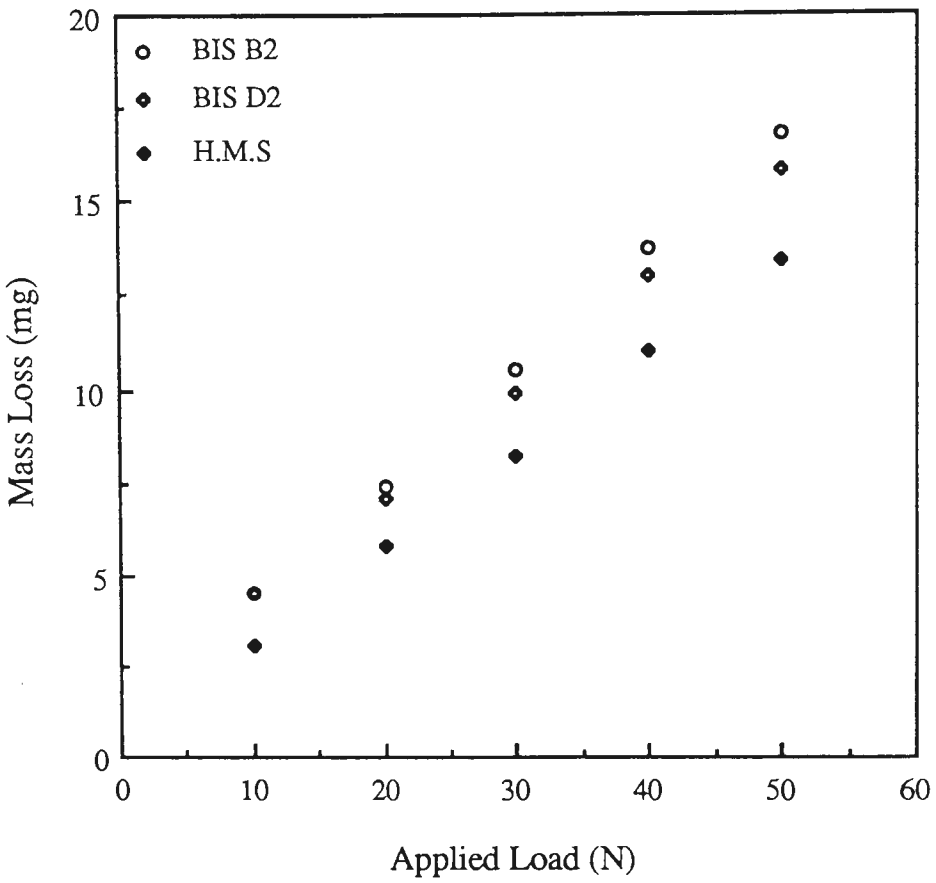

Fig.7.43 Diagrams showing relationship between mass loss and applied load for specimens BIS B2, BIS D2 and H.M.S.. Wear test condition: V=50mm/s, L=20N and X=6m, 180# silicon carbide paper.

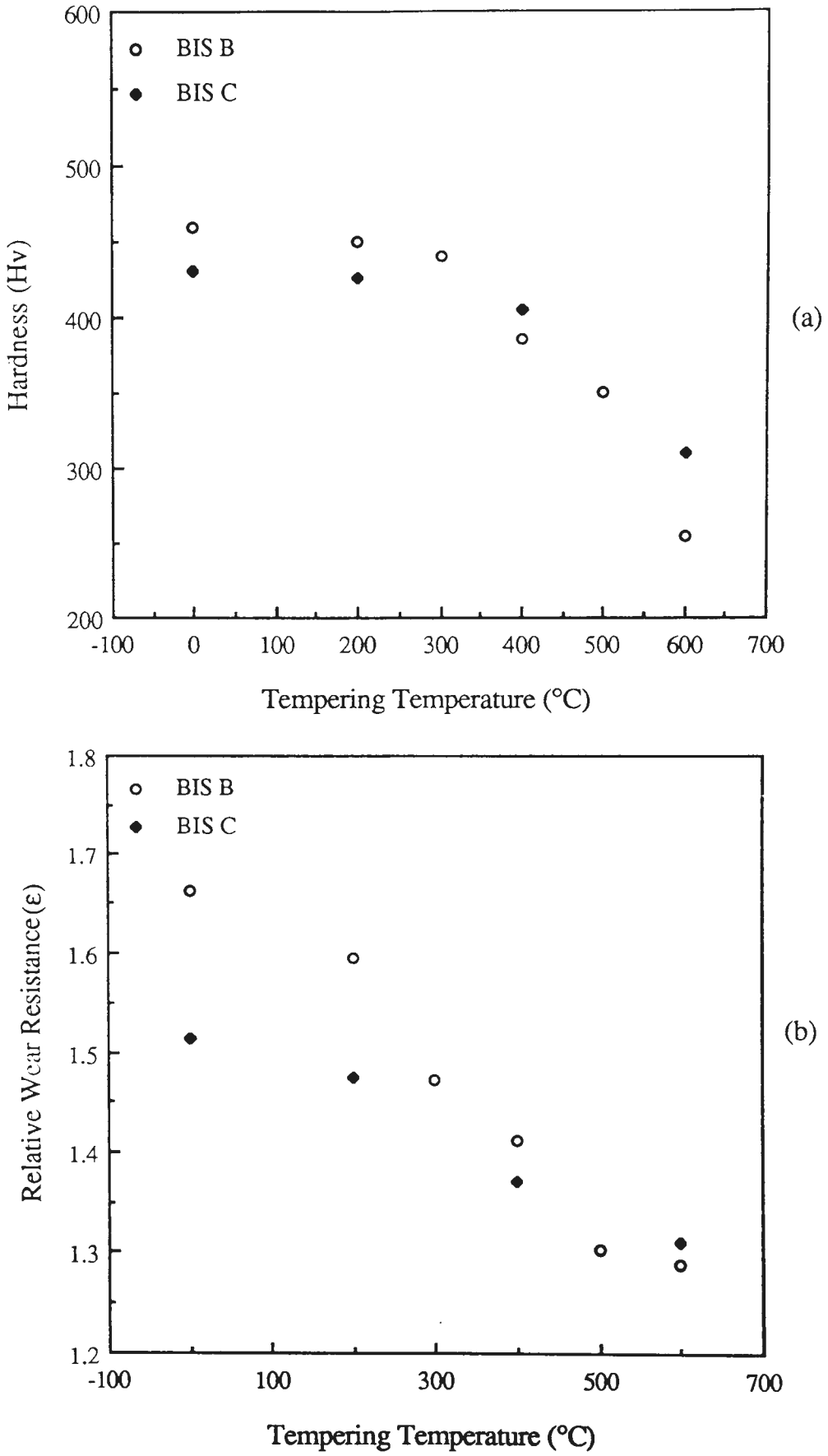

Fig.7.41 Diagrams showing the effect of tempering temperature on: (a) hardness and (b) relative wear resistance for specimens of BIS B and BIS C alloys. Wear test condition: V=50mm/s, L=20N and X=6m.

7.4.3.2 Hardness

Both hardness and relative wear resistance for the specimens of BIS B alloy (0.18%C and 0.003%Mo) were found to decrease non-linearly with the tempering temperature, as shown in Fig.7.41.

For the quenched and the quenched and 200°C tempered conditions, both hardness and relative wear resistance values for specimens of BIS B alloy, BIS B0 and BIS B2, were higher than for corresponding specimens of BIS C alloy (0.18%C and 0.19%Mo), BIS C0 and BIS C2. After tempering at 400°C and 600°C, specimens of BIS C alloy, BIS C4 and BIS C6, were slightly harder than the specimens of BIS B alloy, BIS B4 and BIS B6, but the relative wear resistance for 400°C tempered BIS C alloy, BIS C4, was slightly lower than for 400°C tempered BIS B alloy, BIS B4. Difference in relative wear resistance between 600°C tempered specimens, BIS B6 and BIS C6, was not apparent. Consequently, relationships between relative wear resistance and hardness for both BIS B and BIS C alloys were non-linear as shown in Fig.7.42. Clearly, within the test range, relative wear resistance increased very slowly with increase in hardness from Hv250 to Hv350, and then increased very rapidly from Hv400 to Hv460.

Figure 7.43 shows that the relationship between mass loss and applied load was linear for the specimens, BIS B2 (0.18%C), BIS D2 (0.27%C) and H.M.S (austenitic Hadfield's manganese steel). Clearly, mass loss from specimen BIS D2 was lower than for the specimen BIS B2 and the difference between mass loss was significant at high applied load, although the hardness value for both specimens were similar. Significantly, the mass loss for H.M.S was unexpectedly much lower than for both specimens BIS B2 and BIS D2, even though the hardness of H.M.S was much lower than for each alloy (Table 6.9).

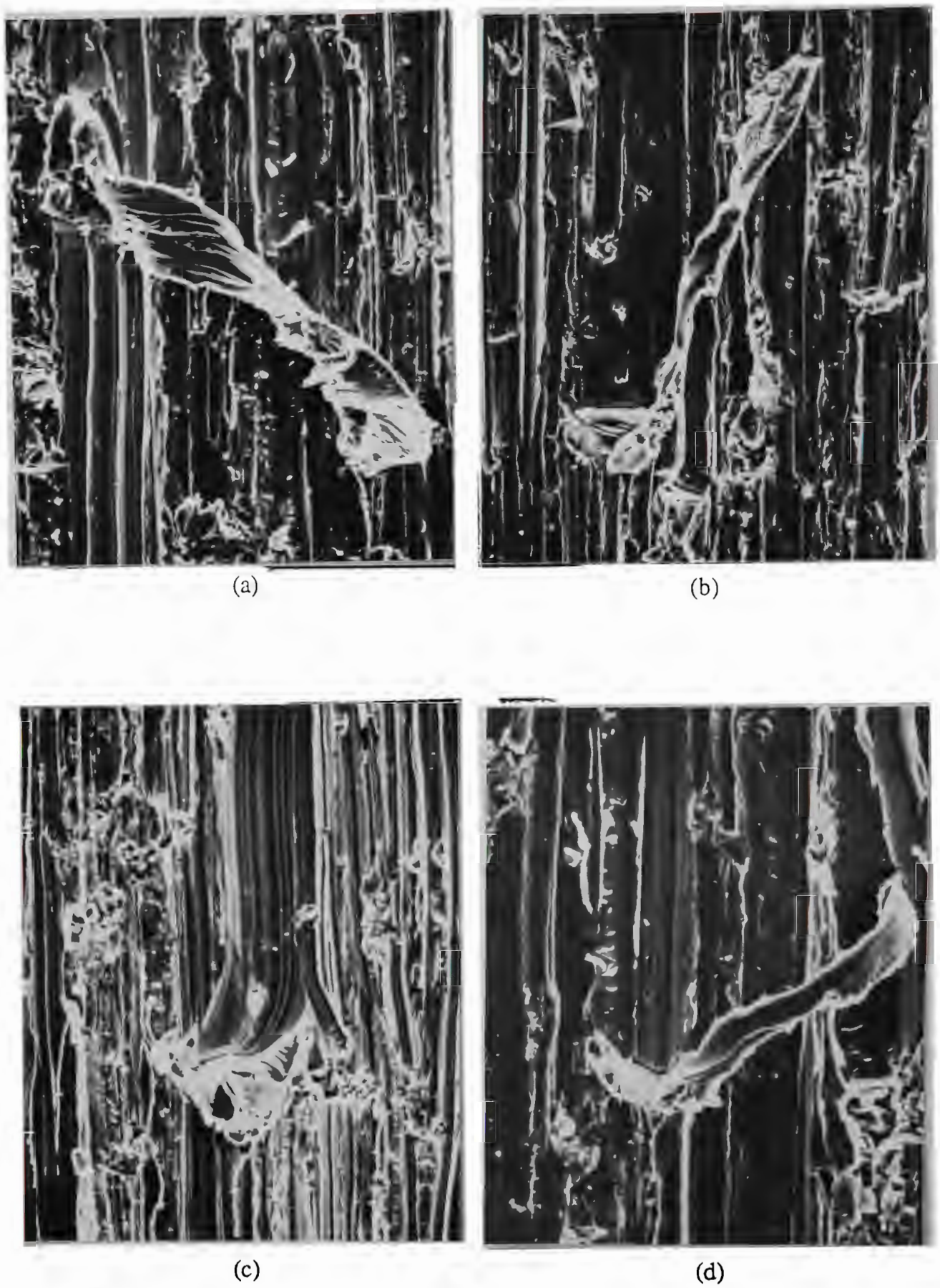

Fig.7.46 Scanning electron micrographs showing wear topography: (a) cut chip formation, specimen BIS B4, (b) delamination involved in separating chip from the matrix, specimen BIS A6, (c) microploughing during abrasion, specimen BIS A0, and (d) bulge cut by subsequent abrasive particle, specimen BIS A6. X500. Wear test condition: V=50mm/s, L=20N and X=6m, 180# silicon carbide paper.

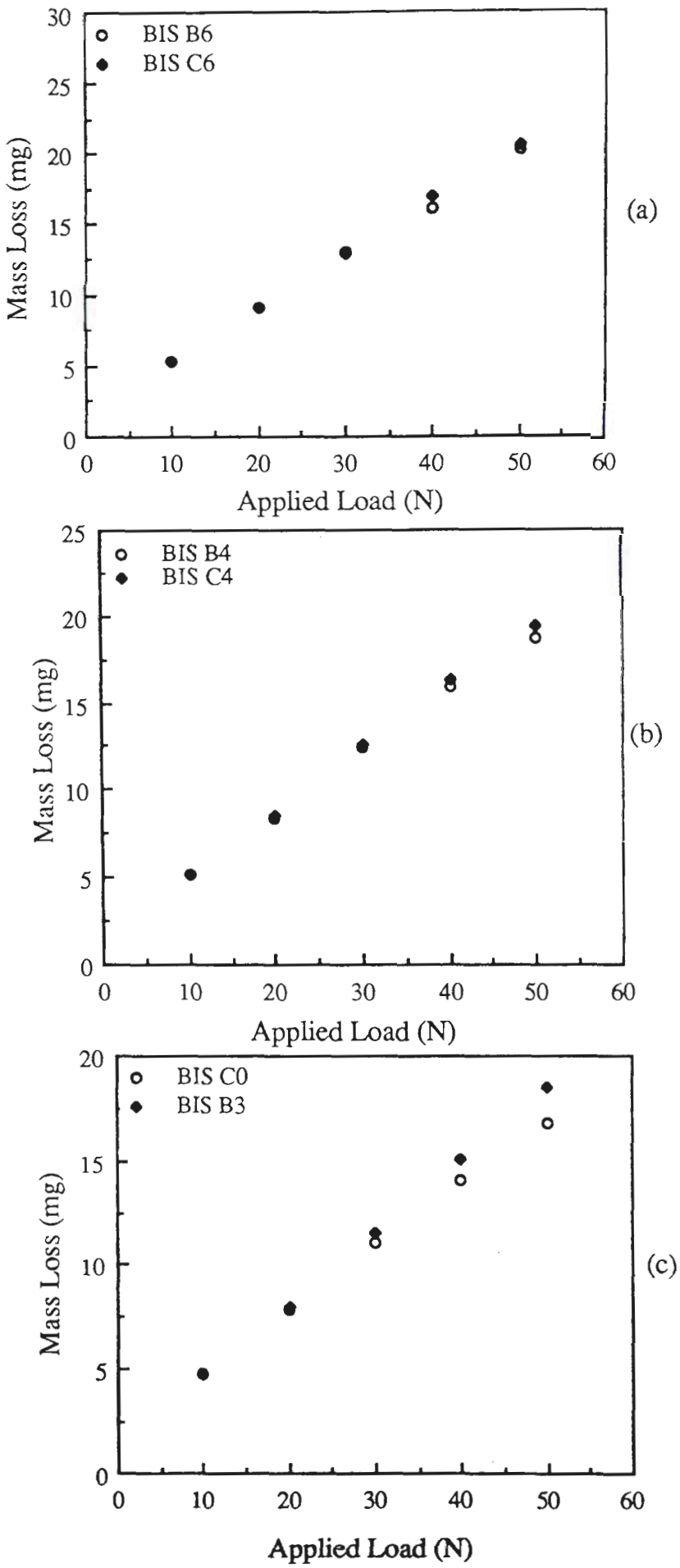

Fig.7.45 Diagrams showing relationships between mass loss and applied load for specimens of BIS B and BIS C alloys: (a) 600°C tempered BIS B6 and BIS C6, (b) 400°C tempered BIS B4 and BIS C4 and (c) same hardness group of BIS B3 and BIS C0. Wear test condition: V=50mm/s and X=6m, 180# silicon carbide paper.

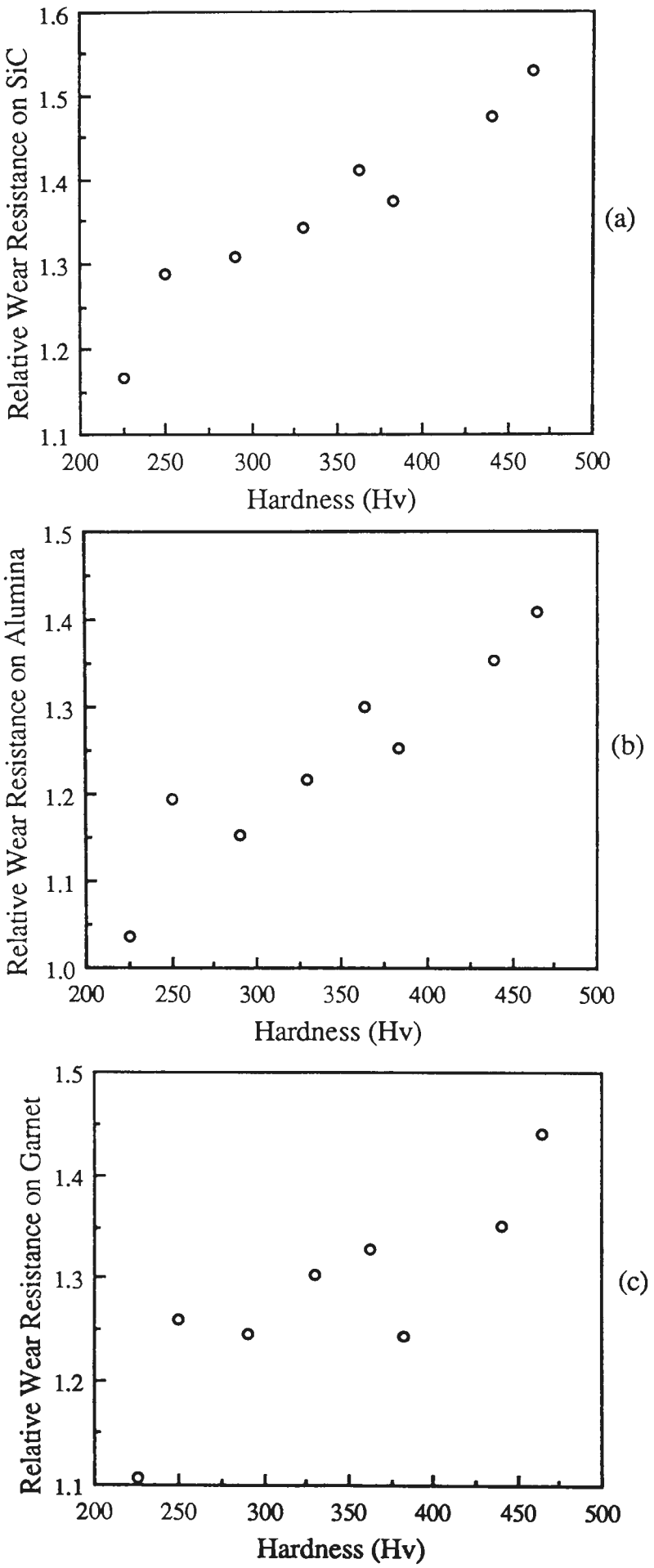

Fig.7.44 Diagrams showing relationships between relative wear resistance and hardness for the particular specimens in Bisalloys identified (*) in Table 6.9, using 180# abrasive paper: (a) silicon carbide, (b) alumina and (c) garnet. Wear test condition: V=50mm/s, L=20N and X=6m.

Figure 7.44 shows that the relationship between relative wear resistance and hardness was non-linear for the selected Bisalloy specimens marked * in Table 6.9, under the test condition of 20N applied load, 50mm/s sliding speed, 6m wear path, and silicon carbide, alumina and garnet abrasive papers.

7.4.3.3 Molybdenum Concentration

The presence of molybdenum in BIS C alloy, which was derived from BIS B alloy, resulted in a lower hardness in the quenched and in the quenched and 200°C tempered conditions, whilst after tempering at 400°C and 600°C, the hardness values of the specimens BIS C4 and BIS C6, were slightly higher than those of corresponding specimens BIS B4 and BIS B6 of BIS B alloy, as shown in Table 6.9. The mass loss from the two specimens, BIS C4 and BIS C6, however, was slightly higher than for the specimens BIS B4 and BIS B6, under high applied loads, as shown in Figs.7.45(a) and (b), for abrasion with silicon carbide paper. Similar wear results were obtained under abrasion with alumina and garnet papers.

Further, for the specimens of the Hv430 hardness group, i.e. quenched BIS C alloy (0.18%C and 0.19%Mo), BIS C0, and 300°C tempered BIS B alloy (0.18%C and 0.003%Mo), BIS B3, mass loss for specimen BIS C0 was lower than for specimen BIS B3, and the difference between mass losses increased with the increase in applied load, Fig.7.45(c).

7.4.4 Wear Topography and Debris

Scanning electron microscopical study of the wear topography for the specimens abraded with silicon carbide paper, indicated that microcutting was the major mechanism for metal removal (Fig.7.46(a)), while delamination was involved in separating chips from the matrix, as shown in Fig.7.46(b). Microploughing was

(a)

(b)

(c)

(d)

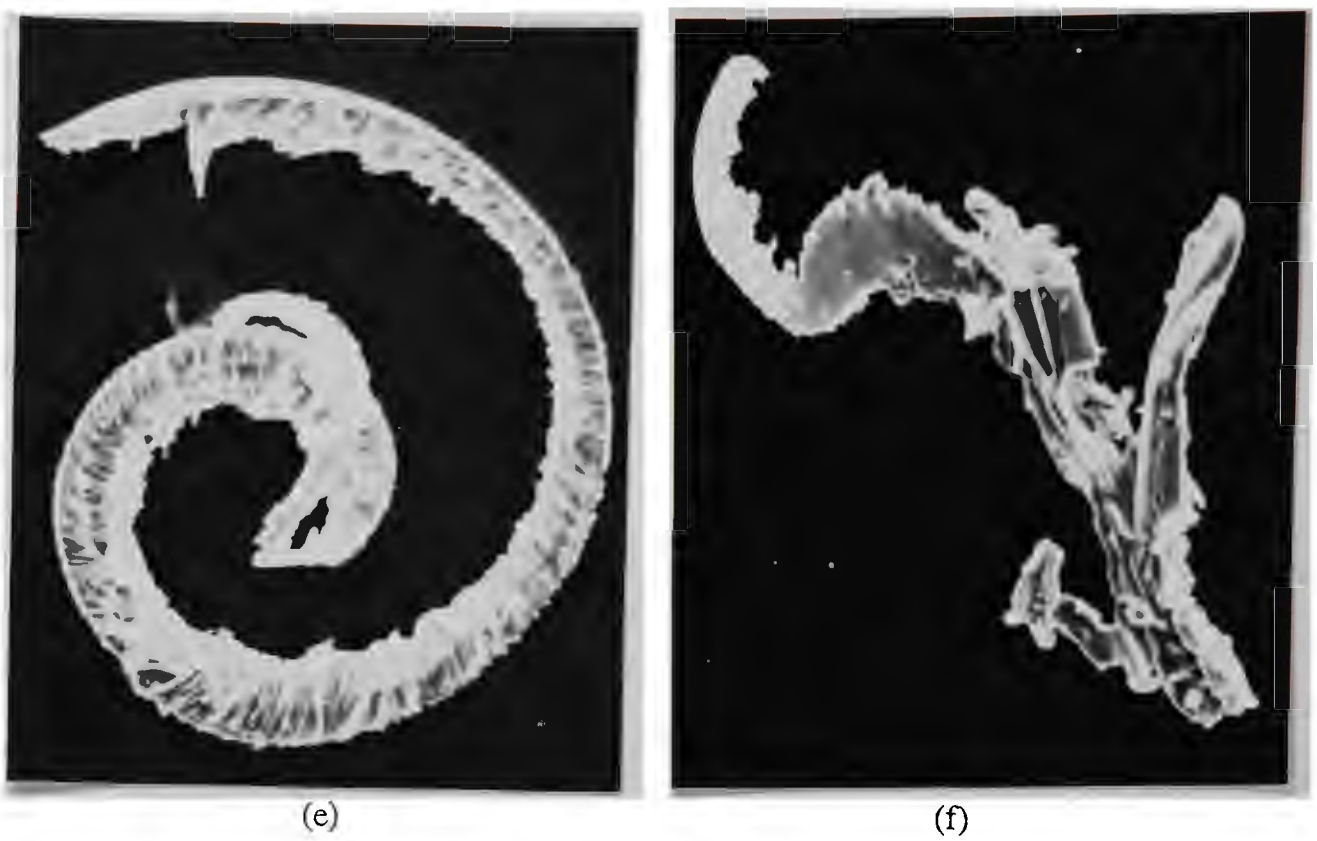

(e) (f)

Fig.7.49 Scanning electron micrographs showing wear debris: (a) cut chip with serrations at the surface, specimen BIS B3; X400, (b) cut chip with delaminated serrations, specimen BIS B3; X700, (c) cut chip with a large ploughed prow ahead, specimen BIS D2; X500, (d) ploughed prow fractured from cut chip, specimen BIS A6; X500, (e) cut chip from side-formed cut chip, specimen BIS E2; X600, and (f) longitudinal serrations along cut chip, specimen H.M.S.; 400. Wear test condition: V=50mm/s, L=20N and X=6m, 180# garnet paper.

Fig.7.48 Scanning electron micrograph showing cut chip formed on the worn surface of specimen H.M.S.. X500. Wear test condition: V=50mm/s, L=20N and X=6m, 180# alumina paper.

Fig.7.47 Scanning electron micrographs showing wear topography: (a) large cut chip, specimen BIS B3, (b) side-formed cut chip, specimen BIS A6, and (c) delamination on the bulges of the ploughed groove, specimen BIS D2. X500. Wear test condition: V=50mm/s, L=20N and X=6m, 180# garnet paper.

significantly involved in the grooving process, as indicated in Fig.7.46(c) by a prow formed at the end of the groove and bulges built up at the groove sides. The bulges were often cut by a subsequent abrasive particle (Fig.7.46(d)).

After abrasion using alumina paper, the wear topography was very similar to that observed for silicon carbide paper.

For garnet abrasive paper, the dominant mechanism for metal removal was microcutting, similar to abrasion with silicon carbide and alumina papers. Additionally, cut chips and side-formed chips generated with the garnet abrasive (Figs.7.47 (a) and (b)) were larger than those formed with silicon carbide or alumina. Further, delamination was also involved in the ploughed groove formed by garnet abrasion (Fig.7.47(c)), resulting in serrated groove ridges.

Wear topography for H.M.S showed little fracture debris, Fig.7.48, and abrasion grooves that were shallower than for Bisalloys. Plastic deformation for H.M.S specimen was severe, but the extent was not as great as for Bisalloys.

Scanning electron microscopical study of wear debris confirmed that microcutting was the dominant mechanism for metal removal. However, the wear debris produced by the abrasion of silicon carbide paper was quite different from that produced by abrasions of alumina or garnet abrasive papers.

Microcutting was characterized by ribbon-like chips, with a smooth surface on the machine tool (abrasive particle) side and serrations on the other surface (Fig.7.49(a)). Also, delaminated serrations were observed on some cut chips(Fig.7.49(b)), which were observed to commence mostly from a ploughed prow (Fig.7.49(c)) that, sometimes, fractured from the chip (Fig.7.49(d)). In some cases, the cut chips

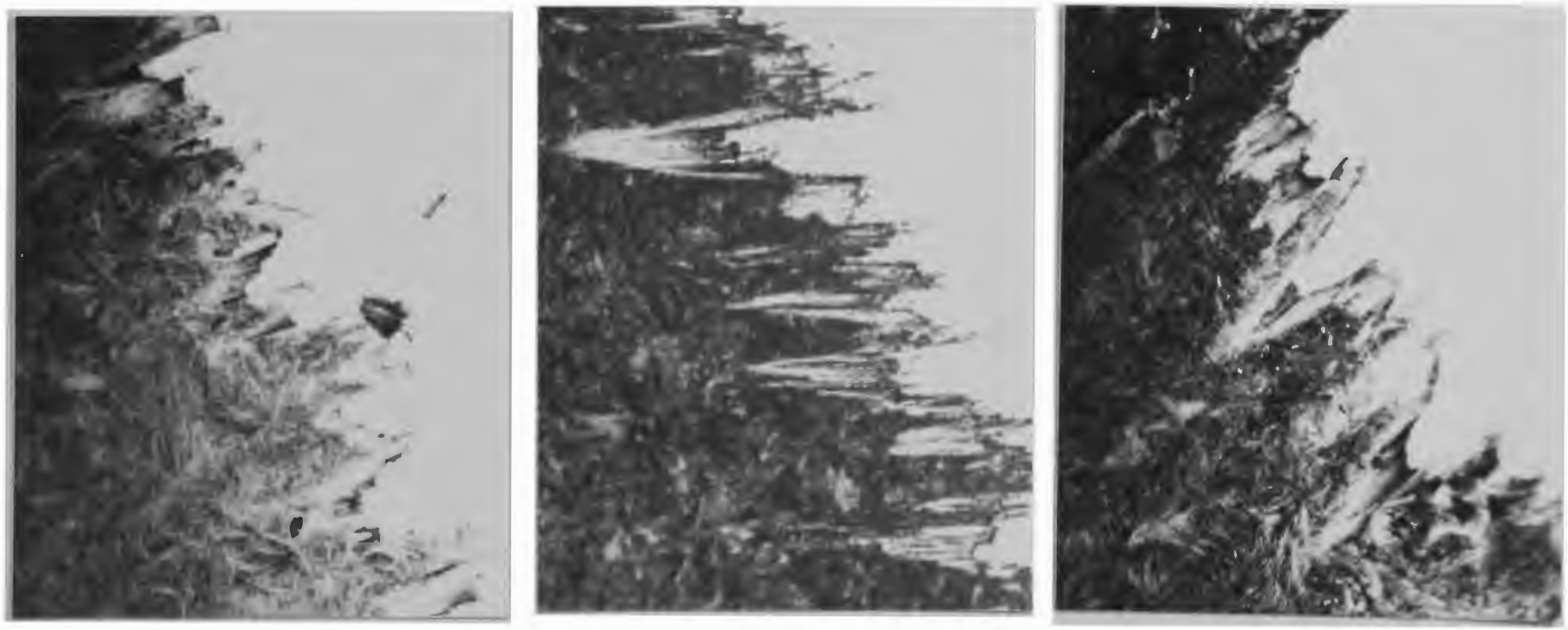

(a) (b) (c)

Fig.7.50 Optical photomicrographs showing white layer on 5° taper surface for the quenched and 250°C tempered 1.2%C steel under the applied load of: (a) 10N, (b) 20N and (c) 50N. Etchant: 2.5% nital. X600. Wear test condition: V=50mm/s, L=20N and X=6m, 180# silicon carbide paper.

commenced from side-form chips, as shown in Fig.7.49(e). Wear chips from the specimen of H.M.S were different to those from Bisalloy specimens in that the serration direction was mostly longitudinal (Fig.7.49(f)).

7.5 WHITE LAYER

A 'white layer' was generated during some of the abrasive wear tests. This layer was featureless and white under optical microscopy and could be observed between the original structure and the copper coating; see Fig.7.50, and was observable in both longitudinal and transverse sections of the abrasion groove.

To elucidate the detailed phenomena of the white layer, and to relate the white layer to the original structures of wear surface, the following optical microscopical observations were carried out on 5° taper sections prepared normal to the grooving direction, then etched with Picric-HCl-Ethanol for high-carbon high-chromium steels and nital for the other steels and alloys. Wear tests were carried out with 50mm/s sliding speed, 6m wear path, 180# silicon carbide abrasive paper, and the applied load of 20N for tool steels and Bisalloys and of 10N, 20N and 50N for carbon steels.

7.5.1 Effect of Prior Microstructures

The white layer was observed to be generated on the quenched or quenched and low temperature tempered specimens for the 0.75%C steel, 0.38%C, 1.2%C steels and the Ni-Cr-Mo-C tool steel, as well as specimen BIS D2; additionally, for the particular steel, the layer was thinner for the quenched specimen, and thicker for the low temperature tempered martensitic (Fig.7.51) or austempered bainitic specimens.

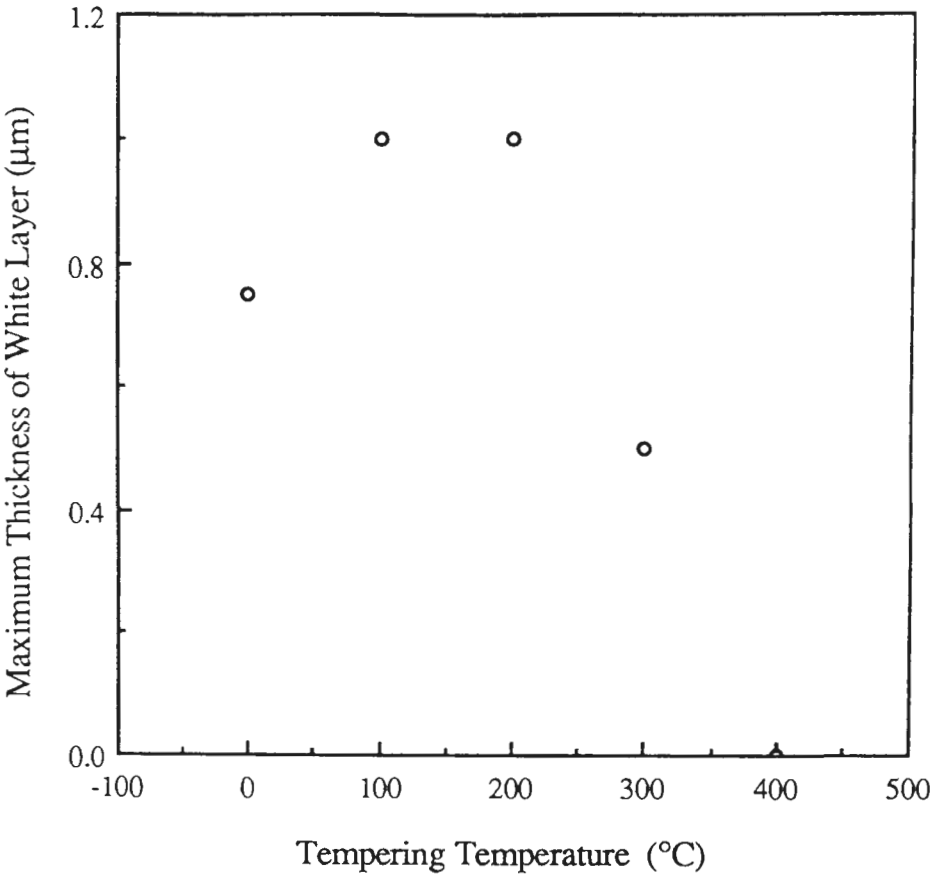

Fig.7.51 Diagram showing effect of tempering temperature on the maximum thickness of white layer for Ni-Cr-Mo-C steel. Wear test condition: V=50mm/s, L=20N and X=6m, 180# silicon carbide paper.

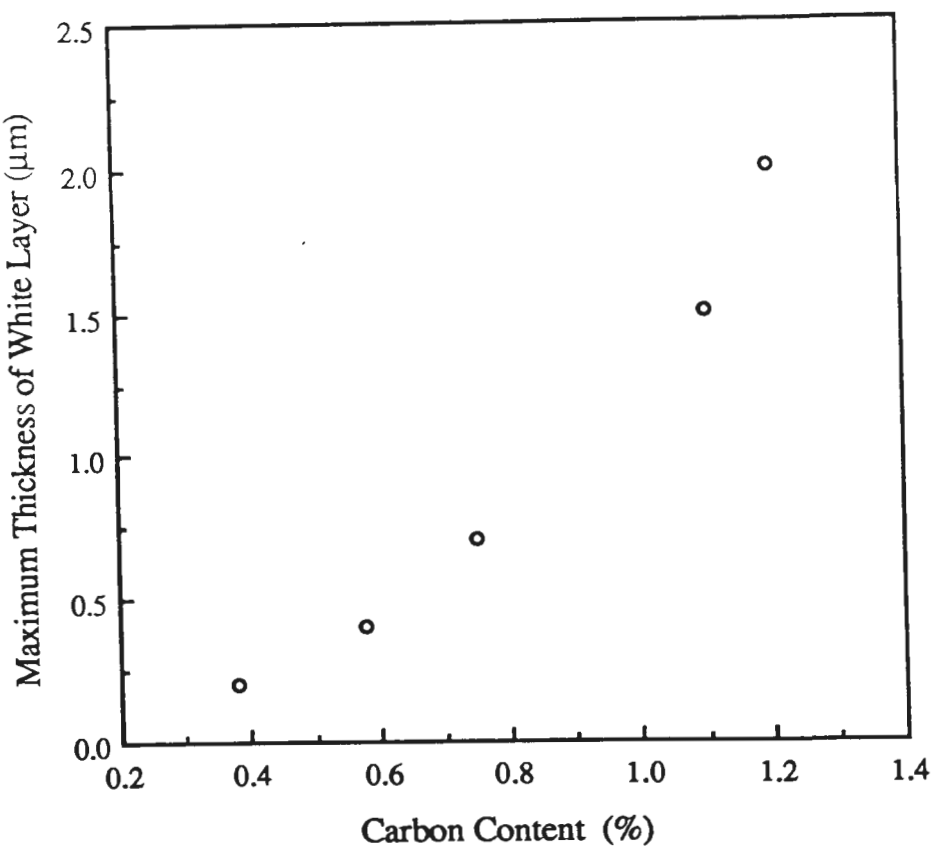

Fig.7.52 Diagrams showing the effect of carbon content on the maximum thickness of white layer for the quenched and 250°C tempered specimens in carbon steels. Wear test condition: V=50mm/s, L=20N and X=6m, 180# silicon carbide paper.

There was no white layer observable for plain carbon steels with equilibrium hypoeutectoid, pearlite or hypereutectoid structures, or on specimens after quenching and 650°C tempering, or on quenched 0.10%C steel.

For high-carbon high-chromium steels, no white layer was generated on specimens with structures comprising a martensitic matrix and massed carbides after heat treatments of quenching and tempering twice at 150°C (for XW-5) and 200°C (for Chrome).

7.5.2 Effect of Carbon Content

Figure 7.52 shows clearly that, for 250°C tempered martensitic specimens, the thickness of the layer increased slowly with carbon content from 0.38% to 0.75%, then more rapidly with further increase of carbon content to 1.2%.

For Bisalloys, the white layer was observed on the higher carbon specimen BIS D2 (0.27%C), but no white layer was observed on the lower carbon (0.18%C) specimens of BIS B and BIS C alloys even in the quenched and the quenched and 200°C tempered conditions, or quenched BIS A alloy (0.085%C).

7.5.3 Effect of Tempering Temperature

Figure 7.51 shows the relationship between the maximum thickness of the white layer and tempering temperature for single-quenched and tempered martensitic specimens of the Ni-Cr-Mo-C steel. It is clear that the thickness of the white layer for specimens tempered at 100°C and 200°C was greater than for the quenched and the 300°C tempered specimens; no white layer was observed at the 400°C tempered specimen.

7.5.4 Effect of Applied Load

Optical photomicrographs, Fig.7.50, show the white layer generated under the applied loads of 10N, 20N and 50N in the quenched and 250°C tempered 1.2%C steel. Evidently, the maximum thickness of the white layer did not change significantly with applied load.

Chapter 8

DISCUSSION

In optimizing abrasive wear resistance in terms of material characteristics, it is important to understand the inter-relationships between wear resistance, composition, microstructures and hardness. However, these parameters are inter-affected and the relationships are rather complicated. This Chapter is concerned with the analysis of the wear behaviour based on the results presented in Chapter 7. The discussion is presented first as an analysis of the effect of the operational variables on wear rate and thereby the standard wear test condition was determined, then of the inter-relationships between wear resistance, composition, microstructures and hardness. The operative abrasive wear mechanisms are deduced from the characteristics of abrasion groove formation and wear debris. Finally, a white layer which formed on some specimens is analysed in relation to the prior microstructural properties and compositions of the specimens, from which, the generation mechanisms are elucidated.

8.1 OPERATIONAL VARIABLES

Operational variables are those parameters which influence the tribology system and which for the pin-on-drum abrasive wear test, usually include applied load, wear path, sliding speed and abrasive paper. As shown in §7.1, these variables directly affect wear rate and wear mechanisms of metal removal, and therefore, influence the relationship between wear resistance and material properties.

The individual effects of these variables were studied for two reasons. First, to elucidate those individual effects and secondly to determine an appropriate value of each of them to identify a standard test condition for the wear tests conducted in the main part of the investigation.

8.1.1 Applied Load

Generally, wear rate increases with increase of applied load. For the condition that the abrasive particles were much harder than the test material, as for silicon carbide or garnet to carbon steels and Bisalloys, mass loss increased almost linearly with applied load over the range 10 to 50N (Figs.7.1, 7.2 and 7.43). The proportionality of mass loss to applied load, which is consistent with previous studies[23; 52], indicates that the predominant mechanism of material removal was either unchanged, or, at least, did not change abruptly over the full range of loads. The increase of the mass loss with load may be attributed to an increase in both the groove depth (z in Fig.3.3) and the number of the groove formations[36].

The relationships between mass loss and applied load for the two high-carbon high-chromium steels, shown in Fig.7.3, were strongly dependent upon the ratio of the hardness of the carbides in the structures to the hardness of the abrasives, and the results are consistent with the proposal[66] that mass loss increases as the hardness of the abrasive increases from garnet to alumina to silicon carbide (Table 5.2). For a particular abrasive, mass loss depended significantly on the hardness of the carbides[65; 13]; this dependence was particularly complicated for the condition that the hardness of the abrasive and of the carbides were about the same[63], as was the case for alumina and Cr_7C_3, Fig.7.3(b). The abrupt increase of mass loss at about 30N applied load probably resulted from a change in the predominant wear mechanism. It is probable that the mechanism changed from microploughing-microcutting to microcutting-microcracking when microcracks occurred either in the carbides or at the interface between the carbides and matrix. Normally, microcracking occurs for the case that the actual stress, which is implied by applied load (stress) and flow stress, at the worn surface exceeds the fracture limit of the carbides or the bond stress between carbides and matrix, and can contribute substantially to high mass loss for some materials[84]. It is known[89] that the harder the material, the higher is the value of the

critical stress for fracture. Therefore, for the condition that the abrasive particles were harder than the carbides, as was silicon carbide to Cr_7C_3, microcracks occurred mainly in the carbides; otherwise, for the case that the abrasive particles were softer than the carbides (garnet to Cr_7C_3), microcracks occurred preferably in the garnet abrasives, which resulted in a low mass loss (Fig.7.3(c)).

8.1.2 Wear Path

It is commonly recognized[50; 52; 55] that the relationship between wear rate and the wear path is linear. This is consistent with the result that mass loss was linearly related to the wear path (Fig. 7.4), which indicates that there is no significant change in the predominant mechanism of metal removal over the 6m wear path.

8.1.3 Sliding Speed

The relationship between mass loss and sliding speed is controversial[22; 50]. The results presented in Fig.7.5 indicates that this relationship was influenced by the ratio (η) of material hardness to applied load:

$$\eta = \frac{\text{Material hardness (Hv)}}{\text{Applied stress (MPa)}} \qquad (8\text{-}1)$$

Under the condition that η had a high value, such as for annealed 0.75%C steel abraded under an applied load of 20N (0.71MPa, Hv220, η = 310), the result presented in Fig.7.5(a) confirmed the conclusion of Khruschov and Babichev[22] that mass loss was independent of the sliding speed.

For cases in which η had a low value, such as for annealed 0.10%C steel abraded under an applied load of 20N (0.71MPa, Hv80, η = 112.7) or annealed 0.75%C steel abraded under an applied load 50N (1.77MPa, Hv220, η = 124.3), the relationship between mass loss and sliding speed, Fig.7.5, is similar to that observed by Misra and

Finnie[50] in which mass loss decreased with speed increase in the low speed range, then became almost constant. Clearly, the decreasing rate of mass loss with speed for the 0.10%C steel (Fig.7.5(a)) was much higher than for the 0.75%C steel (Fig.7.5(b)), even though, the values of η for both cases were similar. This result indicated that the relationship between mass loss and sliding speed is influenced mainly by hardness, so that the harder the material and the higher the value of η, the less is the effect of sliding speed on mass loss.

An applied load of 20N (0.71MPa) was selected for study the effect of sliding speed on wear rate as the associated mass loss (§8.1.1) was pronounced. Additionally, the applied stress (0.71MPa) is popularly used for wear testing[13] as it is lower than the fracture stress for most materials. For 20N abrasion, the decrease of mass loss from the annealed 0.10%C steel in the low speed range may be attributed to an increase in strain-rate which increases the flow stress of the material. Generally, the larger the thickness of the surface layer in which the plastic deformation can be accommodated, the higher is the strain rate during abrasion, and the higher is the flow stress[50] which the material can achieve. Clearly, for low hardness ferrous alloys, such as annealed 0.10%C steel (Hv80), the allowable amount of plastic deformation is much larger than for a higher hardness ferrous alloy, such as annealed 0.75%C steel (Hv220). Consequently, the influence of sliding speed on mass loss was greater for the annealed 0.10%C steel than for the annealed 0.75%C steel. Further, the flow stress may reach a critical value at the fracture limit, then become constant with further increase of strain-rate; correspondingly, mass loss was almost insensitive with further increase in the sliding speed.

The annealed 0.75%C steel was selected for study of the effect of applied load on the relationship between mass loss and speed. Clearly, at the high applied load of 50N, mass loss decreased in the low speed range (3 to 25 mm/s in Fig.7.5(b)) and then

became constant, which indicates that the flow stress can probably increase slightly with increase of sliding speed only at the low speed range. However, for a low applied load, such as 5N or 20N, the flow stress was not influenced significantly by the sliding speed, resulting in a constant mass loss over the test speed range.

8.1.4 Abrasive Paper

The effect of the abrasive paper on two-body abrasive wear includes effects of the size, the shape, the hardness and the density of the abrasive, as reviewed in §3.3.5. For this investigation, the size, the shape and the density of particles of the abrasive were considered to be the same for all 180# silicon carbide, or 120# or 180# alumina, or 180# garnet papers, for the same batches for each kind of papers manufactured by the same company. Analyses of the effect of abrasive on wear resistance was, therefore, limited to the effect of hardness, which is considered in §8.2.2 and §8.2.3.

8.1.5 Standard Test Condition

From the discussion presented in §8.1.1, §8.1.2 and §8.1.3, it is clear that wear rate is strongly related to the operational variables. Therefore, it was necessary to set up a "standard wear test condition" for this investigation so that the inter-relationship between wear resistance, composition, microstructure and hardness could be analysed, and the wear mechanisms studied. The selected standard wear test condition was:

applied load -- 20N
sliding speed -- 50mm/s
wear path -- 6m

Criteria for selecting these variables were:

(a) the applied stress should be less than the yield stress of the test materials,

(b) the mass loss under the applied load should be significant for a single wear test,

(c) the mass loss should not be influenced by slight variation of speed, and wear test machine should not work at the limiting speed condition (3 or 60 mm/s);

(d) the mass loss from the single wear path should be significant, and wear path should be manually controlled easily by the operator; and

(e) the wear mechanisms should be elucidated by microscopical observations of the wear topography, worn subsurface and collected wear debris.

8.2 WEAR RESISTANCE, COMPOSITION, MICROSTRUCTURES and HARDNESS

Wear resistance can be related to the composition, the hardness and the microstructures of materials, however, the inter-relationships are rather complicated. For ferrous alloys, carbon content is an important factor in influencing wear resistance and is particularly significant for plain carbon steels. The effect of carbon content in this investigation was examined using the set of plain carbon steels in the annealed, the quenched, and the quenched and tempered conditions, and the set of Bisalloys in the quenched and tempered conditions. The effect of molybdenum concentration on wear resistance was studied using two of the Bisalloys, and the effects of tungsten and vanadium was studied using two high-carbon high-chromium tool steels. Effects of heat treatment on wear resistance was investigated using a Ni-Cr-Mo-C tool steel.

Hardness and microstructure are often inter-dependent factors in influencing wear resistance, and in this investigation, hardness was examined as a measure of wear resistance for different alloys having the same microstructures. The included effects, such as the effect of carbon content for quenched steels or the effect of tempering temperature for tempered martensitic steels, were also analysed. Finally, the effects of

microstructure and composition the same hardness level were examined for comparison purposes.

8.2.1 Carbon Steels and Pure Metals

Ten carbon steels with annealed, normalized, quenched, quenched and tempered, and austempered structures were studied. A wide range of abrasive wear tests (Appendix 1) were carried out to study inter-relationships between wear resistance, hardness, carbon content and microstructure under the standard test condition which was discussed in §8.1.5.

Several pure annealed metals were also examined to relate wear resistance to hardness for the purpose of comparison with the annealed carbon steels.

8.2.1.1 Annealed Structures

For pure metals, the results presented in Fig.7.8(b) confirmed the conclusion of Khruschov[44] and Richardson[23] that the relationship between relative wear resistance and hardness is approximately linear, and the extrapolation passes through the origin. Clearly, this linear relationship can exist only for the single phase metals, for which hardness is determined solely by the inherent characteristics of the (annealed) metals, and there is no inter-phase effect on either hardness or wear resistance. Also, it is possible that the slope for the relationship straight be slightly different for different types of crystal structure as proposed by Tylczak[69] for wear tests carried out with a wide range of pure metals.

For the annealed carbon steels, the results presented in Figs.7.6(a), 7.7 and 7.8(a) are different from the that of pure metals. These results indicate that grain boundary allotriomorphs of cementite and the cementite in pearlite have different effects in increasing hardness and in increasing wear resistance. Also, it is clear that a linear

relationship between wear resistance and hardness can exist only for annealed steels having similar microstructural characteristics and, for this condition, hardness can be used as a predictor of wear resistance as shown in the equation 7-5 ($\varepsilon = \alpha\ Hv + \beta$) presented in §7.2.1.2.

This equation is actually a modified form of the equation

$$\varepsilon = \alpha\ Hv$$

proposed by Khruschov and Babichev[63], which tends to oversimplify the relationship by assuming it to be the same as that for single phase metals with no provision for microstructural variation. This is not the case for annealed steels, for as shown in Fig.7.8(a), the linear extrapolations of the relationship between wear resistance (ε) and hardness (Hv) do not pass through the origin, and the constant β is not equal to zero for either hypoeutectoid or hypereutectoid structures (Table 7.1). Furthermore, it is evident from Figs.7.6(a), 7.7 and 7.8(a) that the linear relationship between wear resistance and hardness is a direct consequence of linear relationships between hardness and carbon content ($Hv = \alpha_1 C + \beta_1$) and between wear resistance and carbon content ($\varepsilon = \alpha_2 C + \beta_2$).

The scanning electron microscopical observation that microcracking loci were halted at, or avoided the pearlitic colonies, Fig.7.14, clearly indicates that pearlite inhibited microcracking through the ferrite. For hypoeutectoid steels therefore, the higher the carbon content, the higher is the volume fraction of pearlite and the higher is the wear resistance. For hypereutectoid steels, however, the higher the carbon content, the thicker are the grain boundary allotriomorphs of cementite. These carbides cannot sustain plastic deformation[127] during abrasion resulting in fracture cracking along the grain boundaries, Figs.7.13(c) and 7.15(a), which was most severe for the annealed 1.4%C steel, Fig.7.15(b). Such fracture contributed significantly to material removal. Nevertheless, the higher the carbon content, the higher was the hardness (Fig.7.6(a)),

the smaller was the sectional size of the abrasion groove[47], and the lower was the overall wear rate. As a consequence, the increase in relative wear resistance with carbon content was more significant for hypoeutectoid steels than for hypereutectoid steels.

8.2.1.2 Martensitic and Bainitic Structures

Martensitic and bainitic ferrous alloys are popularly used in industrial applications demanding wear resistant and therefore for these alloys, it is practically important to elucidate the wear properties from the structures. However, the properties are rather complicated due probably to phase transformation during the abrasion process[139].

For quenched martensitic steels, relative wear resistance was non-linearly related to hardness (Fig.7.9(b)) as a direct consequence of the non-linear dependence of both hardness and relative wear resistance on carbon content (Figs.7.6(b) and 7.9(a)). Clearly, both hardness and relative wear resistance increased with increase in carbon content for the case that the structure was almost fully martensitic (<1.0%C[126]). For carbon content in excess of about 1.0%, there was a rapid increase in the amount of retained austenite[127] which reduced hardness[127] but increased wear resistance[90]. Additionally, the high concentration of carbon in the martensite resulted in microcracking[146] which reduced wear resistance by acting as internal notches during wear processing. For these relations, overall relative wear resistance of the 1.2%C and 1.4%C steels was higher than for the 0.45%C and 0.38%C steels, although the hardness levels of the 1.2%C and 0.45%C steels and the 1.4%C and 0.38%C steels were similar. It appears evident that the increase of wear resistance due to the presence of the retained austenite was more than the decrease due to the microcracks.

The relationship between wear resistance and hardness of tempered martensitic structures for a particular ferrous alloy was proposed[74] to be affected by the work

hardening exponent so that a linear relationship could exist only under the condition that the exponent is constant over the relevant range of tempering temperatures. As the exponent for tempered martensite, in fact, varies with tempering temperature[74], it follows that the relationship between wear resistance and hardness should be non-linear, as observed from the results for the 0.75%C steel, Fig.7.10(c). This non-linear relationship is actually a consequence of non-linear relationships between both hardness and relative wear resistance, with tempering temperature (Fig.7.10(a) and (b)).

Figure 7.11 confirmed[90; 92], that for the same hardness and carbon content less than 1.0%, bainite, produced by austempering, had the highest wear resistance followed by quenched and tempered structures and annealed structures. It also confirmed that for tempered martensite at a hardness of Hv500, the higher the carbon content, the higher was the wear resistance[93; 100]. Zum-Gahr[90] attributed the higher wear resistance of bainitic structures to the presence of retained austenite as it was claimed that lower bainite contains three to four times the amount of retained austenite present in martensitic structures. As austenite is face centred cubic, the toughness is higher than body centred phase due to the availability of numerous slip systems during deformation processing[126]. The high toughness reduces the cutting efficiency of abrasive particles[13] and consequently, decreases the relative wear rate.

For the same hardness level, the higher wear resistance of higher carbon tempered martensitic structures might be attributed to both retained austenite and precipitated carbides, for which, wear resistance has been proposed[100] to be proportional to $\lambda^{-1/2}$, where λ is the mean spacing between the carbides. The measured mean inter-carbide spacing for Hv500 tempered martensitic specimens and the amount of retained austenite in quenched martensitic specimens, shown in Table 7.2, indicate that the higher the carbon content, the larger was the amount of retained austenite and the

smaller was the spacing between carbides. Therefore, the relative wear rate would be expected to decrease with an increase of carbon content as was observed, Fig.7.12. Further, the large amount of retained austenite, which should remain untransformed in specimens tempered at temperatures below 300°C[146], resulted in higher toughness and lower wear rate.

The relative wear resistance of the quenched and tempered 1.2%C steel was lower than for the bainitic 0.75%C steel, at the same hardness and with a similar amount of retained austenite, probably due to microcracks in the martensite as proposed by Krauss[146], and as observed in this work by both optical and scanning electron microscopy. These microcracks remained in the tempered martensite and provided internal notches[90] during abrasive wear, resulting in low wear resistance.

The results (Fig.7.7) that the relative wear resistance of tempered martensite was higher than that of annealed structures for C<1.0%, were due probably to the increased toughness of the tempered martensite[13]. However, for the 1.2%C steel, the wear resistance for the tempered martensite was lower than for the annealed structure at the same hardness. This behaviour again might be attributed to the presence of microcracks in the martensitic structure for the same reasons as discussed above.

8.2.1.3 Normalized and Spheroidized Structures

Steels with normalized and spheroidized structures, and annealed steels, are usually used for similar applications. The hardness value of normalized steels was confirmed to be higher than for annealed steels due to the finer structures resulting from more rapid cooling[126], Table 7.3. However, the similar relative wear resistance of the 0.38%C steel in both normalized and annealed conditions can be attributed to the microstructural characteristics, which in both structures were pearlitic colonies distributed in a ferritic matrix. Clearly, metal removal by microcutting or microcracking

occurred mainly in the ferritic matrix, as shown in Figs.7.13(a) and 7.14(b). For the normalized structure, the pearlitic colonies, were often smaller than the groove width, and were possibly removed without deformation, during a single wear pass, resulting in an increase in wear rate. On the other hand, the increased hardness of the normalized structure should decrease the wear rate. Consequently, the combined effects resulted in the overall wear resistance being similar to that for the annealed structure.

For 0.75%C steel, the higher wear resistance of the normalized structure, compared with the annealed structure, is understandable as the lamellae in the normalized pearlite were about one sixth (1/6) the thickness of those in annealed structure. The thinner ferritic lamellae resulted in a narrower deformation zone, because plastic deformation took mainly place at the ferritic lamellae[39], Fig.7.13(b). Consequently, the abrasion groove was shallower, resulting in a lower wear rate compared with the annealed structure.

The result that the spheroidized structure, which was the original structure of the 1.2%C steel, had the lowest wear resistance among the structures studied agrees with a previous report[100] that wear rates of spheroidized structures are 10% higher than for pearlitic structures with the same hardness. Apparently, the spheroidal carbides were often removed during a single wear pass without any deformation, as their size was much smaller than the width of the abrasion groove, as shown in Fig.7.15(c). Clearly, spheroidized carbides cannot resist abrasive wear as well as lamellar carbides.

8.2.2 Tool Steels

Abrasive wear resistance is especially important for tool steels as they are often used for applications imposing high abrasion stress and for which abrasive wear is the major problem. For this investigation, a Ni-Cr-Mo-C tool steel was studied to determine how the wear resistance could be optimized by generating the appropriate

microstructure by specific heat treatment. Specimens were prepared by either single-quenching or double-quenching and then tempering at 100°C, 200°C, 300°C and 400°C.

Also, two high-carbon high-chromium tool steels were studied to assess the effect of composition, and type and distribution of massed carbides on wear resistance.

8.2.2.1 Ni-Cr-Mo-C Tool Steel

The wear behaviour shown in Fig.7.23 indicates that the relationship between wear resistance and tempering temperature was strongly affected by the quenching treatment (single-quenching or double-quenching), clearly due to the influence of microstructure and carbide characteristics. The quite different untempered structures, which were bainite and martensite for the single-quenched specimen and martensite together with carbides for the double-quenched specimen, can be interpreted in terms of the austenitization process that preceded the air cooling

During initial austenitization, all carbon and alloying elements became dissolved in the austenite to produce a homogeneous solid solution which, upon air-cooling (single-quenching), transformed to martensite and bainite, specimen 10 (Fig.7.21(a)). During re-heating to re-austenitize prior to the second quenching, the martensite and the ferritic constituent of the bainite transformed to austenite, and the bainitic carbides remained at least partially undissolved. These carbides probably spheroidized and coalesced to some degree; and incidentally, inhibited austenitic grain growth[146]. Further, both carbon and alloying element concentrations in the austenite were reduced due to the presence of the undissolved carbides. During the second quenching by air-cooling, the lower concentrations of carbon and alloying element resulted in the austenite transforming to martensite only, in which the original, but modified, bainitic carbides

were dispersed, Fig.7.21(b). The small austenite grain size resulted in fine grained martensite after the second quenching treatment (Fig.7.20).

The lower hardness and relative wear resistance of the double-quenched specimens, 20 and 21, compared with the single-quenched specimens, 10 and 11, (Figs.7.23 and 7.24), can be attributed to the presence of the coarse spheroidal carbides which reduced the amount of carbon and alloying elements in the martensite. Additionally, for the single-quenched specimens, 10 and 11, the large amount of austenite presented in the bainitic structure[90] contributed to the higher wear resistance. This austenite remained untransformed on tempering at 100°C, but probably transformed partially during tempering at 200°C and above, resulting in reducing wear resistance for the specimens 12, 13 and 14.

The improved wear resistance of double-quenched specimen 22 can be attributed to finely dispersed carbides in a fine martensitic matrix, which is consistent with the conclusion[187] that a structure comprising a high density of precipitated carbides in a martensitic matrix has excellent wear resistance. The predominant finely dispersed spheroidal carbides in the double-quenched specimen 22, Fig.7.22(b), were formed by transformation of the martensite and retained austenite during the tempering process probably as a transition form as suggested by Krauss[146]. Additionally, the carbides were probably semi-coherent with the structure of the martensite[127], with consequential beneficial effect on hardness and relative wear resistance. The predominant lath-shaped carbides in the single-quenched specimen 12, Fig.7.22(a), must have derived from the bainitic carbides and the carbides formed by transformation of the coarse martensite and austenite.

The result that the relative wear resistance of the double-quenched specimen 23, which contained predominantly spheroidal carbides, was lower than that of the single-

quenched specimen 13, which contained predominantly lath-like carbides, agrees with previous work[93; 39]. For 400°C tempered specimens, 14 and 24, both hardness and relative wear resistance were significantly higher for the single-quenched specimen 14, (Figs.7.23 and 7.24), indicating that the large amount of carbon and alloying elements in solution in the single-quenched martensite retarded relatively the tempering processes at 400°C, thus increasing wear resistance.

Further, the results shown in Fig.7.24 confirmed earlier work[121] that hardness decreased with tempering temperature from 200°C to 400°C, but the decreasing rate for double-quenched specimens was higher than for single-quenched specimens, due to the larger amount of alloy elements dissolved in the single-quenched martensitic structure retarding the tempering process.

The non-linear relationship between relative wear resistance and hardness shown in Fig.7.25 indicates that parameters other than hardness must influence wear resistance. Also, the form of the relationships for both single-quenched and double-quenched specimens was not influenced significantly by the hardness of the abrasive, although there were differences in the actual values of the relative wear resistance under abrasion with silicon carbide and with garnet.

8.2.2.2 High-Carbon High-Chromium Steels

For the high-carbon high-chromium steels, the carbide volume fraction of carbide was as high as 40% (Fig.7.30), and the massed carbides had the important role in providing wear resistance. The effect of the carbide distribution and carbide type (hardness) on wear rate was examined in this study.

The effect of applied load and abrasive hardness on wear rate has been discussed in §8.1.1. The complex relationship, for the abrasion on alumina, between mass loss and

applied load consisted of three stages (Fig.7.3(b)). First, at applied loads less than 15 N, the wear rate of the XW-5 steel increased slowly with applied load, presumably due to the effect of the M_7C_3 type carbides (Figs.7.31 and 7.32, and Table 7.4) in obstructing the low stress cutting efficiency of the alumina particles. Additionally, the M_7C_3 type carbides appeared to be as effective as the harder MC type carbides (Figs.7.31(a) and 7.32(d), and Table 7.4) in providing wear resistance. Further, the irregular morphology of the massed carbides in XW-5 (Fig.7.30(b)) probably contributed to the wear resistance of the material. The higher wear rate of the Chrome steel may be attributed to the directional distribution of carbides which resulted in a long mean path between the massed carbides. This path was frequently 40μm, and was occasionally as large as the width of the abrasion groove so that the softer martensitic matrix and fine M_3C type carbide particles (Fig.7.31 and Table 7.4) could be removed easily.

For the second stage (15 to 30N applied load), it is likely that the abrasion stress implied by the applied load and flow stress was close to the fracture stress of both the Cr_7C_3 carbides and the alumina abrasive, which have similar hardness values (Table 5.2), and should have similar fracture stress. Microcracking commenced in either alumina abrasive or Cr_7C_3 carbides, and the microcracks of Cr_7C_3 carbides contribute to mass loss. The occurrence of microcracking firstly in either alumina abrasive or Cr_7C_3 carbides is complex, resulting in abrupt change of the predominant wear mechanisms from the microcutting-microploughing to microcutting-microcracking with increase of applied load. Consequently, the relationship between mass loss and applied load had a minor discontinuity.

For loads exceeding 30N, microcracking and spalling (Figs.7.33 and 7.34) were dominant. These processes can occur only under the condition that the local abrasion stresses at contact exceed the failure stress[48], thereby resulting in fracture of the

carbides. Clearly, Chrome had the higher wear resistance due to the influence of MC type carbide, VC, which was harder than alumina, Table 5.2, had high shear strength[124; 49], and was therefore highly resistant to cracking.

In the case that hardness of the abrasives, such as silicon carbide, was much higher than the hardness of massed carbides (Cr_7C_3), the abrasive particles transmitted large shear stresses in addition to normal stresses[65] during the abrasion process, resulting in increased tendency to microcutting. The approximately linear relationship between mass loss and applied load (Fig.7.3(a)) indicates that no abrupt change of the wear mechanism occurred within the range of applied loads from 10 to 50 N.

For the condition that the abrasive (garnet) was much softer than carbide, mass loss increased almost linearly with the applied load, and the difference in mass loss for the two steels increased with increase of load, Fig.7.3(c). This effect is probably due to the influence of the very hard VC particles in Chrome becoming increasingly significant in providing resistance to abrasion with increase of applied load.

8.2.3 Bisalloys

Bisalloys are a type of high-strength low-alloy steel marketed Bisalloys Pty. Ltd. Australia, and are normally used in the quenched and tempered conditions. Wear resistance is the important characteristic of the alloys as they are used for application demanding high resistance to wear[182]. The objective of this study was to examine the effects of tempering temperature and concentrations of carbon and molybdenum on wear resistance.

8.2.3.1 Effect of Tempering Temperature

The results presented in Fig.7.42 confirms, again, the conclusion by Mutton and Watson[25] that for tempered martensite, the relationship between wear resistance and

hardness is non-linear. This non-linear relationship is a direct consequence of non-linear relationships between both hardness and relative wear resistance, and tempering temperature (Fig.7.41). The different forms of the non-linear relationships for tempered BIS B, BIS C alloys (Fig.7.42), 0.75%C steel (Fig.7.10(b)) and Ni-Cr-Mo-C steel (Fig.7.25), can be attributed to the effect of composition. Also, the high increasing rate of relative wear resistance occurring over different hardness ranges for these alloys, such as was at Hv350 to Hv460 for BIS B alloy and Hv400 to Hv430 for BIS C alloy, was due to the characteristics of the carbides precipitated during tempering. Clearly, the non-linear relationship between relative wear resistance and hardness was affected significantly by the work hardening exponent which is determined by tempering temperature and composition[74], and by precipitated carbides[100] as both carbide size and inter-carbide spacing were related non-linearly to the tempering temperature (Fig.7.39).

8.2.3.2 Effect of Molybdenum Concentration

The concentration of alloying elements such as molybdenum in a steel alters the shape of the TTT curve[145] and thereby changes the quenched microstructure. The presence of 0.19% molybdenum in BIS C alloy, which is derived from BIS B alloy (0.003%Mo), resulted in the quenched structure being bainite, as shown in Fig.7.36. After tempering, martensitic and bainitic structures are indistinguishable (Fig.7.37), due to the carbides precipitated from the martensite. In particular, for the 600°C tempered structure, the martensitic matrix has transformed to ferrite consequent upon rejection of carbon to form carbides[127].

Both hardness and relative wear resistance of bainitic specimen BIS C0 were confirmed[21] to be lower than for quenched martensitic specimen BIS B0 (Fig.7.41). However, for the same hardness level, the quenched bainitic specimen BIS C0 had higher wear resistant than for the 300°C tempered martensitic specimen BIS B3,

Fig.7.45(c). This result is consistent with previous results for plain carbon steels[39], as presented in §7.2.2.3 and discussed in §8.2.1.2, and can be attributed to the presence of the large amount of retained austenite in the bainitic structure[90].

For the same tempering temperature (400°C or 600°C), the slightly higher hardness values of BIS C alloy specimens (Table 6.9), BIS C4 and BIS C6, compared with BIS B alloy, indicates that the presence of significant molybdenum in the bainitic structure retards tempering at temperatures ≥ 400°C, and the higher hardness should contribute to improving wear resistance. On the other hand, the coarse carbides with large inter-carbide spacing in tempered bainitic BIS C (Figs.7.38(c) and (d) and Table 7.5) increased mass loss[100]. Probably, for the 400°C tempered BIS C4, the increase of mass loss due to carbide coarsening was more than the decrease due to molybdenum strengthening of the matrix. Consequently, overall mass loss of BIS C4 was higher than for BIS B4 (Figs.7.45(b)) and it was significant at an applied load of ≥ 40N. For the 600°C tempered specimens of BIS B and BIS C alloys, the effect of molybdenum increased, compared with 400°C tempered specimen, although the carbides in BIS C6 were coarser than in BIS B6. As a consequence, the mass loss for both specimens were similar.

The larger size of the carbides and larger inter-carbide spacing λ for specimens of the BIS C alloy was a consequence of simple coarsening of the carbides in the bainitic structure during the 30 minute tempering treatment. The large value of λ contributed to a low wear resistance for the bainitic structure tempered at 400°C (BIS C4) or 600°C (BIS C6), according to the relationship proposed by Larsen-Badse[100] that wear resistance is inversely proportional to the square root of the inter-carbide spacing. For the martensitic steel, however, the tempering process comprises precipitation of transition carbides during the first stage, then dissolution of the transition carbides, and formation and coarsening of cementite during the third stage at a temperature above

300°C. It could be expected that during tempering for a time more than 1/2 hour, the rapid diffusion of carbon would result in coarsening of the carbides in the martensitic specimens of BIS B alloy, whereas carbide coarsening in BIS C is slow due to adverse effect of molybdenum.

8.2.3.3 Effect of Carbon Content

The effect of concentration of carbon on wear resistance of Bisalloys was studied with BIS A (0.085%C), BIS B (0.19%C) and BIS D (0.27%C) after heat treatment by quenching and tempering.

For specimens with approximately the same hardness level, quenched BIS A0 and 400°C tempered BIS B4, Fig.7.40(a), the lower mass loss for BIS B4 resulted from increased toughness associated with the carbides precipitated during 400°C tempering. For the 200°C tempered martensitic specimens, BIS B2 and BIS D2, the result presented in Fig.7.43, is consistent with the previous work[39] that the higher the carbon content, the higher is the wear resistance for the tempered martensitic specimens with the same hardness level .

For the 600°C tempered specimens, BIS A6 and BIS B6, the lower hardness and fewer carbides precipitated during tempering of BIS A6 (0.085%C), Fig.7.38(b), resulted in lower hardness and higher mass loss, compared with BIS B6 (0.18%C), Fig.7.40(b).

8.2.3.4 Effect of Hardness

The results presented in Fig.7.44 confirms[100] that hardness is not the only indicator for wear resistance. Clearly, there is tendency for wear resistance to increase with hardness, but for the particular case, specimen BIS B4 (Hv385) has the higher relative wear resistance than the specimen BIS C4 (Hv405), due to the effects of

microstructure and composition. Hardness can only be an indicator of the wear resistance for a steel under relevant conditions of microstructure and composition, such as the case for the annealed plain carbon steels presented in §8.2.1

8.3 WHITE LAYER

The white layer was recognized as featureless and white by optical microscopy and can be formed under various conditions of mechanical machining and high stress abrasion[188]. For the most cases, the white layer was generated preferably at the 'untempered' martensitic structure[189], and was proposed to be beneficial to wear resistance because of its high hardness[131]. Additionally, the thickness of the white layer is the important role in increasing wear resistance[132].

In this study, the generation and thickness of the white layer was examined in relation to the prior microstructures to elucidate the mechanisms by which it formed under the laboratory abrasive wear testing condition. A possible structure for white layer is proposed based on the present work and review of the literature.

8.3.1 Mechanism of Formation

The results presented in §7.5 indicate clearly that, under the standard abrasive wear test condition, a white layer was generated only on the surface of specimens with prior microstructures of low temperature tempered martensite, or bainite, with a moderate carbon content. Such specimens were the Ni-Cr-Mo-C tool steel tempered at ≤ 300°C, Fig.7.51, and BIS D2 (0.27%C), §7.5.2. It is probably that the generation of the white layer is related to the retained austenite, as both bainite and low temperature (<300°C) tempered martensite contain a certain amount of austenite in the structure[127]. Additionally, the relationship between the maximum thickness of the layer and the carbon content (Fig.7.52) was similar to the relationship between the

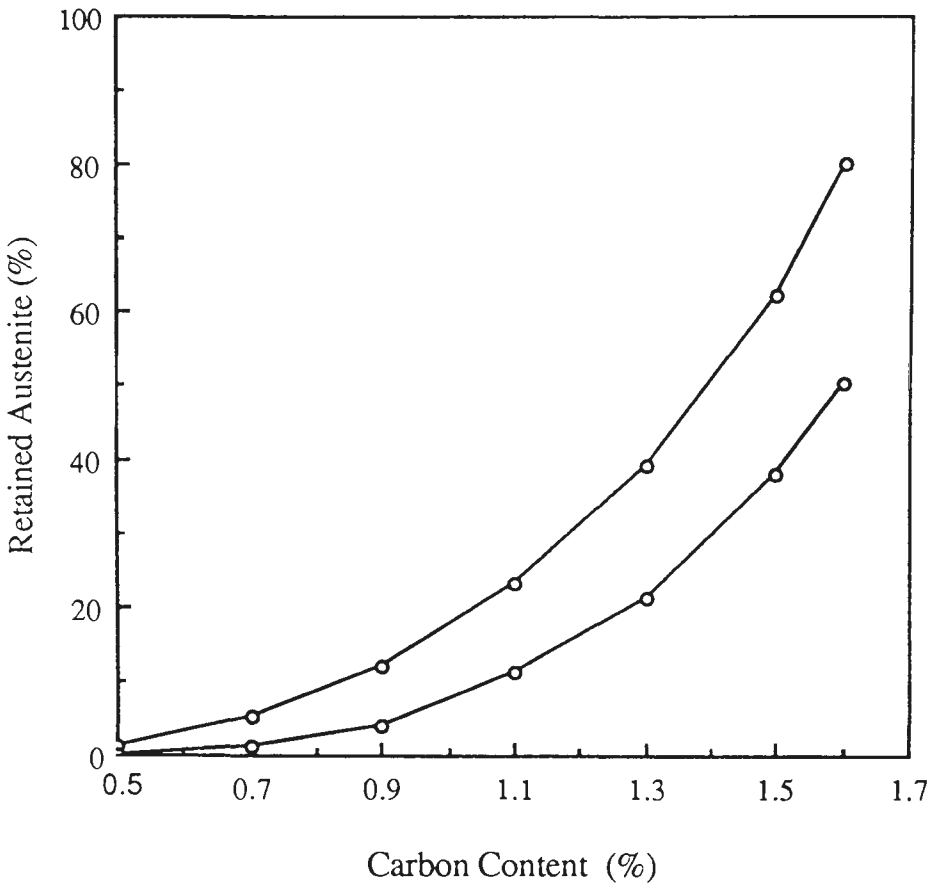

Fig.8.1 Diagram showing the relationship between the amount of retained austenite and the carbon content for quenched carbon steels[127], where two curves indicate the up and low levels of the retained austenite content.

amount of retained austenite and the carbon content (Fig.8.1[127]) for plain carbon steels, which indicates that the larger the amount of retained austenite in the prior microstructure, the thicker the was white layer that was generated during the abrasion process. The austenite, being metastable at ambient temperature, is easily transformed to other structures[102] under a small driving energy, such as deformation stress[190].

The result, for the Ni-Cr-Mo-C steel, that a thick white layer was generated on martensitic specimens tempered at about 200°C, while only a very thin layer was generated on quenched (martensitic) specimens, suggestes that the layer was generate from a prior microstructure of martensite and retained austenite which had partially transformed to dispersed carbides. Also, for 250°C tempered carbon steels, the higher the carbon content, the higher was the density of the precipitated carbides (Table 7.2), and the thicker was the white layer which was generated. It appears that the thickness of the white layer increased with increasing of the amount of precipitated carbides.

Figures 7.13 and 7.19 confirmed[152; 191] that severe plastic deformation occurs at the worn surface; however, the extent of plastic flow is independent of the applied load[58] once the plastic deformation zone reaches a limit; i.e. the thickness of the plastic zone will not change with applied load once the plastic deformation has reached a critical value, such as occurrence of fracture or formation of wear debris. Therefore, the plastic deformation zone that resulted from the applied load of 10N should be similar to that for 50N. Therefore, the result presented in Fig.7.50, that the maximum thickness of the white layer did not change significantly with applied load increasing from 10N to 50N, strongly indicates that the white layer is a consequence of plastic deformation. On the other hand, plastic deformation could not only cause cold work hardening, but also lower both the temperature at which the structure of martensite changes significantly and retained austenite transforms[102], i.e. plastic deformation provides the small amount of energy to accelerate the phase transformation[127]. This plastic

deformation produces local shear and transforms the near-surface microstructure of metastable martensite or austenite[192] to ultra-fine-grained structures[193]. Probably, the deformation energy produced during the abrasive wear test condition was not enough to drive the transformation of equilibrium phases, such as annealed structures, whereas a metastable structure was ideal for such phase transformation.

It is evident that the thickness of the white layer can be related to two contributing factors:

(i) prior microstructure of metastable tempered martensite or bainite with retained austenite and fine precipitated carbides, together with
(ii) severe plastic deformation.

Other factors such as a thermal influence due to sharp heating produced from the high speed grinding, followed by self-cooling, could result in the surface of the specimen being quenched, thereby influence the mechanism of the white layer formation. However, for this study, such influence should not be significant as the wear test was carried out at a low sliding speed of only 50mm/s and the contacting diameter of pin specimen was small (6mm).

8.3.2 Proposal of Structures

For this study, the white layer structure can be categorized as austenitic-martensitic type as proposed by Grozin and Iankevich[134]. It is possibly to propose, on the basis of the discussion in §8.3.1, that the generation of a white layer from tempered martensite, or bainite, and retained austenite, involved severe plastic deformation and partial phase transformation driven by deformation energy. It could be suggested that the structure of the white layer was abnormal (deformed) martensite or bainite, containing extremely fine carbides and ultra-fine-grained structures[128; 144; 194]. The

high hardness of white layer may be attributed to severe cold work hardening, combined with phase transformation hardening[195], which includes precipitation of very fine carbides or formation of extremely fine subgrains with characteristic dimensions of 0.1-1μm[191].

Metastable tempered martensite and retained austenite seem to be necessary structures in generating the white layer under the laboratory abrasive wear test conditions. The fine carbides could interact with dislocations to increase hardness[194], while the retained austenite is mechanically unstable[196] and could be transformed easily to another structure. However, the amount of retained austenite is related to the carbon content of the steels, whilst the stability of retained austenite is determined by the tempering temperature[127]. The result that the thickest white layer was generated on the 1.2%C steel tempered at 250°C is consequence of the large amounts of both retained austenite and fine carbides in this steel.

8.4 ABRASIVE WEAR MECHANISMS

Wear mechanisms are important in understanding the characteristics of the wear debris formation in relation to microstructural properties. In this investigation, wear mechanisms were studied using taper sections of wear surfaces, wear topography and wear debris collected under the standard wear test condition.

8.4.1 Wear Debris Formation

Generally, material is removed from the specimen by the formation of wear debris during abrasive wear. The results presented in §7.2.3, §7.3.1.4, §7.3.2.4 and §7.4.4, indicate clearly that wear debris was formed mainly by microcutting or microcracking, with microploughing as a precursor process. Microploughing is a consequence of plastic deformation, and should occur inevitably on any worn surface[191; 196] forming

built-up bulges[37] at the two edges of the groove and a prow at the end of the groove (Fig.7.26(c)). The bulges, with high stress resulting from plastic deformation, were often cut to produce side-formed chips or fracture debris during subsequent abrasion, Fig.7.26(b). Also, the side-cut chip could be a precursor for the main cut chip as shown in Fig.7.27(b) or as a by-product located at the side of the main cut chips, Fig.7.27(c).

Practically, the abrasion groove was often formed by microcutting combined with microploughing. For this cases, the wear chips were characterized by a ploughed prow at the head, a smooth surface on the cutting tool (abrasive particle) side and serrations on the other surface, as shown in Figs.7.16, 7.27, 7.35(a) and 7.49. These serrations indicate that intensive shear deformation was involved in chip formation. The fracture wear debris was characterized by flat sheets (Fig.7.17), in which microcracks were observable. The occurrence of these microcracks was dependent upon the characteristics of the microstructure of the specimen. Clearly, the fracture debris from hypereutectoid specimens had allotriomorphic cracks (Fig.7.17(b)), while from spheroidized specimens had granular cracks, Fig.7.18(b).

It is clear from the predominance of prow-forming chips shown in Fig.7.35(a) that the dominant mechanism of metal removal was microcutting by which material was initially ploughed by an abrasive particle to form a groove with a prow and bulged edges. These bulges and prows were then sheared, to form chips, by following abrasive particles. These observations also confirmed the proposal[197] that during abrasive wear, only a small fraction of the abrasive particles take part in the cutting action, and that the effective cutting area of a particle is that very small part positioned critically for both rake angle and inclination angle. Thus the chips were much smaller than the abrasive particles, Fig.7.35(b), and the flow direction of the chip being cut depending mainly on the position of the rake angle[31].

Additionally, protruded massed carbides were either detached from the matrix, Fig.7.35(d), or cracked, Fig.7.34(a) in forming small wear debris after the soft matrix was attacked by abrasive particles. The built-up-edge formed on the abrasive particle (Fig.7.35(c)) during cutting action[32] was often fractured to small fragments during the further cutting in forming fine wear debris.

Both large cut chips and small fracture debris can be either free particles separated from the specimen surface together with detached abrasive particles, or particles located on the used abrasive paper (Figs.7.28 and 7.29). The free wear chips or debris were easily collected in the tray underneath the rotating drum and then analysed using scanning electron microscopy, as shown in Figs.7.16, 7.17, 7.18 7.27, 7.35 and 7.49,

8.4.2 Dominant Wear Mechanisms

In considering the abrasive wear process, it is well known[31; 198] that the individual abrasive particles function as cutting tools with random distribution of rake angle. Pure cutting can occur only for those particles having a critical orientation of rake angle, while pure ploughing can occur only for particles positioned with a sufficiently negative rake angle to cause flow of material to form ridges terminating in a prow[37]. Practically, microcutting and microploughing often occurred together, which was indicated by cut chips with a ploughed prow head (Fig.16(b)), by bulged ridges at the cut groove (Fig.7.26(c)) and by the plastically deformed zone at the edges of the cut groove observed in the slight taper section (Fig.7.13(b)). Microcracking occurred frequently in forming fracture debris for specimens with high carbon content (Figs.7.17(b) and 7.18(b)), and was observable on the wear topography (Figs.7.12, 7.26 and 7.33) and in the slight taper section for the annealed 1.2%C and 1.4%C steels (Figs.7.15(a) and (b)).

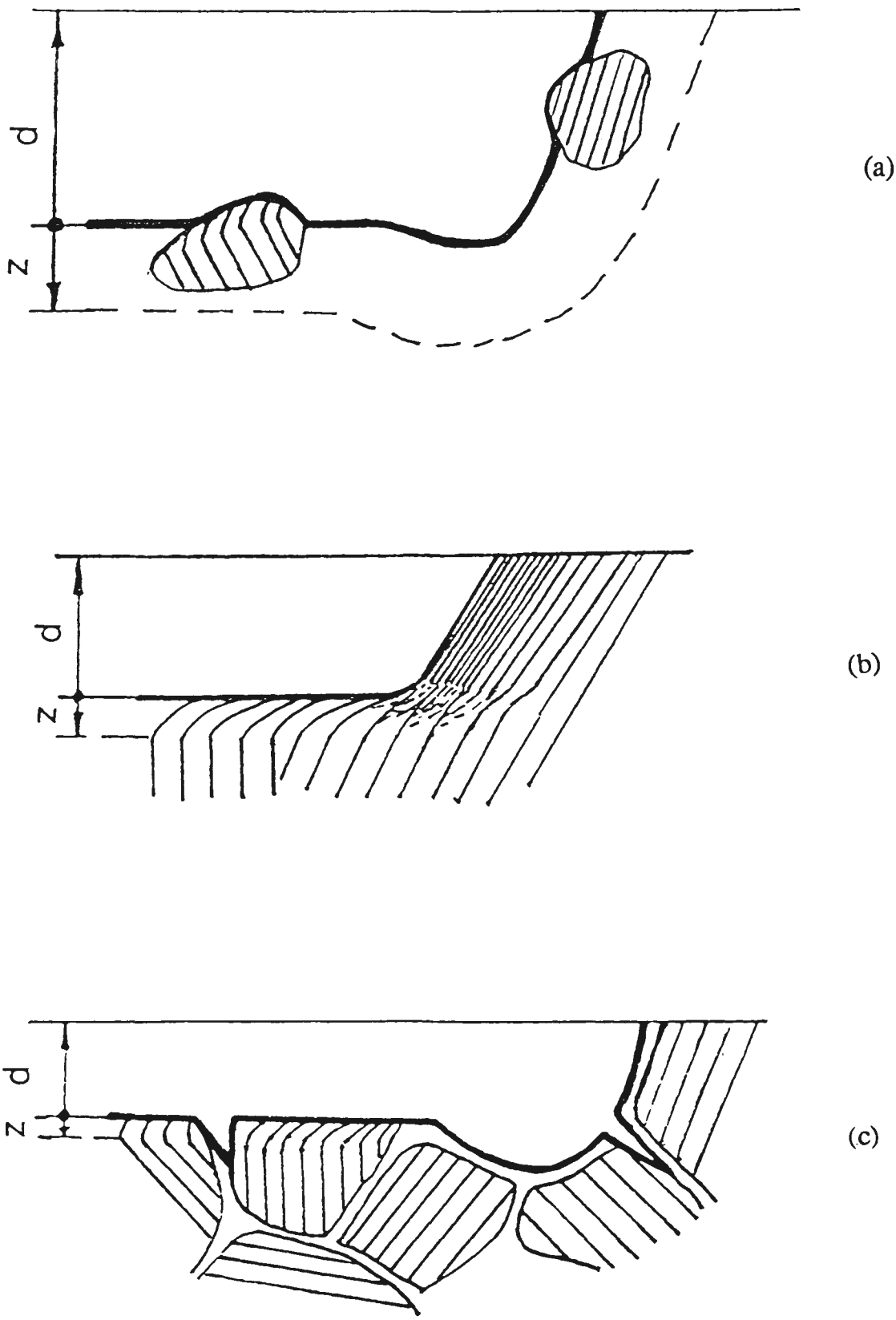

Fig.8.2 Diagrams showing models of the abrasion grooving for annealed steels: (a) very low carbon, (b) pearlitic, (c) hypereutectoid; d indicates the depth of the abrasion groove from the polished surface, and z indicates the thickness of plastic deformation zone.

Figure 8.2 presents three grooving models corresponding to typical abrasion grooves in annealed plaincarbon steels shown in Fig.7.13. It is evident in Figs.7.13(a) and 7.19 that for an annealed steel with very low carbon level, the main wear mechanism was microcutting, but significant microploughing was involved in producing the large abrasion grooves and the plastic deformation zones[58] must be quite thick. For microploughing, the substantial mechanism for metal removal was fracture cracking, occurring through the ferritic matrix when the stress, which resulted from plastic flow, exceeded the strength of the material[89]. For pearlitic steels, wear occurred mainly by microcutting characterized by a sharp ended groove, Fig.7.13(b), with some microploughing. In the thin plastic deformation zone, the ferritic lamellae were deformed more severely than the cementite lamellae, as shown in Fig.8.2(b), and indicated that plastic deformation of pearlite was sustained mainly by the ferrite. For hypereutectoid steels, the hard and brittle grain boundary cementite resisted plastic deformation resulting in a shallow groove and a very thin deformation zone; occasionally, cracking and spalling occurred at the groove end, Figs.7.13(c) and 8.2(c).

Practically, microploughing-microcutting was the predominant mechanism for metal removal for the specimens with low carbon content such as the 0.10%C and 0.38%C carbon steels, the Ni-Cr-Mo-C tool steel (Fig.7.27) and Bisalloys (Figs.7.46 and 7.49). Microcutting-microcracking was the predominant mechanism for the specimens with high carbon content or containing carbide forming alloying elements, as shown in Figs.7.12, 7.26 and 7.33. For the spheroidized structure of the 1.2%C steel, microcutting with a small amount of ploughing was the dominant characteristic for grooving, and the small cementite carbides were commonly removed in single abrasion pass in which the microcutting and ploughing took place in the ferritic matrix (Fig.7.15(c)).

For the martensitic and bainitic specimens, wear mechanisms were dependent upon the tempering temperature. Apparently, microcutting-microcracking was the predominant mechanism for the low temperature tempered specimens, as shown in Fig.7.26(a); probably, phase transformation was involved with the chip formation process, which was indicated by the white layer formation as discussed in §8.4.1. For the high temperature tempered martensitic specimens, however, microcutting-microploughing was the dominant mechanism as shown in Fig.7.12(d), due to the high toughness of the specimen achieved during the tempering process.

8.4.3 Secondary Wear Mechanisms

The secondary wear mechanisms involved with the process of wear debris formation were mainly adhesion and delamination. It is clear from Fig.7.35(c) that an adhesive mechanism was involved in generating small particles of wear debris as indicated by the built-up-edge formed on the cutting region of some abrasive particles, agreeing with the formation of prows during adhesive wear[197]. In the present case, metal was removed by welding-on over a small area of an active abrasive particle, followed by fracture at the built-up-edge to form small fragments.

The delamination mechanism was involved with the wear chip formation characterized by the serrations on the groove edge (Fig.7.47(c)) and at the side of the cut chip (Fig.7.49(b)) for specimens of Bisalloys. Clearly, it was the plastic flow that resulted in the formation of serration and the concentration of high stress at the worn surface. Consequently, the subsurface cracked or the deformed material at the wearing surface was sheared[9].

The longitudinal direction of the serrations for the H.M.S. specimen (Figs.7.48 and 7.49(f)) can be attributed to the austenitic structure which, being face centred cubic,

had different flow directions to the martensitic structure[126]. Further, microfatigue was probably involved with the delamination process as described by Suh[9], but, it can hardly be observed under this test condition.

8.5 COMMENTS

The inter-relationships between wear resistance, hardness, composition and microstructure are complex and are influenced by the operational variables, especially the applied load. Wear resistance for a particular steel can be optimized by applying proper heat treatment to obtain the appropriate microstructure.

The generation of the white layer under the abrasive wear test condition was very much related to the prior microstructures. The thickness of the white layer is influenced by the tempering temperature for a particular steel, and by the carbon content for the plain carbon steels.

The dominant wear mechanisms for this investigation are microcutting-microploughing for low carbon or high toughness steels and microcutting-microcracking for high carbon or brittle steels. The secondary wear mechanisms were found to be adhesion and delamination.

Chapter 9

CONCLUSIONS

Based on the discussion presented in Chapter 8, it is possible to determine the effect of the operational variables on wear behaviours and the inter-relationships between wear resistance, composition, microstructures and hardness according to the characteristics of the investigated plain carbon steels, tool steels and Bisalloys. Additionally, it is also possible to analyse the prevailing wear mechanisms and the conditions under which the the white layer was formed.

1. Operational Variables

i). Applied Load

The relationship between mass loss and applied load was approximately linear for the cases in which the abrasive particles were much harder than the test steels. For the tool steels with a large amount of massed carbides, the relationship was dependent upon the relative hardness of the abrasive particles and the massed carbides. This relationship was complex for the case that the abrasive particles were as hard as the massed carbides, such as alumina and Cr_7C_3, and was almost linear for the condition that abrasive particles were much harder or softer than the massed carbides.

ii). Sliding Speed

The relationship between mass loss and sliding speed was dependent upon the hardness of the test steels and the ratio (η) of the specimen hardness to the applied stress, due to the effect of the flow stress. Additionally, the relationship was influenced by hardness more significantly than by η. The harder the test steels and the lower the value of η, the less was the mass loss influenced by the speed.

iii). Wear Path

Mass loss was linearly related to the wear path.

2. Wear Resistance, Composition, Microstructures and Hardness

i). Carbon Steels

a). For annealed steels, both wear resistance and hardness were linearly related to carbon content with different slopes for hypoeutectoid and hypereutectoid compositions. Consequently, the relationships between relative wear resistance and hardness were linear, with different slopes, neither of which projected through the origin. Thus, hardness can be used as a predictor of wear resistance for annealed steels only with the same type of microstructure.

b). Normalizing treatment for the 0.75%C steel increased both hardness and wear resistance significantly, but for hypoeutectoid 0.38%C steel, normalizing increased only hardness.

c). Carbon content increased wear resistance more prominently for hypoeutectoid steels than for hypereutectoid steels. For the martensitic steels with the same hardness, the higher the carbon content, the higher was the wear resistance. Wear resistance of quenched steels increased with the increase in carbon content to about 1.0%, then decreased for further increase of carbon content.

d). Microstructure was as important in determining wear resistance as was hardness or as carbon content. At the same hardness and carbon content less than 1.0%, bainitic structures had the highest wear resistance, followed by quenched and tempered structures, then annealed structures and spheroidized structures. However, for a 1.2%C steel, the wear resistance of tempered martensite was lower than that of the annealed structure.

e). For a particular steel under the quenched and tempered condition, the relationship between wear resistance and hardness was complex, so that hardness was not a direct indicator for wear rate. For tempered martensitic steels, wear resistance increased with increase of carbide size and decrease of inter-carbide spacing.

f). Under the condition of constant microstructure, the relationship between wear resistance and hardness was non-linear for the cases that both wear resistance and hardness were non-linearly related to the third factor, such as carbon content for quenched (martensitic) steels or tempering temperature for tempered steels.

ii). Ni-Cr-Mo-C Tool Steel

a). The effect of tempering temperature on wear resistance was strongly related to the quenching treatment. For single-quenched specimens, the relative wear resistance decreased non-linearly with tempering temperature; for double-quenched specimens, relative wear resistance had a maximum value at 200°C.

b). The relationship between relative wear resistance and hardness was influenced by the quenching treatment. For single-quenched specimens, relative wear resistance increased with hardness to a maximum value at Hv610 (specimen 10), then decreased with further increase in hardness. For double-quenched specimens, relative wear resistance increased non-linearly with hardness to the highest value available in the study, Hv660. Additionally, relative wear resistance for the double-quenched specimen, tempered at 200°C was the highest value among all the Ni-Cr-Mo-C tool steel specimens examined.

c). The relative wear resistance was optimized with the microstructure of high density of finely dispersed carbides in a fine tempered martensitic matrix, such as in the double-quenched and 200°C tempered specimen.

iii). High-Carbon High-Chromium Tool Steels

a). The relationship between wear rate and applied load depended significantly on the relative hardness of the abrasive particles and massed carbides in the steels. Linear relationships were found under the condition that the hardness of the abrasive was considerably higher, or lower, than that of massed carbides in the specimen, as was the case for silicon carbide abrasive or garnet abrasive. For abrasive which was harder than the massed carbides, the difference in wear rate for the two steels was constant over the range of applied load. This difference increased significantly for abrasive softer than the massed carbides. However, for the condition that the hardness of the abrasive was similar to that of the massed carbides, the relationship between wear rate and applied load was complex.

b). Carbide hardness and distribution strongly affected wear rate for the condition that the hardness of the abrasive was similar to that of the massed carbides. The randomly distributed irregular M_7C_3 type carbides in XW-5 resulted in a lower wear rate under low stress abrasion while the harder VC in Chrome contributed to a higher wear resistance under higher stress abrasion.

c). It appears that wear resistance of a tool steel with a large amount of massed carbides can be optimized with the microstructure of randomly distributed massed carbides of the hard MC type mixed with M_7C_3 type in a tempered martensitic matrix.

iv). Bisalloys

a). For the quenched and tempered martensitic, or bainitic, alloys, the relationship between relative wear resistance and hardness was non-linear. For a particular

steel, the shape of the relationship was strongly influenced by the concentrations of carbon or alloying elements.

b). At the same hardness level, bainite had higher wear resistance than tempered martensite. However, after tempering at temperatures above 300°C, tempered bainite had lower wear resistance than tempered martensite, due to the large inter-carbide spacing in the tempered bainitic structure. For the tempered Bisalloys, the higher the carbon content, the higher was the wear resistance.

3. **White Layer**

i). The favourable prior microstructure for generating the white layer under the laboratory abrasive wear test was low temperature tempered martensite or bainite containing dispersed carbides. The higher the carbon content, the thicker was the white layer. For a particular Ni-Cr-Mo-C tool steel, the white layer was thick on specimens tempered at 100°C and 200°C, thin on quenched specimen and 300°C tempered specimen, and absent on the 400°C tempered specimen.

ii). The generation of the white layer can be attributed to a prior microstructure of metastable tempered martensite or bainite containing retained austenite and dispersed carbides, and severe plastic deformation which occurred during wear processing.

iii). The structure of the white layer is probably a kind of abnormal martensite or bainite, which contains extremely fine carbides or subgrains.

4. Abrasive Wear Mechanisms

i). The dominant wear mechanisms were microcutting together with minor microploughing or microcracking. The occurrence of microploughing and microcracking was dependent upon composition and microstructure. Microploughing, which occurred significantly at low hardness or in low carbon steels, often a precursor for cutting or cracking. Microcracking occurred when the abrasion stress reached the fracture stress and, for higher carbon steels such as annealed 1.2%C steel, and the harder structure, the more cracking which occurred during abrasion.

ii). Secondary wear mechanisms were dependent upon mechanical properties. For hard materials such as high-carbon high-chromium tool steels, the adhesive mechanism was involved in forming built-up-edges and then fracture into small wear debris, whilst delamination was significant for softer materials such as Bisalloys.

iii). Wear debris comprised free particles together with the broken abrasive particles, or material that was deposited on the worn abrasive paper and on the specimen wear topography. The cut wear chips were very similar to machined chips with a curled shape, serrations and built-up-edge. Therefore, each abrasive particle could be considered as a temporary machining tool with randomly distributed rack angle and cutting angle.

iv). The process of wear chip formation was complex, with severe plastic deformation occurring on the wear surface.

Chapter 10

SUGGESTIONS

1. The relationship between wear resistance and hardness for this investigation was obtained under the test conditions of 20N applied load, 50mm/s and 6m wear path. It appears that this relationship should change if the test condition is varied. Further work carried out under an applied load of 30N, 40N or 50N, to elucidate effect of applied loads on wear behaviour is suggested as it is probable that the relationships are influenced by the applied load, and the fracture properties may be important for wear resistance under the higher applied loads.

2. To further elucidate wear mechanisms, especially the shear process during the wear chip formation, it is suggested that simulation of wear test be carried out so that the possible mathematical relationship can be sought out to relate wear resistance to material properties. This kind of wear test can be designed with one or more regularly shaped abrasive particles positioned either directionally or randomly, and the test model can be based upon a single wear mechanism, such as microcutting, or microploughing, or microcracking, or mixed mechanisms. The investigation can be carried out to study the effects of the arrangement and the shape of the 'abrasive particles', and the applied load on wear behaviour, and therefore, wear resistance can be related mathematically to material properties for either a single mechanism or mixed mechanisms.

3. For martensitic and bainitic specimens, it is desirable to further elucidate details of the wear mechanisms, such as plastic deformation or phase transformation, involved in the abrasion processes. Further work is suggested to relate wear resistance to toughness and characteristics of precipitated carbides in these structures.

4. For the white layer, further work can be carried out on:

a). the effect of the layer on increasing wear resistance;

b). the effect of thickness of the white layer on wear resistance; and

c). the structure of the white layer.

APPENDICES

Appendix 1

OPERATIONAL VARIABLES and ABRASIVE PAPERS SELECTED for the WEAR TESTS

Specimen	Variable	Test Condition	Abrasive Paper
10F	V	L=20N, X=6m	Silicon carbide
10F	L	V=50mm/s, X=6m	Silicon carbide
10F	X	L=20N, V=50mm/s	Silicon carbide
10M		L=20N, V=50mm/s, X=6m	Silicon carbide
38FP	V	L=20N, X=6m	Silicon carbide
38FP	L	V=50mm/s, X=6m	Silicon carbide
38FP	X	L=20N, V=50mm/s	Silicon carbide
38NFP		L=20N, V=50mm/s, X=6m	Silicon carbide
38M650		L=20N, V=50mm/s, X=6m	Silicon carbide
38M600		L=20N, V=50mm/s, X=6m	Silicon carbide
38M450		L=20N, V=50mm/s, X=6m	Silicon carbide
38M300		L=20N, V=50mm/s, X=6m	Silicon carbide
38M250		L=20N, V=50mm/s, X=6m	Silicon carbide
38M200	L	V=50mm/s, X=6m	Silicon carbide
38M200	X	L=20N, V=50mm/s	Silicon carbide
38M	L	V=50mm/s, X=6m	Silicon carbide
45FP		L=20N, V=50mm/s, X=6m	Silicon carbide
58FP		L=20N, V=50mm/s, X=6m	Silicon carbide
58M650		L=20N, V=50mm/s, X=6m	Silicon carbide
58M250		L=20N, V=50mm/s, X=6m	Silicon carbide
58M		L=20N, V=50mm/s, X=6m	Silicon carbide
75P	V	L=10N, 20N, 50N, X=6m	Silicon carbide
75P	L	V=50mm/s, X=6m	Silicon carbide
75P	X	L=20N, V=50mm/s	Silicon carbide
75NP		L=20N, V=50mm/s, X=6m	Silicon carbide
75M650	L	V=50mm/s, X=6m	Silicon carbide
75M500		L=20N, V=50mm/s, X=6m	Silicon carbide
75M350		L=20N, V=50mm/s, X=6m	Silicon carbide
75M250	V	L=20N, X=6m	Silicon carbide
75M250	L	V=50mm/s, X=6m	Silicon carbide
75M250	X	L=20N, V=50mm/s	Silicon carbide

Cont. OPERATIONAL VARIABLES and ABRASIVE PAPERS SELECTED for the WEAR TESTS

Specimen	Variable	Test Condition	Abrasive Paper
75M150	L	V=50mm/s, X=6m	Silicon carbide
75M	L	V=50mm/s, X=6m	Silicon carbide
75B	L	V=50mm/s, X=6m	Silicon carbide
75B	X	L=20N, V=50mm/s	Silicon carbide
80P		L=20N, V=50mm/s, X=6m	Silicon carbide
85P		L=20N, V=50mm/s, X=6m	Silicon carbide
100PC		L=20N, V=50mm/s, X=6m	Silicon carbide
100M650		L=20N, V=50mm/s, X=6m	Silicon carbide
100M		L=20N, V=50mm/s, X=6m	Silicon carbide
120PC	L	V=50mm/s, X=6m	Silicon carbide
120S	L	V=50mm/s, X=6m	Silicon carbide
120M650	L	V=50mm/s, X=6m	Silicon carbide
120M250	L	V=50mm/s, X=6m	Silicon carbide
120M	L	V=50mm/s, X=6m	Silicon carbide
140PC		L=20N, V=50mm/s, X=6m	Silicon carbide
TS 00		L=20N, V=50mm/s, X=6m	Silicon carbide, Garnet
TS 10		L=20N, V=50mm/s, X=6m	Silicon carbide, Garnet
TS 11		L=20N, V=50mm/s, X=6m	Silicon carbide, Garnet
TS 21		L=20N, V=50mm/s, X=6m	Silicon carbide, Garnet
TS 12		L=20N, V=50mm/s, X=6m	Silicon carbide, Garnet
TS 22		L=20N, V=50mm/s, X=6m	Silicon carbide, Garnet
TS 13		L=20N, V=50mm/s, X=6m	Silicon carbide, Garnet
TS 23		L=20N, V=50mm/s, X=6m	Silicon carbide, Garnet
TS 14		L=20N, V=50mm/s, X=6m	Silicon carbide, Garnet
TS 24		L=20N, V=50mm/s, X=6m	Silicon carbide, Garnet
BIS A0	L	V=50mm/s, X=6m	Silicon carbide, Alumina, Garnet
BIS A6	L	V=50mm/s, X=6m	Silicon carbide, Alumina, Garnet
BIS B0	L	V=50mm/s, X=6m	Silicon carbide
BIS B2	L	V=50mm/s, X=6m	Silicon carbide
BIS B3	L	V=50mm/s, X=6m	Silicon carbide, Alumina, Garnet
BIS B4	L	V=50mm/s, X=6m	Silicon carbide, Alumina, Garnet
BIS B5	L	V=50mm/s, X=6m	Silicon carbide, Alumina, Garnet

Cont. OPERATIONAL VARIABLES and ABRASIVE PAPERS SELECTED for the WEAR TESTS

Specimen	Variable	Test Condition	Abrasive Paper
BIS B6	L	V=50mm/s, X=6m	Silicon carbide, Alumina, Garnet
BIS C0	L	V=50mm/s, X=6m	Silicon carbide
BIS C2	L	V=50mm/s, X=6m	Silicon carbide
BIS C4	L	V=50mm/s, X=6m	Silicon carbide, Alumina, Garnet
BIS C6	L	V=50mm/s, X=6m	Silicon carbide, Alumina, Garnet
BIS D2	L	V=50mm/s, X=6m	Silicon carbide, Alumina, Garnet
H.M.S.	L	V=50mm/s, X=6m	Silicon carbide, Alumina, Garnet
XW-5	L	V=50mm/s, X=6m	Silicon carbide, Alumina, Garnet
Chrome	L	V=50mm/s, X=6m	Silicon carbide, Alumina, Garnet

Note: The range of the operational varibles selected for this study are: applied load L=10N to 50 N, sliding speed V=3 to 60 mm/s, and wear path X=1.5 to 6 m; and the standard wear test condition is: L=20N, V=50 mm/s and X=6m.

Figure A2 **Structural drawing of the pin-on-drum wear test machine**

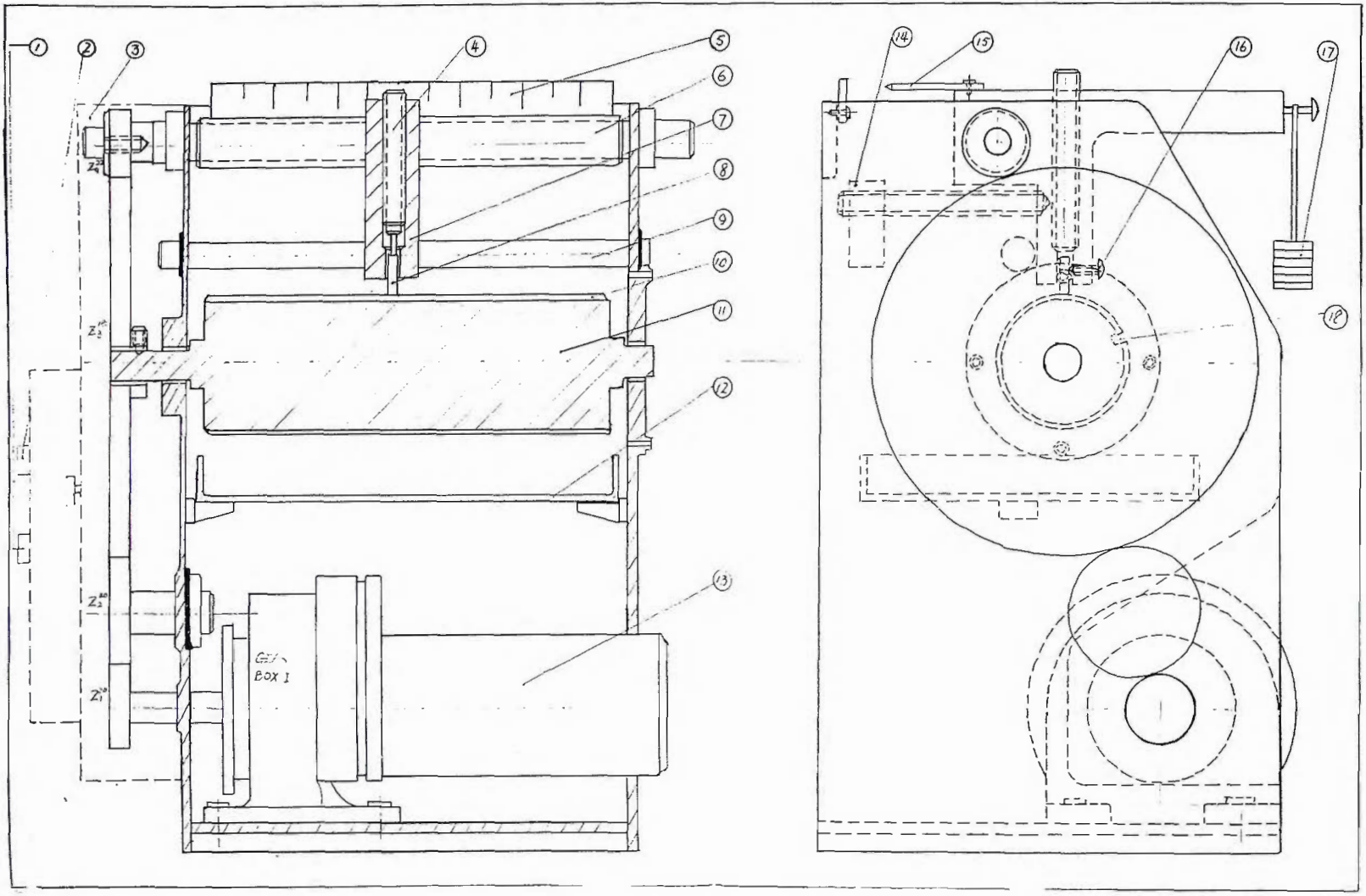

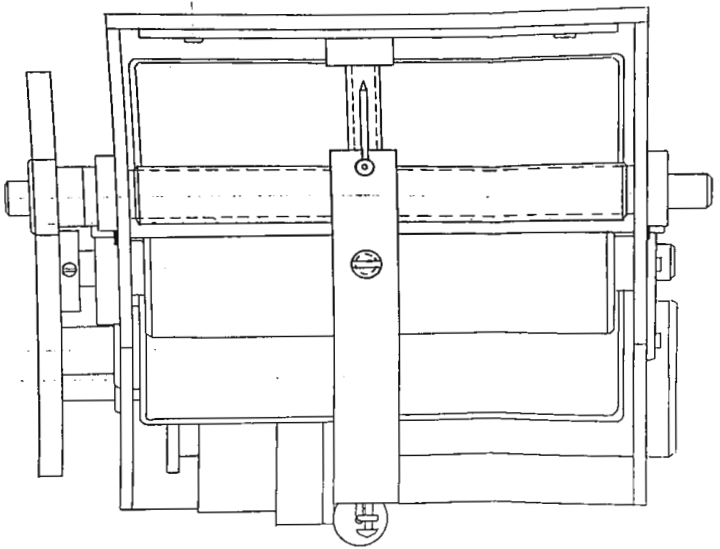

18	SLOT
17	APPLIED LOAD
16	SPECIMEN LOCK SCREW
15	HAND
14	BALANCE WEIGHT
13	VARIABLE SPEED MOTOR
12	TRAY
11	DRUM
10	ABRASIVE PAPER
9	GUIDE SHAFT
8	PIN SPECIMEN
7	SPECIMEN HOLDER
6	GUIDE SCREW
5	RULER
4	SPECIMEN FIXER SCREW
3	GEAR BOX II
2	SPEED SWITCH
1	POWER SWITCH

MATERIALS ENG. DEPARTMENT
WOLLONGONG UNIVERSITY
ABRASIVE WEAR TEST MACHINE
6/5/91 | ZIQUN XU

Appendix 2 DESIGN and WEAR TEST of the PIN-ON-DRUM MACHINE

The pin-on-drum configuration was selected according to the wear devices recommended by the American Society of Lubrication Engineering[199]. The structural drawing of the pin-on-drum wear test machine is shown in Fig.A2. The machine is electrically powered through switch [1], by a variable speed motor [13] with a speed range of 60 to 1200 rpm. The pin specimen, 6mm in diameter and 20 to 35mm in length, moves along a helix locus on the rotating drum covered with abrasive paper. The horizontal distance of specimen movement during one rotation of the drum is 8.2mm, as presented in §6.1.1, which ensures that the specimen always encounters unused abrasive paper. The relationship between the movement of the pin specimen and the rotating drum is obtained by the gear box II with gearing of Z_3 and Z_4 at a ratio of 90/11, and the guide screw having 1mm/teeth. This screw drives the specimen holder horizontally. The rotation speed of the drum is, therefore, transferred from the motor by the gear box I with speed reduction ratio of 1/10, and the gear box II gearing of Z_1, Z_2 and Z_3, with a ratio of 1/9.

The diameter of the drum, 86mm, provides a circular length of 280 mm which is just less than the length of commercially available abrasive paper. The length of the drum, 300 mm, allows a total allowable wear path of 7m (Table 6.2), to provide a practical testing wear path of 6m manually controlled using the power switch according to the wear path indicated at the ruler [5] by a pointer [15]. The commercial abrasive paper is attached to the drum by inserting one end in a narrow slot [18] on the drum and affixing the other end to drum using double-sides adhesive.

The sliding speed between the pin specimen and the drum ranges from 3 to 60 mm/s (Table 6.3), and is manually controlled by switch [2]. The applied load [17] is obtained by adding weight to the end of the specimen holder arm [7], and the actual applied load on the specimen is measured by weighing at the top of the specimen holder at the fixer

screw [4] using a spring balance. The friction force between the guide screw [6] and the specimen holder [7] strongly influences the actual applied load, and therefore, it is important to keep the guide screw [6] clean by frequent greasing. Clean paper inserted between the tray [12] and the drum [11] collects wear debris for scanning electron microscopical observations.

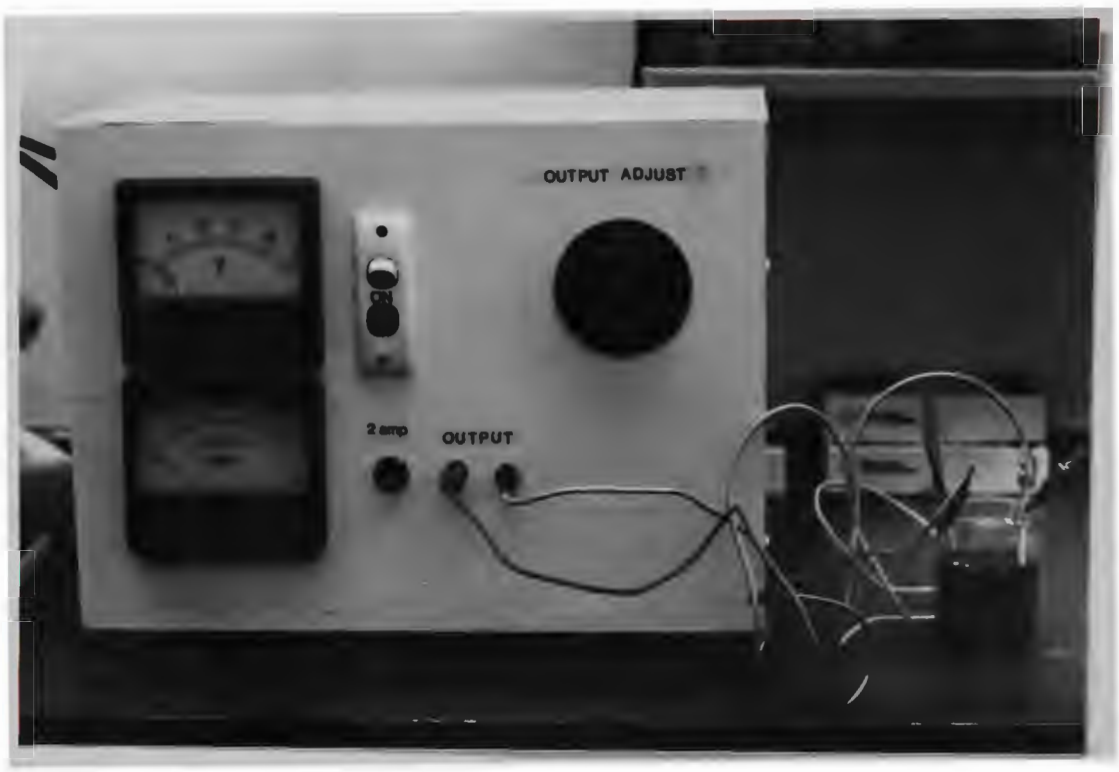

(a)

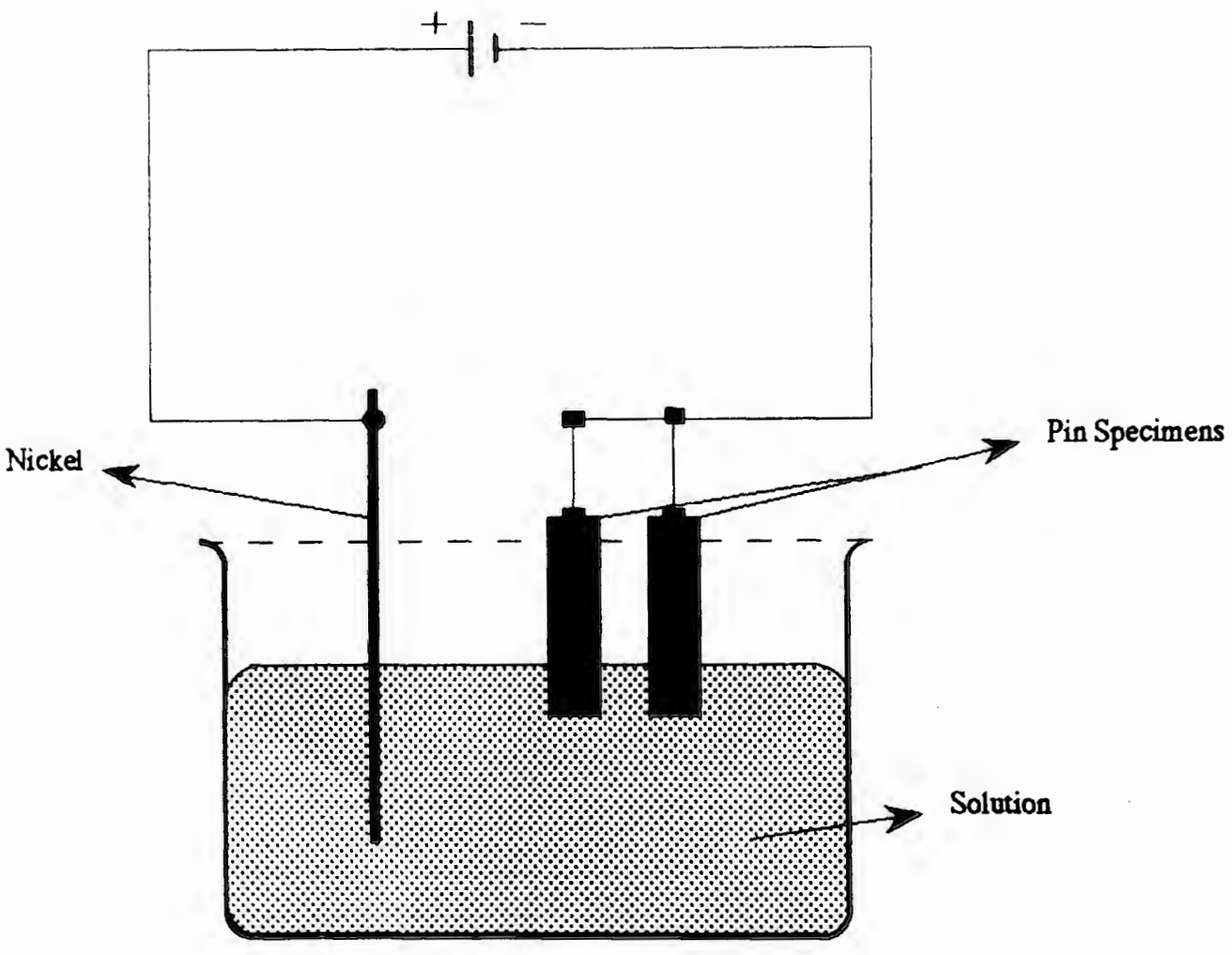

(b)

Fig.A3.1 A nickel electro-plating device showed by: (a) photograph and (b) drawing.

Appendix 3 NICKEL ELECTRO-PLATING

A nickel electro-plating device was constructed for this investigation, as shown in Fig.A3.1, according to the principle and technique suggested by the International Nickel Company (Mond) Limited[200]. In the electro-deposition process, nickel was plated on the negative electrode (the cathode) from an aqueous solution of nickel salts. A piece of pure nickel served as the anode at which nickel atoms could enter the electrolyte to form nickel ions and migrate to cathode. The specimen in the bath, which was connected with the cathode, gained the nickel ions.

The electro-solution[201] used for this nickel-plating was:

nickel sulphate (250g) + nickel chloride (50g) + boric acid (30 to 40g)

per litre of distiled water. The nickel sulphate provided the main source of nickel ions, and the nickel chloride served to prevent anode passivity by providing a source of chloride ions. It also furnished additional nickel ions and increased the conductivity of the electrolyte. Boric acid acted as a buffer to prevent an excessive charge in hydrogen ion concentration in the vicinity of the cathode.

The pH value of the solution is an important factor for nickel plating. The appropriate pH value for this plating was found to be between 4.5 to 4.8, which was adjusted by adding of sulphuric acid to the solution. A higher pH value (>5) caused the cathode (specimen) to oxidize, and a lower pH value (<4) caused nickel sulphate to deposit on the cathode to form a barrier film for the nickel plating. The current was controlled at about 1mA.

The thickness of plating was required to be about 1mm to protect the specimen during preparation of the making 5° taper section. Normally, it took about 24 hours to complete the 1mm plating, so that for efficiency, two specimens were plated simultaneously, for which the working principle of electrical circuit is shown in Fig.A3.2.

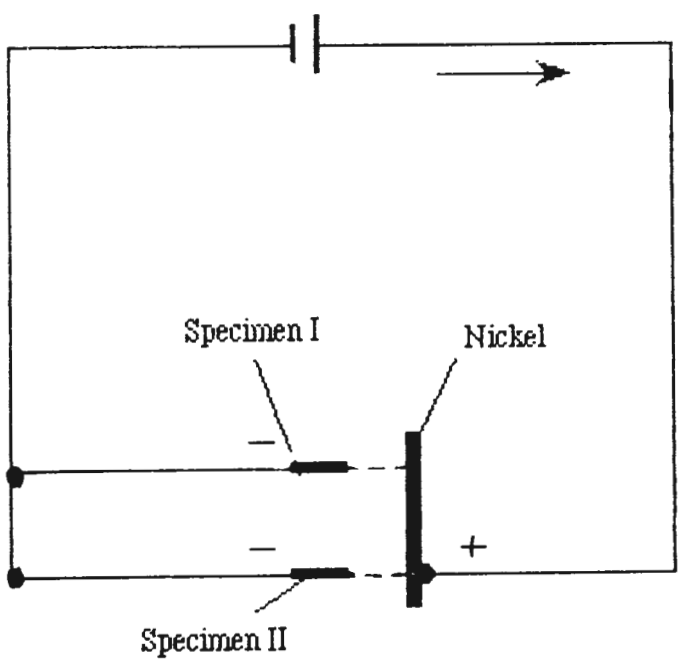

Fig.A3.2 Diagram showing electrical circuit for nickel electro-plating of two specimens simultaneously.

REFERENCES

1. D. Dowson, "Wear oh Where ?", *Wear*, Vol.103, (1985), pp191-203.

2. D. Tabor, "Wear-A Critical Synoptic View", *J. Lubr. Tech.* Oct., (1977), pp387-395.

3. M. A. Moore, "Laboratory Simulation Testing for Service Abrasive Wear Environments", *Intern. Conf. Proc. Wear of Materials 1987,* Texas, ed. Ludema, ASME, 1987, pp673-687.

4. Research Group on Wear of Engineering Materials, *Glossary of Terms and Definitions in the Field of Friction, Wear and Lubrication--Tribology*, OECD Publications, Paris, 1969.

5. D. Tabor, "Friction and Wear -- Developments Over the Last Fifty Years", *Proc. Inst. Mech. Eng.-- Friction Lubrication and Wear, Fifty Years on 1987,* pp157-172.

6. National Foundry Council, *Wear of Abrasion Resistant Materials--Technical Note*, MTIA Australia, (1986).

7. M. E. Merchant, "Mechanism of Static Friction", *J. Applied Physics,* Vol.11, No.3 (1940), p230.

8. F. P. Bowden and D. Tabor, *The Friction and Lubrication of Solids*, Clarendon, Oxford, England, (1950).

9. N. P. Suh, "The Delamination Theory of Wear", *Wear*, Vol.25, (1973), pp111-124.

10. N. P. Suh and Colleagues, *Wear*, Vol.44, (1977), pp1-161.

11. T. S. Eyre, "Wear Characteristics of Metals", *Source Book on Wear Control Technology*, 1978, (ed. D. A. Rigney & W. A. Glaeser), pp1-10.

12. A. G. Gray, "Wear Control Takes on New Significance", *Metal Progress*, Nov. (1977), Vol.112, p29.

13. K. H. Zum-Gahr, *Microstructure and Wear of Materials*, Tribology Series 10, Elsevier, 1986.

14. A. Misra, *A Study of Abrasive Wear*, Ph.D Thesis, University of California, Berkeley, (1979).

15. H. S. Avery, *Selecting Materials for Wear Resistance, in Surface Protection against Wear and Corrosion.* ASM, Cleveland, 1954, p10.

16. H. S. Avery, "Classification and Precision of Abrasion Tests", *Intern. Conf. Proc. Wear of Materials 1977,* ASME, New York, 1977, pp148-157.

17. R. Blickensderfer, B. W. Madsen and J. H. Tylczak, "Comparison of Several Types of Abrasive Wear Tests", *Intern. Conf. Proc. Wear of Materials 1985*, ASME, New York, 1985, pp313-319.

18. C. G. Massieon, "Abrasive Wear Testing", *Wear and Fracture Prevention, Mat./Met. Working Tech. Series, Proc. of Conf. ASM*, (1980), Metals Park, Ohio, pp23-37.

19. M. M. Khruschov and M. A. Babichev, *Research on the Wear Metals*, Moscow, Chap.18, (1960).

20. E. Rabinowicz, *Friction and Wear of Materials*, Wiley, New York, (1965).

21. M. A. Moore, *Fundamentals of Friction and Wear of Materials*, ASM Materials Seminar, (1980), Pittsburgh.

22. M. M. Khruschov and M. A. Babichev, *Research on the Wear of Metals*, Moscow, Chap.II, (1960).

23. R. C. D. Richardson, "The Wear of Metals by Hard Abrasives", *Wear*, Vol.10, (1967), pp291-309.

24. D. V. Doane, "Abrasive Wear -- The Alloy Question", *Wear and Fracture Prevention, Mat./Met. Working Tech. Series, Proc. of Conf. ASM*, (1980), Metals Park, Ohio, pp3-21.

25. P. J. Mutton and J. D. Watson, "Some Effects of Microstructure on Abrasive Resistance of Metals", *Wear*, Vol.48, (1978), pp385-398.

26. A. Kasak and T. A. Neumeyer, "Observations on Wear of High-Hardness Steels",*Wear*, Vol.14, (1969), pp445-454.

27. B. Pugh, *Practical Lubrication*, London, Newnes-Butterworth, 1970, p146.

28. G. V. Toporov, "The Influence of Structure on the Abrasive Wear of Cast Iron", *Friction and Wear in Machinery*, No. 12, ASME, New York, (1960), pp39-59.

29. E. Rabinowicz, L. A. Dunn and P. G. Russell, "A Study of Abrasive Wear Under Three-Body Condition", *Wear*, Vol.4, (1961), pp345-355.

30. A. Misra and L. Finnie, "A Classification of Three-Body Abrasive Wear and Design of a New Tester", *Wear*, Vol.60, (1980), pp111-121.

31. L. E. Samuels, "The Mechanisms of Abrasive Machining", *Scientific American,* Nov. (1978), pp132-152.

32. M. C. Shaw, *Metal Cutting Principles*, Oxford, Clarendon Press, New York, 1984.

33. A. J. Sedriks and T. O. Mulhearn, "The Effect of Work-Hardening on the Mechanics of Cutting in Simulated Abrasive Process", *Wear*, Vol.7, (1964), pp451-459.

34. K. Hokkirigawa and K. Kato, "The Effect of Hardness on the Transition of the Abrasive Wear Mechanism of Steel", *Wear*, Vol.123, (1988), pp241-251.

35. T. O. Mulhearn and L. E. Samuels, "Abrasion of Metals: A Model of the Process", *Wear*, Vol.5, (1962), pp478-498.

36. J. Larsen-Badse, "Influence of Grit Diameter and Specimen Size on Wear During Sliding Abrasion",*Wear*, Vol.11, (1968), pp213-222.

37. M. J. Murray, P. J. Mutton and J. D. Watson, "Abrasive Wear Mechanism in Steels", *J. Lubr. Tech. Trans., ASME, Trib.*, Vol.104, (1982), pp9-15.

38. L.Xu and N. F. Kennon, "A Laboratory Study of Abrasive Wear of Liner Materials for Refractory Industry", Accepted by *Materials Forum, Australasia*, Nov., 1990.

39. L. Xu and N. F. Kennon, "A Study of the Abrasive Wear of Carbon Steels", Accepted by *Wear*, Feb. 1991.

40. P. Heilmann and D. A. Rigney, "Experimental Evidence for Fatigue During Sliding Wear", *Metal. Trans.*, Vol.12A, (1981), pp686-688.

41. J. F. Archard, "Contact and Rubbing of Flat Surface", *J. Applied Physics*, Vol.24, (1953), pp981-988.

42. E. Rabinowicz, *Friction and Wear of Materials*, Wiley, New York, (1965).

43. *Evaluation of Wear Testing*, A Symposium Presented at the Seventy-first Annual Meeting, ASTM, San Francisco, Philadelphia, 1969.

44. M. M. Khruschov, "Resistance of Metals to Wear by Abrasion, as Related to Hardness", *Inst. Mech. Eng., Proc. Conf. on Lubr. and Wear, London*, (1957), pp655-659.

45. M. M. Khruschov and M. A. Babichev, "Resistance to Abrasive Wear of Structurally Inhomogeneous Materials", *Friction and Wear in Machinery*, Vol.12, (1958), pp5-23.

46. R. T. Spurr and T. P. Newcomb, "The Friction and Wear of Various Materials Sliding Against Unlubricated Surfaces of Different Types and Degrees of Roughness", *Inst. Mech. Engrs., Proc. of Conf. Lubr. and Wear*, (1957), pp269-275.

47. K. H. Zum-Gahr, "The Influence of Fracture Toughness on the Friction Force in Abrasive Wear", *Z. Metallkde*, Vol.67, (1976), pp678-682.

48. K. H. Zum-Gahr, "Relation Between Abrasive Wear Rate and the Fracture Toughness of Metallic Materials", *Z. Metallkde,* Vol.69, (1978), pp643-650.

49. J. Larsen-Basse, "Effects of Hardness and Local Fracture Toughness on the Abrasive Wear of WC-Co Alloys", *Proc. Inst. Mech. Eng., Tribology -- Friction Lubrication and Wear*, (1987), pp277-282.

50. A. Misra and I. Finnie, "Some Observations on Two-Body Abrasive Wear", *Wear*, Vol.68, (1981), pp41-56.

51. J. Larsen-Badse, "Influence of Grit Diameter and Specimen Size on Wear During Sliding Abrasion", *Wear*, Vol.12, (1968), pp35-53.

52. G. K. Nathan and W. J. D. Jones, "The Empirical Relationship Between Abrasive Wear and the Applied Condition",*Wear*, Vol.9, (1966), pp300-309.

53. C. J. Wang and J. C. M. Li, "Wear Behaviour of an Amorphous Alloy", *Wear*, Vol.98, (1984), pp45-61.

54. V. Aronov, A. F. D'Souza, S. Kalpakjian and I. Shareef, "Interactions Among Friction, Wear, and System Stiffness-Part 1: Effect of Normal Load and System Stiffness. ", *J. Tribology,* Jan., (1984), pp54-57.

55. A. F. Smith, "The Friction and Sliding Wear of Unlubricated 316 Stainless Steel at Room Temperature in Air", *Wear*, Vol.96, (1984), pp301-318.

56. B. W. E. Avient, J. Goddard and H Wilman, "An Experimental Study of Friction and Wear During Abrasion of Metals", *Proc. Roy. Soc. (London), Ser. A* ,Vol.258, (1960), pp159-179.

57. R. C. D. Richardson, " The Wear of Metals by Relatively Soft Abrasives", *Wear*, Vol.11, (1968), pp245-275.

58. M. A. Moore and R. M. Douthwaite, "Plastic Deformation Below Worn Surfaces", *Metal. Trans.*, Vol.7A, (1976), pp1833-1839.

59. R. W. Johnson, " A Study of the Pick up of Abrasive Particles During Abrasion of Annealed Aluminium on Silicon Carbide Abrasive Papers", *Wear*, Vol.16, (1970), pp351-358.

60. G. W. Patterson and T. O. Mulhearn, "The Fracture of Idealized Abrasive Particles", *Wear*, Vol.13, (1968), pp175-182.

61. M. A. Moore and P. A. Swanson, "The Effect of Particle Shape on Abrasive Wear: A Comparison of Theory and Experiment", *Intern. Conf. Proc. Wear of Materials 1983*, ASME, New York, 1983, pp1-11.

62. M. M. Khruschov, "Principles of Abrasive Wear", *Wear*, Vol.28, (1974), pp69-88.

63. M. Khruschov, "Investigation of the Effect of Abrasive Hardness on Wear of Metals", *Friction and Wear in Machinery*, Vol.11, (1956), pp13-19.

64. E. Rabinowicz, "The Wear of Hard Surfaces by Soft Abrasives", *Intern. Conf. Proc. Wear of Materials 1983*, ASME, New York, 1983, pp12-18.

65. E. Blank and E. Luchsinger, "Microstructure and Abrasive Wear Resistance of Cast Ni-Cr-C Alloys", *Wear*, Vol.117, (1987), pp289-308.

66. R. B. Gundlach and J. L. Parks, "Influence of Abrasive Hardness on the Wear Resistance of High Chromium Irons", *Wear*, Vol.46, (1978), pp97-108.

67. M. M. Khruschov and M. A. Babichev, "An Investigation of the Wear of Metals and Alloys by Rubbing on an Abrasive Surface", *Friction and Wear in Machinery*, Vol.11, (1956), pp1-12.

68. B. Pugh, *Friction and Wear*, Newnes-Butterworth, 1973.

69. J. H. Tylczak, "A Study of the Abrasive Wear of Pure Metals Using a Pin-on-Drum Apparatus", *Wear*, Vol.135, (1990), pp305-318.

70. K. Hokkirigawa and Z. Z. Li, "The Effect of Hardness on the Transition of Abrasive Wear Mechanism of Steel", *Intern. Conf. Proc. Wear of Materials 1987*, Texas, ed. Ludema, ASME, 1987, pp585-593.

71. F. Borik, "Metallurgy of Ferrous Materials for Wear Applications", *Wear Control Handbook*, (M. B. Perterson and W. O. Winer ed.), ASME, New York, (1980), pp327-343.

72. R. C. D. Richardson, "The Maximum Hardness of Strained Surface and the Abrasive Wear of Metals and Alloy", *Wear*, Vol.10, (1967), pp353-382.

73. P. J. Alison and H. Wilman, "Different Behaviour of Hexagonal and Cubic Metal in Their Friction Wear and Work Hardening During Abrasion", *Brit. J. Applied Physics,* Vol.15, (1964), pp281-189.

74. J. Larsen-Badse, "The Abrasion of Some Hardened and Tempered Carbon Steels", *Trans. MIME*, Vol.236, (1966), pp1461-1466.

75. Myer Kutz, *Mechanical Engineers' Handbook*, New York, Wiley, 1986.

76. K. H. Zum-Gahr, "How Microstructure Affects Wear Resistance", *Metal Progress,* Sept. (1979), Vol.116. pp46-52.

77. A. Ball and H. Böhm, "The Design and Performance of Steels in an Abrasive-Corrosive Mining Environment", *Proc. Inst. Mech. Eng., Tribology -- Friction Lubrication and Wear, Fifty Years on 1987,* pp595-602.

78. W. M. Garrison *Jr* and R. A. Garriga, "Ductility and the Abrasive Wear of an Ultrahigh Strength Steel", *Wear,* Vol.85, (1983), pp347-360.

79. W. M. Garrison *Jr*, T. A. Lechtenberg and J. Kim, "Ductility and the Abrasive Wear Resistance of Hot Work Die Steels", *Wear*, Vol.116, (1987), pp33-41.

80. W. A. Glaeser, "High Strain Wear Mechanisms in Ferrous Alloys" *Intern. Conf. Proc. Wear of Materials 1987,* Texas, ed. Ludema, ASME, 1987, pp155-162.

81. I. R. Kramer and N. Balasubramanian, "Metallographic Study of the Surface Layer", *Acta Metallurgia,* Vol.21, (1973), pp695-699.

82. E. Hornbogen, "The Role of Fracture Toughness in the Wear of Metals", *Wear,* Vol.33, (1975), pp251-259.

83. M. A. Moore and F. S. King, "Abrasive Wear of Brittle Solids", *Intern. Conf. Proc. Wear of Materials 1979*, ASME, New York, 1979, pp275-285.

84. K. H. Zum-Gahr, "Modeling of Two-Body Abrasive Wear", *Wear*, Vol.124, (1988), pp87-103.

85. K. H. Zum-Gahr, "Formation of Wear Debris by the Abrasion of Ductile Metals", *Wear*, Vol.74, (1981), pp353-373.

86. M. M. Khruschov and M. A. Babichev, "Abrasive Wear Resistance and the Modulus of Elasticity of Heat-treated Steels", *Friction and Wear in Machinery*, Vol.17, (1962), pp9-18.

87. K. J. Bhansali and W. L. Silence, "Metallurgical Factors Affecting Wear Resistance of Metals", *Metal Progress*, Nov. (1977), Vol.112, pp39-43.

88. A. R. Rosenfield, "Elastic-Plastic Fracture Mechanics and Wear", *Wear*, Vol.72, (1981), pp245-254.

89. M. A. Moore, R. C. D. Richardson and D. G. Attwood, "The Limiting Strength of Worn Metal Surfaces", *Metal. Trans.*, Vol.3A, (1972), pp2485-2491.

90. K. H. Zum-Gahr, "Relation Between Abrasive Wear Rate and the Microstructure of Metals", *Intern. Conf. Proc. Wear of Materials 1979*, ASME, New York, 1979, pp266-274.

91. M. A. Moore, "A Review of Two Body Wear", *Wear*, Vol.27, (1974), pp1-17.

92. N. N. Serpik and M. M. Kantor, "Effect of Heat Treatment on Abrasive Resistance of Steels for Earth Moving Equipment", *Metalloved Obrab. Metal.*, Vol.7, (1958), pp46-50.

93. M. A. Moore, "The Relationship Between the Abrasive Wear Resistance, Hardness, and Microstructure of Ferritic Materials", *Wear*, Vol.28, (1974), pp59-68.

94. C. K. Kwok and G. Thomas, "Microstructural Influence on Abrasive Wear Resistance of High Strength, High Toughness Medium Carbon Steels", *Intern. Conf. Proc. Wear of Materials 1983*, ASME, New York, 1983, pp140-147.

95. J. W. Jang and I. Iwasaki, "Effect of Martensite and Austenite on Grinding Media Wear", *Wear*, Vol.122, (1988), pp285-299.

96. K. H. Zum-Gahr and D. V. Doane, "Optimizing Fracture Toughness and Abrasion Resistance in White Cast Irons", *Metal. Trans.*, Vol.11A, (1980), pp613-620.

97. K. H. Zum-Gahr, "Abrasive Wear of White Cast Iron", *Wear*, Vol.64, (1980), pp175-194.

98. K. H. Zum-Gahr, "Friction and Wear of a Precipitation Hardenable Austenitic Steel Under Abrasive Conditions", *Z. Metallkde*, Vol.68, (1977), pp381-389.

99. J. Larsen-Badse, "Abrasion Resistance of Some SAP-Type Alloys at Room Temperature",*Wear*, Vol.12, (1968), pp357-368.

100. J. Larsen-Badse and K. G. Mathew, "Influence of Structure on the Abrasion Resistance of a 1040 Steel",*Wear*, Vol.14, (1969), pp199-205.

101. K. H. Zum-Gahr, "Abrasive Wear of Two-Phase Metallic Materials with a Coarse Microstructure", *Intern. Conf. Proc. Wear of Materials 1985*, ASME, New York, 1985, pp45-58.

102. Z. Nishiyama, *Martensitic Transformation*, New York Academic Press, (1977), ed. M. E. Fine, M. Meshii and C. M. Wayman.

103. J. Y. Su, Y. Q. Chen and Q. D. Chen, "Prolonging the Service Life of Shot-Blaster Blades Made From High Chromium Cast Iron",*Wear*, Vol.135, (1990), pp391-402.

104. I. M. Feng, "Plastic Roughening and Wear", *Inst. Mech. Eng., Proc. Conf. on Lubr. and Wear, London*, (1957), pp635-639.

105. T. Yamamoto, Y. Imada and K. Nakajima, "The Effect of Grain Size on the Wear Behaviour of Mn-Zn Ferrite", *Proc. Inst. Mech. Eng., Tribology -- Friction Lubrication and Wear, Fifty Years on 1987*, pp671-677.

106. M. D. Tumuluru, "Wear Resistance of Quenched and Tempered AISI 4237H Steel", *Metal. Trans.*, Vol.17A, (1986), pp295-306.

107. P. W. Leach abd D. W. Borland, "The Unlubricated Wear of Flake Graphite Cast Iron", *Wear*, Vol. 85, (1983), pp257-266.

108. D. Shen. "Friction and Wear of Eutectoid and Hypoeutectoid Steels", *Intern. Conf. Proc. Wear of Materials 1985*, ASME, New York, 1985, PP194-204.

109. U. Herold-Schmidt and R. Hinsberger, "Abrasive Wear Resistance of Anisotropic Two Phase Fe-Ni-C Steels", *Wear*, Vol.120, (1987), pp151-160.

110. C. K. Kwok and N. Thomas, "Microstructure-Abrasive Wear Characteristics of Low Carbon Dual Phase Steels", *Intern. Conf. Proc. Wear of Materials 1985*, ASME, New York, 1985, pp612-620.

111. M. A. Moore, "A Preliminary Investigation of Frictional Heating During Abrasive Wear",*Wear*, Vol.17, (1971), pp51-58.

112. J. Larsen-Basse and S. S. Sokoloski, "Influence of Atmospheric Humidity on Abrasive Wear -- II. Two-Body Abrasion",*Wear*, Vol.32, (1975), pp9-14.

113. W. Glaeser, "Wear Resistant Materials", *Wear Control Handbook*, pp313-325. M. B. Perterson and W. O. Winer ed., ASME, New York, (1980).

114. L. E. Doyle, *Manufacturing Processes and Materials for Engineers*, Pub. Englewood Cliffs, N.J. Prentice-Hall, (1985).

115. C. H. White and R. W. K. Honeycombe, "Structural Changes During the Deformation of High-Purity Iron-Manganese-Carbon Alloys", *J. Iron and Steel Inst.* Vol.200, (1962), pp457-466.

116. N. F. Kennon and L. Xu, "Wear Resistance of BIS-alloys", *A Final Report to Bisalloy Steel Works*, December, 1990.

117. M. Kehoe and P. M. Kelly, "The Role of Carbon in the Strength of Ferrous Martensite", *Scripta Met.*, Vol.4 (1970), pp473-476.

118. J. D. Watson, P. J. Mutton and I. R. Sare, "Abrasive Wear of White Cast Irons", *Metal Forum,* Vol.3, No.1 (1980), pp74-88.

119. S. Hogmark and O. Vingsbo, "Mechanisms of Dry Wear of Some Martensitic Steels", *Source Book on Wear Control Technology*, 1978, ed. D. A. Rigney & W. A. Glaeser, pp147-169.

120. J. J. Sidorin and N. A. Dolgova, "The Wear Resistance of Tool Steels in Relation to the Distribution of Alloying Elements", *Izv. Vyssh. Ucheb. Zaved. Mashinostr.* Vol.5, (1970), pp155-157.

121. R. A. Grange, C. R. Hribal and L. F. Porter, "Hardness of Tempered Martensite in Carbon and Low-Alloy Steels", *Metal. Trans.*, Vol.8A, (1977), pp1775-1785.

122. T. Minemura, A. Inoue, Y. Kojima and T. Masumoto, "Formation of Metastable Austenite in Splat Quenched High Alloy Steels Containing Cr, Mo or W", *Metal. Trans.*, Vol.11A, (1980), pp671-673.

123. H. Berns and A. Fischer, "New Abrasion Resistant Alloys",*Proc. Inst. Mech. Eng., Tribology -- Friction Lubrication and Wear, Fifty Years on 1987,* pp603-608.

124. W. Fairhurst and K. Röhrig, "Abrasion-Resistance High-Chromium White Cast Iron", *Foundry Trade Journal*, May 30 (1974), pp685-697.

125. M. A. Grossmann, *Principles of Heat Treatment,* Cleveland, Ohio, ASM, 1962.

126. M. Shi,*Metal Materials and Heat Treatments*, (Chinese), Metallurgical Industries Press, China, 1983.

127. Y. Liu, *Heat Treaments of Steels*, (Chinese), Metallurgical Industries Press, China, (1986).

128. D. M. Turley, "The Nature of White-Etching Surface Layers Produced During Reaming Ultra-High Strength Steels", *Materials Science & Engineering*, Vol.19, (1975), pp79-86.

129. B. J. Griffiths and D. C. Furze, "Tribological Advantages of White Layers Produced by Machining", *J. of Trib., Trans. of ASME,* Vol.109, (1987), pp338-342.

130. T. S. Eyre and A. Baxter, "The Formation of White Layers at Rubbing Surface", *J. of Trib.*, Dec. 1972, pp256-261.

131. Y. I. Babei, V. M. Golubets, I. P. Vygovskii, B. F. Rynbov and N. N. Gnatyshak, "Effect of White Layer on the Wear Resistance of Steel 50Kh", *Sov. Mat. Sci.* Vol.7, (1971), No.5, pp511-514.

132. W. J. Tomlinson, L. A. Blunt and S. Spraggett, "Running-in Wear of White Layer Formed on EN24 Steel by Centreless Grinding", *Wear,* Vol.128, (1988), pp 83-91.

133. V. D. Kuznetsov, K. V. Savitskiy and N. N. Sukharina, "Some Structure of White Layers", *Physics of Metal and Metallography,* Vol.15, (1963), pp135-137.

134. B. D. Grozin and V. F. Iankevich, "The Structure of White Layers", *Friction and Wear in Machinery*, Vol.15, (1962), pp143-152.

135. R. C. Glenn and W. C. Leslie, "The Nature of 'White Streaks' in Impacted Steel Armor Plate", *Metal. Trans.,* Vol.2A, (1971), pp2945-2947.

136. D. Furze and B. J. Griffiths, "White Layers at Machined Surfaces and Their Wear Resistance", *Proc. Conf. Eng. the Surface* held at London, May, (1986), Pub. Institute of Metals, part 31, pp1-2.

137. J. A. Bailey, S. Jeelani and S. E. Becker, "Surface Integrity in Machining AISI 4340 Steel", ASME *J. Engineering for Industry,* (1976), pp999-1007.

138. N. Jost and I. Schmidt, "Friction-Induced Martensitic Transformation in Austenitic Manganese Steels", *Wear*, Vol.111, (1986), pp377-389.

139. L. A. Blunt, W. J. Tomlinson and S. Spraggett, "Metallurgical Effects Associated with the Centreless Grinding of EN 24 Steels", *Advances in Manufacturing Technology II, Proc. 3rd Nat. Conf. on Production Research,* (1987), pp393-397.

140. A. L. Wingrove, "A Note on the Structure of Adiabatic Shear Bands in Steel", *J. Aust. Inst. Metals,* Vol.16, No.1 (1971), pp67-70.

141. D. M. Turley, E. D. Doyle and L. E. Samuels, "The Structure of the Damaged Layer on Metals", *Proc. Intern. Conf. on Production Engineering*, Held in Tokyo 1974, Part 2, Pub. Japan Soc. Prec. Eng., pp142-147.

142. B. J. Griffiths, "White Layer formations at Machined Surfaces and Their Relationship to White Layer Formations at Worn Surfaces", *J. of Trib., Trans. of ASME,* Vol.107, (1985), pp165-171.

143. B. J. Griffiths, "Mechanisms of White Layer Generation With Reference to Machining and Deformation Processes", *J. of Trib., Trans. of ASME,* Vol.109, (1987), pp525-530.

144. D. V. Wilson, "Effect of Plastic Deformation on Carbide Precipitation in Steel", *Acta Met.* Vol.5, (1957), pp293-302.

145. "Metallurgy, Structures and Phase Diagrams", *Metals Handbook*, Vol.8, 8th ed. ASM, Handbook Committee, (1961).

146. G. Krauss, *Principles of Heat Treatment of Steels,* Metals Park, Ohio, ASM, 1980.

147. K. Nakazawa and G. Krauss, "Martensite and Fracture in 52100 Steel", *Metal. Trans.,* (1978), Vol.9A, p681-689.

148. R. P. Brobst and G. Krauss, "The Effect of Austenite Grain Size on Microcracking in Martensite of an Fe-1.22C Alloy", *Metal. Trans.,* Vol.5, 1974, p457-462.

149. A. R. Marder and A. O. Benscoter, "Microcracking in Fe-C Acicular Martensite", *Trans ASM*, Vol.61, (1968), p293-199.

150. M. G. Mendiratta, J. Sasser and G. Krauss, "Effect of Dissolved Carbon on Microcrackig in Martensite of an Fe-1.39C Alloy", *Metal. Trans.*, (1972), Vol.3, p351-353.

151. G. Krauss, "The Effect of Austenitizing on Microstructure and Fracture of Hardened High Carbon Steels",*Wear and Fracture Prevention, Mat./Met. Working Tech. Series, Proc. of Conf. ASM*, (1980), Metals Park, Ohio, pp147-161.

152. S. F. Wayne, S. L. Rice, K. Minakawa and H. Nowotny, "The Role of Microstructure in the Wear of Selected Steels", *Wear*, Vol.85, (1983), pp93-106.

153. S. Bhattacharyya, "Wear and Friction in Steel, Aluminium and Magnesium Alloy --I, Pearlitic and Spheroidized Steels", *Wear*, Vol.61, (1980), pp133-141.

154. "Tool Steels", ASM Committee on Tooling Materials, *Metals Handbook,* (1980), Vol.3, p421, 9th ed., ASM Metals Park, Ohio.

155. J. E. Denton, "Selection of Tool Materials for Structural Components", *Metals Handbook,* (1980), Vol.3, p558, 9th ed., ASM Metals Park, Ohio.

156. R. Wilson, *Metallurgy and Heat Treatment of Tool Steels*, McGraw-Hill Book, 1975.

157. M. R. Ghomashchi and C. M. Sellars, "Microstructural Changes in as-Cast M2 Grade High Speed Steel During High Temperature Treatment", *Metal Science*, Vol.48, (1984), pp44-48.

158. H. E. Boyer and T. L. Gall, *Metals Handbook*, Desk Edition, Metals Park, Ohio, ASM, 1984.

159. D. A. Rigney, "Wear Resistance", *Metals Handbook,* (1980), Vol.1, p597, 9th ed., ASM Metals Park, Ohio.

160. H. Berns and W. Trojahn, "Wear of Ledeburitic Chromium Steels", *Intern. Conf. Proc. Wear of Materials 1985*, ASME, New York, 1985, pp186-192.

161. H. Berns and W. Trojahn, "New Cold Working Tool Steels", *Metals and Materials,* July (1986), pp421-425.

162. M. R. Ghomashchi, "The Morphology of Eutectic Carbides in M2-Grade High Speed Steel", *Metal. Trans.*, Vol.16A, (1985), pp2341-2342.

163. W. L. Silence, "Effect of Structure on Wear Resistance of Co-, Fe-, and Ni-Base Alloys",*Trans. of ASME, Tribology,* Vol.100, (1978), pp428-435.

164. A. G. Shchulepnikova, "The Effect of Composition, Structure, and Changes in the Surface Layer of Steel on Its Resistance to Abrasive Wear by Iron Ores and Agglomerates (Sinters)", *Friction and Wear in Machinery,* Vol.19, (1965), pp16-27.

165. V. M. Desai, C. M. Rao, T. H. Kosel and N. F. Fiore, "Effect of Carbide Size on the Abrasion of Co-Base PM Alloys" *Intern. Conf. Proc. Wear of Materials 1983*, ASME, New York, 1983, pp32-37.

166. S. Junyi and J. Yuding, "The Effect of Orientation and Thickness of Carbides on Abrasive Wear Resistance of High Chromium Iron", *Intern. Conf. Proc. Wear of Materials 1987,* Texas, ed. Ludema, ASME, 1987, pp661-671.

167. L. J. Venne, "Abrasion Resistant Materials for Earthmoving and Coal Mining",*Wear and Fracture Prevention, Mat./Met. Working Tech. Series, Proc. of Conf. ASM*, (1980), Metals Park, Ohio, pp39-46.

168. L. Fang, Q. Rao and Q. Zhou, "Abrasive Wear Resistance of Chromium Family of White Cast Iron", *Intern. Conf. Proc. Wear of Materials 1987,* Texas, ed. Ludema, ASME, 1987, pp733-741.

169. D. E. Diesburg and F. Borik, "Optimizing Abrasion Resistance and Toughness in Steels and Irons for the Mining Industry", *Source Book on Wear Control Technology*, 1978, (ed. D. A. Rigney & W. A. Glaeser), pp94-120.

170. A. J. DeArdo, *Processing, Microstructure and Properties of HSLA Steels*, TMS, Warrendale, Pennsylvania, 1988.

171. "High-Strength Low-Alloy Steels and High Strength Intermediate Manganese Steels", *AISI Steel Products Manal*, Vol.17, (1967).

172. M. Cohen and W. S. Owen, "Thermo-Mechanical Processing of Microalloyed Steels", *Microalloying 75*, Proceedings International Symposium on HSLA Steels, New York, (1977), pp2-8.

173. J. H. Woodhead and S. R. Keown, "The History of Microalloyed Steels", *HSLA Steels Conf. Proc.*, Beijing, China, (1985), (ed. J. M. Gray *et al.*), pp15-27.

174. S. W. Poole, "High-Strength Structural and High-Strength Low-Alloy Steels", *Metals Handbook*, (1980), Vol.1, pp403-420, 9th ed., ASM Metals Park, Ohio.

175. G. A. Rosier and J. E. Croll, "High Strength Quenched and Tempered Steels in Structures", The Association of Consulting Structural Engineers of NSW Seminar "*Steel in Structures*" Held in Sydney, August, 1987.

176. J. E. Croll, "Production and Usage of QT Steel Plate in Australia", *HSLA Steels Conf. Proc.*, Wollongong, Australia, (1984), (ed. D. P. Dunne and T. Chandra), pp247-250.

177. K. Norring, H. Harvig and B. Lindwall, "Improvements in Thick-Plate Steel for Heavy Structures", *Microalloying 75*, Proceedings International Symposium on HSLA Steels, New York, (1977), pp684-691.

178. A. Cigada, T. Pastore, G. Re, G. Rondelli and B. Vicentini, "Stress Corrosion Cracking in Seawater of HSLA Steel Type API 5L X65" *HSLA Steels conf. Proc.*, Beijing, China, (1985), (ed.J. M. Gary *et al.*), pp785-792.

179. H. Zhang, N. Xhou, S. Jiang, T. Jin, Y. Zhou and K. Huang, "A 65kgf-25CrMoTi-SSCC Resisting Steel", *HSLA Steels conf. Proc.*, Beijing, China, (1985), (ed.J. M. Gary *et al.*), pp793-798.

180. L. Meyer, C. Straβburger and C. Schneider, "Effect and Present Application of the Microalloying Elements Nb, V, Ti, Zr, and B in HSLA Steels", *HSLA Steels conf. Proc.*, Beijing, China, (1985), (ed.J. M. Gary *et al.*), pp29-44.

181. T. Gladman, D. Dulieu and I. D. McIvor, "Structure-Property Relationships in High-Strength Microalloyed Steels", *Microalloying 75*, Proceedings International Symposium on HSLA Steels, New York, (1977), pp32-55.

182. J. E. Croll, "The Use of High Strength and Abrasion Resistant QT Steel Plates", *AIM NZ Branch Metals Materials Symposium*, Lower Hutt, 1983, pp91-94.

183. M. S. Bhat, W. M. Garrison, *Jr*, N. J. Kar and T. A. Lechtenberg, "Abrasive Wear of Ultra High Strength Steels", *Wear and Fracture Prevention, Mat./Met. Working Tech. Series, Proc. of Conf. ASM*, (1980), Metals Park, Ohio, pp47-69.

184. J. H. Pollard, *A Handbook of Numerical and Statistical Techniques*, Cambridge University Press, (1977), p80.

185. *Metallography Principles and Procedures*, Leco Corporation, LECO, 1985.

186. H. Modin and S. Modin, *Metallurgical Microscopy*, ed. T. J. Baker, London, Butterworths, 1973.

187. N. F. Kennon and L. Xu, "Effects of Heat Treatment on Abrasive Wear Behaviour of a Ni-Cr-Mo-C Tool Steel", Accepted by *Materials Forum, Australasia*, 1991.

188. N. C. Welsh, "Structural changes in rubbed steel surfaces", *Proc. Inst. Mech Engrs.* Conf. Lubrication & Wear, (1957), Paper 77, PP701-706.

189. M. Field, W. P. Koster, J. B. Kohls, R. E. Snider and J. Maranchik,*Machining of high strength steels with emphasis on surface integrity*, Air Force Machinability Data Centre Report No. AFMDC-70-1, (1970).

190. C. N. Sastry, K. H. khan and W. E. Wood, "Mechanical stability of retained austenite in quenched and tempered AISI 4340 steel", *Metal. Trans.*, Vol.13A, (1982), PP676-680.

191. D. A. Rigney and W. A. Glaeser, "The Significance of Near Surface Microstructure in the Wear Process", *Wear*, Vol.46, (1978), pp241-250.

192. M. M. Shteynberg, Y. N. Goykhenberg and D. A. Mirzayev, "A Study of Features of the Martensitic Transformation During Plastic Deformation of Fe-Ni-Si Alloys", *Fiz. Metal. Metalloved*, 30 No6 (1970), pp1200-1206.

193. D. A. Rigney, L. H. Chen and M. G. S. Naylor, "Wear Processes in Sliding System", *Wear*, Vol.100, (1984), pp195-219.

194. M. Kawamoto, K. Okabayashi, "Wear of cast iron in vacuum and the frictional hardened layer", *Wear*, Vol.17, (1971), P123-138.

195. O'Niell, *Hardness Measurement of Metals and Alloys*, Pub. Chapman & Hall, 2nd ed. (1967).

196. S. L. Rice, H. Nowotny and S. F. Wayne, "Formation of Subsurface Zones in Impact Wear", *Trans. of ASLE*, Vol. 24, (1980), pp264-268.

197. S. Hogmark and O. Vingsbo, "Adhesive Mechanisms in the Wear of Some Tool Steels", *Wear*, Vol.38, (1976), pp341-359.

198. R. T. Spurr, "The Abrasive Wear of Metals", *Wear*, Vol.65, (1981), PP315-324.

199. *Friction and Wear Devices*, Park Ridge, Ill., ASLE, 1976.

200. *Nickel Plating Technique and Application*, The international Nickel Company (Mond) Limited.

201. *Nickel Plating*, International Nickel Limited, Thames House Millbank, London SW1.

PUBLICATIONS

1. A. Wingrove and L. Xu, "The Influence of Welding Voltage on the Microstructure of Manual Metal Arc Weld Deposits", *Australian Welding Research* , Vol.16, 1988, pp12-14.

2. L. Xu and N. F. Kennon, "A Laboratory Study of Abrasive Wear of the Liner Materials for Refractory Industry", *Materials Forum,* IMMA, Vol.15, 1991, pp191-196.

3. L. Xu and N. F. Kennon, "A Study of the Abrasive Wear of Carbon Steels", *Wear,* Vol.148 , 1991, pp101-112.

4. N. F. Kennon and L Xu, "Effects of Heat Treatment on Abrasive Wear Behaviour of a Ni-Cr-Mo-C Tool Steel", *Materials Forum,* IMMA, Vol.15, 1991, pp287-292.

5. L. Xu and N. F. Kennon, "Taper Sectioning of Abraded Surfaces", *Conference Proceeding 'Metallography & Minerology'*, IMMA, Melbourne, July, 1991.

6. L. Xu and N. F. Kennon, "Optimization of Abrasive Wear Resistance", *1991 IMMA Annual Conference 'Materials Processing and Performance',* Melbourne, Sept. 1991, pp202-205.

7. L. Xu and N. F. Kennon, "Generation of White Layer During Laboratory Abrasion Test", to be published in *Materials Forum,* IMMA, 1991.